Ana Isabel Machado Mouquinho
Mestre em Bioorgânica

New Polymeric films for Smart Windows with Permanent Memory Effect

Dissertação para obtenção do Grau de Doutor em
Química Sustentável

Orientador: Prof. Doutor João Carlos da Silva Barbosa Sotomayor, Professor Auxiliar, FCT-UNL

Júri

Presidente: Prof. Doutor Manuel Luís de Magalhães Nunes da Ponte
Arguentes: Prof. Doutor José Virgílio de Sousa Coelho Prata
Prof. Doutor João Luís Maia Figueirinhas
Vogais: Prof. Doutora Maria Helena Figueiredo Godinho
Prof. Doutor João Francisco Alves Martins
Doutora Krasimira Todora Markova-Petrova

FACULDADE DE CIÊNCIAS E TECNOLOGIA
UNIVERSIDADE NOVA DE LISBOA

Setembro, 2019

Ana Isabel Machado Mouquinho

Mestre em Bioorgânica

New Polymeric films for Smart Windows with Permanent Memory Effect

Dissertação para obtenção do grau de doutor em
Química Sustentável

Orientador: Professor Doutor João Carlos da Silva Barbosa Sotomayor, Professor Auxiliar, FCT-UNL

To Manuel, Gabriel and João

New Polymeric films for Smart Windows with Permanent Memory Effect

Acknowledgments

Firstly, I would like to express my sincere gratitude to my advisor, Professor João Sotomayor for the freedom and confidence placed in the chosen research routes, which was decisive for my scientific development. Thank you for your knowledge, for always treating me with cordiality, respect and equality.

Similar, gratitude goes to Professor Maria Teresa Barros, for being as dedicated as if she were a secondary advisor. Thank you for your immense knowledge, comments and encouragement over the years. I am particularly indebted for providing me the opportunity to work in her laboratory.

My sincere thanks also go to Dr. Krasimira Petrova for her friendship, support and accessibility that positively influenced the results.

Special mention goes to Professor João Figueirinhas, who provided me an opportunity to use his research laboratory and for the profitable theoretical discussions.

I am grateful to Professor Madalena Dionísio for her friendship, kindness and for her lab support in particular in differential scanning calorimeter.

I would like to acknowledge Professor Mário Eusébio for the development of a computer program essential to the electro-optical studies. Professor João Martins and Dr. Fernando Monteiro are acknowledged for their support in the experimental setup to measure the electro-optical properties of PDLC devices.

Special mention goes to Professor Gabriel Feio, Dr. Pedro Almeida and Dr. Marta Corvo for collaboration in solids magnetic resonance studies.

I am thankful to Professor Luís Pereira for the photolithography process, Professor Elvira Fortunato and Dr. Mafalda Costa for the confocal microscopy measurements, Professor Rita Branquinho for profilometry measurements and Dr. Daniela Gomes for scanning electron microscopy measurements. I also would like to thank Dr. Luz Fernandes for valuable help in discussing the results of MALDI-TOF.

Thanks to Faculdade de Ciências e Tecnologia da Universidade Nova de Lisboa and especially to the Department of Chemistry that welcomed me and the availability of infrastructure, technical and human resources indispensable for the laboratory practice of this work.

Thanks to Fundação para a Ciência e Tecnologia for the financial support granted under the PhD scholarship (SFRH/BD/91870/2012).

I am grateful to colleagues and friends of the Faculdade de Ciências e Tecnologia. In particular, I am grateful to Andreia Forte.

Special thanks to my mother for all the love and support. No word serves to measure this thanks. Because no matter how hard I try, I will never show all the gratitude I have with me.

I am especially indebted to my husband, Victor for all that we have achieved. With love, understanding, sense of humor and effort this PhD completes another achievement.

Finally, I would like to express my profound gratitude to my lovely children, Manuel, Gabriel and João. The three were born during my PhD and they are my true masterpieces and so I dedicate this thesis to them.

Abstract

In the field of the liquid crystals in device applications, the polymer dispersed liquid crystal (PDLC) with permanent memory effect can become feasible in technological applications. Although studies of the liquid crystals in technological applications were extensively reviewed in the literature, not so much has been reported on the permanent memory effect (PME) in PDLCs. PDLCs can change transmittance from a totally opaque state to a totally transparent state during the application of an external electric field. Typically, the opaque appearance returns to the PDLC when the electric field is switched OFF. However, in this work PDLCs have been produced that use the electric field to create a highly transparent state but the transparent state remains even when the electric field is switched OFF giving rise to a permanent alignment state of LC molecules. This property is called a permanent memory effect (PME). For optimizing this effect a series of linear polyethylene glycol di(meth)acrylate and multi-arm polyethylene glycol with linear chains arms extending radially from a central core with reactive (meth)acrylate end groups were synthesized and characterized. The resulting pre-polymers and also some commercial ones were then tested in preparation of PDLCs.

The 70 % of PME and the reproducibility even after multiple repetitions of the heating and electric field cycles application make the poly(ethyleneglycol) dimethacrylate of molecular weight 875 g mol^{-1} the most appropriate pre-polymer in preparation of PDLCs with PME. This effect is also dependent on the thermal polymerization which produces a polymer ball morphology type in the polymer matrix. In addition, PME is also highly dependent on the alignment layer type coating the glass PDLC cell (homogeneous alignment).

With the high transparent state permanently displayed at room temperature through PME (70 %), an efficient procedure to allow the PDLC to acquire its opaque state has been achieved. A method of removing the PME has been outlined by Joule effect with the application of the electric current to the conductive layer (ITO) of the glass PDLC cell. This procedure makes the experimental setup to destroy the LC alignment structure simpler and more practical than by radiation heat.

Conventional PDLCs need continuity of energy supply for keeping the ON state, which can be a very limiting aspect for many applications. However, PDLCs with PME besides having lower power consumption can be used in digital memory devices based on write-read-erase cycles. For this, a prototype has been assembled as proof of the concept to be used in the digital process of recording information with the binary language.

Keywords: Liquid crystal, PDLC, poly(ethyleneglycol), permanent memory effect.

Resumo

No campo dos cristais líquidos (CL) com aplicação em dispositivos, o cristal líquido disperso numa matriz polimérica (PDLC) é viável para aplicações tecnológicas. Apesar dos diversos estudos de cristal líquido neste tipo de aplicação, pouco está referenciado sobre o efeito de memória permanente (EMP) em filmes de PDLC. Normalmente, dispositivos de PDLCs podem alternar a transmitância de um estado totalmente opaco para um estado totalmente transparente durante a aplicação de um campo elétrico. Contudo, o PDLC retoma a um estado opaco quando o campo elétrico é desligado. No entanto, neste trabalho foram produzidos PDLCs que usam o campo elétrico para criar um estado de elevada transparência mas um estado transparente permanece mesmo quando o campo é desligado dando origem a um estado de alinhamento permanente das moléculas de cristal líquido. Para otimizar este foi sintetizado e caracterizado uma série de polietilenoglicol dimetacrilato e diacrilato de cadeia linear e uma série de cadeia ramificada com os grupos metacrilato ou acrilato como grupos funcionais terminais.

A percentagem de 70 % de efeito de memória permanente e a reprodutibilidade após múltiplas repetições de aquecimento e aplicação de campo elétrico fazem com que o polietilenoglicol dimetacrilato com uma massa molecular de 875 g mol^{-1} seja o mais apropriado para preparar PDLCs com efeito de memória permanente. Este efeito é também dependente da polimerização térmica que possibilita uma morfologia do tipo “polymer ball”. Adicionalmente, o efeito de memória permanente é também dependente do tipo de camada de alinhamento que reveste o vidro da célula de PDLC (alinhamento homogêneo).

Com o estado de alta transparência permanentemente exibido pelo efeito de memória permanente (70 %) foi desenvolvido um procedimento eficiente para estes PDLCs adquirirem novamente um estado opaco. Este método foi delineado pelo efeito de Joule com aplicação de corrente elétrica à camada condutora (ITO) da célula de vidro de PDLC. Este procedimento faz com que a destruição do alinhamento das moléculas de CL seja mais simples e prático do que a aplicação de calor por radiação.

Os PDLCs convencionais precisam continuamente de energia para manter o estado ligado, o que pode ser um aspeto muito limitativo para muitas aplicações. No entanto, os PDLCs com efeito de memória permanente além do menor consumo de energia podem ser utilizados em dispositivos de memória digital baseados em ciclos de gravar, ler e apagar informação digital. Para isso, um protótipo foi montado como prova de conceito para ser utilizado num processo digital de gravação de informação em linguagem binária.

Palavras-chave:

Cristal líquido, PDLC, polietilenoglicol, efeito de memória permanente.

List of Contents

List of Figures

List of Figures

List of Tables

List of Symbols and Abbreviations

8OCB	4,4´-n-octyloxycyanobiphenyl
5CT	4´n-pentyl-4-cyanoterphenyl
5CB	4-cyano-4´-pentyl-1,1´-biphenyl
7CB	4-n-heptyl-4´cyanobiphenyl
AC	Alternating Current
$n_{\parallel}$	An alternative designation for the extraordinary refractive index of the nematic liquid crystal (n_e)
$n_{\perp}$	An alternative designation for the ordinary refractive index of the nematic liquid crystal (n_o)
A	Ampere
Bit	Binary digit
^{13}C-NMR	Carbon Nuclear Magnetic Resonance Spectroscopy
T_{CC}	Cold-crystallization temperature
COSY	Correlation spectroscopy
J	Coupling constant
Tc	Crystallization temperature
Tcc	Cold-crystallization temperature
Da	Dalton
$CDCl_3$	Deuterated chloroform
$\Delta\varepsilon$	Dielectric anisotropy
$\varepsilon_{\parallel}$	Dielectric constants according to the direction parallel to the director
$\varepsilon_{\perp}$	Dielectric constants according to the direction perpendicular to the director
DSC	Differential Scanning Calorimetry

$\vec{p}_{\parallel}$	Dipole moment vector parallel to the molecular axis
$\vec{p}_{\perp}$	Dipole moment vector perpendicular to the molecular axis
DC	Direct Current
$\vec{n}$	Director of the liquid crystal
DEPT	Distortionless Enhancement by Polarization Transfer spectroscopy
dd	Double doublet
d	Doublet
E_{90}	Electric field required for the PDLC reaches 90% of its maximum transmittance
ε	Electric permittivity
P	Electric Power
I	Electrical Current Intensity
n_e	Extraordinary refractive index of the nematic liquid crystal
T_g	Glass transition temperature
HSQC	Heteronuclear Single Quantum Correlation Spectroscopy
HPDEC	High Power Proton Decoupling Pulse Sequence spectroscopy
H-PDLC	Holographic PDLC
ITO	Indium Tin Oxide
$\alpha_{\parallel}$	Induced dipole moments per unit electric field parallel to the molecular axis
$\alpha_{\perp}$	Induced dipole moments per unit electric field perpendicular to the molecular axis
IPS	In-Plane Switching
LEDs	Light Emitting Diodes
LC	Liquid Crystal

LCD	Liquid Crystal Display
T_{MAX}	Maximum transmittance of PDLC during electric field ON
T_m	Melting temperature
MSC	Memory state contrast
mW cm^{-2}	Milliwatts per square centimeter
T_0	Minimum transmittance for the initial opaque state of PDLC at electric field off
AIBN	*N*,*N*-azobisisobutyronitrile
E7	Nematic liquid crystal from *Merck*
T_{NI}	Nematic to isotropic transition temperature
M_n	Number average molecular weight
Δn	Optical anisotropy
n_o	Ordinary refractive index of the nematic liquid crystal
ppm	Parts per million
wt.%	Percentage by weight
PME	Permanent Memory Effect
POM	Polarized Optical Microscopy
PEG	Poly(ethylene glycol)
PPGA	Poly(Propylene Glycol)Acrylate
PPGM	Poly(Propylene Glycol)Methacrylate
PDI	Polydispersity index
PDLC	Polymer Dispersed Liquid Crystal
PIPS	Polymerization Induced Phase Separation

List of Symbols and Abbreviations

^{1}H-NMR	Proton Nuclear Magnetic Resonance Spectroscopy
n_i	Refractive index of the nematic liquid crystal in the isotropic phase
n_p	Refractive index of the polymer
R	Resistance
V_{RMS}	Root Mean Square Voltage
SEM	Scanning Electron Microscopy
s	Singlet
^{13}C CPMAS	Solid State Cross-Polarization Magic Angle Spinning carbon spectroscopy
^{13}C MAS	Solid State Magic Angle Spinning carbon spectroscopy
SIPS	Solvent-Induced Phase Separation
v	Speed of light in the material
c	Speed of light in vacuum
STN	Super Twisted Nematic
TMS	Tetramethylsilane
TIPS	Thermally Induced Phase Separation
TFT	Thin Film Transistor
TLC	Thin Layer Chromatography
V_{th}	Threshold Voltage
T_{OFF}	Transmittance of PDLC after removing electric field
NEt_3	Triethylamine
TN	Twisted Nematic
M_w	Weight average molecular weight

Chapter I

1 Liquid Crystal Fundamentals and Applications

1.1 Basic Types and Structures of Liquid Crystals

Liquid crystals (LC) are compounds with properties between crystalline solid and isotropic liquid. This is due to the fact that they exhibit optical birefringence as crystalline solids and can flow and not support shearing as isotropic liquids. In this way, LC are liquids but with properties of crystalline solids. A stable LC phase known as mesophase is characterized by having a degree of molecular order intermediate between the orientational and positional order of crystalline solids and the disorder of isotropic liquids[1].

1.2 Classification of Liquid Crystals

LCs can be divided into two principal groups according to the parameters that influence the phase transitions. The thermotropic LCs, when the most relevant parameters are temperature and pressure and therefore mesophases are stable at defined temperatures and pressures[1,2] and the so-called lyotropic LCs when the mesophases are formed by molecules dissolved in an appropriate solvent in a suitable concentration. Lyotropic LCs usually consist of amphiphilic molecules with two distinct parts: a hydrophilic polar group and a hydrophobic nonpolar group often a hydrocarbon tail. In high enough concentration amphiphilic molecules form ordered structures, molecules arranged themselves such either the polar ends are turned out in a polar solvent or the nonpolar ends are turn out in a nonpolar solvent. For instance, in a polar solvent such as water, the hydrophobic tails arranged together and present the hydrophilic heads to the solvent (Figure 1.1)[1,3,4]. For low concentration, the amphiphilic molecules distributed randomly throughout the solvent and on interfaces.

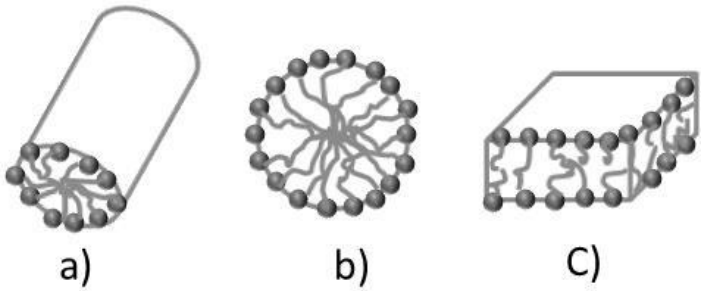

Figure 1.1 – Schematic illustration of aggregate morphologies of lyotropic liquid crystals: a) cylinder; b) sphere and c) lamellar phases (adapted from[3]).

The lyotropic LCs are present in human body cells, brain, nerves, muscles and blood and they are important in biologic functions. For example, organ membranes that are lyotropic LC must be fluid but must maintain structural order. In this way, this type of LC has the fluidity necessary to allow diffusion (proteins and enzymes) keeping the required molecular structure [5]. However, they are not used in technical applications[1]. Therefore this type of mesophase is not discussed in this work. In this way, more details of thermotropic LCs will be referred which are important for technical applications.

1.3 Phase Structures of Calamitic and Discotic Liquid Crystals

Organic compounds with shape anisotropy are able to form thermotropic mesophases. In this way, two principal types of molecules can be identified: ellipsoid or rod-like and discoid molecules. Ellipsoid or rods like molecules give rise to calamitic LCs, which include nematic and smectic LCs. Discoid molecules produce nematic-discotic and columnar LCs. A typical calamitic crystal molecule is 4´-n-pentyl-4-cyano-biphenyl (5CB) and can be regarded as a cylinder (Figure 1.2 a). A typical discotic LC molecule has a rigid core of aromatics surrounded by flexible chains and the molecular shape can be compared to a disk (Figure 1.2 b)[1,2].

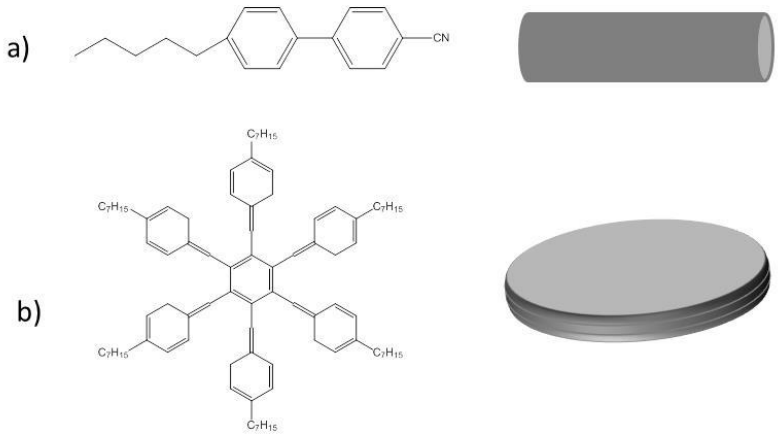

Figure 1.2 – Molecular structures and their templates: a) calamitic liquid crystal molecule and b) discotic liquid crystal molecule (adapted from[1]).

1.3.1 Phase Structures of Calamitic LCs

The transitions that could involve rod-like molecules are shown in Figure 1.3. At high temperatures, the molecules are in an isotropic liquid state where they do not have either positional or orientational order. When the temperature decreases reaching the nematic to isotropic transition temperature (T_{NI}), the material transforms into the nematic phase, which is the most common and simplest LC phase. In this phase, the molecules have orientational order but there is no long-range positional ordering of the molecules. The rod-like molecules tend to align parallel to each other (spontaneous parallel orientation of the molecules) and roughly in

the same direction. The average molecular orientation of molecules is denoted by LC director $(\vec{n})$[1,2].

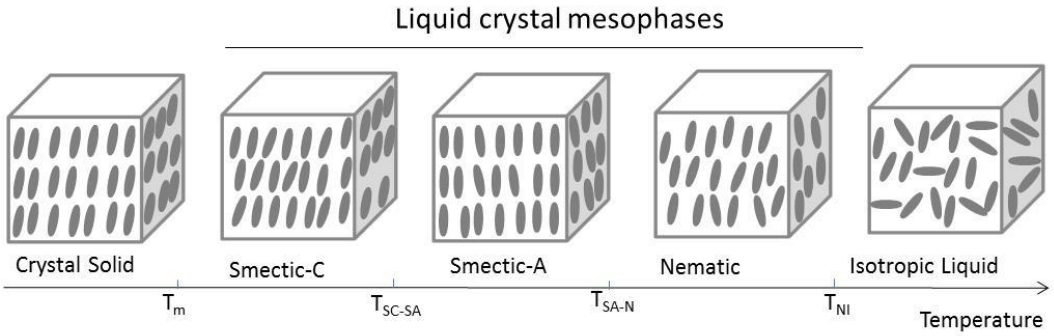

Figure 1.3 – Schematic representation of the sequence of phase transition exhibited by rod-like molecules between a crystalline solid and an isotropic liquid by increasing temperature (adapted from[1]). T_m is the melting transition temperature, T_{SC-SA} is the smectic-C to the smectic-A transition temperature, T_{SA-N} is the Smectic-A to the nematic transition temperature and T_{NI} is nematic to the isotropic transition temperature.

When the temperature continues to decrease the material could reach the smectic phase. In this phase besides the orientational order, the molecules form a layered structure (partial positional order). The lamellar smectic state is classified in subgroups according to the degree of the in-plane positional ordering of the molecules and the tilt orientational ordering of the long axes of the molecules relative to the layer planes. However, the smectic A and smectic C phases are the most common and have been utilized in display devices[2]. In the smectic A phase, the molecules are arranged in layers where the LC director is perpendicular to the layers. The layers can also be organized in semi-bilayer and bilayer structures. This is because of molecules with terminal polar groups, for example, cyano group could interact with the ends of the central cores of adjacent molecules[1,2].

When the temperature is decreased further, the material may transform into the smectic C phase, where the molecules continue arranged in diffuse layers but the LC director is tilted relative to the layer (no longer perpendicular to the layer as smectic-A phase)[1,2]. As the smectic-A phase, other sub-phases of the smectic C phase can also be found[2].

At low temperature, the translational viscosity becomes high and the molecules almost do not diffuse. In this way, the material is in the crystal solid phase where there are both positional and orientational orders. However, not all rod-like molecules exhibit all the LC phases presented in Figure 1.3 they may exhibit only some of the LC phases[1].

The calamitic nematic LC is the less ordered mesophase which results in lower viscosity. These properties allow this LC type to respond more sensitively to the external applied electric field when compared with more ordered mesophases (like smectic mesophase). The application of an electric field could not induce enough change in the optical properties of a smectic LC for

display applications. For this reason, calamitic nematic LCs are the most chosen LC for this type of applications[5–7].

LCs were discovered in 1888 by Austrian botanist Friedrich Reinitzer. At 145.5 ºC cholesteryl benzoate melted from a solid to a cloudy liquid and when temperature continues to increase until 178.5 ºC it became a clear liquid. While temperature decreased a pale blue color appeared as the clear liquid turned cloudy and then a bright blue-violet color as the cloudy liquid crystallized. Later, a German physicist Lehmann studied with a polarized optical microscope and observed that the sample can flow like liquids also exhibit optical properties such as crystals. In this way, these studies established a new thermodynamic state of matter. Lehman first called this new state flowing crystal and later on liquid crystals. The LC that Reintzer observed is a chiral LC. One example of chiral LC is known as CB15 shown in Figure 1.4[5].

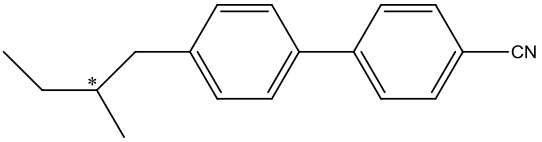

Figure 1.4 **–** Molecular structure of a chiral liquid crystal (CB15).

The structure of chiral calamitic mesophase consists of chiral molecules where they are aligned parallel to each other with the long axis in a plane (similarly to non-chiral nematic phase). However, different orientation of the molecules describes a helical distortion of the LC director along the structure as shown in Figure 1.5. The average orientation within each layer delineates a spiral molecular orientational along the structure[5]. The axis around which the director twists is called helical axis and the distance over which the director rotates by 360º is called the pitch[1].

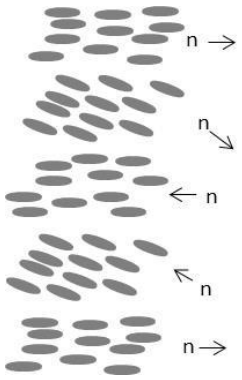

Figure 1.5 – Schematic illustration of the molecular orientation in a chiral calamitic mesophase. The director ($\vec{n}$) within each layer delineates a spiral molecular orientational along the structure (adapted from[5]).

If the pitch length is in order of the wavelength of visible light, light can be selectively reflected. The pitch length is temperature dependent. In general, at higher temperatures due to the higher thermal energy the angle at which the director changes are larger and so the pitch is straight.

However, when temperature decreases the pitch length increases changing the colors selectively reflected[7].

In this way, the color of cholesteric LCs changes with temperature which enables thermographic applications, for example, in the thermal mapping of human skin for the diagnosis of circulatory diseases or the detection of tumors. In industrial applications for direct temperature diagrams, detection of wave fields, locating faults in electronic devices and for thermally activated information display[8].

1.3.2 Phase Structure of the Discotic Liquid Crystal

Some of the LC phases of disk-like molecules are shown in Figure 1.6. At high temperatures, molecules are in the isotropic liquid state where there is no positional and orientational order. When the temperature is decreased, the material transforms into the discotic nematic phase which has orientational order but not positional order. The planes of the disc-like shape molecules are roughly parallel to one another, although the molecules have no positional order. The director is normal to the planes of the discs-like molecules[2].

When the temperature continues to decrease the material transforms into the columnar phase like stacks of disc-like molecules. In this phase, in additional to orientational order there is also a partial positional order. Finally, at low temperature, the material transforms into the crystalline solid phase where beside long-range order the positional order along the columns is achieved. The molecules are normal to the column axis[1]. The columns in columnar and in crystal solid can be hexagonally or orthorhombically closely packed together[2].

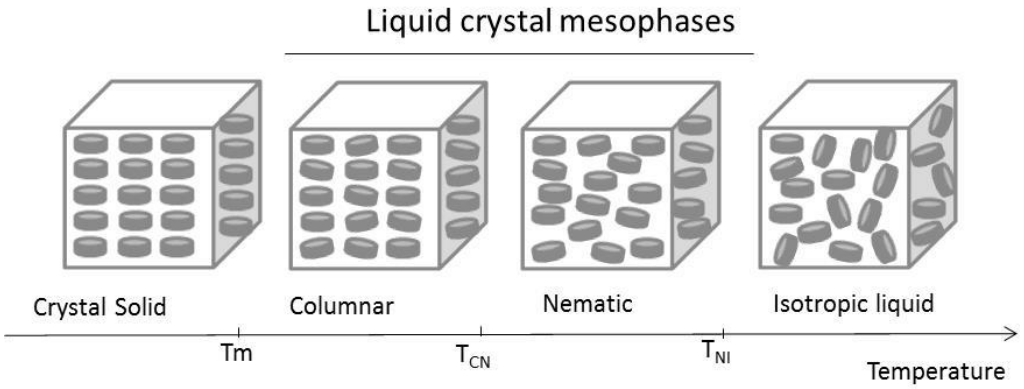

Figure 1.6 – Schematic representation of the sequence of phase transition exhibited by discotic molecules between a crystalline solid and isotropic liquid by increasing the temperature (adapted from[1]). T_m is the melting transition temperature, T_{CN} is the columnar to the nematic transition temperature and T_{NI} is the nematic to the isotropic transition temperature.

Chirality in a discotic phase can be achieved by the incorporation of a chiral unit into one or more flexible chains that surround the benzene groups (discotic core)[1,2].

1.4 Physical Properties of Calamitic Nematic Liquid Crystals

The molecular structure in calamitic nematic LC can be divided in a rigid core (within which mobile charge can respond to an applied electric field), a flexible terminal group (hydrocarbon chain) and at the other end of the core there is a terminal permanent dipole group, as shown in Figure 1.7 [2]. This structure is based on a cyanobiphenyl molecule. If the molecule is completely flexible, it will not have orientational order and if it is totally rigid moves directly from isotropic to a crystalline solid phase with decreasing the temperature[1].

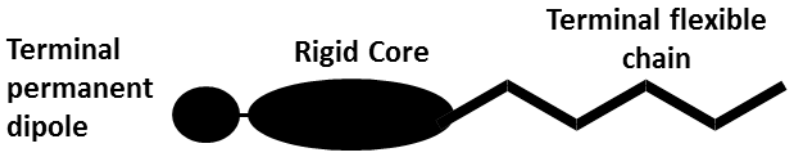

Figure 1.7 – Schematic illustration of typical calamitic nematic liquid crystal molecule (adapted from [2]).

When an electric field is applied to an LC it will induce dipole moments in molecules. The rigid core region (aromatic part) with delocalized electrons provides the mobile charge and the asymmetry. However, if the core had different chemical ring structures the charge would be less mobile giving lower polarizability. Properties such as transition temperatures, viscosity, dielectric permittivity, birefringence, and response time can be controlled by the selection of the structure of the rigid or aromatic part of a mesogen and the lengths of the aliphatic chains. The rigid core becomes polarized with the positive charge moving in the direction of the electric field and negative charge moving in the opposite direction. The electric dipole moment vector is defined as $\vec{p}$ = q$\vec{d}$, where q is the magnitude of the charge and $\vec{d}$ is the distance vector from (- q) to (+ q). Under an external electrical field, the local polarization is aligned to the field direction. The greater the distance between the separate positive and negative charges the greater the electric dipole moment. For this reason, rod shape of the polarizable core molecules originates a stronger induced dipole moment $\vec{p}_{||}$ parallel to the molecular axis and a smaller dipole moment $\vec{p}_{\perp}$ perpendicular to the molecular axis (Figure 1.8)[2]. Corresponding polarizabilities, $\alpha_{||}$ and $\alpha_{\perp}$ are the induced dipole moments per unit electric field parallel and perpendicular to the molecular axis, respectively. In the case of polar LC molecules, there is a contribution of the permanent dipole for the induced dipole moment. In this way, if the permanent dipole is parallel to the molecular axis, the dipole contribution can originate an increase in $\vec{p}_{||}$ but if it is perpendicular to the molecular axis can cause an increase in $\vec{p}_{\perp}$. LC molecules with specific induce dipole moment vector can be achieved by polar groups in appropriate positions on the LC molecule. Nevertheless, even for nonpolar LC with calamitic molecules, the $\vec{p}_{||}$ is greater than $\vec{p}_{\perp}$ [9].

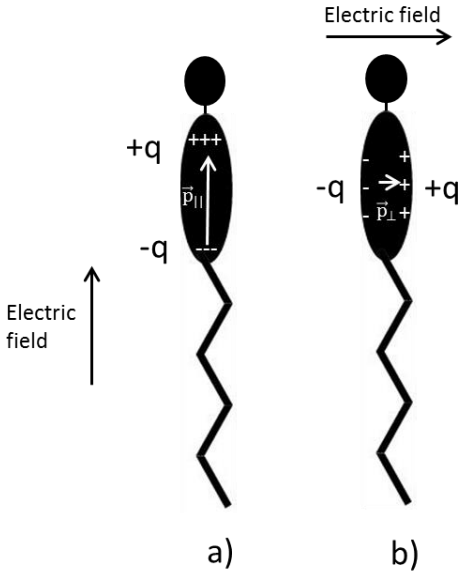

Figure 1.8 – Schematic illustration of the effect of an electric field in calamitic liquid crystal molecules applied parallel (a) or perpendicular (b) to the core the molecule and the induced dipole moment vector: $\vec{p}_{||}$ and $\vec{p}_{\perp}$, respectively (adapted from [2]).

1.4.1 Order in Calamitic Nematic Liquid Crystals

As previously mentioned, the average direction of the long axes of an ensemble of rod-like molecules in the nematic phase is parallel to each other, despite not having a positional order. Due to this orientational order, LCs possess anisotropic physical properties, that is, in different directions, they have different responses to external fields such as electric or magnetic fields. Three axes can be attached to elongated LC molecules to describe its orientation. One is the long molecular axis and the other two axes are perpendicular to the long molecular axis. The molecules are free to rotate around the long molecular axis and in some degree about their short axes. The molecules are rotationally and orientationally disordered with respect to their short axes (there is no preferred direction for the short axes) and thus the nematic LC is usually uniaxial[1].

The direction of the n-director is an average of the molecular orientations in a given region. It can be considered that the end with the dipole is equally likely, on average, to point along the n-director as it is to point the opposite direction to the n-director[2]. In other words, the dipole has equal probability to point up or down. This means that without an applied electric field the bulk of LC molecules have no net electric polarization. The nematic order parameter S, is used as a quantitative measure of the amount of order defined by

$$S = \frac{\langle 3cos^2\Theta - 1 \rangle}{2}$$

where Θ is the angle between the optical axis and long molecular axis of an LC molecule[10]. The order in a nematic LC lies between a perfect orientational order like in a crystalline solid and orientational disorder in an isotropic liquid. As shown in Figure 1.9, S=1 corresponds to perfect order, S=0 for no preferred molecular direction and in the nematic LC phase S lies between 0.3 and 0.9[2].

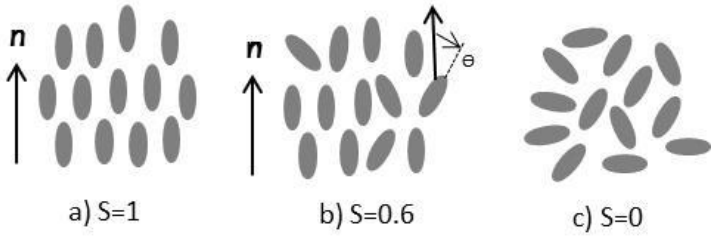

Figure 1.9 – Schematic illustration of the states of rod-shaped molecules with different orientational order in a) perfect orientational order; b) the high degree of orientational order as nematic liquid crystal and c) without order as found in isotropic liquids (adapted from [2]).

The bulk anisotropic physical properties of nematic LC materials are decided besides the chemical structure of the individual molecules by the extent of the order of the molecules in the nematic phase[2].

1.4.2 Refractive Index

A simple way to express the interaction between electromagnetic radiation and a material is through the refractive index (n) given by the ratio between the speed of light in a vacuum (c) and the speed of light in the material (v). The value of the refractive index of a nematic LC is defined by the polarization of electrons in the molecules and from the polarization of the electrons in the constituent atoms. The refractive index is a bulk property that besides depending on the polarizabilities of the individual molecules depends also on the order of the molecules**.** As previously mentioned, for rod-like molecules the induced dipole moment is higher parallel to the molecular axis than perpendicular to the molecular axis (Figure 1.8) which results in an anisotropy in the molecular polarizability with $\alpha_{\parallel}>\alpha_{\perp}$. For this reason, when the polarized visible light falls on a region with nematic LC molecules, if the electric field vector of the electromagnetic wave is parallel to the director then the light wave will experience the refractive index of the nematic LC parallel to the n-director, $n_{\parallel}$. If the electric field vector is perpendicular to the director, the light wave will experience the refractive index of the nematic LC material perpendicular to the n-director, $n_{\perp}$. In most LC materials, the largest index is along the n-director (also the optic axis) and the smallest refractive index is perpendicular to this direction.

In this way, a light ray entering in a calamitic nematic LC is in general divided into rays, which travel through the LC with different velocities, and usually in different directions. The refractive index along the optic axis is designated by an extraordinary refractive index n_e and is equal to

$n_{||}$. The refractive index perpendicular to the optic axis is called an ordinary refractive index n_o and is equal to $n_{\perp}$. The optical anisotropy of this medium is given by $\Delta n = n_e - n_o = n_{||} - n_{\perp}$, which results in birefringence.

If the molecules were perfectly ordered (crystalline solid) all molecules aligned parallel to the n-director. In this way, just $\alpha_{||}$ would contribute to $n_{||}$, and just $\alpha_{\perp}$ would contribute to $n_{\perp}$. If molecules were randomly oriented (isotropic liquid) the polarizability of the medium on average would be the same in all directions. The refractive indices would be equal $n_{||} = n_{\perp}$ and the material would be optically isotropic with $\Delta n = 0$. In general, liquids are not birefringent even when individual molecules have directionally dependent polarizabilities. The random orientation originates that the refractive index is independent of the electric field orientation. However, in nematic LC with orientational but without positional order of the molecules, there is a contribution from both $\alpha_{||}$ and $\alpha_{\perp}$ to $n_{||}$, and from both $\alpha_{||}$ and $\alpha_{\perp}$ to $n_{\perp}$. Further, in LC molecules the molecular polarizability can be very different along to the molecule axis and perpendicular to it[2].

1.4.3 Dielectric Properties

Dielectric properties are associated with the response of LC molecules to the application of an electric field. Without a magnetic response, the relative electric permittivity (ε) for a material is given by the square of its refractive index. Thus, if the refractive index is determined by the induced polarization the electric permittivity it is also determined by the induced polarization of the material when an electric field is applied. Usually, dielectric constants are proportional to the molecular polarizability. For this reason, in a nematic LC the permittivity parallel to the n-director ($\varepsilon_{||}$) is generally different from the permittivity perpendicular to the n-director ($\varepsilon_{\perp}$), thus the dielectric anisotropy giving by the expression $\Delta\varepsilon = \varepsilon_{||} - \varepsilon_{\perp}$ is different from zero.

For rod-shaped molecules when a permanent dipole is a terminal group makes the component of the permanent dipole moment along the molecule (and the n-director) larger than perpendicular to it. In this way, the material shows a large positive dielectric anisotropy[2]. When a permanent dipole is a lateral group of the molecule the contribution of polarization gives a negative dielectric anisotropy where the highest permanent dipole moment is perpendicular to the n-director[1]. The Figure 1.10 a),b) illustrates the response of nematic LC molecules with positive dielectric anisotropy (dielectric constant parallel to the n-director, $\varepsilon_{||}$ is the largest) in presence of an electric field. For this reason, the LC responds to the applied electric field by polarizing, predominantly parallel to the n-director. The separated charge rotates the n-director to reorient along the direction of the electric field. This is an example of an out-of-plane rotation. Figure 1.10 c),d) represents the situation for a nematic LC molecule with negative dielectric anisotropy (dielectric constant perpendicular to the n-director $\varepsilon_{\perp}$ is the largest). In this case, the polarization in response to the applied electric field is perpendicular to the n-director and the

separated charge exerts a torque that rotates the n-director perpendicular to the direction of the electric field. This is an example of an in-plane rotation.

The friction between the molecules limits the speed which the molecules can rotate. The frequency is usually higher when the dielectric constant perpendicular to the n-director $\varepsilon_{\perp}$ is the largest because there is less resistance to molecules rotating around their long axis than about the short molecular axis[2].

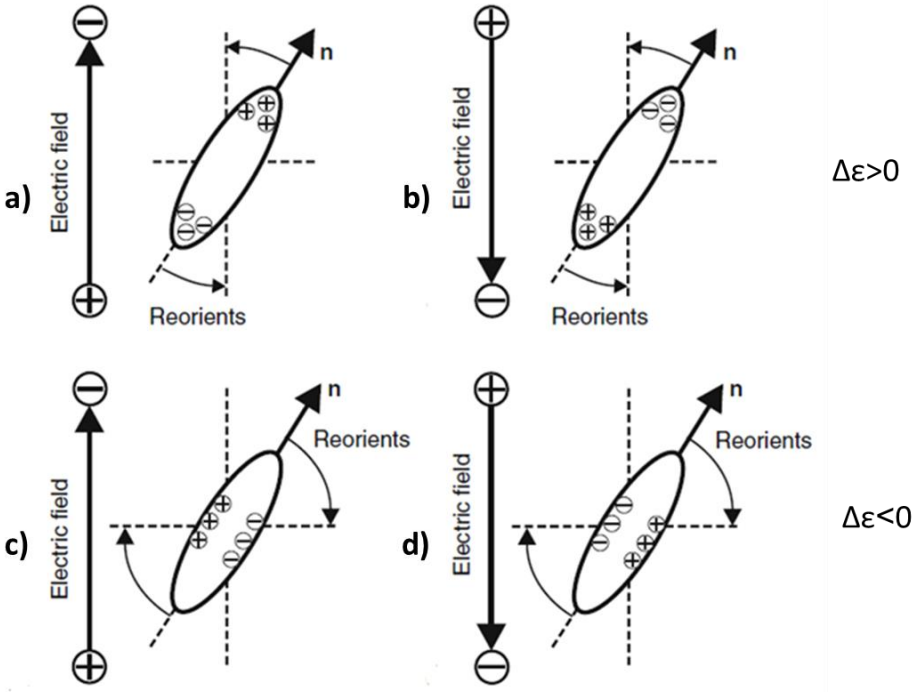

Figure 1.10 – Schematic illustration of the effect of electric field in reorientation of the n-director and in the polarization of LC molecule: a) and b) in nematic liquid crystal molecules with positive dielectric anisotropy ($\Delta\varepsilon>0$) and c) and d) in nematic liquid crystal molecules with negative dielectric anisotropy ($\Delta\varepsilon<0$) (adapted from [2]).

1.4.4 Elastic Constants

When the nematic phase is limited by a surface created by contact with another phase (solid, liquid, gas), its orientation may change due to the surface normally imposes some preferred directions, called anchoring directions**.** These directions are spontaneous orientations of the LC director on the surface (in the absence of an external torque). The minimum energy configuration in contact with a substrate surface is with the n-director lie in a certain direction. But the LC n-director could not remain in a uniform direction throughout the sample (bulk). The distortion of the n-director is opposed by elastic torques and has an associated elastic energy cost because the elastic forces tend to keep the configuration. Although LC director deformations cost energy, it is relatively easy to occur due to spatial confinements, impurities, irregularities, and externally applied fields[1,2]. Any type of deformation in a nematic LC is

described in terms of the contributions from three basic spatial distortions of the n-director. Representations of undistorted, pure, splay, twist and bend distortions are representing in Figure 1.11 a), b), c) and d), respectively[2]. In theory, the elastic energy associated with each of the splay, twist and bend distortions are quantified by the K11, K22 and K33 elastics constants, respectively[2]. The elastic parameters are restoring forces that restored the lowest energy configuration upon removal of the distorting force.

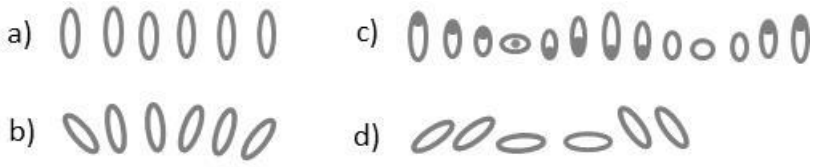

Figure 1.11 – Schematic representation of the spatial variation of n-director in a) undistorted nematic LC; b) with a splay distortion; c) with a twist distortion and d) when there is a bend distortion (adapted from[2]).

1.5 Liquid Crystalline Alignment Surfaces

As previously mentioned, the most important properties of LCs are due to the fact of the molecules are anisotropic and the orientational order is present. However, in a bulk sample of an LC, the director is not constant and samples will not be characterized by any macroscopic anisotropy. The physical properties of a nematic sample depend on the spatial distribution of the LC director. In this way, in order to observe the anisotropy of the LC, it is necessary to promote the director orientation. This is usually achieved by LC molecules in contact with a substrate that induces a preferential alignment. Several techniques to modify surfaces have been used in order to exhibit preferential alignment. These treated surfaces are called alignment surfaces. The nematic LC is easy to align compared with other LC phases. The surface alignment controls not only the alignment direction but also the pretilt angle of the LC. The pretilt angle is the tilt angle of the LC director relative to the substrate surface. The bulk properties of LCs depend strongly on the molecular structure and on the molecular interactions. The surface properties depend on the interaction of the LC molecules with the surface[11].

1.5.1 Types of Surface Alignment

The LC orientation near the substrate surface affecting the LC orientation in the bulk by molecular interactions is usually achieved by an LC sandwich between two parallel glass plates separated by a very small gap (of the order of microns) where surfaces have been treated in order for the director to assume a particular direction. In this way, when the alignment of LC molecules adjacent to a single surface refers to both surfaces of a LC cell, the director alignment is extended to the bulk[2]. The terminologies used to describe LC orientations can be divided in homogeneous, homeotropic and tilted cases (Figure 1.12 a), c) and b) respectively) when the directors of the LC molecules are aligned in one fixed direction. In this type of

alignment, the director (fixed direction) of the LC phase can be parallel, perpendicular or tilted at an intermediate angle to the interface. While in splay, twist, bend, hybrid and super-twisted nematic cases the directors are not fixed in one direction, as illustrated in Figure 1.12d), e), f), g) and h) respectively. The type of preferential alignment plays an important role in determining the electro-optical properties of LC devices[2,12].

Depending on the required electro-optical effect it is necessary an appropriate surface treatment method. However, in order to maximize the contrast ratio of the display, the orientation of the LC director in any local region of the fluid should be the same throughout the fluid whether the applied voltage is ON or OFF. Two examples of maximum order are homeotropic and homogeneous alignments[6].

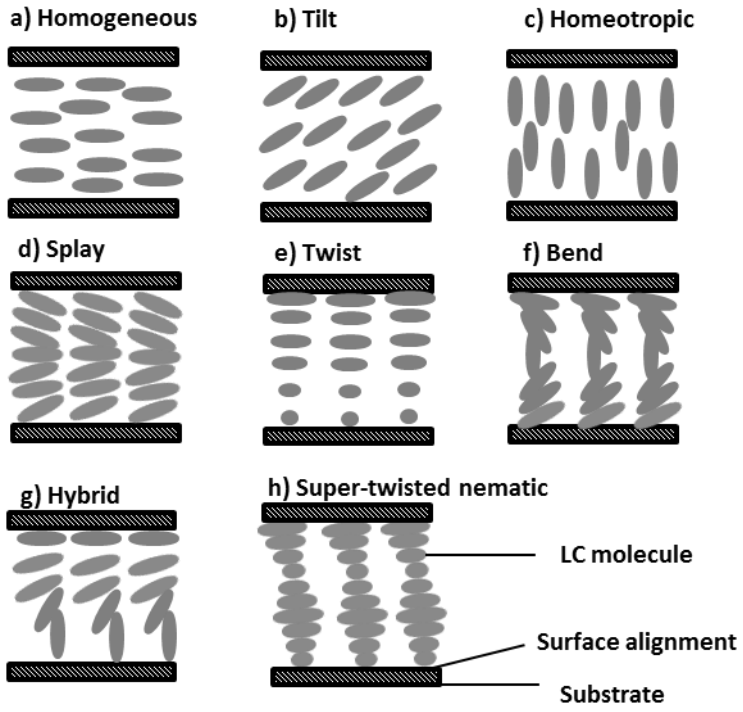

Figure 1.12 – Schematic illustration of a typical orientations of nematic liquid crystals when sandwich in two parallel substrates with different surface alignment: a) homogeneous; b) tilt; c) homeotropic; d) splay; e) twist nematic; f) bend; g) hybrid and h) super-twisted nematic alignment (adapted from[12]).

In homogeneous alignment when both surfaces are homogeneously aligned but in opposite direction, the alignment directions are antiparallel and in the same direction are parallel. These types of cells are also described as Fréedericksz and π-cells, respectively as shown in Figure 1.13 [2].

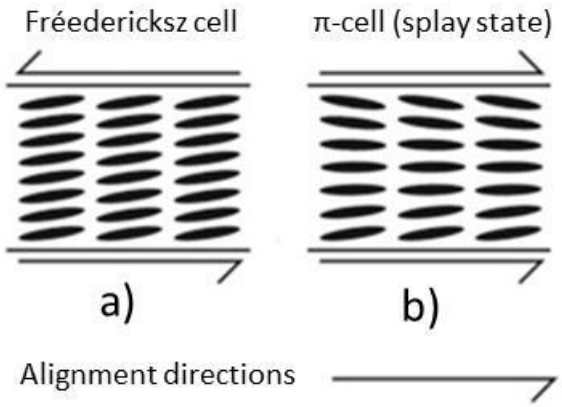

Figure 1.13 – Schematic illustration of LC cell with homogeneous alignment but with a different direction of alignment: a) antiparallel directions result in Fréedericksz cell and b) in the same directions of alignment result in π-cells (adapted from[2]).

1.5.2 Methods and Materials to Create Homeotropic and Homogeneous Alignments

Orienting surfaces can be created by various methods and materials to control the organization of LC molecules. A simple method to obtain a homeotropic alignment is by deposition of surfactants, such as monomolecular layers of lecithin (Figure 1.14 a)) in a substrate. The hydrophilic polar head is chemically attached to the glass and the hydrophobic tails are arranged perpendicular to the surface. The intermolecular interaction between the LC molecules and the surfactant promotes the homeotropic alignment (Figure 1.14 b)). The dipolar interactions between polar groups at one end of the LC molecules or surface agents and the silanol groups on the glass surface and the van der Waals interactions between nonpolar alkyl-(butyl)-groups of the LC and the aligned nonpolar alkyl-groups of surface agents (lecithin) give rise to homeotropic alignment[8]. An alternative to the use of lecithin is the deposition of a hydrophobic polymer layer which also promotes homeotropic alignment[1,2]. In this way, some type of polyimide films have been developed and used in this type of alignment and silicone compounds such as alkoxysilanes or chlorosilanes react with the substrate surface and polymerize to form polysiloxane structures near the surface[12].

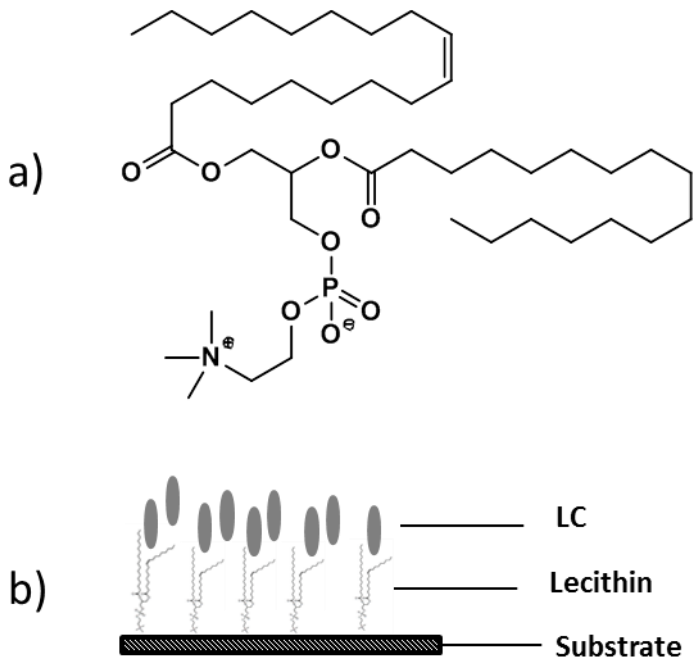

Figure 1.14– Schematic illustration of homeotropic alignment using lecithin: a) chemical structure of lecithin and b) homeotropic alignment using lecithin (adapted from [2]).

The most described method used to create a homogeneous alignment is the mechanical polymer unidirectional rubber technique. The first step is to coat a substrate with an alignment material (usually a specific polymer) and then rubbing the surface in a uniform direction (about 100 times) with soft tissue (cotton cloth) (Figure 1.15 c)). The polymer rubber technique depends not only on the rubbing strength but also on the structure of the rubbing fiber and the alignment material[2,12].

The first polymers (alignment material) used were polyvinyl alcohol (PVA), acrylic polymers and vinyl polymers. The most common is PVA (Figure 1.15 a)) or polyimide (Figure 1.15 b)). Two types of polyimide are used: solvent soluble pre-imidized polyimide and polyamic acid type. The polyimide has been widely used due to the higher stability (thermal and chemical) and electric characteristics[12]. The way that a rubbed polymer can homogeneously align an LC is not yet very clear but it is considered that it is a mechanical effect[2]. The reorientation of polymer chains (alignment material) along the rubbing direction creating a series of nano grooves that exercise certain elastic energy. When LC molecules are in contact with this surface, it costs less elastic energy for the molecules to align parallel to the nano grooves than perpendicular to them as depicted in Figure 1.15 d) [2,12]. The simple rubbing of the substrate (without alignment material) created a weak anchoring strength (10^{-5} J m^{-2}) and for this reason, the widely used homogeneous alignment layers are rubbed the coated surface with polyimides in order to increase the anchoring energy (10^{-3} J m^{-2})[1].

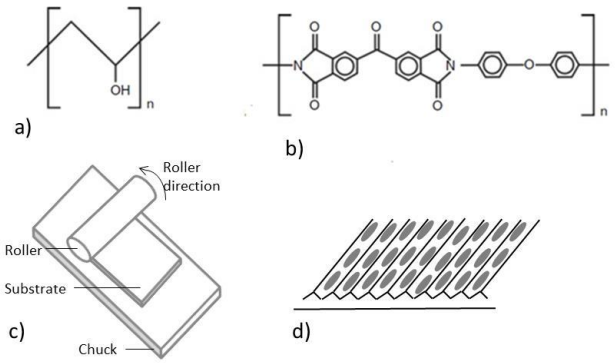

Figure 1.15– Chemical structure of rubbing polymers a) Polyvinyl alcohol (PVA), b) polyimide (PI2555), c) schematic illustration of rubbing technique and d) LC molecules align along the direction of the grooves (adapted from [1,2]).

The chemical changes in rubbed surface have been also studied by the measurement of the polarity of a rubbed surface using water contact angle measurements. Rubbing polyimides films with a cotton cloth decreases the water contact angle for polyimides containing polar groups or linear alkyl side chains. The microscopic reorientation exposes the polar groups to the surface or moves the nonpolar side chains into the bulk. In the strong rubbing, the surface chemistry and roughness have dominant effects on the pretilt angle and the anchoring energy. The increase in surface polarity and a larger reoriented surface area enhance the attractive interaction between the LC and the rubbed surface and anchoring energy will increases.

Depending on the alignment materials, the pretilt angle can decrease or increases with an increase in rubbing strength. The increase of the rubbing strength, increase the surface polarity (side chains are merging into the bulk) that promote the interaction between the LC molecules and the alignment material. The rubbing strength could also change the surface wave structure that decreases in average the tilt angle. The pretilt angle of LCs on a surface can be increased by the use of long side chains (nonpolar regions) and the use of fluorinated moieties in the polymer main chain of alignment material. The fluorinated moiety increases the roughness of the surface that causes the increase of the pretilt angle of the LC. In a homogeneous alignment, the pretilt angle is generally between 0^0 and 10^0 [12].

However, although rubbed polymer is the dominant alignment process, it can insert small particles, static charges onto the substrates and pretilt angle fluctuation, reducing the efficiency of the process[2,12]. In this way, several LC alignment methods have been developed such as oblique evaporation of silicon oxide and photo-alignment[2].

In summary, the strength of the physicochemical forces (van der Waals, hydrogen and dipolar bonding) and geometric factor at the liquid crystal-solid interface are the most important factors that determine parallel or perpendicular orientation[6].

1.6 The Liquid Crystal in Device Applications

The liquid crystal devices (LCDs) are one of the most important optical displays because of the large area of the flat panel, light weight, high definition, high viewing quality, low driving voltages and low power consumption[13]. LCDs could be seen as an array of light valves where plane polarized light intensity that traverses an LC cell can be modulated by applying an electric field due to dielectric anisotropic of LC[1,2]. LCDs are widely used for watches, calculators, cellular phones, display monitors of computers, TV screens and so on. LCDs have the advantages of a flat panel, light weight, energy saving and low drive voltage[1]. Although the LC state was discovered in 1888, the most widely used LCD mode called twisted nematic (TN) was invented by Schadt and Helfrich in 1970. In addition to twisted nematic, some important display modes for device applications are super-twisted nematic (STN), in-plane switching (IPS), and polymer dispersed LC (PDLC). The most common LC display employ the twist nematic technology[12].

It is possible to designated various LC cell structure. The LC cell construction depended on the configuration of the display and the switching mode (dielectric anisotropy). For the proper operation of LC display devices, appropriate cell construction is necessary[2].

1.6.1 Liquid Crystals used in Displays

The main requirements of physical properties of LCs for a good response to the externally applied electric field include.

- The higher value of dielectric anisotropy that can be positive or negative, depending on the LC molecular structure.
- Optical anisotropy must be large for a visible electro-optical effect.
- The switching time is proportional to the rotational viscosity of the LC and proportional to the square of the cell gap in the display. For this reason, low viscosity and small cell gap give rise to a small switching time.

However, the challenge is to achieve LCs with a high T_{NI} for allowing broad operating temperature, low viscosity for fast switching and also with the high value of dielectric anisotropy. Moreover, LC must be chemically, photochemically and electrochemically stable[2]. One way to achieve these characteristics in an LC is by a mixture of compounds. In this way, it could be possible to obtain LCs with lower viscosity keeping or even improving the other features. In 1974, Raynes made a eutectic mixture known as E7 (Table 1.1). In this table, it is evident that nematic mixture E7 that contains four cyanoparaphenylene derivatives, that not only give rise to a high value of Δn (0.2195) but also $\Delta\varepsilon$ (14.5). Its T_{NI} occurs at 58 ºC, exhibiting liquid crystalline properties until the glass transition at - 62 ºC[9,14]. The range of temperature in which LC properties are displayed is fundamental in applications. For nematic LC this range should be about - 40 to 100 ºC for automotive applications, - 20 to 70 ºC for mobile applications and 0 to

50 ºC for indoor applications like PC monitors or TV screens. The T_{NI} of LC should be at least 10 ºC higher than the operating temperature of the device[2].

Table 1.1– Physical properties of isolated compounds in an LC mixture known as E7[9,14].

Structure	Designation	IUPAC Name	n_e	n_o	$\varepsilon_{\parallel}$	$\varepsilon_{\perp}$	Phase Transitions (ºC)
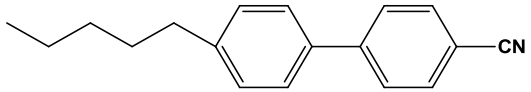	5CB	4-cyano-4´-pentyl-1,1´-biphenyl	1.7304	1.5335	17.9	6.9	Cr – N 23 N – I 35
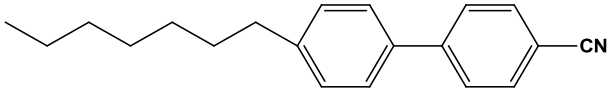	7CB	4-n-heptyl-4´cyanobiphenyl	1.7115	1.5203	15.7	6.0	Cr – N 28 N – I 42
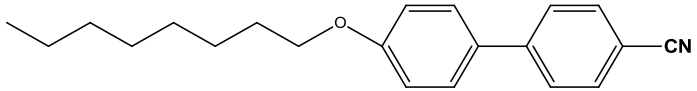	8OCB	4,4´-n-octyloxycyanobiphenyl	1.6983	1.5028	14.7	6.2	Cr – SA 54 SA – N 67 N – I 80
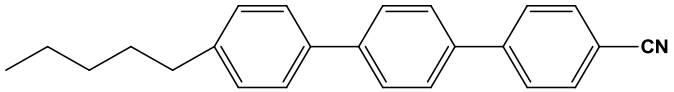	5CT	4´n-pentyl-4-cyanotriphenyl	1.891	1.542	26.4	4.3	Cr – N 130 N – I 229
Eutectic mixture							
Structure	**Designation**	**Composition (wt.-%)**	**n_e**	**n_o**	**$\varepsilon_{\parallel}$**	**$\varepsilon_{\perp}$**	**Nematic range Temperature (ºC)**
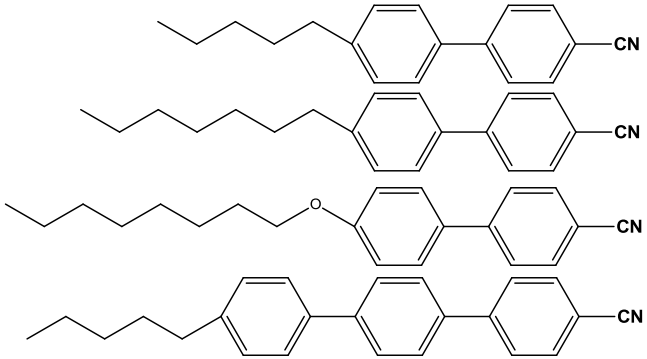	E7	51, (5CB) 25, (7CB) 16, (8OCB) 8, (5CT)	1.7378	1.5183	19.6	5.1	Cr – N -62 N – I 58

1.6.2 The Fréedericksz Transition

As previously mentioned, the type of response (distortion of the n-director) with the applied voltage depends on the dielectric anisotropy of the LC. If the LC has a positive dielectric anisotropy, $\Delta\varepsilon>0$ (dielectric constant parallel to the n-director, $\varepsilon_{\parallel}$, is the largest), an electric field applied makes LC molecules rotate out-of-plane parallel with the electric field. Nevertheless, as previously mentioned, the elastic energy tends to keep the initial LC configuration. This elastic energy is overcome when the voltage is further increased above a critical voltage called Fréedericksz threshold voltage (Vth), the dielectric torque exceeds the elastic torque and the n-directors mostly align with the electrical field, as shown in Figure 1.16 c). If the voltage is below the Fréedericksz threshold voltage, the LC molecules remain in an undistorted configuration as shown in Figure 1.16 a). When a voltage is applied above the threshold voltage, the nematic n-director begins to distort within the layer, as shown in Figure 1.16 b). Common threshold values for nematic LC materials are of the order of 1V.

In general, substrates are coated with an LC alignment layer with very strong anchoring and even when the voltage is greater than the threshold voltage the n-director at the boundaries has a fixed orientation and LC molecules cannot rotate. In the bulk, all LC molecules are surrounding by others and interaction energy is weaker than on the interface where the same of surrounding molecules are also LC molecules and others are alignment layer molecules. This means that in boundaries molecules cannot easily change their direction like in bulk. The relaxation back to the undistorted state is a viscoelastic process that is not dependent on the voltage. Although the viscosity limits the speed of reorientation, the elasticity allows the return to the equilibrium state[2].

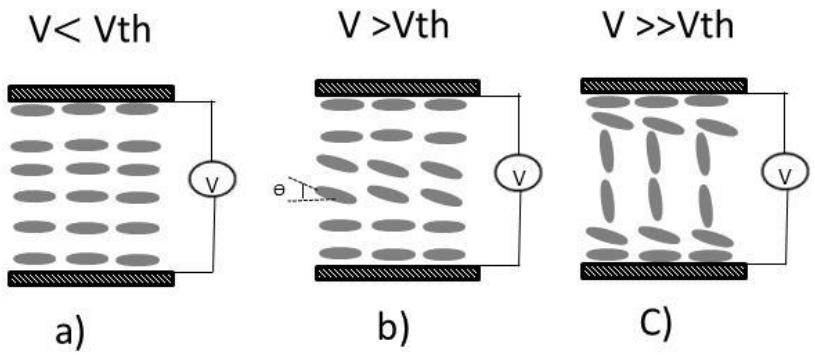

Figure 1.16– Schematic illustration of Fréedericksz transition of a liquid crystal with positive dielectric anisotropy sandwiched between two parallel substrates treated in homogeneous alignment when: a) V<Vth; b) V> Vth and c) V>> Vth (adapted from[2]).

1.6.3 Twisted Nematic (TN) and Super-Twisted Nematic (STN)

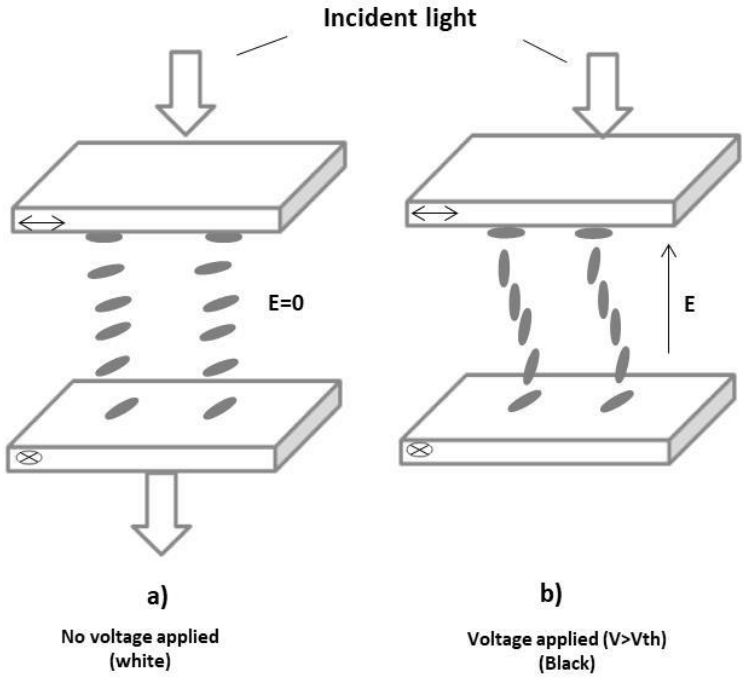

Figure 1.17– Schematic illustration of the operation of a twisted nematic (TN) cell when a) no voltage applied (white) and b) with a voltage applied above the Vth (black) (adapted from[12]).

The schematic representation of the operation of TN-LCD is illustrated in Figure 1.17. The electrodes of the LCD cell must be transparent in the visible spectral keeping an excellent electrical conductivity. In this way, usually, LC cell consists of two layers of glass coated on one side with a transparent conducting deposit, such as indium tin oxide (ITO). ITO or Sn-doped In_2O_3 ($Sn:In_2O_3$) belongs to the family of transparent electronic conductors. ITO has excellent electrical conductivity and optical transparency and is therefore used as transparent electrodes[2]. Each ITO glass substrate is coated with a homogeneous alignment layer (for example, rubbed polyimide film). The rubbing directions of the alignment layers of the two glass substrates are perpendicular to each other and therefore LC molecules perform a 90^0 twist through the thickness of the LC cell. Each polarizer is placed on the outside of the substrates in order that a transmission axis of each polarizer is parallel to the rubbing direction of each alignment layer which results in cross polarizers.

At no voltage applied (OFF state) (Figure 1.17 a)) the light incident on display is polarized by the first polarized and when passes through the LC layer its polarization direction rotates 90^0. In this way, light can pass through the second polarizer. With the application of an electric field (ON state) (Figure 1.17 b)) the LC molecules ($\Delta\varepsilon>0$) tend to reorient parallel to the electric field (except near to the alignment layers) distorting the uniform twisted structure. The light passing

through the first polarizer and through the LC layer (parallel align to the electric field) experiences no rotation of the polarization direction. In this way, incident light reaches the second polarizer in a direction perpendicular to this polarizer and light will be blocked. When the electric field is switched OFF the LC molecules restore the uniformly twisted state and the light is again transmitted [2,12]. This operating LC cell is known as the normally white mode. This mode is used in portable low-power applications such as watches and calculators which use ambient light. While black mode results in an OFF state black are used in applications such as mobile phones and applications[2]. The TN is improved by a super twisted nematic (STN) where the torque imposed to the LC molecules can reach 270^0, unlike the 90^0 in TN, which increases speed the transition between the OFF and ON state[12].

1.6.4 In-Plane Switching (IPS)

The in-plane switching devices have a better horizontal viewing angle performance than twisted nematic (TN). For this reason, it is widely used for large area display applications.

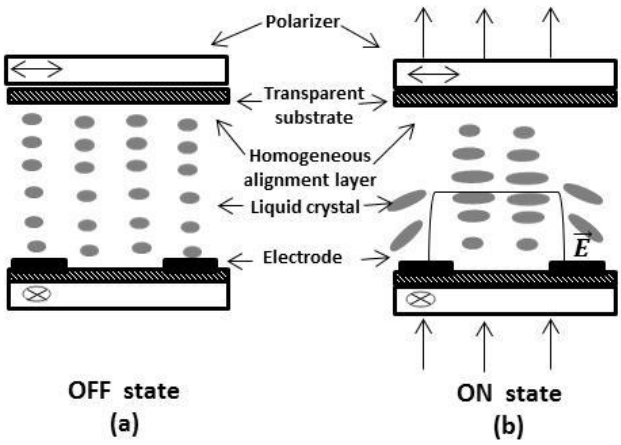

Figure 1.18– Schematic representation of the basic principle of the IPS switching mode in the OFF and ON state (adapted from [15]).

The rubbing directions of the homogeneous alignment layers are parallel to each other in order to be parallel with the axis of the polarizers. In this way when light passes through the LC layer (OFF state) it will be blocked that results in a black display screen (Figure 1.18 a))[15].

To achieve an in-plane electric field inside the LC cell, electrodes should be placed side by side on the same glass substrate inside in the upper and lower substrates. In this way, when an electric field is applied between the two electrodes (on the lower substrate) the LC with positive dielectric anisotropy align parallel to the in-plane electric field (LC directors rotate in the plane) allowing light to pass through the second polarizer result in a white display screen (Figure 1.18 b))[2,15].

1.6.5 Addressing Principles of Passive and Active Matrix in LCDs

The LC devices previously mentioned are the principle of operation of common LC displays where each picture element (pixel) has the same operating device that the LC cell. Each element has its own electrodes that are separated from the electrodes of other elements. The image displayed on the screen is made by adjusting the polarization direction of light passing through pixel by pixel in response to an electrical voltage[1,2].

In an LCD matrix display, independent wiring for each pixel is impractical and the pixels are addressed via rows and columns of electrodes. In this way, the electric wiring is reduced from millions to thousands. The matrix displays are done by integrated circuits that are connected to the display glass and the data source. The electrical addressing of LCD can be divided into the passive matrix and active matrix[9].

In a simple way, the passive matrix is made by two glass substrates sandwiching the LC, where one of the substrate is coated by columns and the other by rows of transparent conductive material. The rows and columns are connected to integrated circuits that control when a charge is sent to a specific column or row. The row and column intersect is a display element referred to as pixel (Figure 1.19).

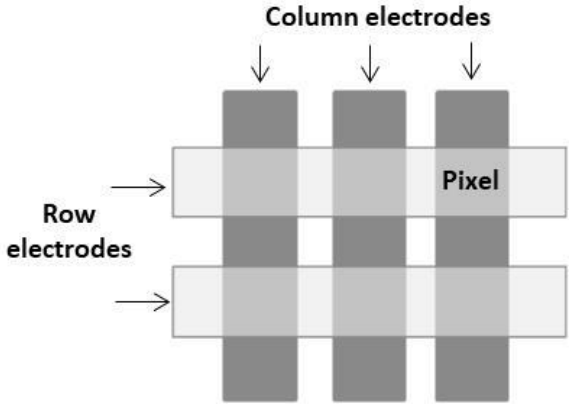

Figure 1.19 – Schematic representation of a passive address matrix in. The row drivers (left) and column drivers (above) are used to addressing every pixel in the matrix (adapted from [16]).

For display consisting of N rows and M columns, there are NxM pixies, but only N+M electrodes. To turn on a pixel, a potential difference is applied between the corresponding row and column electrodes by the integrated circuit. Figure 1.19, provides the principles of a passive matrix. However, with this simply matrix it is easy that a voltage which is applied to a row affects all pixels on this row and the same for columns (cross talk). That results in slow response time and imprecise voltage control. Because of poor image quality and resolution, this matrix is applied in cheap devices and relative small-size display devices which do not need high quality.

In order to achieve better performance, the active matrix was developed which increase in complexity. The most important technology is a transistor employed at each pixel (occupy a small fraction of the pixel area) to isolate each pixel from its neighboring pixels on the same row and column (Figure 1.20). These transistors are fabricated on a thin film of silicon deposited on a glass panel and are known as thin film transistors (TFTs). The transistor functions as an electrical gate. In this way, when a voltage is applied to a pixel and a charge is built upon the capacitor containing the LC, the gate is closed. This makes possible electrical isolation during the addressing of neighboring pixels. Only the capacitor at the designated pixel receives a charge and all the other pixels are not affected. This results in complete independent addressing of each pixel. With the TFT it is possible to maintain an applied voltage at any pixel, independent of the voltages of the neighboring pixels. The capacitor is able to hold the charge until the next refresh cycle. The control of the amount of voltage supplied to each pixel allows better control of the amount of light creating a gray scale[9].

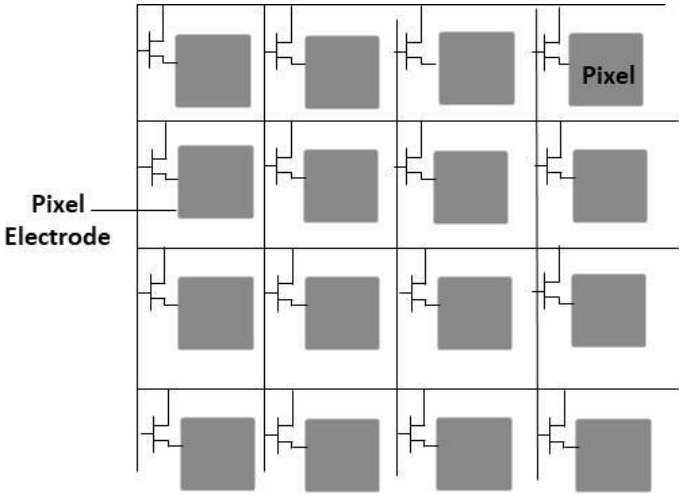

Figure 1.20– Schematic representation of active address matrix display (adapted from [16])

In colorful displays, the image it is also made by pixels and the operation is similar to previously described. However, to display color information, each pixel is divided into three parts or sub-pixel through color filters of red, green and blue which designate the name used in the RGB color screens by pigment filters, dye filters and metal oxide filters. The array of color filters is coated on the inner surface of the glass plate facing the viewer[9]. The electrodes control light intensity in each sub-pixel allowing varies the mixing and intensity of the three basic colors giving all other colors to yield thousands or millions of possible colors combinations for each pixel[1,2,9].

1.7 Polymer Dispersed Liquid Crystal (PDLC)

Liquid crystal polymer composites are constituted by low molecular weight LCs and high molecular weight polymers but in a phase separated state. These composites can be divided in

polymer dispersed liquid crystals (PDLCs) and polymer stabilized liquid crystal (PSLCs). In PDLC the concentration of polymer and LC are similar and in a PSLC the concentration of LC is much higher than polymer[1,5]. Whereas in PDLC the polymers are involved in optical and mechanical effects, in PSLC the polymer role is only to stabilizing the LC alignment or for increase the mechanical stability of the device[2]. However, in most publications, liquid crystal polymer composites are always referred to as PDLC regardless of the LC concentration[1,5].

As previously mentioned, in LCDs such as twisted and super-twisted nematic displays their contrast is achieved through absorption at polarizers but in PDLC films it is achieved through scattering. Although the LC in a PDLC can be chiral, cholesteric, smectic or nematic the most common PDLC is a polymer dispersed nematic liquid crystal[1]. PDLCs films consist of LC domains dispersed in a solid polymer matrix and their optical response is based on the electrically controlled light scattering properties of the LC domains. In absence of an electric field, the refractive index mismatch between the LC and the polymer matrix, as well as that between different LC domains, is crucial to obtain a scattering state. During the application of an external electric field, LC molecular arrangement change and if the ordinary refractive index of the LC and the one of the polymer match, the PDLC becomes transparent[17].

PDLC devices are constituted by two layers of transparent substrates that can be glass, plastic, quartz or some other type of transparent substrate material. Each of the transparent layers is coated on one side with a transparent conducting deposit. The two transparent conductive layers sandwich a layer of LC domains dispersed in a transparent polymer. PDLCs are configured to apply an electric field to the upper and lower electrodes[2]. To assure a scattering state LC domains must be comparable (± 1 μm) to or larger than an optical visible light wavelength, usually 2-5 μm [1]. The spacing between top and bottom glass plates varies from 5 to 50 μm, the most common is 10 to 20 μm. The spacer composition should be an inert material such as glass frits and even Teflon and Mylar can also be used as spacer materials[6]. Although no alignment layers neither polarizers are necessary for the operation of PDLC, they have high addressing voltages compared for example with twisted nematic displays.

PDLCs can be prepared by several methods that can be grouped in emulsion and phase separation techniques. In emulsion technique, the nematic LC, water and polymer (water soluble) are mixed together. The emulsion is placed on a conductive transparent substrate and after water evaporation, a second substrate is laminated to form the PDLC. Droplet size and shape are determined by speed and duration of stirring and by solvent evaporation rate[1,2].

In phase separation techniques the LC is mixed with the pre-polymer or with the polymer dissolved in a solvent. The phase separation process occurred by solvent induced phase separation (SIPS), by thermally induced phase separation (TIPS) or by phase separation by polymerization (PIPS).

- Solvent-induced phase separation (SIPS): The LC and polymer are dissolved in a solvent forming a homogeneous solution. When solvent evaporates, it results in phase separation with polymer precipitation[1]. The further process consists of warm the film to dissolve again the LC in the polymer and cooled at a rate chosen to achieve the desired droplet shape. This further process (thermal annealing) adds flexibility to PDLC films[2,17]. After solvent evaporation, another substrate is needed to sandwich the PDLC film.
- Thermally induced phase separation (TIPS): A mixture of polymer and LC forms a homogeneous solution at elevated temperature. The polymer should be thermoplastics in order to melt below their decomposition temperature. The mixture in an isotropic phase is cooled causing the phase separation between LC and polymer. The domain size is control by the rate of cooling and viscosity[1,17].
- Phase separation by polymerization (PIPS): This technique is preferably used when the monomer is miscible with low molecular weight LC. The solubility of the LC decreases with the stiffening of the polymer during photochemical polymerization (P-PIPS) or thermal polymerization (T-PIPS) until the LC phase separates, forming domains of LC dispersed in a polymer matrix. The LC domains grow until the stiffer of the polymer. Domains size is controlled by the types of LC and polymers, concentrations of both and physical parameters such as viscosity. The rate of polymerization is controlled by cure temperature and light intensity for thermally and photochemical polymerization, respectively[17]. Unlike the above techniques, the PIPS technique the assembled LC cell can be directly filled with a homogeneous solution by capillarity. Polymerization reactions can occur directly within the cell because there is no solvent evaporation. With this technique, it is easier to achieve a uniform thickness of the PDLC film.

The optical characteristics of PDLC films are dependent on the LC properties and are also related to the polymer structure and rate of polymerization mechanism. For this reason, controlling the polymerization mechanism is important to achieve the desired properties in PDLC films[17]. Due to the importance of controlling PDLC properties, the most convenient method used for the preparation of PDLC film is the PIPS method.

1.7.1 Morphology of Polymeric Matrix

After phase separation especially in the PIPS method, the PDLC film results in a solid polymeric film called matrix containing a large number of small cavities filled with an LC called domains of LC[2]. The polymer matrix can acquire two different morphologies called swiss cheese or polymer ball (Figure 1.21). In swiss cheese morphology, the polymer forms a continuous medium with the LC dispersed as isolated droplets from one another. The polymer ball morphology is characterized by a continuous LC phase embedded in a polymer matrix. This morphology of

polymer network can be comparable to polymer fibrils where LC was continuous dispersed[18]. The polymeric morphology type and characteristics, in addition, to depending on the molecular structure and molecular weight of monomers used to be incorporated as a polymeric matrix, can be also affected by polymerization conditions [19–26].

The electro-optical properties of PDLC beside dependent on the type of LC and polymer also dependent on the morphology of the polymer matrices[1]. Therefore, with an understanding of the relationships between morphology and electro-optical properties, it is possible to control PDLC properties.

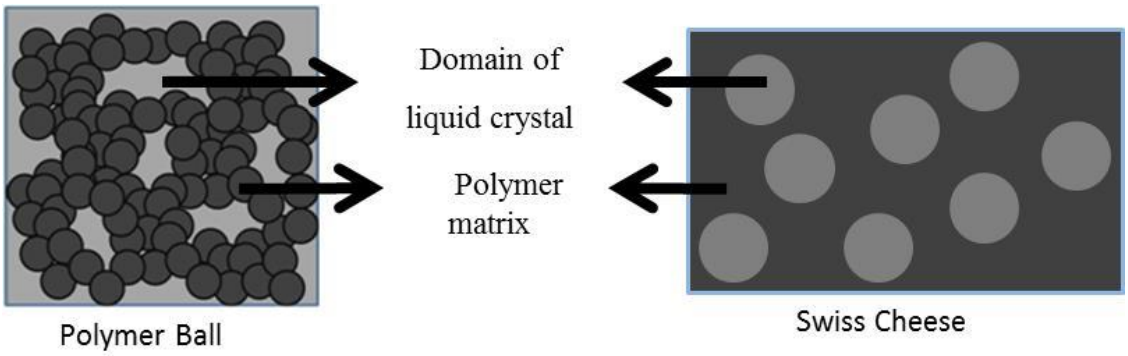

Figure 1.21– Simple schematic illustration of the microstructure of the polymer matrix with a polymer ball morphology type (left) and swiss cheese morphology type (right).

1.7.2 Important Features of The Polymer to Be Used in PDLCs

The most important features of polymers to be used in the production of PDLC by PIPs method devices are its film-formation ability, chemical inertness in relation to an LC, good miscibility of polymer precursor with LC in a liquid state and immiscibility in a solid polymer. The polymers should be highly transparent and do not scatter light. A polymer should have also good mechanical properties, low brittleness, elasticity and resistance to mechanical strokes, especially in flexible PDLC[17]. The polymer through its chemical structure and properties enables LC domain formation, providing their mechanical support also determining shape, size, distribution and LC domain alignment which in turn influences the PDLC properties.

In a PDLCs film, unlike in other types of liquid crystal devices, the liquid crystal molecules are trapped as liquid crystal domains within a polymeric matrix. For this reason, the properties of PDLC depend much more strongly on the polymer phase than on many of the liquid crystal physical properties. In this way, the polymer matrix not only provides thermal and mechanical stability to PDLC films but the suitability of PDLC applications depends on the nature of the matrix [18]. In this way, a depth study of the polymer matrix is crucial for optimized PDLCs applications.

1.7.3 Polymer Structure and Properties

Polymers are a class of macromolecules consisting of repeated chemical units. Each repeating unit is called a mer or basic unit with “poly-mer” meaning many repeating units. The monomers are chemical compounds that are capable of reacting to form a polymer. When there is only one type of repeating unit the corresponding polymer is a homopolymer and if there is more than one type it is a copolymer[27]. Oligomers are also a type of polymer but formed by a few numbers of repeating units and therefore with a molecular mass comparatively lower than polymer formed by a large number of repeating units. The oligomers can be named according to the number of repeating units present in their structure. In this way, when two repeating units are linked, it forms an oligomer called a dimer, three repeating units forms a trimer and four repeating units form a tetramer and so on [27].

Polymers can be classified in several different ways due to their complexity. A possible classification can be according to:

- Structure: linear, branched and network (Figure 1.22)
- Molecular forces: thermoplastic, elastomers and thermosetting
- Types of polymerization reactions: addition or chain-growth polymerization and condensation or step-polymerization.

According to structure, they can be linear, branched or crosslinked polymers. Branched-chain polymers restricted the polymers to pack together as closely as linear molecules can and the forces holding these polymers together tend to be much weaker. The crosslinked polymers result when branches of different chains become interconnected[28].

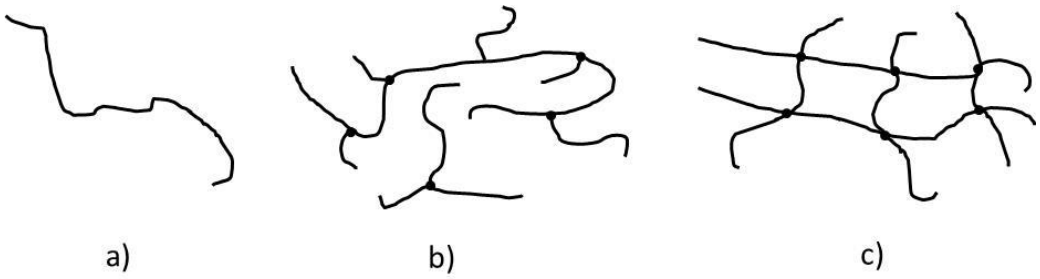

Figure 1.22- Schematic representations of different polymer structures: a) linear, b) branched and c) crosslinked (adapted from [27]).

The classification by molecular forces in thermoplastic, elastomers and thermosetting is linked to polymer structures. The molecular forces determine if polymers chains tend to form crystalline or an amorphous arrangements[29].

Linear or branched polymers formed thermoplastic polymers. This type of polymer softens or melts when heated and can be molded and remolded by heating. On cooling, they form a glass

below the glass transition temperature (T_g) or they may crystallize even partially. An elastomer is a lightly crosslinked polymer which deforms and then returns to its original shape. When unstretched they have randomly coiled molecules[27]. The elastic behavior is due to flexible chains with weak forces between them. Some segments of the chain molecule may have freedom of movement while the molecule itself is not free to move[30]. On cooling, elastomer becomes glassy below T_g because the structure is sufficiently irregular to crystallize[29]. During the heating, the polymer cannot melt because polymer chains cannot flow due to the cross-links. The other very important feature is that T_g for these polymers is below room temperature, so elastomer polymer can resemble a rubbery state at room temperature[27]**.** The higher extensibility and elasticity of rubber are a result of the great flexibility that this confers on the molecular chains. There are many single bonds in the backbone, leading to the easy formation of non-linear structures.

Normally, thermosetting is network polymers in which a crosslinking reaction occurs promoting chemical bonding between macromolecular chains and creating a three-dimensional network [29]. For this reason, they are normally rigid (their shape is permanent) and cannot melt on heating decomposing if the temperature is too higher [27].

Polymers can also be classified according to polymerization reactions which in turn can be classified in addition or chain-growth polymerization and condensation or step-growth polymerization. The addition polymerization reactions may occur by way of radical, cationic or anionic intermediates[31]. From these three reactions, free radical reactions have been the most applied method in forming PDLC films[18]. The most important functional groups in polymerizable monomers that can participate in free radical polymerizations are the carbon-carbon double bond in alkenes and the carbon-oxygen double bond in aldehydes and ketones. The common polymerizable monomers used to produce PDLC by PIPS method are those with carbon-carbon double bond derived from acrylate, methacrylate or vinyl families[18].

The free radical polymerization has at least three different reaction steps as initiation, chain propagation and chain-terminating steps, as shown in Figure 1.23.

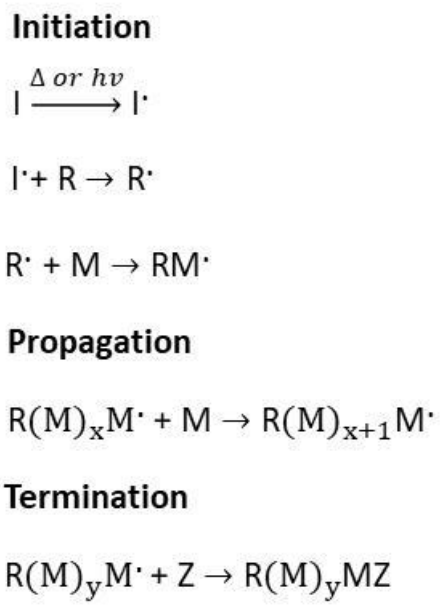

Figure 1.23– Generalized simply mechanism for free radical polymerization (adapted from [18,32]).

Free radicals must be introduced into the system to start the reaction. In this way, in the initiation step, the thermal or photoactivation of the initiator (I) produces fragments with unpaired electrons, the so-called free radicals initiators a free radical ($R^{\cdot}$). As this species is produced it reacts with the reactive group of monomer (M) producing new activated species ($M^{\cdot}$) which completes the initiation process. During the propagation stage subsequent attacks of the activated species with monomer leads to rapid chain growth. The termination reaction occurs between the product radical and another radical forming a chain with non-reactive groups that cannot participate in further reactions. However, molecules containing thousands or tens of thousands of repeat units are formed because propagation is very much probable than termination [27]. In free radical addition reactions, the chains tend to grow rapidly (few seconds) unless the system viscosity is very high [18,31].

1.7.4 Anchoring Effects in PDLCs

As previously mentioned, when LC molecules are limited by a surface (solid or liquid) LCs orientation changes. The molecular interaction between LC and polymer matrix results in energy of adhesion between LC and polymer surface known as anchoring effect[33]. The strength of the interaction between the LC and the polymer matrix depends on the nature of polymer film and the shape and size of LC domains[17]. Interplay between the applied field, elastic and viscous torques of the LC but also the anchoring strength on the interface between LC domain and polymer surface contribute to the free energy of the nematic which determines electro-optical properties of the PDLC. In a simple way, by applying an electric field to PDLC domains, there is a balance between three energies involved: elastic energy, surface energy and electric energy[17].

Threshold voltage could be calculated, taking into account spherical LC domains with strong planar surface anchoring, using the following equation:

$$V_{th} \approx \frac{1}{R}\sqrt{\frac{K}{\Delta\varepsilon}}$$

Where R is the radius of spherical LC droplet, K is the LC elastic constant and Δε is the liquid crystal dielectric anisotropy [2]. Due to the threshold voltage dependency on droplet size, it is possible to yield information beyond the droplet size, also anchoring strength. In PDLCs with strong anchoring, the threshold voltage is usually high. On the contrary, in PDLCs, with weak anchoring, the threshold voltage is usually low[1].

1.7.5 Liquid Crystal Domains Configurations in PDLCs

In PDLC with swiss cheese or polymer ball morphology the LC director are not aligned uniformly along one direction neither inside the domains neither from one domain to another. As previously mentioned, between two planar LC alignments surface LC directors acquire typical configurations (Figure 1.12) but when LC molecules are confined in another type of shape structure several other configurations can be obtained. In swiss cheese morphology LCs directors inside spherical domains can acquire four main types of configuration as shown in Figure 1.24 a) bipolar droplet, b) toroidal droplet, c) radial droplet and d) axial droplet. The global configuration inside each domain is due to the boundaries between LC and polymer (anchoring effect)[1].

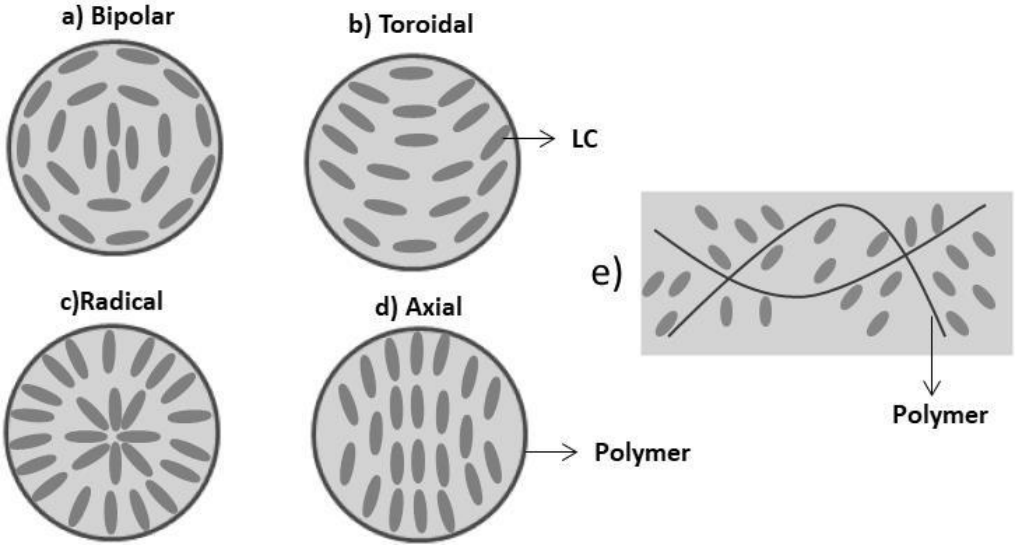

Figure 1.24– Schematic illustration of the liquid crystal director configuration inside spherical domains (left) and (adapted from[12]) and irregular domains (right).

In PDLCIs with swiss cheese morphology type, the bipolar and radial are the most common configurations for the nematic director. The electrical field acts in order to align the nematic director (positive electric anisotropy) parallel to the field direction. This reorientation tends to be easier for little distortion of the initial director configuration inside the droplets. Therefore, in toroidal configuration, a higher anchoring strength does this configuration relatively stable[12]. In polymer ball morphology the LC domains are not spherical and have not the same LC director configuration as swiss cheese morphology. However as shown in Figure 1.24 e), although LC near the polymer network is aligned along the polymer network, a multi-domain structure each with a different alignment of LC is formed. Regardless of the morphology type, the LC is in the directorial configuration in which the sum of the elastic and surface energies are minimized[1].

1.7.6 Scattering and Switching In PDLCs

In OFF state (zero electric fields), the misalignment of nematic directors inside each domain causes a random domain director inside the PDLC cell. A light ray passing through a domain with a normal incident direction is divided into two rays, which travel with different velocities and usually different directions. One of these rays has the extraordinary refractive index (n_e) that varies with the angle Θ measured from the incident direction of the light ray to the nematic director and is expressed as follows:

$$n_e = \frac{n_{\parallel} n_{\perp}}{\left(n_{\parallel}^2 cos^2\Theta + n_{\perp}^2 sin^2\Theta\right)^{1/2}}$$

The other one has the ordinary refractive index (n_o) that does not vary with Θ and is given by $n_o = n_{\perp}$. In OFF state (misalignment of LC directors), the extraordinary optical refractive indices for incident light rays are distributed between $n_{\perp}$ and $n_{||}$ that makes it impossible to match refractive indices of all domains to the polymer index (n_p) and light rays are scattered by domains and PDLC appears opaque[1,34].

As previously mentioned, the transparent state of PDLC can be achieved by applying an electric field but also can be obtained by thermally switched through heating the PDLC film. The degree of scattering depends on the birefringence. Since n_e increases and n_o decreases with decreasing temperature the birefringence increases. As a result, incoming light rays probe a range of refractive indices between n_0 and n_e and light rays are scattered by the domains. The transparent state can be achieved by heating the PDLC film above the T_{NI} and if the refractive index of the polymer (n_p) is close to the refractive index of the isotropic LC (n_i) the PDLC behaves as an optical homogeneous isotropic material[13].

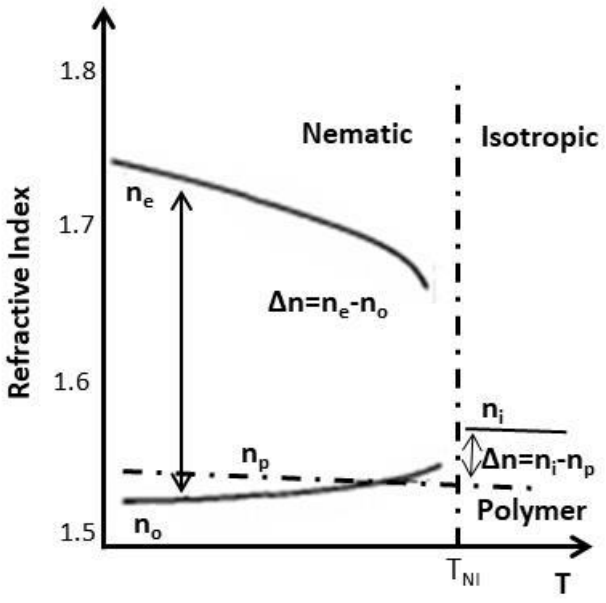

Figure 1.25– The relationship between temperature and refractive indices ordinary (n_o) and extraordinary (n_e) of a typical nematic liquid crystal and for an isotropic liquid crystal (n_i) (solid lines) and the refractive index of a typical polymer (n_p) (dashed line) (adapted from [35]).

As the temperature decreases below the T_{NI} the n_o of the LC decreases while the n_p increases, the mismatch them increases (Figure 1.25) and the transmittance decreases. Above the T_{NI} the birefringence disappears and only refractive index n_i is observed, that should match with n_p, and the transmittance will be maximum.

When the PDLC is voltage driven, for an initial opaque state the LC must be in its nematic phase that is below T_{NI}. With the application of electric field (ON state) above threshold field for LC with positive dielectric anisotropy, the LC directors within each domain become uniformly reoriented parallel with the applied field direction and domains director align parallel to the normal of the cell. When the normal incident light propagates through the LC domains, it encounters only the refractive index n_o. If the refractive index of the polymer n_p is the same as n_o, PDLC became isotropic and the light goes through the device without scattering and the PDLC will appear transparent (Figure 1.26)[1,35].

It is preferable to choose n_p to match the n_o than to choose a match between n_p and n_e. Because small changes in the composition of an LC which may occur either during its preparation or during the PDLC film preparation are more probability to destroy a match between n_e and n_p than a match between n_o and n_p. It is also hard to obtain a stable polymer material with refractive indices in the range of the extraordinary refractive indices of LC. In additional, PDLC films with n_e matched to n_p would always scatter unpolarized light in the on state[35]. When the applied electric field is removed, the alignment in the LC domains is lost and PDLC reverts to its OFF state.

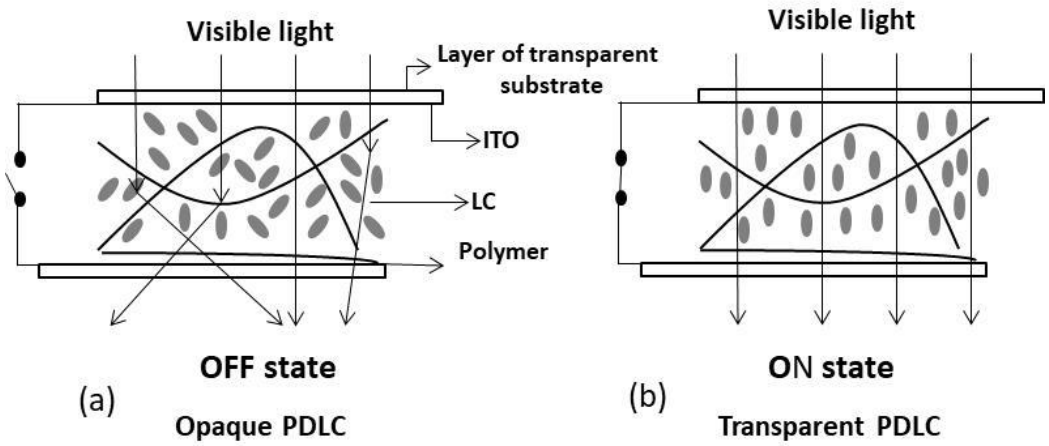

Figure 1.26 – Schematic representation of a PDLC with a) randomly orientation of the domains director producing a highly scattering state and b) with the application of an applied field LC molecules ($\Delta\varepsilon>0$) align up with the field matching the refractive indices (n_o and n_p) and a highly transparent state is achieved.

1.7.7 Permanent Memory Effect (PME)

The typical behavior of light transmittance versus electric field applied across a PDLC is shown in Figure 1.27 a) where the transmittances measured with increasing electric field match with the transmittance measured with decreasing electric field.

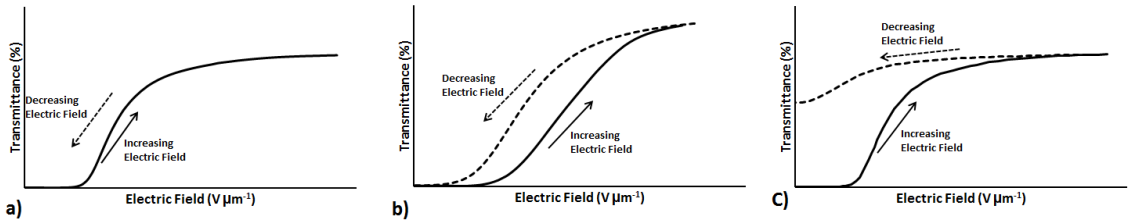

Figure 1.27– Electro-optical response of PDLC a) with no hysteresis, b) with hysteresis and c) with permanent memory effect

When the transmittances measured during switching ON and switching OFF are different, a hysteresis can be seen such in Figure 1.27 b). PDLCs films exhibit some amount of hysteresis because they do not regain their initial levels of transmittance instantaneously after switching OFF the electric field[36]. This behavior can be associated with the difference in response time of bulk and boundaries surface of LC domains[13,36]. In much less common cases, an orientational order is partially or fully recorded by the system after removal electric field (Figure 1.27c)).

The memory behavior in pure LC devices is called memory effect or bistability. In PDLCs this effect is called as a permanent memory effect (PME). In other words, PDLC in an initial opaque state (OFF-state) with an application of an electric field change to a transparent state (ON-state) but a high transparent state is retained after the applied electric field has been switched OFF. This transparent permanent memory state could be preserved over a period of years because the two long-lived states are separated by an energy barrier that could be overcome reaching

the T_{NI} of LC[18]. This type of PDLCs has one important advantage over PDLC without PME because it can maintain a transparent state without any holding technique. It will be necessary only energy to turn ON and after to turn OFF the PDLC, not during the operation of the PDLC for keeping it on. The majority of cases reported in the literature have been done to optimize PDLCs without PME (Figure 1.27 a) and b))[18,37–39]. Which result in a lack of understanding of fundaments for PME[40–48]. However, the switching properties of the PDLC films and particularity the PME depend on same variables such interfacial forces between the polymer matrix and the nematic molecules (anchoring effect), nature of the polymer, the type of microstructure of the polymer matrix (polymer ball and swiss cheese morphology type) and polymerization conditions[19–24,26,49].

1.7.8 Some Useful Parameters to Characterize PDLCs

The important electro-optic parameters of PDLCs are dependent on the application type. For example, for smart windows applications, high transparent and scattering states are required, while other parameters such as driving voltage and switching speed are relatively unimportant. However, for display applications, low driving voltage and fast response times are essential. In this way, in order to characterize a PDLC, several parameters are used, which includes:

- Contrast ratio: Contrast measurement is defined as the ratio between of highest on transmittance (T_{MAX}) over the lowest transmittance (T_0)[13].
- Driving voltage: Voltage at which the transmitted intensity reaches 90 % of the highest transmittance obtained, called V_{90} [13].
- Response (rise and decay) times: rise time is the time for the transmitted intensity to achieved 90 % of the saturation value during the application of electric field (the rate at which the PDLC becomes transparent) and decay time is the time needed for transmitted intensity to fall to 10 % of the saturation value when the electric field is switched OFF (the rate at which the PDLC becomes opaque)[13].
- Hysteresis: the differences between electric field needed to reach half of the maximum transmittance intensity during the switching field ON and switching field OFF[13].
- Haze: The droplet refractive index contradistinction to the isotropic polymer is an angle-dependent. The haze is caused by the increased effective refractive index of the droplets when viewed at oblique angles. In this way, the haze in ON state can limit the applications of PDLC for other than normal viewing angles[50].
- Percentage of permanent memory effect (%PME) can be calculated by the equation:

$$\%(PME) = \frac{T_{OFF} - T_0}{T_{MAX} - T_0} \text{x } 100$$

where T_0 is the transmittance for the initial opaque state (zero electric fields), T_{MAX} is the maximum transmittance upon applying an electric field and T_{OFF} is the transmittance after removing the applied field[26].

- Percentage of memory state contrast (%MSC) is defined as the difference between T_{OFF} and $T_{0.}$

1.7.9 Special PDLCs

1.7.9.1 Reverse-mode PDLCs

PDLCs are potentially useful for a wide variety of applications ranging from switchable windows to LCD devices due to their electro-optical and mechanical properties. In controlling daylight or interior lighting, the most common device used LC with positive $\Delta\varepsilon$ where it is opaque in OFF state and transparent when an electric field is applied. However, switchable windows transparent in the OFF state can be also useful resulting in reverse mode for PDLC[13]. In this mode, PDLCs transmits light in state OFF and scatter light in state ON. The former should be prepared with mesogenic monomers with rigid cores and flexible tails (similar to the chemical structure of LC molecules) and with a concentration less than 10 %. The mixture of this monomer type and negative dielectric anisotropy LC is photochemically polymerized inside an LC cell with the homeotropic alignment layer. In this way, the polymer formed and LC molecules are perpendicular to the cell surface. For this reason, an electric field-OFF light goes through the PDLC without scattering, for $n_o = n_p$. At the electric field-ON, LC directors align tilted away from the field and light is scattered[1,5].

1.7.9.2 Holographic PDLCs (H-PDLCs)

In PDLCs, the most attractive properties for display applications are their electrically controllable light scattering. Nevertheless, in holographic PDLCs (H-PDLCs) it is a wavelength selective reflection. As previously mentioned, in PDLCs the LC director inside domains is randomly and uniformly distributed. However, special configurations can be created by non- uniform conditions during phase separation (polymerization conditions). The simplest one to achieve this condition is by irradiating with a patterned UV laser light from both sides of the cell, which lead monomers to diffuse into high light intensity regions (bright regions) forming a polymer and LCs diffuse into dark regions. The polymerization rate is higher in the bright region and lowers in the dark region forming polymer and LC rich layers, as shown in Figure 1.28[1,2,33].

Since the droplet sizes (≈ 100 nm) in H-PDLC are smaller than the visible wavelength, light is not scattering and the change between the diffraction state and transmission state is achieved by application of an electric field. At electric field-OFF, the incident light will be diffracted by phase grating formed by the LC-polymer that has different refractive indices (Figure 1.28 a)).

When an electric field is applied, the LC director ($\Delta\varepsilon>0$) lining up with the field matching the ordinary refractive index of LC molecules and polymer (Figure 1.28 b)). The Bragg grating disappears and light passes through the material without reflection. A disadvantage for this PDLC type is difficult to achieved uniformity on the sizes of LC domains[33]. H-PDLC can be used for switchable mirrors and reflective displays[1].

Unlike in conventional PDLC, in H-PDLC due to the high anchoring strength between the small droplets and the polymer a higher threshold field (20-30 V μm^{-1}) is required. This higher electric field can be reduced by adding a small quantity of surfactant (≈10 wt. %) in the monomer/LC mixture that forms a layer between polymer and LC during phase separation decreasing anchoring energy. The grating pitch can reflect red, green, or blue light, which makes it potentially useful in displays[2].

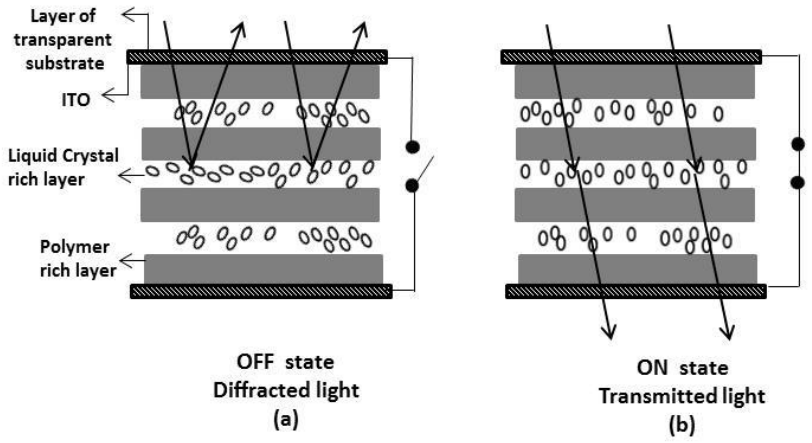

Figure 1.28– Schematic representation of holographic PDLCs at zero electric field with randomly orientation structure of LC. The cell has a periodic refractive index and light is highly reflected (a) and with the application of an applied field (b) LC molecules ($\Delta\varepsilon>0$) align with the field matching the refractive indices of the polymer rich layer and liquid crystal rich layer and light is transmitted (adapted from[1]).

1.7.9.3 Dichroic Dye-Doped PDLCs

The dichroic dye-doped PDLCs combine the effects of scattering and absorption of light. When an electric field is parallel to the transition dipole moment of the dichroic dye the light is absorbed when the electric field is perpendicular to the transition moment the light is not absorbed. Positive dichroic dyes have transition dipole moments parallel to the long molecular axis while negative have transition dipole moments perpendicular to the long molecular axis[1].

These molecules have good solubility in LC unlike in polymer. In this way, after phase separates dye molecules are inside the droplets and can be switched. The orientation of the elongated dye molecule is governed by the nematic LC director inside the domains. The dyes molecules tend to arrange with their long axes aligned along the LC director. At zero electric field state the misalignment of nematic and dyes molecules directors inside each domain with

respect to droplet director increasing scattering and adsorption (light is scattered by LC molecules and absorbed by the dyes), while in the high electric field state will be weakly absorbing and transparent. The change in LC director orientation causes a change in the orientation of the dye´s molecules and the color of the electro-optical cells also change. In this way, the incorporation of dichroic dyes substantially improves the contrast of PDLC[1,51].

1.7.10 Applications of PDLCs

PDLC can be used in applications that other type of LC devices cannot due to their properties:

- PDLCs do not require polarizers and rigid substrates (such glass) so they can be easily produced in a large scale.
- The amount of LCs, in general, is lower than in other LC devices and therefore PDLCs are more economic devices.
- Although the thermal switching effect can be often undesired, it can be also used in some applications[13].

1.7.10.1 Digital Memory Devices based on Write-Read-Erase Cycles

Optical storage in LC composites have been described [52–55] and the applications of these properties in developing a novel digital memory devices based on write-read-erase cycles can be envisaged by permanent memory effect in PDLCs using nematic LC. For optical storage materials by electrically writing, optically read and thermally erased multiplexing drive a pixel array is needed where optical elements (pixels) are formed by PDLC units with PME. The PDLC units are individually controllable and can be transparent or opaque whether or not an electric field is applied to define the ON and OFF state, respectively. In this way, information can be digitally written by an electric field individually applied to different PDLC units that turn these pixels to the transparent state and if no electric field is applied to a given pixel it remains an the opaque state. The storage information given by transparent or opaque pixels can be optically read by a low-intensity laser light beam that scans the PDLC units that transformed light scattered by the PDLCs into binary code. In a binary system, only two digits or states (on and off, 1 and 0) are involved. The bit is an abbreviation for the binary digit that is the smallest unit of information. A bit is represented by the numbers 1 and 0, which correspond to the states on and off, true and false, or yes and no. Bits are combined into larger units called bytes. One byte equals 8 bits. This means that a byte can represent 2^8 or 256 possible states (0-255). Bytes are also the major unit for measuring quantities of data or data storage capacity. Data quantity is commonly measured in kilobytes (1,000bytes), megabytes (1 million bytes), or gigabytes (1 thousand million bytes) [56]. Each PDLC unit can represent two distinct states represent 0 or 1, opaque and transparent state, respectively.

Finally, the storage information can be thermally erased by heating the PDLCs units array until the T_{NI} of the LC and rewrite it again.

1.8 Green Chemistry

"Green chemistry refers to the design, development and application of chemical products and processes that reduce or eliminate the use or production of substances that are hazardous to human health and the environment"[57]. The breadth of the green chemistry concept is summarized by twelve principles as shown in Figure 1.29. "Sustainable Chemistry is the implementation of the concept of sustainability in the production and use of chemicals and chemical products and the application of chemistry and chemical products to enable sustainable development" [58]. The first part of this overlap is related to green chemistry which is summarized by the twelve green chemistry principles. In the second part, it is clear that should also have a contribution for sustainable and not just in a green manner "the benefits of modern chemistry and chemical products should be made available to all communities". In this way, "a sustainable chemical product should be supplied at a price that enables it to be accessed by its users while at the same time being commercially viable for its producers"[58].

The use of green and inexpensive chemistry reagents, such as polyethylene glycol [59–62], provides green and economic features to this work. Also, the polymer dispersed liquid crystal devices with permanent memory effect use an economic and environmentally sustainable technology through the reduction of energetic waste.

1 – Preventation
It is better to prevent waste than to treat or clean up waste after it has been created

2 – Atom Economy
Synthetic methods should be designed to maximize the incorporation of all materials used in the process into the final product.

3 – Less Hazardous Chemical Syntheses
Wherever practicable, synthetic methods should be designed to use and generate substances that possess little or no toxicity to human health and the environment.

4 – Designing Safer Chemicals
Chemical products should be designed to affect their desired function while minimizing their toxicity.

5 – Safer Solvents and Auxiliaries
The use of auxiliary substances (solvents, separation agents, etc.) should be made unnecessary wherever possible and innocuous when used.

6 – Design for Energy Efficiency
Energy requirements of chemical processes should be recognized for their environmental and economic impacts and should be minimized. If possible, synthetic methods should be conducted at ambient temperature and pressure.

7 – Use of Renewable Feedstocks
A raw material or feedstock should be renewable rather than depleting whenever technically and economically practicable.

8 – Reduce Derivatives
Unnecessary derivatization (use of blocking groups, protection/ deprotection, temporary modification of physical/chemical processes) should be minimized or avoided if possible, because such steps require additional reagents and can generate waste.

9 – Catalysis
Catalytic reagents (as selective as possible) are superior to stoichiometric reagents.

10 – Design for Degradation
Chemical products should be designed so that at the end of their function they break down into innocuous degradation products and do not persist in the environment.

11 – Real time analysis for Pollution Prevention
Analytical methodologies need to be further developed to allow for real-time, in-process monitoring and control prior to the formation of hazardous substances.

12 – Inherently Safer Chemistry for Accident Prevention
Substances and the form of a substance used in a chemical process should be chosen to minimize the potential for chemical accidents, including releases, explosions, and fires.

Figure 1.29 – The twelve principles of green chemistry (adapted from[63]).

Chapter II

2 Materials and Experimental Techniques

In this chapter, materials and preparation of the PDLCs are described as well as the instruments and experimental techniques utilized to characterize the pre-polymers synthesized.

2.1 Electro-Optical Characterization

To study the change in optical properties resulting from the application of electric field, a system for measuring the electro-optical properties of PDLCs has been developed. Optical transmission of PDLC films is sensitive to external alternating current (AC) electric fields. Usually, AC is used in addressing LCDs in which the LC molecules interact with applied electric fields through dielectric interaction. The LC reorientation dynamics depends on the square of the electric field so it is independent on the polarity of the electric field. However, if the LC is reoriented by a direct current (DC) for too long, then ions from the alignment layer will form a thin layer at the interface with LC molecules that shield the voltage. To reduce this inconvenient DC voltage effect, an AC voltage should be used[1].

In order to measure this optical effect in a PDLC under the action of an applied electric field, the experimental arrangement developed for recording the electro-optic data is depicted in Figure 2.1. The electro-optical properties of PDLC films were studied in terms of light transmission coefficient changes by a driving AC field, at room temperature.

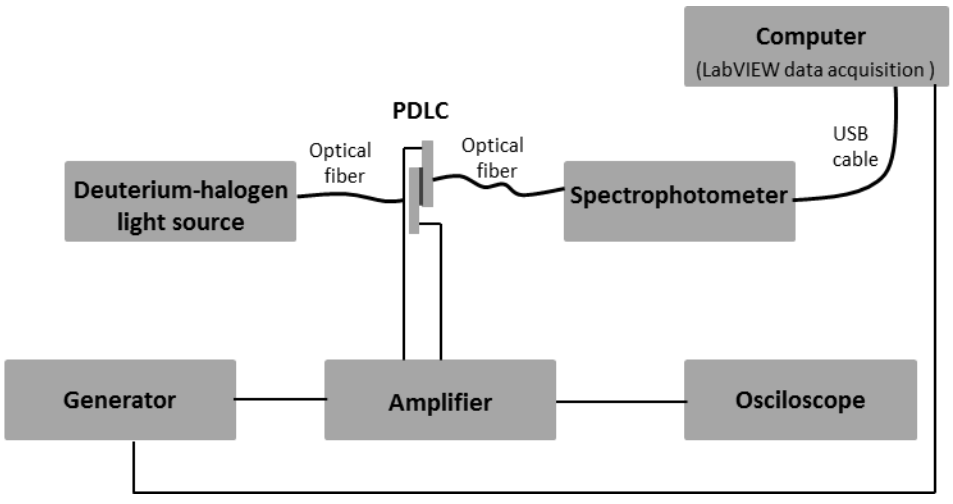

Figure 2.1– Schematic of the experimental set-up developed to measure the electro-optical properties of the PDLC devices.

The PDLC films were held in a cell holder on an optical bench and measurements were performed in normal transmission geometry. The AC electric field was supplied by a function generator (Tektronix AFG 3021C) whose output was amplified by a voltage amplifier (Vtrek TP-430) and applied to the conducting electrodes (ITO-coated glass plates) for sample excitation. Spectroscopic PDLC coefficient transmissions were performed using a fiber optic spectrophotometer Avantes Avasped-2048-2 equipped with an Avalight DH-S deuterium-halogen light source (wavelength 633). The advantage of this method is the relative simplicity of the equipment with a source of light a spectrometer and fiber optics for delivering the light on the PDLC sample and the other to collect the transmitted light. The light intensity transmitted through a PDLC is referred to as transmittance (T). The transmittance is the ratio between the light intensity transmitted through the sample (I_i) and the intensity transmitted through the reference blank (empty cell holder) (I_0) and is represented as a percentage.

The samples were submitted to short bursts of a square wave with 1 kHz AC voltage with 200 ms of duration, followed by 1000 ms to allow relaxation to off-state while the transmission coefficient was recorded at five different times, three during the pulse and two after removal of the applied pulse. At 180 ms was recorded the maximum transmittance. The voltage excitation scheme consisted of 210 experimental points comprising a sequence of increasing step ramp up to a maximum value (Vmax) followed by a decreasing step ramp down to the starting value at 0 V. The voltage dependent transmittance curves were integrated by the LabVIEW data acquisition system.

The measurements were corrected using appropriate calibration standards. To confirm the validity of measurements by calibration of voltage amplifiers, a calibration set-up as depicted in Figure 2.2 was used.

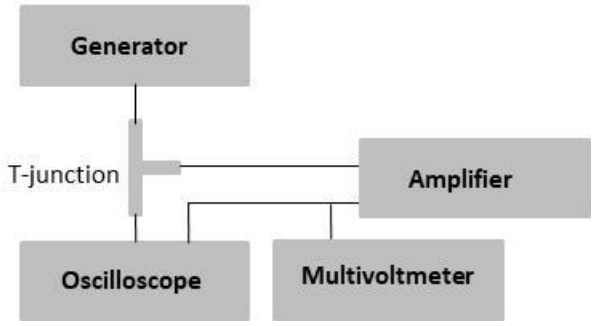

Figure 2.2– Schematic representation of a calibration set-up of voltage amplifier using a signal generator.

The sine-wave generator reference was sweep manually between 1 and 20 V (1KHz, high impedance) and characteristics of output signal were the measurement by oscilloscope. The amplified signal was observed on an oscilloscope screen and compared with the original signals applied by the generator. The signal generator is coupled directly to the input of the voltage amplifier and oscilloscope (TekTronix TBS 1102B-EDU) via a coaxial T-junction. The

measurands of this set-up are the input voltage of the amplifier from a calibrated generator voltage (*Vin*) and the output voltage of the amplifier (*Vout*). In terms of the following equation:

$$Vout = 0.1961Vin^2 + 39.04Vin$$

2.2 Polarized Optical Microscopy (POM)

The light sources usually emit lights formed by electromagnetic waves that vibrate in several directions (nonpolarized light). However, in polarized light, the electric vectors of all waves vibrate in the same plane and can occur at any angle.

For achieving polarized light from nonpolarized light filters called polarizers are needed. Polarizers have a unique transmission axis that defines the plane of vibration of the transmitted rays producing polarized light. This concept is illustrated in Figure 2.3 where only rays from the random incident light whose electric vectors vibrate in a plane parallel with the transmission axis of the filter are transmitted (passes through polarizer) as a linearly polarized light. The other rays are partially transmitted or blocked by the polarizer[64].

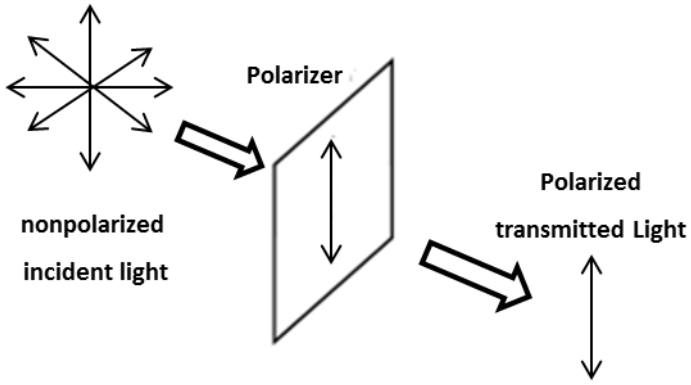

Figure 2.3– Schematic explanation of how to get polarized transmitted light from random light (adapted from[64]).

Two polarizers are used in the optics of a polarizing microscope. Which make the fundamental concept of a polarizing microscope, as demonstrated in Figure 2.4.

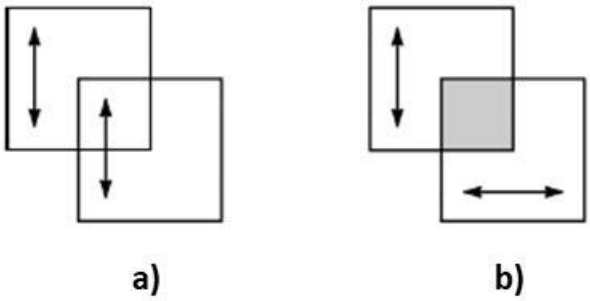

Figure 2.4– Schematic representation of a) align and b) cross-polarizer (adapted from[64]).

In Figure 2.4 a), when a normal light wave passes through the first polarizer also passes through the second polarizer placed in the microscope above the first one, because its transmission axis is parallel to that of the first polarizer. In this way, the transmission axes of the two polarizers are aligned and this configuration produces light polarized. However, when a light wave passes through the first polarizer if the second polarizer is placed in the microscope above to the first one, with its main axis perpendicular with respect to the first polarizer (crossed polarizers), no light passes (Figure 2.4 b)[64]. The main advantage in polarized light microscopy is that the easy and fast identification of birefringent samples because they will appear bright even when viewed through crossed polarizers. As previously mentioned, when the polarized light beam from polarizer enters the birefringent medium, it is refracted and divided into two separate components, ordinary and extraordinary rays, vibrating parallel to the crystallographic axes and perpendicular to each other. These components travel with different velocities and are initially out of phase. Nevertheless, the components of these waves that pass through the analyzer are vibrating in the same plane. Because one wave is retarded with respect to the other, waves are recombined with constructive or destructive interface when they pass through the second polarizer, as shown in Figure 2.5 [65]. As a result, birefringent material acquires a spectrum of color when observed in white light through crossed polarizers. In a simple way, if a birefringent sample containing oriented macromolecules is placed between two crossed polarizer filters, their repetitive structure rotates the axis of the light emerging from the first polarizer and light will pass through to the second one. In this way, the sample will appear as a bright structure[66].

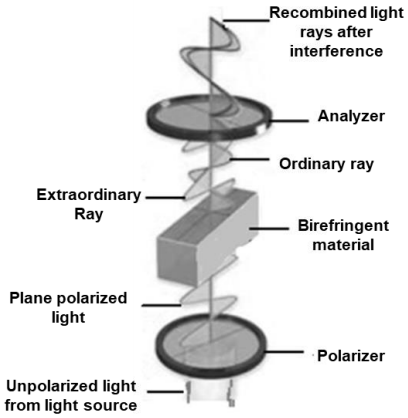

Figure 2.5– Schematic illustration of the interaction of birefringent material with polarized light between crossed polarizers in an optical microscope (adapted from [65]).

Because of these above features, the dispersion of LC domains in PDLC films was analyzed by polarized optical microscopy (POM) with crossed polarizers. These studies were performed by an Olympus CX31P optical polarizing microscope. The microstructure of the samples was obtained by taking microphotographs using an Olympus SC-30 digital camera interfaced to a computer. Images were obtained at a magnification of 100x.

2.3 Scanning Electronic Microscopy

A scanning electron microscope (SEM) provides details surface characteristics of the sample, such as three-dimensional structure and particle size. For this, a finely focused electron beam is moved sequentially from point to point across the sample surface. When the incident electrons come in contact with the metal atoms produces reflected electrons and secondary electrons emitted from the surface of the sample. SEM instruments always have at least one detector and usually a secondary electron detector. Secondary electrons and backscattered electrons are commonly captured by a detector and transmitted to amplifiers. The resulting signal is processed to produce a black and white three-dimensional image on a monitor. In this way, the sample to be characterized by SEM must have a good superficial electronically conductive. Otherwise conductivity can be achieved by coating samples with a thin layer of conducting material, such as carbon or gold or other metal. However, metal coatings are most effective for high resolution electron imaging applications[66,67]. In this way, SEM has been used to provide images of the morphology of the polymeric matrix in the PDLC. For these analyses glass substrates of PDLCs cells were first separated and immersed into acetonitrile until LC molecules were extracted and then polymer samples were dried under vacuum for 24 hours. Afterward, the resulting samples were mounted on aluminum stubs carbon cement (D-400, Neubaeur Chemikalien) and examined after gold or carbon coating using a dual ion beam sputter coating apparatus. The measurements were performed using an SEM Hitachi S-2400 instrument.

2.4 Confocal Laser Scanning Microscope

Confocal microscopy involves scanning the sample at successive focal planes with a focused light beam. The light from a laser source hits the sample plane and is reflected. The beam splitter directs the reflected light to a pinhole and later to a detector. Light above or below of the focused plane is blocked. Digital images captured at many individual spots in a very thin plane of focus are used to produce an optical section of that plane. A series of optical sections of focal planes can be used to digitally reconstruct a three-dimensional image[66].

This technique is a non-invasive method to analyze the morphology through the entire thickness of the PDLC cell in order from top to bottom of the cell. In this study, PDLC samples were directly observed by confocal laser microscopy without any other preparation, such as the introduction of a fluorescent probe as mentioned in literature[22,68,69]. The PDLC with polymer-ball morphology was analyzed in a transparent state (permanent memory effect) with 20 µm of thickness between glass substrates and PDLC with swiss-cheese morphology was analyzed with 5 µm of thickness for reducing the light scattering. Confocal visible microscopy scans were recorded through the entire thickness of the PDLC sample from top to bottom. The confocal micrographs were made using a confocal laser scanning microscope Carl Zeiss LSM 700.

2.5 Differential Scanning Calorimetry

The differential scanning calorimetry (DSC) allows recording the difference in enthalpy which occurs between the sample and a reference material while both are heated under the same conditions. The term differential is related to the use of two identical measuring sensors, one for the sample and one for the reference. The DSC instrument provides calorimetric information (measurement of the heat changes which occur during a process) where the energy difference provided to a substance and the reference is determined as a function of temperature.

In this work, the results from DSC have been obtained by heat flux DSC instruments. In this DSC type, the instrument signal is derived from the temperature difference (converted into heat flow) established when the sample and reference are heated in the same heat source (Figure 2.6 a). The power compensating DSC has two independently furnaces where each one is provided with a heating unit and a temperature sensor (Figure 2.6 b) [70].

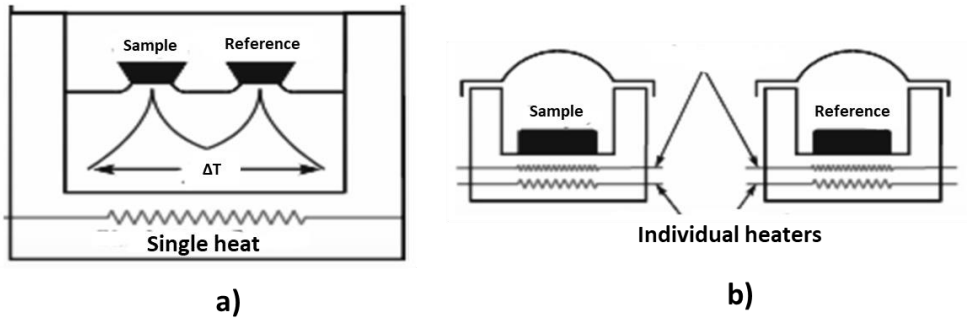

Figure 2.6– Schematic illustration of different instruments used in DSC to detect energy changes occurring in a sample: a) heat flux DSC and b) power compensation DSC (adapted from[71]).

The thermal energy changes correspond to endothermic and exothermic effects. The fusion transition is an endothermic event that requires higher heat flux flowing to the sample to increase the temperature at the same rate as in the reference. Therefore, the melting temperature corresponds to an endothermic peak. Unlike exothermic effects as crystallization and chemical reactions such as polymerization where it is required a smaller variation of the amount of heat to reduce the temperature of the sample. The T_g was taken at the inflection point of the specific heat capacity increment in the transition.

In heat flux, endothermic answers are described as negative heat flux below the baseline and exothermic peaks are presented as positive heat flux above the baseline (Figure 2.7).

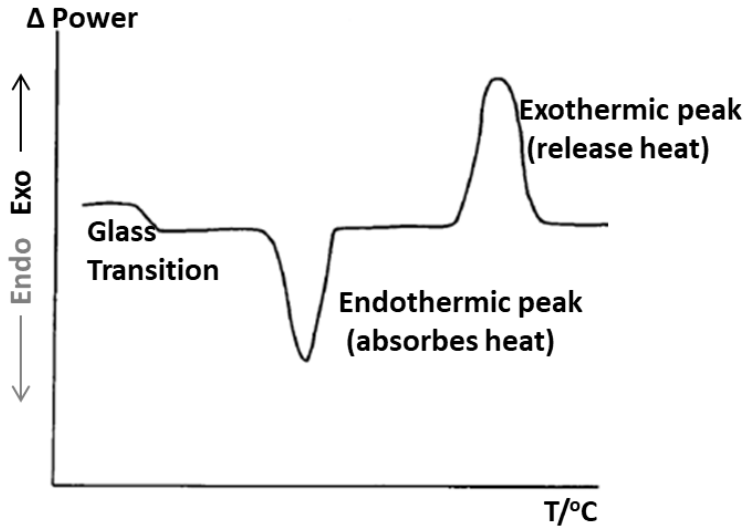

Figure 2.7 – Schematic representation of a DSC curve achieved by the heat flux method where conventionally the endothermic peaks go down unlike exothermic peaks.

Differential Scanning Calorimetry (DSC) analyses were performed using a DSC Q2000 from TA Instruments interfaced with a cooling accessory. Ice-water slurry as coolant and nitrogen purge

(50 mLmin^{-1}) was used. About 5 mg of the sample was weighted and encapsulated in a hermetically sealed aluminium pans. Measurements were carried out under nitrogen gas flowing at 5 ºC min^{-1}. Analysis of the thermal analysis curve is carried out using instrument software (TA instrumental analysis) and the peak area is proportional to the enthalpy change.

2.6 Matrix-Assisted Laser Desorption Ionization-Time of Flight Mass Spectrometry (MALDI-TOF MS)

Polydispersed ethylene glycol samples contain molecular chains of different lengths that result in different molecular mass in the same sample. Therefore, most of these materials cannot be characterized by a single molecular weight. The molecular weight and its distribution are important in determining the physical properties of these samples. For example, the type of distribution of molar masses could determine if a sample (which is in a molten state) cools to a crystalline state or to an amorphous state. Depending on distribution in molar mass, different molecular species crystallize in different temperatures. The high molar mass component crystallizes early and the low molar mass species can crystallize in separate crystal [31] and the presence of short chains could act as plasticizers. These molecules will facilitate the movement of chains and interfere with the packing of long-chain molecules [72].

In this way, it is important and useful to characterize the average molecular mass and molecular mass distribution. It can be defined two different types of average molecular mass: the number average (M_n) and the weight average (M_w), given by:

$$M_n = \frac{\sum N_i M_i}{\sum N_i}$$

$$M_w = \frac{\sum W_i M_i}{\sum W_i} = \frac{\sum (N_i M_i) M_i}{\sum (N_i M_i)} = \frac{\sum N_i M_i^2}{\sum N_i M_i}$$

Where N_i is the number of molecules of molecular mass M_i; $\sum$ is the sum over all i molecular masses and W_i is the total weight of macromolecular chains with molar mass equal to M_i. The number average molecular weight represents all molecules weights of the individual molecules present divided by their total number (each molecule contributes equally to the average). On the other hand in the weight average molecule each molecule in such an average contributes according to the ratio of its particular weight to that of the total. Therefore, M_w is more sensitive to the higher molecular weight species, while M_n is sensitive to the lower ones [28].

The M_w is always higher than the M_n and the ratio of these two averages called polydispersity index (PDI) gives information width of the molecular mass distribution. Therefore, the greater the distribution of molecular sizes, the greater is the difference between averages.

Matrix-Assisted Laser Desorption/Ionization (MALDI) is a soft ionization technique used in mass spectrometry to volatilize polymers and Time of Flight (TOF) mass spectrometers to analyze the ions. The MALDI requires the preparation of within an ionic matrix which is subsequently irradiated by a laser source. This ionization produces molecular ions rather than causing fragmentation as in mass spectrometry. The ions when analyzed by TOF mass spectrometer essentially reflect the molecular weight distribution of the polymer [73]. TOF is an analyzer where ions are separated according to their m/z values. In this technique ions of different m/z are dispersed in time during their flight along a field-free drift path of known length. The lighter ions will arrive earlier at the detector than the heavier ones [74], which convert the mass separated ion current into an electrical signal that can be amplified and computer processed. Magnetic sector and quadrupole mass spectrometers are examples of ion detector [75].

Mass spectra were recorded by matrix-assisted laser desorption ionization time-of-flight (MALDI-TOF) on a Bruker. Autoflex with 2-(4-hydroxyphenylazo) benzoic acid (HABA) was used as the matrix with sodium chloride as the cationizing salt for the MALDI-TOF mass measurements.

2.7 Preparation of PDLC Samples

2.7.1 Materials

The liquid crystal used was E7 (*Merck*) and it was used without further purification. E7 exhibits a nematic to isotropic transition temperature at 58 ºC detected experimentally by POM and DSC. Which is in accordance with literature [14,76].

The initiator used for thermal polymerization was *N,N*-azobisisobutyronitrile (AIBN) used as received from Sigma-Aldrich without further purification. The AIBN has been widely used as a radical initiator in free radical polymerization due to the initiator isobutyronitrile radicals that are easily and rapidly formed by heating the AIBN (Figure 2.8). This thermal cleavage of AIBN is highly favorable by the entropy term for the formation of three molecules from one. In addition, the molecular nitrogen keeps the two radicals far enough apart to minimize their coupling[32].

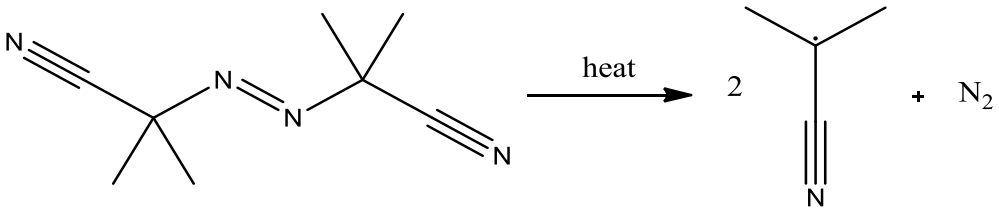

Figure 2.8 – Thermal cleavage of 2,2'-azobisisobutyronitrile (AIBN) to give two isobutyronitrile radicals and molecular nitrogen (adapted from [32]).

The thermal polymerizations were carried out in a handmade oven, equipped with an auto-tune temperature controller (model CAL 3300) provided by CAL Controls and a resistance thermometer, Pt100/RTD-2, whose sensor has a temperature range from - 200 to 400 ºC. The cells filled with the mixture were kept isothermally for several minutes at 55, 60, 66, 70, 74, 80 and 90 ºC.

For photochemical polymerization was used p-xylylene bis-(*N,N*-diethyldithiocarbamate) (XDT) as an initiator which was synthesized as described in literature [77]. This molecule, when subjected to ultraviolet light (*hv*) is decomposed photochemically into a reactive chain-initiating carbon-centered radical Figure 2.9 a) and in a less reactive sulphur-centred dithiocarbamyl radical Figure 2.9 b) [78,79].

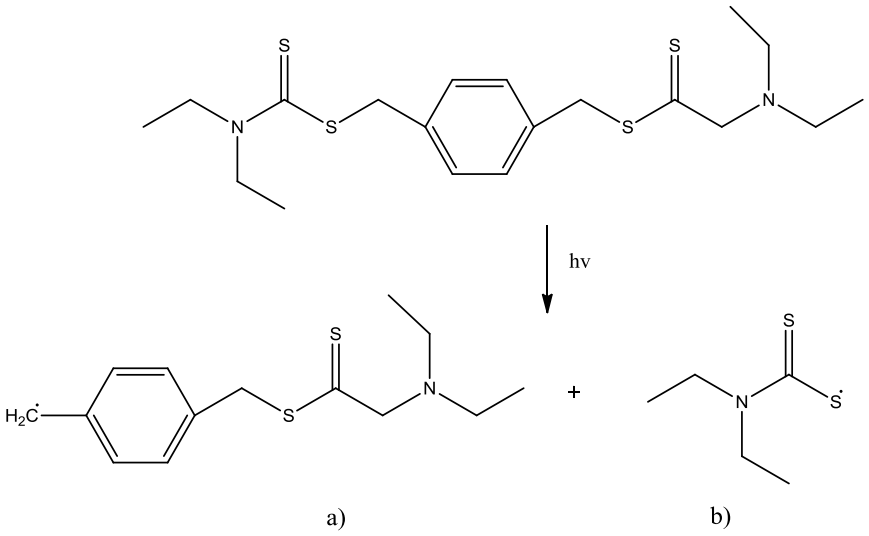

Figure 2.9 – Ultraviolet light-induced decomposition of p-xylylene bis-(*N,N*-diethyldithiocarbamate) (XDT) into a dithicarbamyl and a carbon radicals (adapted from [78,79]).

In this way, the free radical polymerization propagates by the attack of carbon radicals from the XDT molecule to double bonds in the (meth) acrylate monomers. The termination step occurs by carbon-carbon radical termination that results in a dead polymer. However, a carbon-dithiocarbamyl radical termination is also possible forming a polymer where the end group can be reinitiated. Further irradiation breaks the bond between the carbon radical and the sulfur group which reintroduces again a carbon radical and a thiol radical into the reaction [78,79]. In this way, the XDT initiator simulates a “living” radical polymerization [78,79] because polymerization proceeds without the occurrence of irreversible chain breaking process [80].

The photochemical polymerizations were carried out using Oriel 60115 equipment, with a 100W mercury medium pressure lamp powered by Oriel 68800. The samples were irradiated by monochromatic light at 366 nm with two different intensities at 48 and 0.48 $mWcm^{-2}$, using neutral density filters. The cells filled with the mixture were kept under radiation for several minutes and all photochemical polymerizations were carried out at room temperature.

For the preparation of PDLC films, mixtures of 70 wt. % (percentage by weight) of E7 and 30 wt. % of pre-polymer with 1 wt. % of AIBN or XDT for thermal and photochemical polymerization, respectively, were mixed together at room temperature until the mixture became homogeneous. For solid pre-polymers, this mixture was slightly warmed. Samples were prepared by introducing the mixtures by capillarity into the electro-optical cell. If nothing is stated otherwise the thermal polymerization was made at 70 ºC and photochemical polymerization at 48 mW cm^{-2}. A schematic illustration of PDLCs preparation is shown in Figure 2.10.

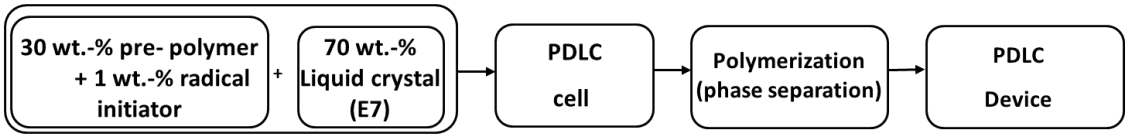

Figure 2.10 – Schematic representation of the preparation of PDLC films by PIPS method.

The electro-optical cells used in this work were manufactured or from commercial sources. The manufactured ones were constructed by a pair of commercial flat glass substrates model D256A-X000 supplied by *Instec Inc*. (Figure 2.11). They are ITO (100 Ω; 0.023 ± 0.005 µm of thickness) coated glass substrate (soda lime glass type) that was covered with rubber polyimide (KPI-300B type; 0.06 µm thickness) alignment layer to promote a homogeneous alignment.

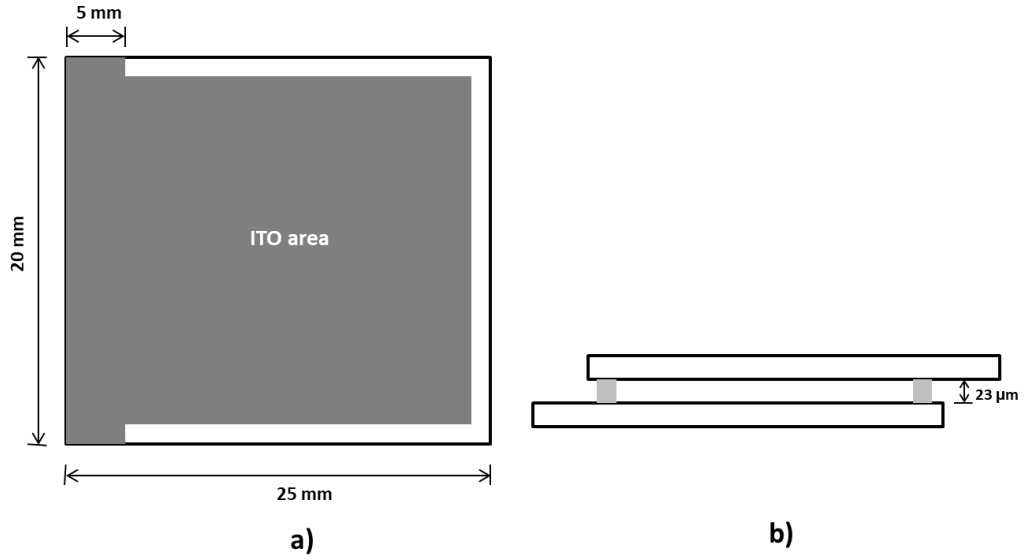

Figure 2.11 – Schematic representation of a) top view of ITO glass substrate model D256A-X000 provide by *Instec Inc* (left) and b) lateral view of a manufactured LC cell (right) (adapted from[81]).

For cell assembly, glass substrates are spaced by a mylar film formed along the edges such that the glass substrates faces form a gap. The mylar spacer, which fixes the thickness of the gap is about 23 µm thick. The substrates are held together by applying a sealing epoxy resin along the edge contour except for an inlet area where the pre-polymer and E7 mixture will be injected into the spacing between substrates.

The commercial cells supplied from *Instec Inc*. (Figure 2.12) have the same substrates features. ITO (100 Ω; 0.023 ± 0.005 µm of thickness) coated glass substrate (soda-lime glass type) that was covered with rubber polyimide (KPI-300B) alignment layer to also promote a homogeneous alignment. The thickness of cells is made by sputtering spacer beads made of transparent ceramics or glass onto the substrate of glass slab before assembly[82]. It is the diameter of these micro-spheres that fixes the cell gap, and in this work, it is about 20 µm.

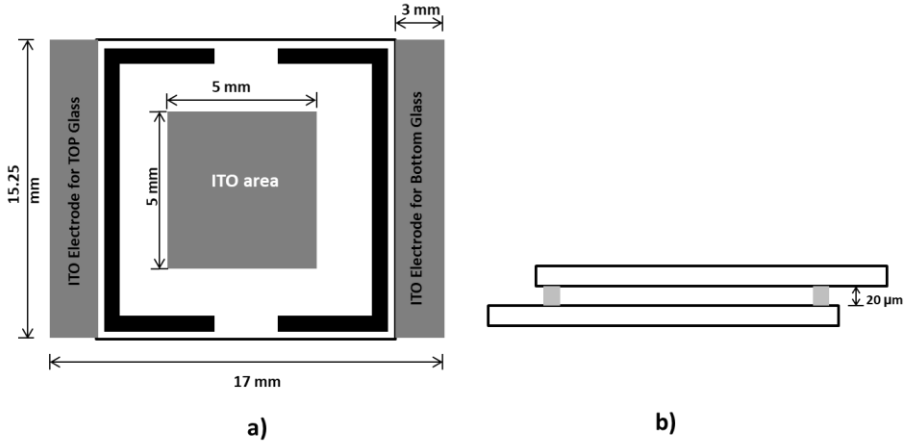

Figure 2.12 – Schematic representation of a top view (left) and lateral view (right) of a commercial LC cell model LC2-20.0 provide by *Instec Inc* (adapted from[81]).

2.8 The Synthesis Reagents

All chemicals were purchased from the Aldrich Chemical Company and used without further purification. Starting material compounds were dried under vacuum over phosphorus pentoxide (P_2O_5) to remove residual water. The solvents used and trimethylamine (Et_3N) were distilled prior to use by standard procedures. Organic solvents were evaporated using a rotary evaporator under reduced pressure at 40 ºC. All reactions were performed under a dry argon atmosphere.

The reactions were monitored by thin layer chromatography (TLC), which were conducted on commercially aluminum plates (*Merck* Kieselgel 60 F_{254}) and compounds were visualized by using a UV lamp (λ=254nm) and staining with a solution of phosphomolybdic acid (5 g) in EtOH (95 mL) and subsequent heating. Flash Chromatography columns were prepared with silica gel from Macherey-Nagel (Kieselgel 60M).

2.9 Commercial Pre-Polymers

The commercial precursors from Sigma-Aldrich of the polymeric matrix were TriEthyleneGlycoldimethacrylate "TriEGDM" (286 g mol^{-1}; n = 3), TetraEthyleneGlycoldimethacrylate "TetraEGDM" (330 g mol^{-1}; n = 4),

Polyethyleneglycoldimethacrylate "PEGDMA550" (≈ 550 g mol^{-1}; n ≈ 10), "PEGDM875" (≈ 875 g mol^{-1};n ≈ 16), poly(propylene glycol)methacrylate "PPGM" (≈ 375 g mol^{-1}; n ≈ 5) and poly(propylene glycol)acrylate "PPGA" (≈ 375 g mol^{-1}; n ≈ 6). These precursors were previously passed through a disposable inhibitor remover column from Aldrich in order to eliminate the hydroquinone stabilizer.

2.10 NMR Spectroscopy

^{1}H-NMR resonance (δ^{H}) and ^{13}C-NMR (δ^{c}) spectra were recorded on a Bruker AMX-400 instrument operating at 400MHz for ^{1}H nuclei and 100 MHz for ^{13}C nuclei. Deuterated chloroform ($CDCl_3$) (99.50 % isotropic purity) was used as NMR solvent and chemical shift values (δ) are reported in parts per million (ppm), using tetramethylsilane (TMS) as the internal standard.

Solid state magic angle spinning carbon-13 (^{13}C MAS), and solid state cross-polarization magic angle spinning carbon-13 (^{13}C CPMAS) NMR spectra of the basic compounds nematic liquid crystal E7, TriEGDM, TetraEGDM, PEGDM550, PEGDM875 and their respective PDLC films were acquired, with a 7 T (300 MHz) AVANCE III Bruker spectrometer equipped with a BBO probe head operating at 75 MHz for ^{13}C nuclei and at 300 MHz for ^{1}H. The samples were spun at the magic angle with a frequency of 5 kHz in 4 mm-diameter rotors at room temperature. The ^{13}C MAS NMR experiments were acquired using a high-power proton decoupling pulse sequence (HPDEC) with a relaxation delay of 2.0 s. The ^{13}C CPMAS NMR was acquired with proton Cross Polarization with a contact time of 1.2 ms, and the relaxation delay of 2.0 s.

Chapter III

3 Di-Functional PEG with linear chain length

From free radically polymerizable monomers, the most commonly used in PDLC by PIPS method processes are those with acrylate or methacrylate as reactive groups. From these acrylate or methacrylate monomers, there is a wide variety of the chemical group attached to the oxygen atom of the acryl- or methacrylic-ester unit that can be used in PDLCs preparation [18]. For E7 liquid crystal with a n_o close to 1.52 [6,83], the n_p should be also close to 1.5. Although, the refractive index of polyethylene glycol depends slightly on the number of ethylene oxide units [84,85] in average the refractive index of this class of polymers is in the range of 1.4640 for $n \approx 12$ and 1.470 for molecular weight higher than 1000 g mol^{-1} (at 20 ºC using chloroform)[85]. This makes this polymer family preferable for use in preparation of PDLCs.

Although acrylates and methacrylates react according to similar pathways in free radical polymerization, under the same conditions, an acrylate forms secondary radicals as the propagating end group, while a methacrylate forms tertiary radicals. This tertiary radical is more stable than the secondary one which in turn lowers the velocity of the polymerization reaction. Additionally the steric effect for the approach the monomer to monomer radical is higher in methacrylate monomers which also hinder the propagation reaction slowing it [86–88].

Ethylene glycol is an ethane-1,2-diol and its molecular formula is $(CH_2OH)_2$. The poly(ethylene glycols) (PEGs) are linear polymeric materials whose chains are composed by oxyethylene units (n) and terminated by one or two end hydroxyl groups called monomethoxy-PEG (mPEG-OH) or diol-PEG (HO-PEG-OH), respectively. The structure of diol-PEG is commonly expressed as $H\text{-}(O\text{-}CH_2\text{-}CH_2)_n\text{-}OH$ and it chemical structure is shown in Figure 3.1. Depending on their average molecular weight, they can be liquids (200 - 800 g mol^{-1}), waxy solids (1000 - 1500 g mol^{-1}), and flakes or solids (2000 - 10000 g mol^{-1})[89].

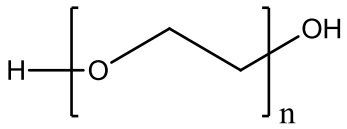

Figure 3.1– Chemical structure of diol-PEG where n is the number of ethylene oxide units.

PEGs are synthesized by living anionic ring-opening polymerization of ethylene oxide producing a family of PEG molecules with wide Gaussian´s distribution of molecular weight. This heterogeneous mixture having a distribution of different molecular weights is characterized by average molecular weights. The length of the chain can be controlled within a desired range by the degree of polymerization of the starting material[90,91].

PEG with reactive chain ends such as acrylate or methacrylates have been synthesized [92–98]. These macromolecules PEGs that contain a reactive end group allow subsequently further polymerization by addition of one or more polymerizable double bonds. These reactive PEGs are called macromers[99,100]. PEGs functionalized with acrylate or methacrylate groups (macromers) form a free radical polymerizable species able to be used as a pre-polymer matrix in PDLC devices. For simplicity, in this work PEG refers to macromolecules whose chains are composed by oxyethylene units and terminated by hydroxyl groups; PEG functionalized (oligomers or pre-polymers) with acrylate group at both ends refer to PEGDA and only at one end refer to PEGA. PEG functionalized with methacrylate group refer to PEGDM and only at one end refer to PEGM. Finally, polymer results from free radical polymerization of PEG functionalized (oligomers) refer to PEGDA polymer, PEGA polymer, PEGDM polymer or PEGM polymer.

The relationship between linear chain (ethylene oxide units) length of polymerizable monomers with morphology, electro-optical properties and ^{13}C NMR relaxation spectroscopy of the corresponding polymer dispersed liquid crystal (PDLC) films were investigated. In this chapter, it is observed that the permanent memory effect of PDLC is greatly influenced by the length of the molecular chain of pre-polymers to be incorporated as a polymer matrix. Increasing the number of ethylene oxide in the pre-polymers chain, maintaining the number of functionalities (polymerizable groups in each monomer molecule), the permanent memory effect of PDLC increased. Among the length of the molecular chain of the polymerizable monomers studied (from n = 3 to n ≈ 16), 70 % of permanent memory effect with 54 % of memory state contrast was obtained for PDLCs films prepared with the longest monomeric chain.

The switching properties of the PDLC films and particularity the permanent memory effect depend on same variables such interfacial forces between the polymer matrix and the nematic molecules (anchoring effect), nature of the polymer, the type of microstructure of the polymer matrix (polymer ball and swiss cheese morphology type) and polymerization conditions [19–24,26,49].

The polymer through its chemical structure and properties enables LC domains formation, providing their mechanical support but also determining the shape, size and LC domain alignment. The interfacial forces between LC molecules and polymer matrix result in an energy of adhesion (anchoring energy) [5,11].

3.1 Electro-Optical Properties

The PDLCs were prepared as described in Figure 2.10 by thermal polymerization at 70 °C, overnight. The electro-optical responses for the PDLCs, prepared by di-functional pre-polymers (TriEGDM, TetraEGDM, PEGDM550 and PEGDM875, are depicted in Figure 3.2 and electro-optical properties are summarized in Table 3.1.

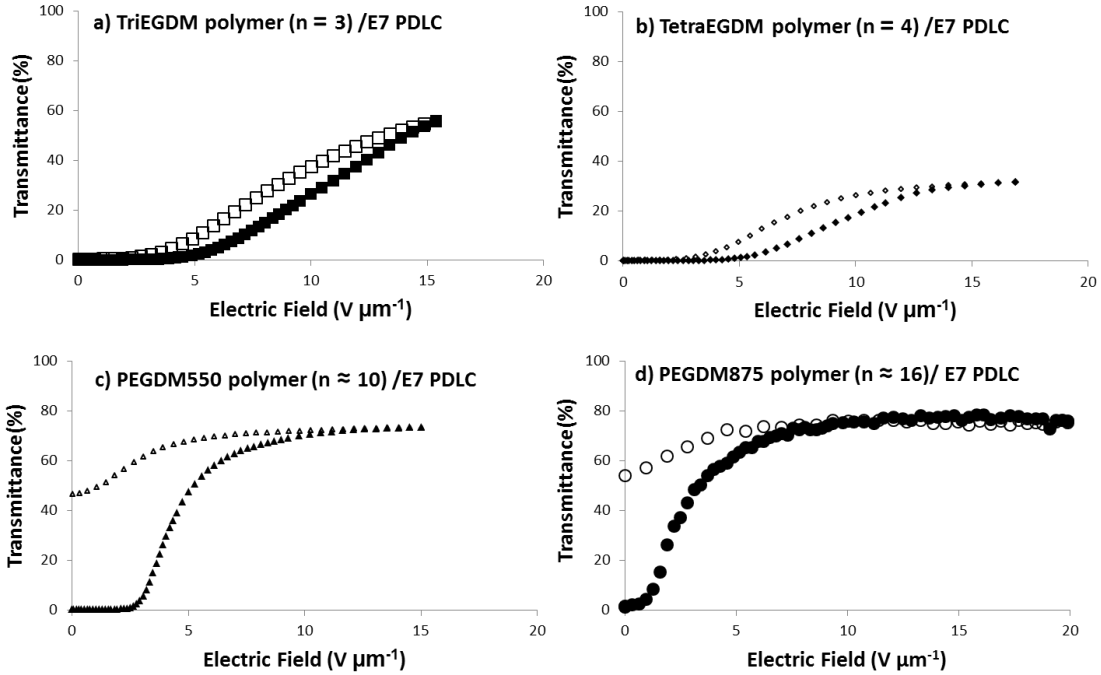

Figure 3.2 – The electro-optical response for PDLC films prepared with a)TriEGDM, b)TetraEGDM, c)PEGDM550 and d)PEGDM875 and E7 with weight ratios of 30/70 (wt%), and 1 wt% of AIBN with respect to the pre-polymer, polymerized at 70 °C, overnight. The transmittance was measured by applying increasing electric field (filled symbols) and decreasing electric field (open symbols).

Table 3.1 – Electro-optical properties for PDLC films prepared with TriEGDMA, TetraEGDMA, PolyEGDMA550 and PolyEGDM875 and E7 with weight ratios of 30/70 (wt. %), and 1 wt. % of AIBN by weight with respect to the pre-polymer.

Electro-optical properties	**Polymer/E7 PDLCs**			
	TriEGDM	**TetraEGDM**	**PEGDM550**	**PEGDM875**
% PME	0.0	0.0	63.0	70.0
E_{90} (V µm^{-1})	13.8	13.2	7.9	6.4
% T_0	0.0	0.0	0.0	0.0
% T_{OFF}	0.0	0.0	46.5	53.8
% T_{MAX}	55.9	31.5	73.1	75.8
% MSC	0.0	0.0	45.5	53.8

It is evident from the electro-optical response (Figure 3.2) that the increase of the number of ethylene glycol oxide units in polymer matrix increases the PME percentage from 0 % (TriEGDM, n=3 and TetraEGDM, n=4) to 63 and 70 % (PEGDM550, n ≈ 10 and PEGDM875, n≈16, respectively). The electrical field required to initiate the transition from light scattering to light transmission (E_{90}) also decreases from 13.8 to 6.4 V µm^{-1}. This indicates that the increase of ethylene oxide units decreases the energy required for LC molecules started aligning parallel to the electric field indicating a decrease of polymer ability to anchor liquid crystal which is agreement with the increase of PME.

3.2 Morphology of Polymer Matrix of PDLC Samples

Micrographs of polymer matrix microstructure are presented in Figure 3.3. In literature, PDLCs with polymer ball morphology tend to exhibit permanent memory effect [18]. However, although not all samples studied have permanent memory effects, all morphologies can be assigned as a polymer ball. This morphology type formed microsized polymer balls that merged together to form a network that is in contact with a continuous LC phase. Nevertheless, with the increase of pre-polymer chain length the polymer beads are progressively tightly merged increasing the PME from 0 % (TriEGDM and TetraEGDM polymers/E7 PDLCs) to 63 and 70 % (PEGDM550 and PEGDM875 polymers/E7 PDLCs, respectively).

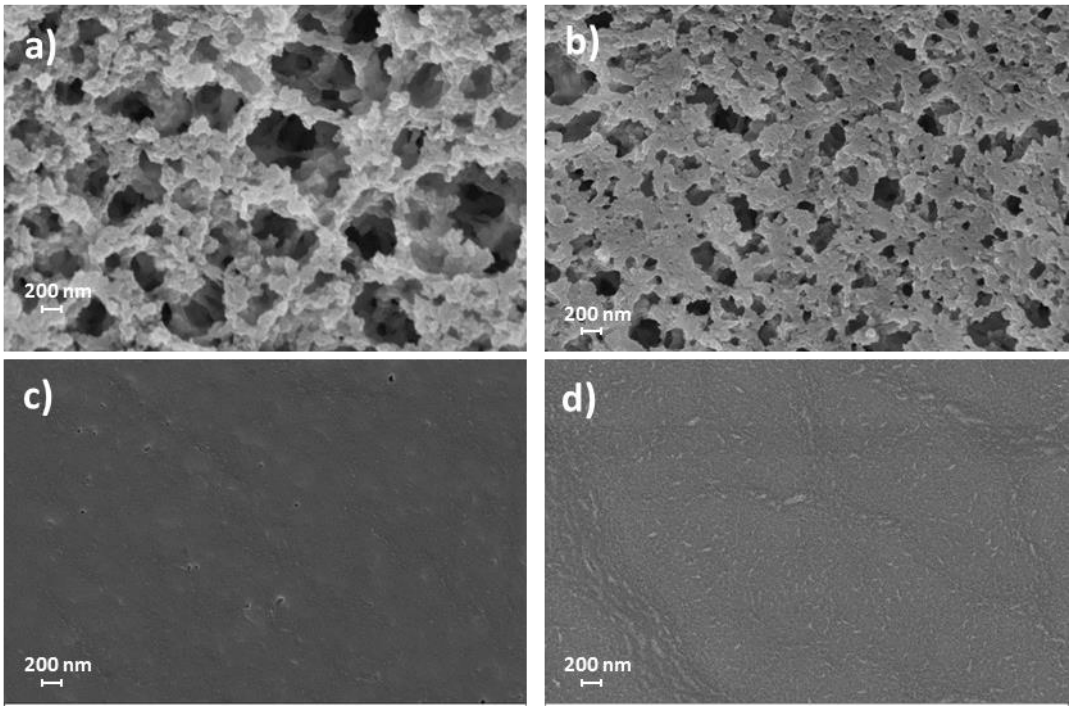

Figure 3.3 – Scanning electronic micrographs for the microstructure of the polymer matrix of the PDLC films prepared with different pre-polymers: a) TriEGDM; b) TetraEGDM; c) PEGDM550; d) PEGDM875. All samples were prepared with pre-polymer and E7 with weight ratios of 30/70 (wt. %), and 1wt. % of AIBN with respect to the monomer.

3.3 Nematic to Isotropic Liquid Crystal Transition

The determination of phase transition temperatures was investigated by POM and for pure LC E7 also by DSC. From DSC measurements (Figure 3.4), the pure LC E7 is characterized by T_g at - 61.69 ºC and a T_{NI} at higher temperatures at about 58.17 ºC. No other transition occurs, which make the nematic phase covers this wide range of temperatures.

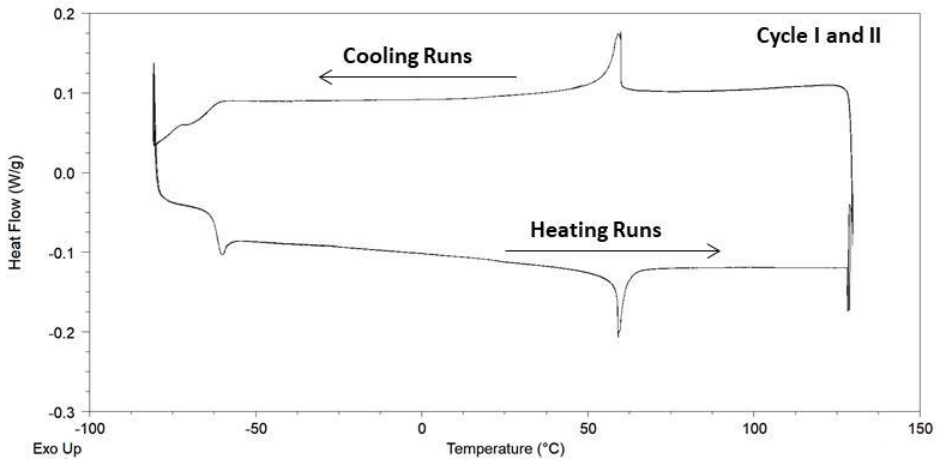

Figure 3.4 – Thermogram obtained from DSC measurement during the Cycle I and II for a pure liquid crystal E7. The cycle I correspond to the first heating and cooling runs and cycle II to the second heating and cooling runs, both at 5 ºC min^{-1}.

For POM experiments a temperature-controlling unit was also used. The samples were heated at a rate of 1 ºC min^{-1} from 25 to 70 ºC. The T_{NI} was taken as the temperature where the sample became optically clear under crossed polarizers. The same heating was repeated two times for each sample. The liquid crystal phase transition temperatures from nematic to isotropic determined by POM are reported in Table 3.2.

Table 3.2 – Nematic to isotropic transition temperatures (T_{NI}) determine by POM under crossed polarized during heating a rate of 1 ºC min^{-1} from 25 to 70 ºC, for TriEGDM/E7, TetraEGDM/E7, PEGDM550/E7, PEGDM875/E7 PDLCs and for pure LC E7.

Sample	T_{NI}(ºC)
TriEGDM/E7 PDLCs	58.9
TetraEGDM/E7 PDLCs	59.2
PEGDM550/E7 PDLCs	59.0
PEGDM875/E7 PDLCs	59.0
E7	58.0

At the nematic-isotropic transition temperature of E7, the PDLC films under crossed polarized became fully transparent. This high transparent state of the PDLCs films is due to a reduction in the refractive index mismatch which results from the thermal motions of the LC molecules[101,102].

Although the different electro-optical response (Figure 3.2) the T_{NI} (Table 3.2) seems to remain identical on average at 59 ºC and independent of polymer matrix type.

3.4 Glass Transition Temperature and Permanent Memory Effect

The glass transition temperature of the polymer matrix could have direct implications in the PME of PDLCs. In this way to determine the transition temperatures and their associated enthalpies

differential scanning calorimetry (DSC) was used. For thermal analysis of polymers, the thermal polymerizations were initiated inside the DSC furnace.

Thermal properties of PEGDM875 and PEGDM550 and result polymers obtained by DSC during the Cycle I and II are shown in Figure 3.5 and Figure 3.6, respectively. The cycle I correspond to the first heating and cooling runs and cycle II to the second heating and cooling runs.

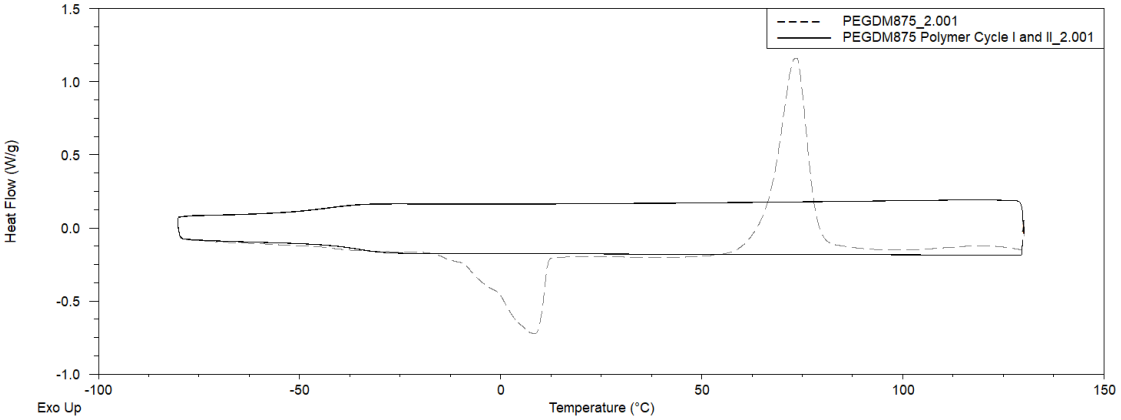

Figure 3.5 – Thermograms (heat flow vs. temperature) of a mixture of PEGDM875 oligomer with 1wt.% of AIBN collected at the heating scan at 5 ºC min^{-1} and for PEGDM875 polymer collected with two heating and cooling cycles at 5 ºC min^{-1}.

In the first heating cycle, the pre-polymer PEGDM875 melt peak is observed at 8.10 ºC followed by a polymerization peak at 73.32 ºC. On cooling PEGDM875 polymer becomes glassy with T_g at - 42.45 ºC and during the heating at -35.51 ºC (Figure 3.5). The EGDMA550 polymer has a similar DSC behavior with a T_g during heating at -12.97 ºC and during cooling at - 13.16 ºC (Figure 3.6).

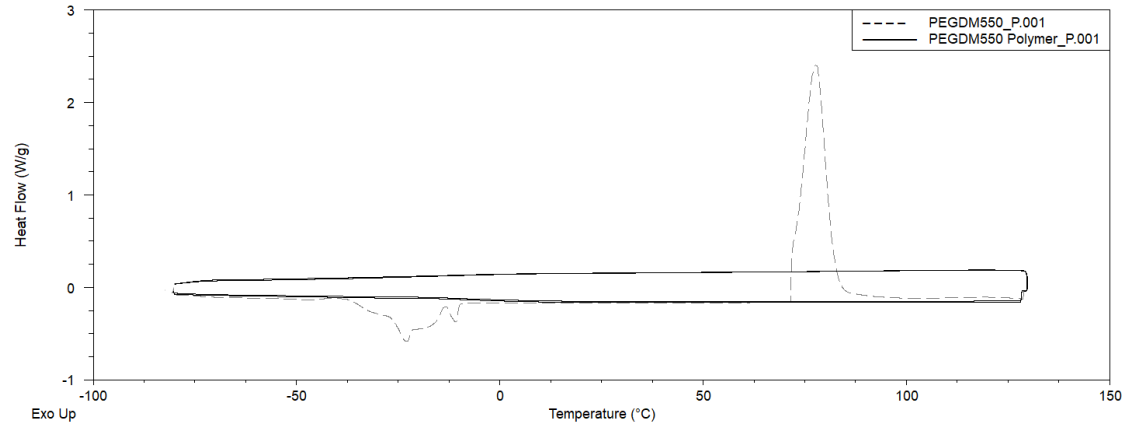

Figure 3.6 – Thermograms (heat flow vs. temperature) of PEGDM550 oligomer with 1wt.% of AIBN collected with a heating scan at 5 ºC min^{-1} and for PEGDM550 polymer collected with two heating and cooling cycles at 5 ºC min^{-1}.

The decrease of polymer chains length in TriEGDM and TetraEGDM polymers increases the attractive forces between chains which hinders the mobility of polymer chains. This result in an increase of the T_g. For this reason, the T_g becomes too flat and diffuse in DSC thermograms and it is not possible to determine the value at the inflection point. In this way, the DSC is not sensitive enough due to the small heat capacity values between glassy and rubbery regions[103]. Nevertheless, in literature, the T_g for TriEGDMA polymer is estimated at 146 ºC [104] and for TetraEGDMA polymer at 125 ºC[104].

The value range of T_g (from T_g = 146 ºC to T_g = - 35.51 ºC) of polymer matrix studied make possible to relate the working principles of PME with polymer plasticity at room temperature.

3.5 Polymer Glass Transition Temperature and Permanent Memory Effect

Polymer around LC domains surface gets entangled LC molecules. During the electric field application, if polymer chain segments mobility is poor (T_g higher than room temperature) means that at boundaries LC molecules have a fixed orientation and even when LC molecules in bulk of domains align with the external electric field, the LC molecules orientation in the surface of polymer matrix remains unchanged. In this way, after switching off the electrical field, the orientations of LC molecules at bulk returns to randomly state because elastic forces that originate at the surface between LC molecules and the polymer action on the free LC molecules to restore the random configuration of lower energy (Figure 3.7 a)). Therefore, LC molecules return to a local energy minimum. So, the alignment achieved will only persist so long as the electric field is applied, and when it is removed, the multi-domain texture will reappear. An applied electric field can reorient the LC molecules so that the PDLC becomes transparent, but the scattering state always returns when the electric field is removed.

However, this limitation might be overcome if the T_g of the polymer matrix is lower than room temperature. In this case, the surface structure of polymer chain segments can be affected by the LC alignment. When LC molecules reoriented along to the electric field easily involve polymer chains at boundaries to form a new conformation. In this case, the electrical field in addition to changes the orientation of the entire LC volume it also changes the orientation of LC molecules in a near polymer boundary layer of LC domains. With the application of an electric field, the preferred alignment of LC director at the surface would be different than in it was before the application of the electric field. LC molecules at the interface with the polymer involve polymer chains in the reorientation process and these LC molecules at boundaries also align. This new preferred anchoring orientation will exert aligning forces on the free molecules trying to keep the LC director align even when the electric field is removed (Figure 3.7 b). The LC molecules also reached a stable state although the opposite order than it was prior to the application of the electric field. The higher transparency obtained in the OFF state permanently persists upon removal of the applied electric field giving rise to a permanent memory effect. The

correlation between PME and polymer thermal properties is related to the anchoring ability of polymer matrix [18,105].

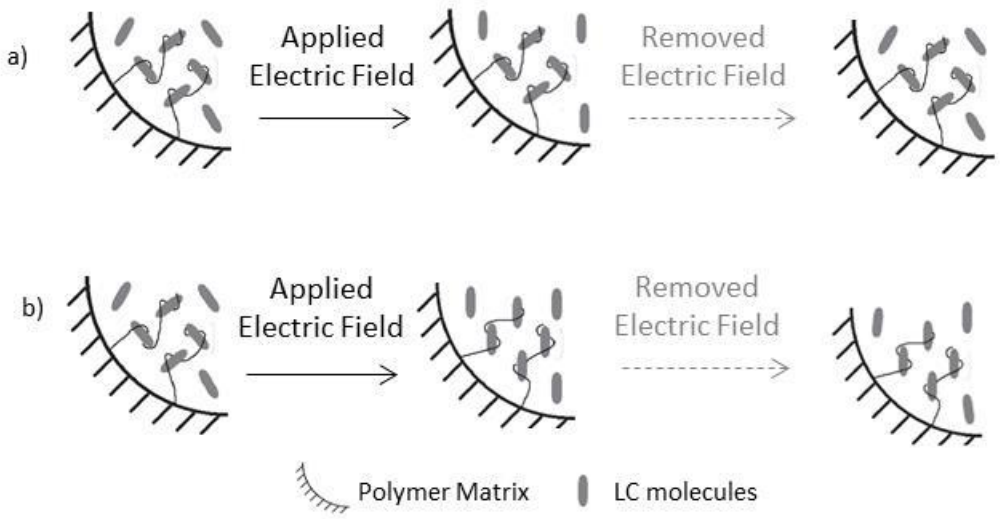

Figure 3.7 – A simplified illustration of liquid crystal orientation influenced by T_g of polymer: a) T_g higher than room temperature (TriEGDM and TriEGDM polymers) and b) T_g lower than room temperature (PEGDM550 and PEGDM875 polymers) (adapted from[106]).

In this way, in PEGDMA550 and PEGDMA875 PDLCs with T_g of polymer lower than room temperature (PEGDM550 polymer at - 12.97 ºC and PEGDM875 polymer at - 35.51 ºC) during the application of electric field LC E7 molecules orient toward the field direction and LC molecules at interface with the polymer involve polymer chains in the reorientation process. The original polymer chain configuration is modified and a new stable configuration is formed. Upon removal electric field, the alignment achieved will persist because polymer structure at boundaries keeps the director of LC align, stabilizing also the LC alignment at bulk which results in a PME (PEGDM 550 PDLC with 63 % of PME and PEGDM 875 PDLC with 70 % of PME). Which indicate that it has memorized the LC alignment induced by the electric field.

However, for T_g of polymer chain higher than room temperature, the polymer at working temperature is glassy (TriEGDM and TetraEGDM polymers) and when the electrical field is applied, most of LC molecules align, except those adjacent to the polymer boundaries. When the electrical field is removed the LC molecules return to the random configuration by elastic forces that originate at the surface between LC and polymer (unchanged LC configuration) and light will be scattered again.

3.6 Solid-State NMR

Solid-state NMR methods have been previously used to study liquid crystal-polymer interactions in PDLCs[107]. Signal intensities recorded with magic angle spinning and cross-polarization are sensitive to the molecular dynamics, and large differences are expected between the solid, liquid-like, and interfacial matter[108]. Depending on the chemical nature of the polymer, the LC

and the preparation techniques, the interface of the LC and polymer will experience different constraints that reflect the molecular dynamics and the protonic environment of the LCs inside the domain. This technique is able to distinguish between an outer layer, with LC molecules anchored and a core of LC molecules which are free to orient under an applied electrical field.

The cross-polarization spectra of E7 and E7/polymer (TriEGDM and PEGDM875) mixtures can be used to distinguish between LC molecules and polymers in rigid and mobile environments. Moreover, it is expectable that upon cross-polarization the signal enhancement will be maximum for rigid materials, while intermediate mobility between solid and liquid will produce smaller enhancements.

In an LC mixture of E7 (Figure 3.8), the methyl, α-methylene and methylene group adjacent to the aromatic core are depicted in grey by CH_3, α-CH_2 and Ar-CH_2, respectively.

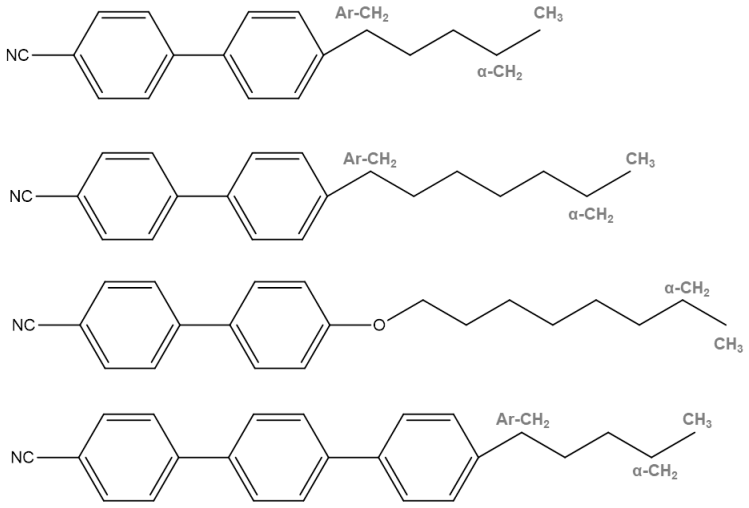

Figure 3.8 – The composition and molecular structures of the components of the nematic LC mixture E7. In the aliphatic chains, the methyl, α-methylene and methylene group adjacent to the aromatic core are depicted in grey by CH_3, α-CH_2 and Ar-CH_2, respectively.

The Figure 3.9 shows the ^{13}C CPMAS spectra of a) E7, b) TriEGDM polymer and c) TriEGDM/E7 PDLC. The Figure 3.10 shows the ^{13}C CPMAS spectra of a) E7, b) PEGDM875 polymer and c) PEGDM875/E7 PDLC. On both Figures, one can clearly identify in the PDLC spectra the contributions of the respective polymer and the LC.

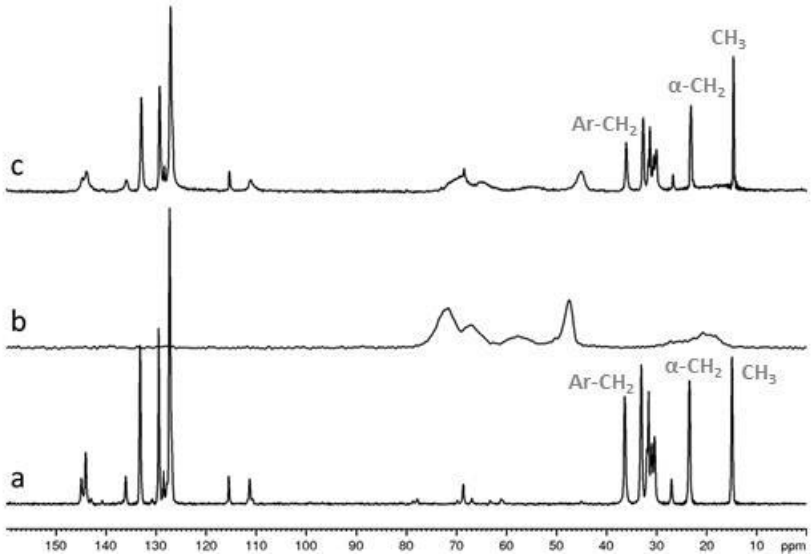

Figure 3.9 – ^{13}C CPMAS spectra of (a) E7, (b) TriEGDM polymer and (c)TriEGDM/E7 PDLC. In aliphatic peaks, the methyl, α-methylene and methylene group adjacent to the aromatic core are depicted in grey by CH_3, α-CH_2 and Ar-CH_2, respectively.

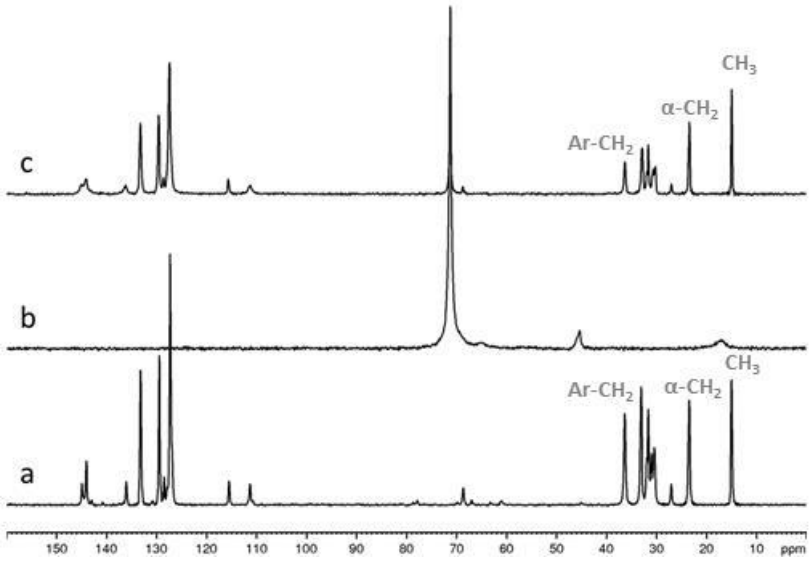

Figure 3.10 – ^{13}C CPMAS spectra of (a) E7, (b) PEGDM875 polymer and (c) PEGDM875/E7 PDLC. In aliphatic peaks, the methyl, α-methylene and methylene group adjacent to the aromatic core are depicted in grey by CH_3, α-CH_2 and Ar-CH_2, respectively.

In Figure 3.11 signal enhancement from cross-polarization is observed not only for the polymer but also from the aromatic and aliphatic E7 signals in all the studied mixtures. It is noticeable that this effect depends on the polymer nature, exhibiting with PEGDM875 a different behavior from the smaller polymer chains TriEGDM. These enhancements can arise either from the liquid crystalline material at the interface between the polymer and the liquid crystal as a consequence of the different protonic environments or the existence of different segmental mobility inside the LC domain. This different mobility is a consequence of different dynamic

properties of PEGDM875 and TriEGDM PDLCs, experimentally evidenced by the T_g and E_{90} measurements.

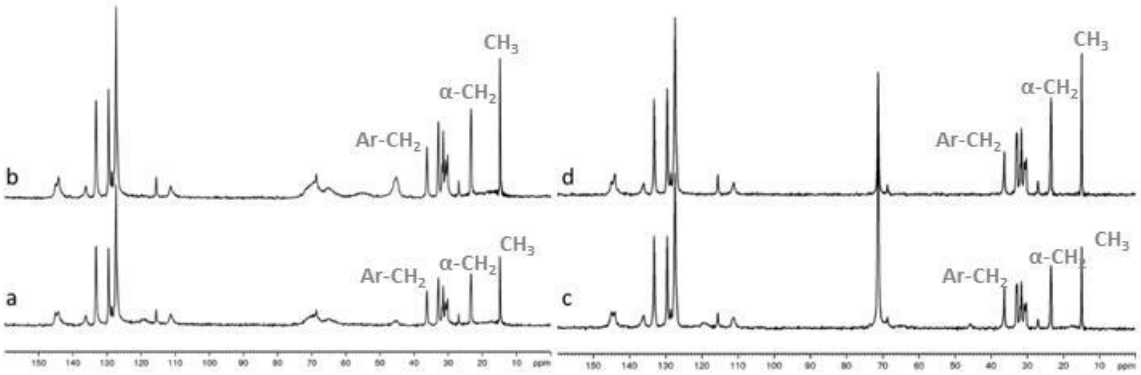

Figure 3.11 – ^{13}C MAS spectra of (a,b) TriEGDM/E7 PDLC and (c,d) PEGDM875/E7 PDLC. The spectra were acquired (a, c) without and (b, d) with cross-polarization. In aliphatic peaks, the methyl, α-methylene and methylene group adjacent to the aromatic core are depicted in grey by CH_3, α-CH_2 and Ar-CH_2, respectively.

The signals enhancement from cross polarization has been measured in the ^{13}C MAS spectra of the two EGDM/E7 PDLCs (Table 3.3). The analysis was accomplished by focusing on the behavior of three different regions in the aliphatic spectral window. The methyl group at 14.9 ppm, the α-methylene group at 23.3 ppm and the methylene group adjacent to the aromatic core (Ar-CH_2-) at 36.3 ppm. The corresponding integrated areas of these signals were normalized to the aromatic core resonances at 127.2-129.5 ppm. In LC E7 the Ar-CH_2- exhibits a much higher enhancement compared to the remaining signals in the result of the proximity to the aromatic core and consequent lesser mobility. The analysis of EGDMA/E7 PDLCs discloses a different behavior.

The higher enhancement, resulting from a stronger contact between polymer and LC, reflects a more favorable protonic environment or a slower dynamic modulation of the interaction, both of them taken as a consequence of a more effective anchoring effect.

Table 3.3 – Normalized peak area (area of the aromatic peaks between 127.2 and 129.5 ppm = 1) for nematic LC E7 and for the two different PDLCs TriEGDMA + E7 and PolyEGDM875 + E7. The increment percentage is calculated having the area of each peak obtained using HPDEC as a reference.

PDLC	NMR Peak	δ / ppm	HPDEC	CPMAS	% relative increment
E7	Ar-CH2-	36.3	0.13	0.24	83.2
	α-CH2	23.3	0.19	0.29	55.2
	CH3	14.9	0.20	0.25	21.5
TriEGDMA + E7	Ar-CH2-	36.3	0.13	0.15	17.5
	α-CH2	23.3	0.19	0.23	21.4
	CH3	14.9	0.17	0.23	36.8
PEGDM875 + E7	Ar-CH2-	36.3	0.14	0.13	-6.3
	α-CH2	23.3	0.19	0.24	26.5
	CH3	14.9	0.17	0.23	39.8

For both EGDM/E7 PDLCs the Ar-CH_2- groups present a much lower increment when compared to the respective α-CH_2 and CH_3, suggesting that the methylene groups closer to the aromatic core have higher mobility or a less favorable protonic environment. The CH_3 groups in EGDM/E7 PDLCs exhibit a higher enhancement as a consequence of the anchoring effect of the terminal carbons. The amplitude of the variation of the enhancements between the terminal CH_3 and the Ar-CH_2 is greater in the case of PEGDM875/E7 PDLC, suggesting that either the methyl groups are more restrained or the Ar-CH_2 groups have more mobility. This last explication is in agreement with lower electric field required to initiate the transition from light scattering to light transmission (6.40 V μm^{-1} for PEGDM875 polymer/E7 PDLC and 13.84 V μm^{-1} for TEGDM polymer/E7 PDLC) and by an increase in polymer segmental mobility in PEGDM875 polymer (T_g = - 35.51 ºC) than in TriEGDM polymer (T_g = 146 ºC) which in turn increase segmental mobility of the LC molecules less subjected to the polymer anchoring forces. This has direct implications in PME of PEGDM875 polymer/E7 PDLC. The lower anchoring ability of PEGDM875 polymer prevents LC molecules to return a multi-domain texture and high transparency obtained in the OFF state permanently persists upon removal of the electric field, giving rise to 70 % of PME.

3.7 Conclusions

In summary, it was observed that the permanent memory effect of PDLC is greatly influenced by the ethylene glycol linear chain length of methacrylate monomers. For the studied molecular chain length the permanent memory effect increased with the number of ethylene oxide from 0 % (TriEGDM, n = 3 and TetraEGDM, n = 4) to 63 % and 70 % (PEGDM550, n ≈ 10 and PEGDM875, n ≈ 16 respectively). The polymer chain length is correlated with the polymer glass transition. The increase of polymer chain length by the increase of the ethylene oxide units decreases the glass transition temperature. With a polymer with a glass transition temperature lower than room temperature (PEGDM550 polymer (- 12.97 ºC) and PEGDM875 polymer (- 35.51 ºC) after the application of an electric field the preferred alignment of polymer chain segments at the interface between polymer and LC would be different than it was before application of the electric field. This new polymer chain segments structure keep LC molecules at interface align which stabilized LC bulk alignment and the order induced by electric field was kept memorized. The strong influence of the chain length in permanent memory effect was also

explained by ^{13}C NMR relaxation spectroscopy applied to PDLCs in terms of LC molecules mobility change as a function of contact between LC and polymer. The segmental motions of the LC molecules in PDLC become more unlimited as polymer chain length increases (from $n = 3$ to $n \approx 16$) which in turn promotes permanent memory effect.

In this way, an intimate relationship exists between the polymer matrix and permanent memory effect in PDLCs. As previously mentioned the polymer matrix is not just a mechanical support of LC domains but influences the efficiency of the permanent memory effect.

Chapter IV

4 Appropriate Polymer Matrix Morphology in appearance of Permanent Memory Effect

In order to better understand the permanent memory effect found in PDLC prepared with the PEGDM875 oligomer, different polymerization conditions of PDLCs preparation were investigated. These conditions include the effect of the curing temperature in thermal polymerization and different UV light intensity in photochemical polymerization as well as time exposure during the polymerizations.

It was found that these two polymerization types differ mainly in morphology acquire by polymer matrix during phase separation which in turn determines the permanent memory effect.

4.1 Morphological Evolution of Polymer Matrix: Comparison between Thermal and Photo-Polymerization

Polymerization type determines the phase separation process and the development of the morphology during polymerization. Therefore, the properties of PDLC films prepared using either thermal or photo-polymerization have been compared. The phase separation phenomenon between LC and polymeric matrix in PDLCs preparation is a kinetic process where the transport parameters, the rate of polymerization and physical parameters as the viscosity of the systems can play an important role on the size and the shape of liquid crystal domains[37,68,109–114]. The relation between size and distribution of the liquid crystal domains in the polymer matrix and the time used in the polymerization of PDLC films was investigated by POM with crossed polarisers. It is obvious from Figure 4.1 of polarized optical micrographs for representative results for thermal polymerizations and Figure 4.2 and Figure 4.3 for photochemical polymerizations that these two types of polymerizations promote different shapes and sizes of LC domains.

In thermal polymerization, the low matrix viscosity promotes a homogeneous diffusion of LC molecules in a continuous LC phase embedded in the polymer matrix. So the initial spherical LC domains dispersed in the polymer matrix (Figure 4.1 a) become in continuous LC dispersion (Figure 4.1 e). It is also evident from (Figure 4.1 f) that even after the electric field was removed, LC molecules remain align (the region where electric field was applied is more bright).

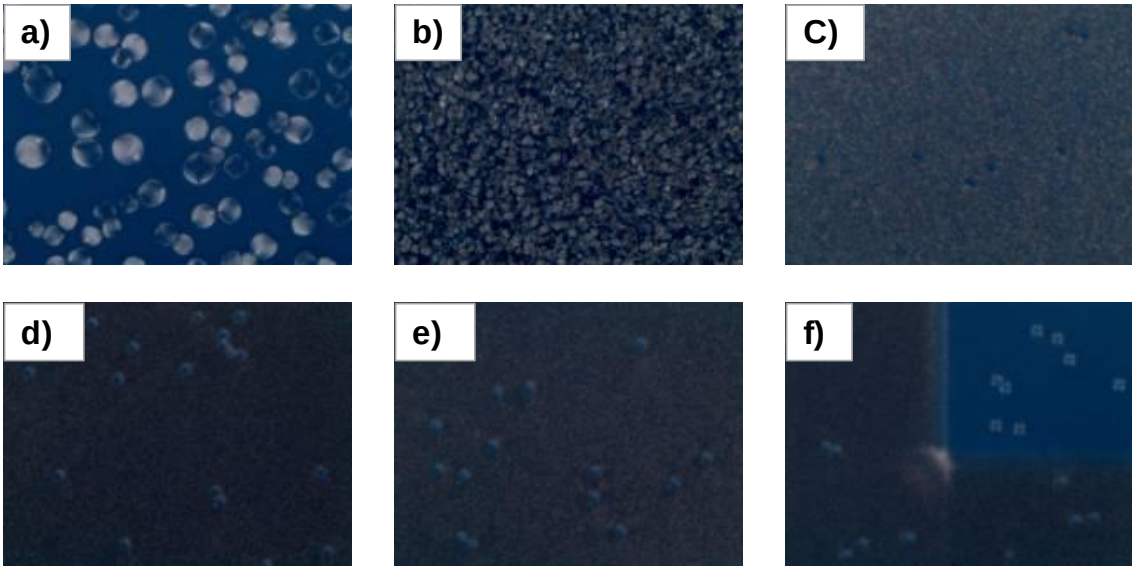

Figure 4.1– The evolution of phase separation morphology observed by polarized optical micrographs with crossed polarizers of PDLC films prepared with the PEGDM875 (1 wt.% of AIBN)+E7 in a weight ratio of 30/70 (wt.%) thermally polymerized at 70 ºC with different polymerization time in initial OFF state: (a) 4 min; (b) 5 min; (c) 6 min; (d) 20 min; (e) 60 min and (f) 60 min in OFF state but upon removal the applied electric field, x100 magnification.

In photochemical polymerization, the viscosity at room temperature shortens the interval between initial phase separation and polymer matrix gelation and LC molecules came out from solution arranged in spherical domains (Figure 4.2 and Figure 4.3).

At high UV curing intensity (48 mW cm^{-2}) a phase separation occurred within 300 s of UV exposure because LC domains diameter in average remains unchanged during exposure time. The diffusion of LC molecules through the highly viscous medium is hindered. In this way, small and monodispersed domains are formed because the diffusion and coalescence of the LC domain cannot follow the gelification of the matrix (Figure 4.2).

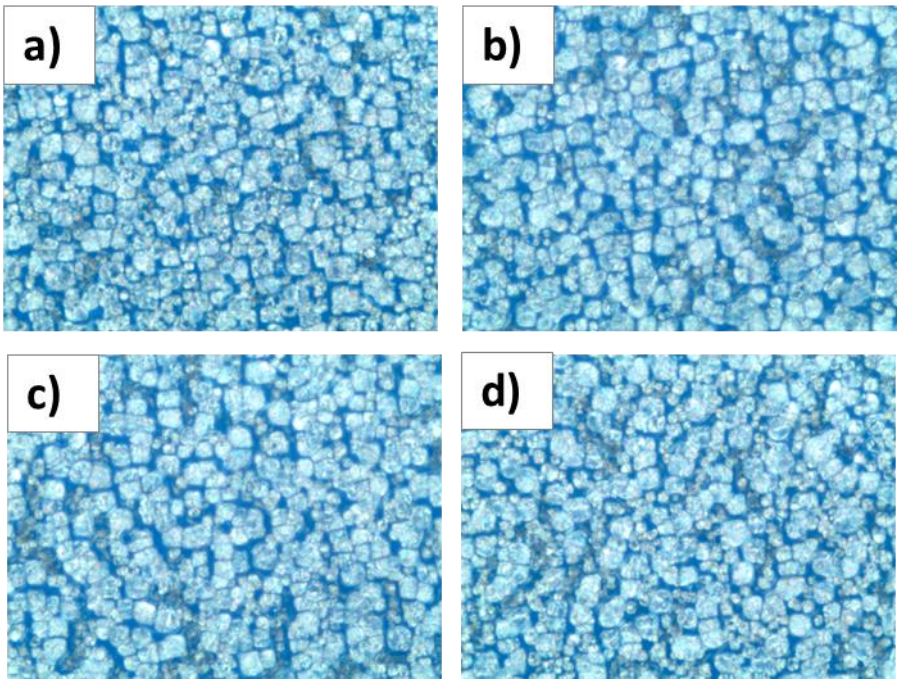

Figure 4.2 –The evolution of phase separation morphology observed by polarized optical micrographs with crossed polarizers of PDLC films prepared with the PEGDM875 (1 wt.% of XDT)+E7 in a weight ratio of 30/70 (wt.%) photochemically polymerized at curing 366 nm UV light intensity 48 $mWcm^{-2}$ with different exposure time: (a) 300 s; (b) 500 s; (c) 700 s and (d) 900 s in initial OFF state, x100 magnification.

However, at low UV curing intensity at 0.48 mW cm^{-2} the polymer gel point is slowly reached and the phase separation process is slow. In this way, the phase separation between liquid crystal and polymer matrix occurs during the slow progress of the cure reaction which allows enough time for growth, diffusion and coalesces of the domains resulting in relatively large LC domains (Figure 4.3).

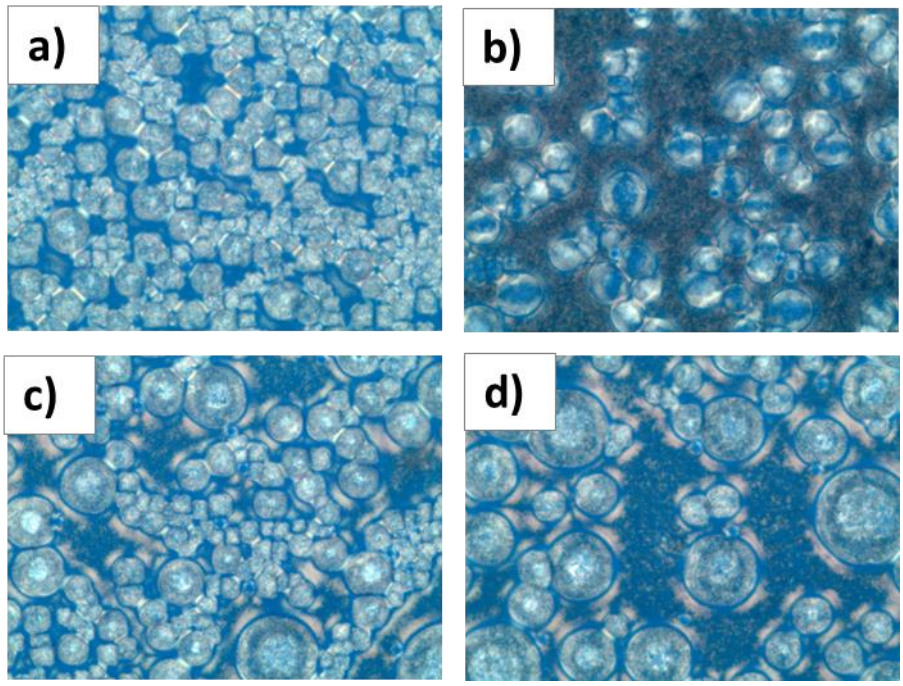

Figure 4.3 – The evolution of phase separation morphology observed by polarized optical micrographs with crossed polarizers of PDLC films prepared with the PEGDM875 (1 wt. % of XDT) +E7 in a weight ratio of 30/70 (wt.%) photochemically polymerized at curing 366 nm UV light intensity at 0.48 mWcm^{-2} with different exposure time: (a) 30000 s; (b) 50000 s; (c) 70000 s and (d) 90000 s in initial OFF state, x100 magnification.

The results described by POM with crossed polarizers for the morphology of the polymer matrix were confirmed with those obtained by scanning electronic microscopy. The representative micrographs of polymer matrix microstructure for samples thermally polymerized are presented in Figure 4.4 and photochemically polymerized in Figure 4.5 and Figure 4.6. In Figure 4.4 the polymer matrices microstructure can be identified as polymer-ball morphology.

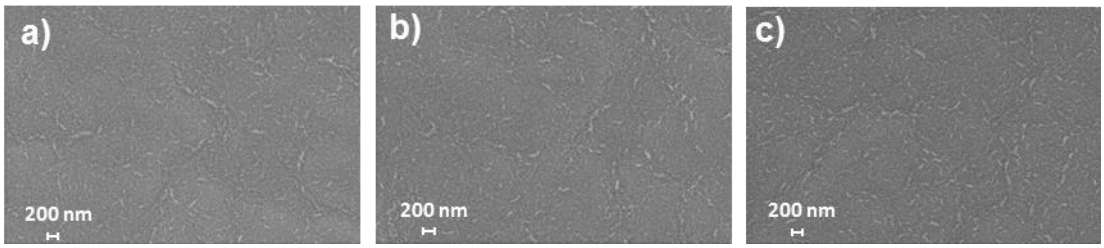

Figure 4.4 – Scanning electronic microscopy micrographs for the microstructure of the polymer matrix of the PDLC films prepared with the PEGDM875(1 wt.% of AIBN)+E7 in a weight ratio of 30/70 (wt.%) thermally polymerized at different temperatures and times: a) 60 ºC, 90 min; b) 66 ºC, 60 min; c) 90 ºC, 10 min.

On the other hand, polymer matrices microstructure in Figure 4.5 and Figure 4.6 can be assigned to swiss cheese morphology where LC molecules were confined within isolated microdroplets. However, the morphologies types were not affecting by polymerization kinetics. In this way, independently of temperature, the thermal polymerization promotes polymer ball

morphology and independently of UV light intensity the photochemical polymerization produces a swiss cheese morphology.

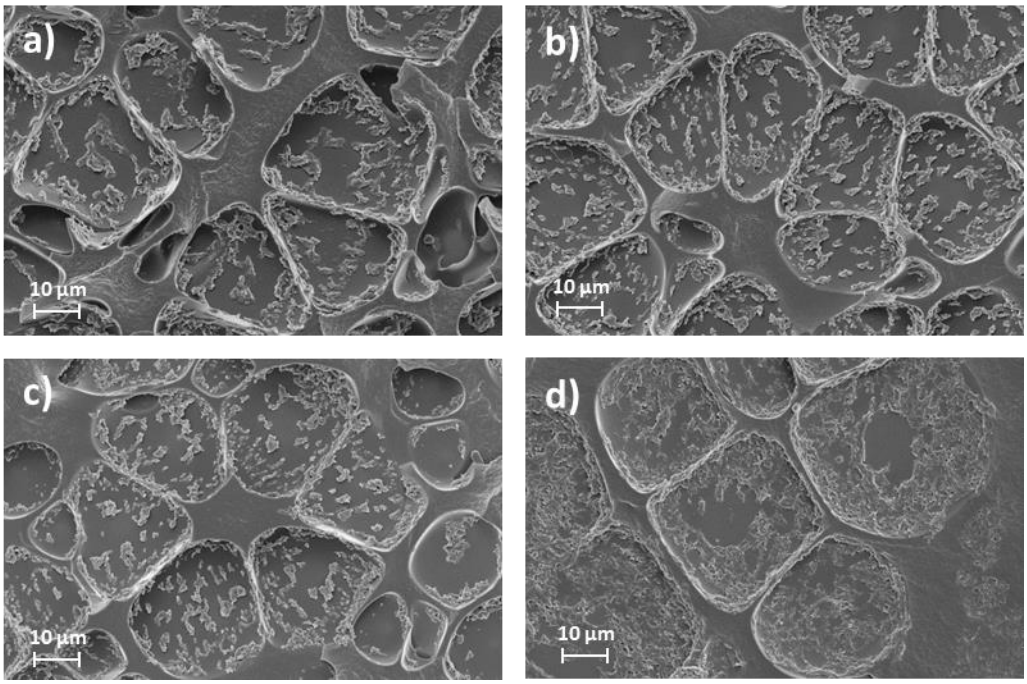

Figure 4.5 – Scanning electronic microscopy micrographs for the microstructure of the polymer matrix of the PDLC films prepared with the PEGDM875 (1 wt.% of XDT)+E7 in a weight ratio of 30/70 (wt.%) photochemically polymerized at 366 nm UV light curing intensity at 48 $mWcm^{-2}$ during different times: a) 300 s; b) 500 s; c) 700 s; d) 900 s.

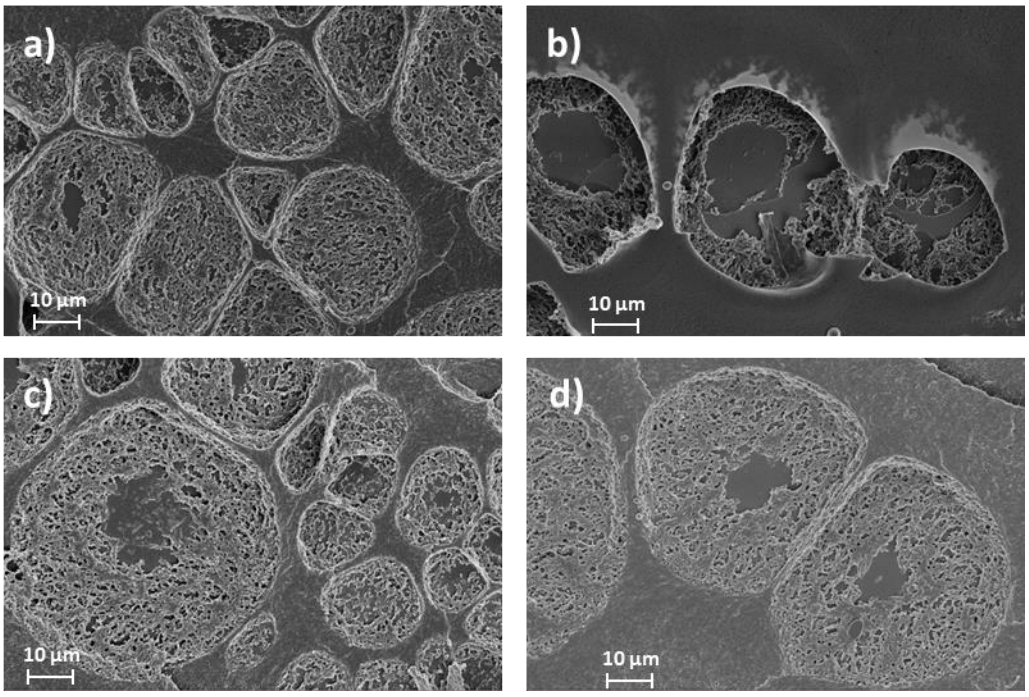

Figure 4.6 – Scanning electronic microscopy micrographs for the microstructure of the polymer matrix of the PDLC films prepared with the PEGDM875(1 wt. % of XDT)+E7 in a weight ratio of 30/70 (wt.%) photochemically polymerized at 366 nm UV light curing intensity at 0.48 $mWcm^{-2}$ during different times: a) 30000 s; b) 50000 s; c) 70000 s; d) 90000 s.

The average LC domain diameter, determined by the analysis of scanning electronic microscopic images is plotted versus curing time for each UV curing light intensity as shown in Figure 4.7.

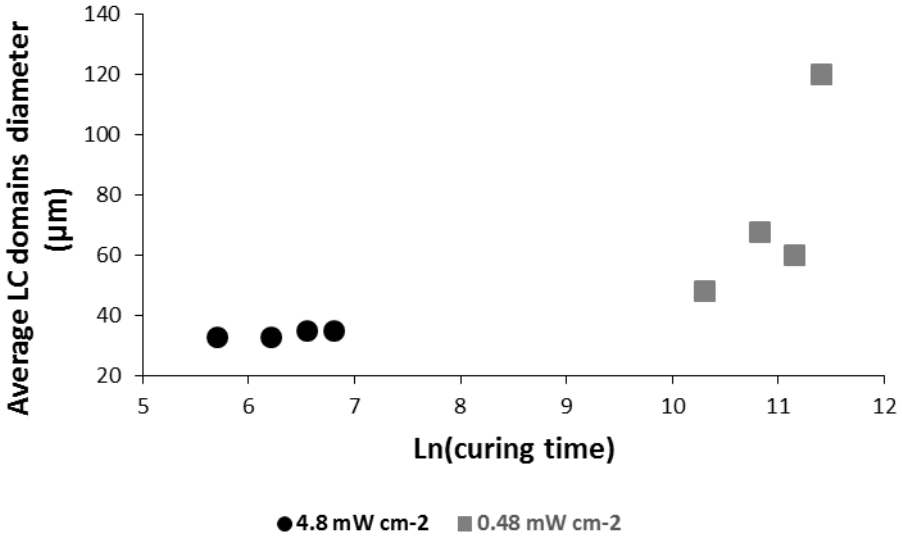

Figure 4.7– Dependence of average LC domains diameter with the UV exposure time for each UV curing light intensity used. The average size of the liquid crystal domains was determined using scanning electronic microscopies images.

The morphologies type identification was also evaluated by confocal microscopic images of PDLC films presented in Figure 4.8 which are also in agreement with the morphologies identified by scanning electronic microscopy in Figure 4.4, Figure 4.5 and Figure 4.6. With confocal microscopy it is possible to better understand that in a polymer ball morphology type for thermally polymerized matrices the LC is a continuous phase embedded in a polymer beads network, such polymer forms a sponge structure (Figure 4.8 a). On the other hand, LC domains isolated from one another dispersed in a continuous polymer matrix are observed for the photochemically polymerized matrices, characteristic of the swiss-cheese morphology type (Figure 4.8 b).

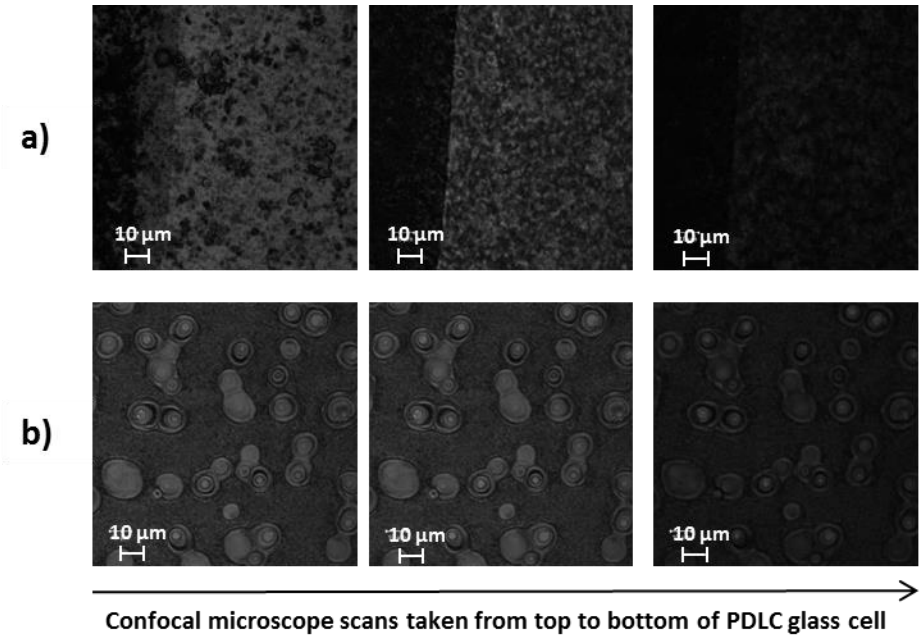

Figure 4.8 – Confocal visible microscopy scans through the entire thickness of the PDLC glass sample: a) 20 µm of PDLC cell thickness for polymer-ball morphology and b) 5 µm PDLC cell for swiss-cheese morphology. In the images, the polymer matrix appears as dark regions and bright regions are LC domains.

Combined polymer matrix morphology characterization by polarized optical microscopy (Figure 4.1,Figure 4.2 and Figure 4.3), scanning electronic microscopy (Figure 4.4, Figure 4.5 and Figure 4.6) and confocal microscopy analysis (Figure 4.8) confirmed that although the PDLC mixture (70 wt.% of E7 and 30 wt.% of PEGDM875) is the same, the thermal polymerization promotes a polymer-ball morphology and photochemical polymerization generates a swiss-cheese morphology, that influences the appearance of PME, as will be shown below.

4.2 Electro-Optical Properties of PDLC

4.2.1 Thermal Polymerization

Representative examples of electro-optical responses for PDLC films thermally polymerized at 55, 70, 74 and 90 ºC are shown in Figure 4.9. The detailed information obtained by the electro-optical measurements (%PME and E_{90}) for PDLC films polymerized at all different cure temperatures (55, 60, 66, 70, 74, 80 and 90 ºC) is summarized in Table 4.1. It is evident that independently of polymerization temperature the correspondently PDLCs have a permanent memory effect. The percentage of this effect it is however dependent on polymerization temperature.

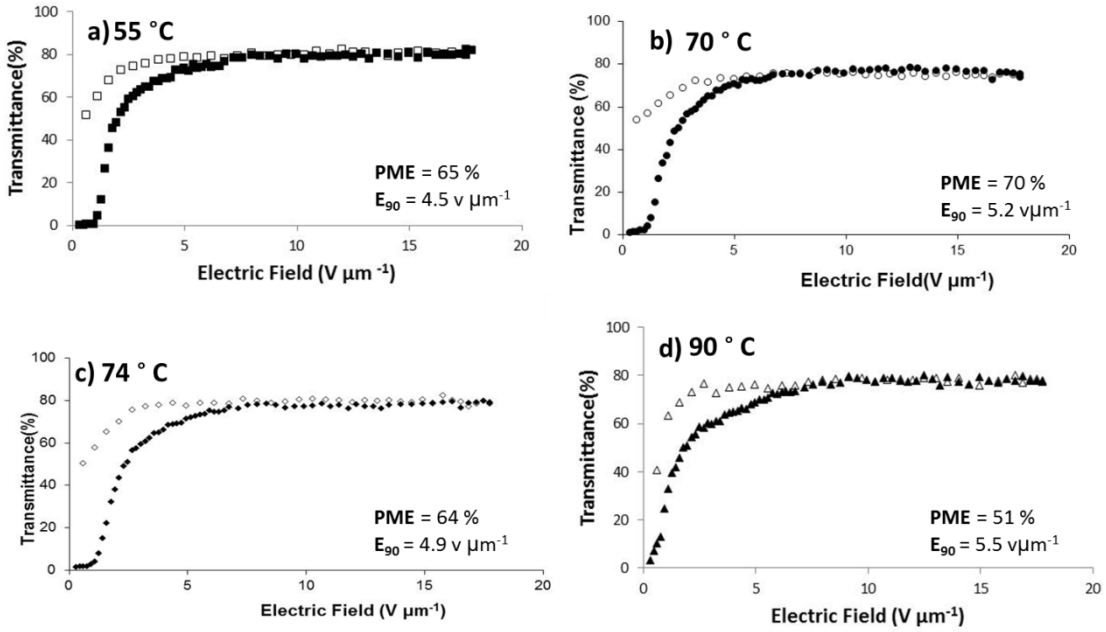

Figure 4.9– The electro-optical response optimized for PDLC films prepared with the PEGDM875(1 wt.% of AIBN)+E7 in a weight ratio of 30/70 (wt.%) and polymerized at different temperatures and times: (a) 55 ºC, 120 min (b) 70 ºC, 120 min (c) 74 ºC, 40 min (d) 90 ºC, 10 min. The transmittance was measured by applying increasing electrical field (filled symbols) and decreasing electrical field (open symbols).

Table 4.1 – Percentage of PME and E_{90} obtained by the electro-optical measurements of PDLC films polymerized at different cure temperatures (55, 60, 66, 70, 74, 80 and 90 ºC).

Polymerization temperature (ºC)	**E_{90} (V µm^{-1})**	**(%) PME**
55	4.5	65
60	3.7	64
66	3.6	69
70	5.2	70
74	4.9	64
80	2.7	57
90	5.5	51

Thus, PDLCs polymerized at 66 ºC and 70 ºC with nearly 70 % of PME, both started from an opaque state (T_0 = 0 %) show the best efficiencies. In addition, for these polymerization temperatures, the permanent memory effect percentages remain unchanged even after all night polymerization time. At higher temperatures such as 80 ºC and 90 ºC, the diffusion of LC molecules cannot follow the rate of polymer matrix gelification which decreases the amount of LC molecules in domains separated from the polymer matrix. Electro-optical properties are affected with respect to lower curing temperatures.

4.2.2 Photochemical Polymerization

The phase separation kinetics was investigated as functions of curing light intensity. In this way, two light intensities at 48 mW cm^{-2} for 300, 500, 700 and 900 s of exposure times and light

intensity at 0.48 mW cm^{-2} for 30000, 50000, 70000 and 90000 s of exposure times, both monochromatic at 366 nm, were used to prepare the PDLC films.

From the dependence of light transmission as a function of the applied electrical field, it is evident that independently of UV light intensity and exposure time the transmittance always returns to its original value corresponding to the initial scattering state when the electrical field was removed. Which result in PDLCs without permanent memory effect. The representative electro-optical responses for the UV light intensity of curing at 48 mW cm^{-2} during 900 s and at 0.48 mW cm^{-2} during 90000 s are shown in Figure 4.10.

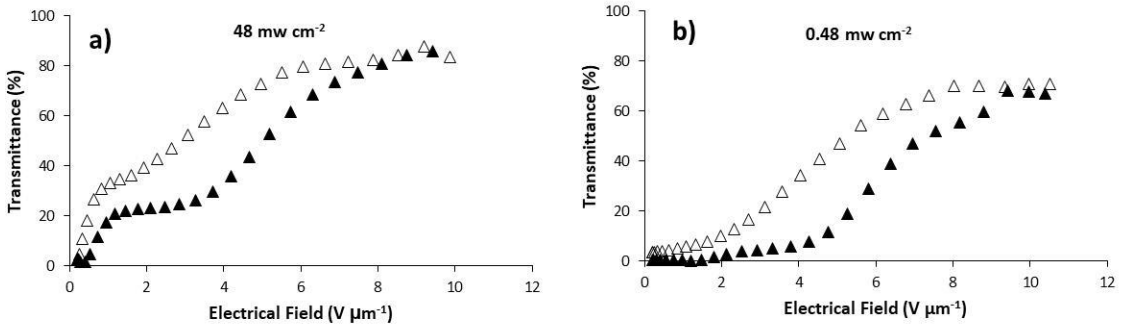

Figure 4.10 – The electro-optical response for PDLC films prepared with the PEGDM875(1 wt.% of XDT)+E7 in a weight ratio of 30/70 (wt.%) and polymerized at different curing UV 366 nm light intensities and times: a) 48 mW cm^{-2}; 900 s; b) 0.48 mW cm^{-2}; 90000 s. The transmittance was measured by applying increasing electrical field (filled symbols) and decreasing electrical field (open symbols).

The increase of exposure time from 500 to 900 s for 48 mW cm^{-2} and from 50000 to 90000 s for 0.48 mW cm^{-2} did not change the behavior of electro-optical response (Figure 4.11).

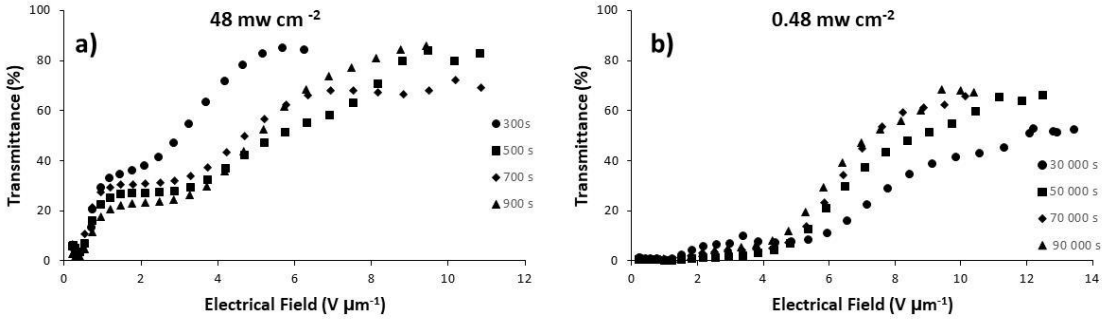

Figure 4.11 – The electro-optical response for PDLC films prepared with the PEGDM875(1 wt.% of XDT)+E7 in a weight ratio of 30/70 (wt.%) and polymerized at different curing UV light intensities and times: a) 48 mW cm^{-2}; 300, 500, 700 and 900 s; b) 0.48 mW cm^{-2}; 30000, 50000, 70000 and 90000 s. The transmittance was measured by applying increasing electrical field (filled symbols) and decreasing electrical field (not shown).

In this way, for each UV light intensity, the exposure times of 500 and 50000 s are times for the major phase separation process.

4.3 Polymer Ball and Swiss Cheese Polymer Matrix Morphology in Permanent Memory Effect

The results obtained confirm that permanent memory effect in PDLCs studies is dependent on the polymerization conditions which determine the morphology of the polymeric matrix. Thermal polymerization promotes polymer ball morphology which promotes PDLC with permanent memory effect unlike those prepared by photochemical polymerization with a swiss cheese morphology.

The shape of liquid crystal domains influences the balance of elastic forces within the domains. Most polymers induce a parallel alignment of the LC molecules and therefore the most common droplet alignment is the bipolar configuration. In this configuration, the nematic director follows the surface curvature from one pole to the other. Liquid crystal domains with a higher degree of curvature provide higher elastic free energy [18].

Polymer ball morphology is an extreme LC spherical domain distorted shape. The polymer appears as an agglomerate of polymer beads forming an irregular network that is in contact with a continuous liquid crystal phase providing a high degree of interconnection between LC domains. It is a complex geometry where LC is a continuous phase embedded in a polymer bead matrix.

In a swiss cheese morphology characterized by spherical domains surrounded by polymer, strong enough electric fields distort the medium from its lowest energy configuration which increases the elastic free energy. This higher elastic free energy in this align state provides the LC directors to relax to the internal curvature of the domains reducing elastic free energy once the electric field is removed. A strong degree of LC domains curvature will raise the elastic free energy upon reorientation of LC molecules with the electric field. Therefore, upon removal of the electric field the LC molecules in each domain go back for a random configuration to minimize the elastic energy and the PDLC film returns to the opaque state. In polymer ball morphology with asymmetric domains structures, the LC directors are not influenced by a higher degree curvature of domains and many degenerate alignment directions (defects) for the LC exist. Upon removal of the electric field, the LCs are not forced to go back to the initial configuration and relax to the nearest degenerate alignment state, which is likely along a direction near to the applied field remain to align parallel to each other in a collective alignment (stable arrangement)[18,115]. LC will adopt the configuration which will minimize both the number and the strength of the defects[116].

The different arrangement of LC molecules in the two types of morphologies determines the strength of restoring forces which control the appearance of permanent memory effect.

4.4 Conclusions

It was clearly shown that polymerization type in PIPS method of PDLC films prepared with poly (ethylene glycol) dimethacrylate with a molecular mass of ≈ 875 $gmol^{-1}$ (PEGDM875) has a profound effect in polymer matrix morphology which determines the permanent memory effect. Thermal polymerization, unlike photochemical polymerization, promotes the attainment of PDLC with great permanent memory effect percentage (70 %). The mechanism of this polymerization type promotes the formation of polymer-ball morphology in contrast to photochemical polymerization which promotes swiss-cheese morphology. The continuous LC phase dispersed in polymer ball morphology minimizes the LC elastic energy and upon removal, the electric field LC molecules tend to remain aligned parallel to each other in a collective alignment. In this way, a highly transparent state was kept resulting in a permanent memory effect. The PEGDM875 polymer with a low glass transition temperature at - 35.51 ºC reflects the rubbery state of the PDLC matrix at room temperature, which also promotes the appearance of permanent memory effect. Although the UV light curing conditions used cannot create permanent memory effect in PDLC films, they can be used to produce morphologies in PDLC films with a controllable gradient of LC domains size.

In summary, the results demonstrate that in thermal polymerization, temperature and time of polymerization are regulatory effects that enhance the permanent memory effect. Electro-optical measurements of PEGDM875 PDLC films prepared with different polymerization conditions showed that devices with permanent memory effect were optimized for thermal polymerization from 66 ºC to 70 ºC, respectively. In these conditions, PDLCs with 70 % of permanent memory effect were developed. The PME percentage remains unchanged even after all night polymerization time.

Chapter V

5 Di-Functional PEG with long linear chain length

As previously shown in chapter III, the increased in the length of the ethylene glycol chain in pre-polymer increases the permanent memory effect. In this way, the relationship between longer linear chain length PEG polymerizable oligomers and electro-optical properties of the corresponding polymer dispersed liquid crystal (PDLC) films was investigated. With these propose a series of di(metha)acrylate oligomers from polyethylene glycol with various molecular masses (M_w = 1000, 2000, 4000 and 6000 g mol^{-1}) to be incorporated as the polymer matrix in PDLCs devices were synthesized. Combined analyses of ^{1}H-NMR, ^{13}C-NMR and MALDI-TOF mass spectroscopy were used to confirm the structure and purity of the products. It was found that the length of the molecular chain of pre-polymers greatly affects the polymer thermal properties (amorphousness and crystallinity), which in turn influence the permanent memory effect.

5.1 Amorphousness and Crystallinity in Polymers

Polymers can form an amorphous or crystalline state. Crystalline polymers have a preferred chain conformation and can form a “regular” structure unlike in amorphous polymers formed by disordered structure[28,117]. In a simple way, this last state can be represented by a tangled mass of chains rather like a bowl of spaghetti. Nevertheless, it is possible that there is some vague and very local order, as in crystalline polymers which can also have local amorphous regions[31].

When sufficiently cooled, amorphous polymers can resemble glass. Above this glassy state, the segmental mobility is not zero and short-range vibrational and rotational motions of the segments are possible. The occurrence of these segmental motions gives the polymer some ductility. At temperatures above the glassy state, larger molecule motion returns and amorphous polymers resemble rubbers, if crosslinked. If uncrosslinked, amorphous polymers resemble very viscous liquids in their properties. The temperature at this transition is T_g[28]. The value of T_g is very dependent on the attractive forces between chains, the repeating unit, the molecular architecture, the number of functionalities and the molecular weight[31].

In general, for linear chains, the decreasing of the molecular weight increased the attractive forces between chains. Therefore, more heat energy to go from a glassy to a rubbery state is required. In this way, the T_g values of the corresponding polymers increase by decreasing the oligomer molecular weight[31,95]. In the other hand, when the molecular chain length increase is too large highly entangled of the long chains in the melt can form a crystalline state[118–120]. The long chain nature of macromolecules makes their mechanism of crystallization and crystal

morphology substantially different from those of small molecules[121]. Therefore, there is a great contrast in the crystallization process between atomic or low molecular weight and macromolecular systems[122]. Polymer chain length between short and longer ones can only form randomly coiled and entangled chains impart amorphoness[95].

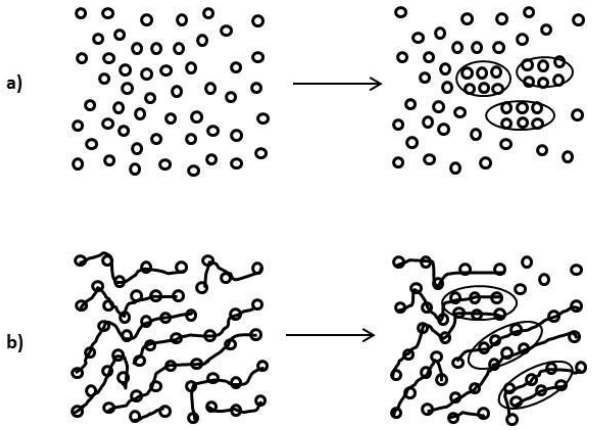

Figure 5.1– Schematic illustration of the crystallization behavior in a) atomic or short chain molecular system and b) macromolecular system (adapted from[123]).

For small molecules, it is easy each atom or molecule can be transported and rearranged independently into crystalline points (Figure 5.1 a). The mechanism for a liquid of small molecules undergoes to a phase transition into a crystal involves the nucleation and growth states. In this way, the first step is the formation of a nucleus of the crystalline phase followed by the growth of such nuclei. However, in macromolecular systems, each molecule from the polymer chain should be transport and rearranged under strong restriction due to the entangled in longer polymer chains. In this condition the chains have to slide along the chain axes for rearrangement into crystalline phase (Figure 5.1 b)[122].Although, chain folding is predominant in crystallization process there are still many chains that remain in a disordered structure. Which result in a semi-crystalline morphology[118].

In this way, the morphology of semi-crystalline macromolecules consists in chains thread their way through several fibrillary crystallites via intermediate amorphous regions. The same chain can pass alternately through ordered and disordered regions[124] (Figure 5.2). When crystallization is carried out from concentrated solutions or melt, multilamellar aggregates are formed. The most common structure consists of radiating arrays of period lamellar from a core that are linked together with the amorphous region in between and crystal aggregates are formed normally in a circular crystalline shape known as spherulites[125].

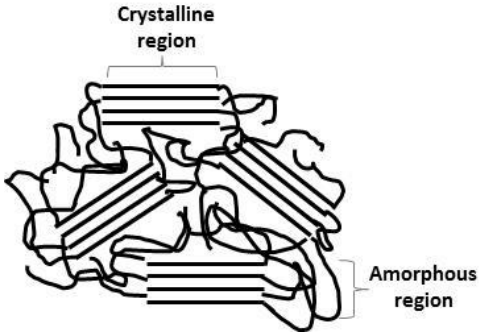

Figure 5.2 – Schematic illustration of a finged-micelle model of the microstructure of semicrystalline macromolecules (adapted from[124]).

For folded chain crystals morphologies result it is necessary a critical molecular weight for chains starts to fold. If the sample is above the critical molecular weight than folded chain crystals can result. A minimum chain length is necessary to form a crystallite, by other words, it is necessary a molecular chain long enough to fold and to crystallize[98,126]. In a highly crystalline polymer, the small amorphous component is severely constrained by the crystals. Molecular chains that have a length lower than the critical length are excluded from the chain fold crystallization[124]. Normally, below of the critical molecular weight polymer chains are only able to interlink like cooked spaghetti forming amorphous regions [30].

Although, it is needed a minimum chain length the crystallinity decreases with a high increase of molar mass. As previously mentioned nucleation is a process that requires the disentanglement of molecular chains to rearrangement into folded conformation. This nucleation process becomes more difficult with increasing molecular weight due to the increase of friction for the sliding diffusion[122]. As the molar mass increases freedom of the chains to rearrange themselves on crystallization decreases and chain folding becomes less regular [124]. Therefore, for to higher molar mass, the sample crystallizes with a larger proportion of chains in the amorphous phase. These chains in the amorphous region can be chains that returning to the same crystal lamella after a spell in the amorphous region[31] (Figure 5.2).

5.2 Synthesis, NMR and MALDI-TOF Characterization of End-Functionalized Poly (ethylene glycols)

5.2.1 Nucleophilic Acyl Substitution Mechanism under Basic Conditions

Although a wide range of PEGDA and PEGDM are commercial, they are extremely expensive. Thus, following some literature procedures[92–94,96,97,99] the synthesis starting from inexpensive commercial PEG. PEGDA (PEG-diacrylate) was prepared by esterification of PEG and acryloyl chloride and PEGDM (PEG-dimethacrylate) by esterification of PEG and methacryloyl chloride (Figure 5.3). The syntheses were performed with commercial PEG of different molecular

weights: 1000 g mol^{-1} (PEG1000), 2000 g mol^{-1} (PEG2000), 4000 g mol^{-1} (PEG4000) and 6000 g mol^{-1} (PEG6000). Their structures were assigned on the basis of their ^{1}H-NMR, ^{13}C-NMR, DEPT, two dimensional NMR (COSY and HSQC) and MALDI-TOF mass spectrometry.

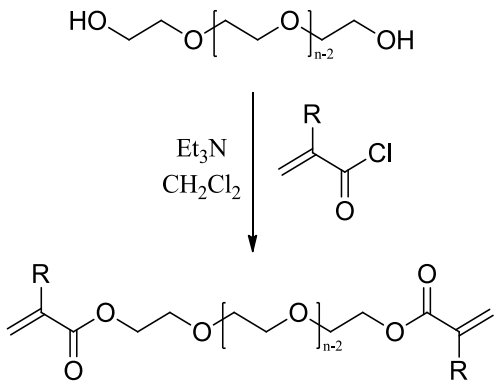

Figure 5.3 – General scheme for the synthesis of PEGDA and PEGDM; R=H or CH_3, n= number of repeating ethylene oxide units (EO).

The methodology used to obtain PEGDM and PEGDA was the reaction of PEG with (meth)acryloyl chloride and is a common procedure[92–98].

The reaction starts by the nucleophile attack from the hydroxyl group to the electrophilic center of the carbonyl group present in (meth) acryloyl chloride, creating an unstable intermediate which reforms the carbon-oxygen double bond (thermodynamically very favorable process). The elimination of the leaving group (Cl^-) leads to the formation of trimethylamine hydrochloride salt ($^+HNEt_3Cl^-$) and the desired ester [127,128]. Among carboxylic acid derivatives, the acyl chlorides (RCOCl) are the most reactive, due to the electronegativity of the chlorine atom, because, in addition to increasing the electrophilicity of the carbon in carbonyl group, it is also a great leaving group. The combination of these two factors makes the reaction very favorable (Figure 5.4)[127].

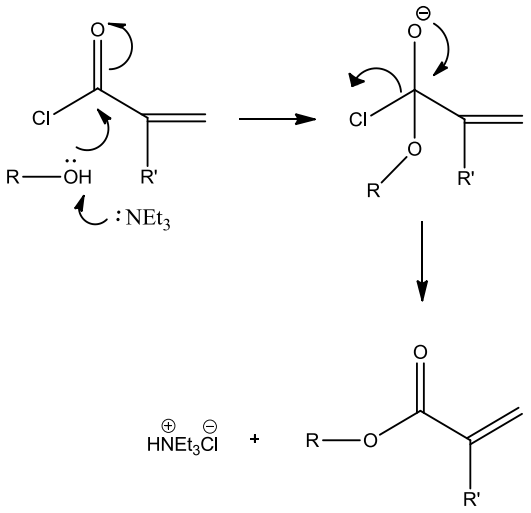

Figure 5.4- Nucleophilic acyl substitution reaction mechanism under basic conditions (NEt_3), R = alcohol side chain (ethylene oxide); R´= H or CH_3.

5.2.2 Poly (ethylene glycol) dimethacrylate

5.2.2.1 PEG2000DM

To a solution of poly(ethylene glycol) (M_w = 2000 g mol^{-1}) (2 g, 1 mmol, 1 eq) in dry CH_2Cl_2 (15 mL) was added triethylamine (0.4 g, 4 mmol, 4 eq) and then cooled to 0 ºC in an ice-water bath. To this solution, methacryloyl chloride (0.42 g, 4 mmol, 4 eq) was added dropwise. After dropping, the mixture was stirred 24h at 40 ºC. The reaction mixture was washed with HCl 0.1M, brine and H_2O. In the end, residual water was removed from the organic phase by treatment with anhydrous Na_2SO_4, filtered and concentrated under reduced pressure. The remaining solution added dropwise to a 300 ml of diethyl ether (cooled on an ice bath). The product was collected by filtration and subsequent washing with diethyl ether. The product was visualized with phosphomolybdic acid by TLC analysis ($CHCl_3$-MeOH 9:1). A white waxy solid (1.67g, 0.78 mmol, 78 %) was obtained. The NMR assignments and structure determination were made by ^{1}H-NMR (
Figure 12.1) and ^{13}C-NMR (Figure 12.2).

^{1}H-NMR (400 MHz, $CDCl_3$) δ 6.13 (s, 2H, =C$\underline{H_2}$), 5.58 (s, 2H, =C$\underline{H_2}$), 4.32 – 4.28 (m, 4H, C$\underline{H_2}$O-(C=O)), 3.76 – 3.72 (m, 4H, C$\underline{H_2}$CH_2O-(C=O)), 3.65 (s, 182H, C$\underline{H_2}$C$\underline{H_2}$O), 1.95 (s, 6H, C$\underline{H_3}$).

^{13}C-NMR (100 MHz, $CDCl_3$) δ 18.13 (C$\underline{H_3}$), 63.99 (C$\underline{H_2}$O-(C=O)), 69.16 (C$\underline{H_2}$CH_2O-(C=O)), 70.56 (C$\underline{H_2}$C$\underline{H_2}$O), 125.75(=C$\underline{H_2}$), 136.17(H_3C-C=), 167.33 (C=O).

5.2.2.2 PEG4000DM

The synthesis and characterization of PEG4000DM and PEG6000DM were similar to synthesis and characterization of PEG2000DMA Instead of PEG2000, PEG4000 and PEG6000 were used, respectively.

Poly(ethylene glycol) (M_w = 4000 g mol^{-1}) (2 g, 0.5 mmol, 1 eq) in CH_2Cl_2 (15 mL) with triethylamine (0.2 g, 2 mmol, 4 eq) and methacryloyl chloride (0.21g, 2 mmol, 4 eq) gave PEG4000DM (1.63 g, 0.39 mmol, 79 %) as a white waxy solid that foamed under vacuum. . The NMR assignments and structure determination were made by ^{1}H-NMR (Figure 12.3) and ^{13}C-NMR (Figure 12.4).

^{1}H-NMR (400 MHz, $CDCl_3$) δ 6.13 (s, 2H, =C$\underline{H_2}$), 5.57 (s, 2H, =C$\underline{H_2}$), 4.31 – 4.28 (m, 4H, C$\underline{H_2}$O-(C=O))3.76 – 3.73 (m, 4H, C$\underline{H_2}$CH_2O-(C=O)),3.65 (s, 69H, C$\underline{H_2}$C$\underline{H_2}$O),1.95 (s, 6H, C$\underline{H_3}$).

^{13}C-RMN (100 MHz,$CDCl_3$) δ 18.33 (C$\underline{H_3}$), 63.879 (C$\underline{H_2}$O-(C=O)), 69.16 (C$\underline{H_2}$CH_2O-(C=O)), 70.58 (C$\underline{H_2}$C$\underline{H_2}$O), 125.75(=C$\underline{H_2}$), 136.18(H_3C-C=), 167.37 (C=O).

5.2.2.3 PEG6000DM

Poly(ethylene glycol) (M_w = 6000 g mol^{-1}) (2 g, 0.33 mmol, 1 eq) in CH_2Cl_2 (15 mL) with triethylamine (0.14 g, 1.33 mmol, 4 eq) and methacryloyl chloride (0.14 g, 1.33 mmol, 4 eq) gave PEG6000DM (1.69 g, 0.28 mmol, 82 %) as a white waxy solid that foamed under vacuum. The NMR assignments and structure determination were made by ^{1}H-NMR (Figure 12.5) and ^{13}C-NMR (Figure 12.6).

^{1}H-NMR (400 MHz, $CDCl_3$) δ 6.12 (s, 2H, =C$\underline{H_2}$), 5.57 (s, 2H, =C$\underline{H_2}$), 4.31 – 4.28 (m, 4H, C$\underline{H_2}$O-(C=O)), 3.83 – 3.79 (m, 4H, C$\underline{H_2}$CH_2O-(C=O)), 3.64 (s, 525H, C$\underline{H_2}$C$\underline{H_2}$O), 1.94 (s, 6H, C$\underline{H_3}$).

^{13}C-NMR (100 MHz, $CDCl_3$) δ 18.36 (C$\underline{H_3}$), 63.92 (C$\underline{H_2}$O-(C=O)), 69.18 (C$\underline{H_2}$CH_2O-(C=O)), 70.61 (C$\underline{H_2}$C$\underline{H_2}$O), 125.77(=C$\underline{H_2}$), 136.20(H_3C-C=), 167.39 (C=O).

5.2.2.4 PEG1000DM

The synthesis of PEG1000DM was similar to described above but the resulting crude product was purified by column chromatography using EtOAC-hexane (5:1) and then $CHCl_3$:MeOH (9:1). Compounds were visualized with phosphomolybdic acid by TLC analysis ($CHCl_3$-MeOH 9:1).

Poly(ethylene glycol) (M_w = 1000 g mol^{-1}) (2 g, 2 mmol, 1 eq) in CH_2Cl_2 (15 mL) with triethylamine (0.81 g, 8 mmol, 4 eq) and methacryloyl chloride (0.84 g, 8 mmol, 4 eq) gave PEG1000DM (2.02 g, 1.78 mmol, 89 %) as a colourless oil that foamed under vacuum. The NMR assignments and structure determination were made by ^{1}H-NMR (Figure 12.7), ^{13}C-NMR (Figure 12.8), DEPT (Figure 12.12) and by two dimensional NMR (COSY (Figure 12.10) and HSQC (Figure 12.11)).

^{1}H-NMR (400 MHz, $CDCl_3$) δ 6.13 (s, 2H, =C$\underline{H_2}$), 5.58 (s, 2H, =C$\underline{H_2}$), 4.32 – 4.28 (m, 4H, C$\underline{H_2}$O-(C=O)), 3.77 – 3.72 (m, 4H, C$\underline{H_2}$CH$_2$O-(C=O)), 3.65 (s, 69H, C$\underline{H_2}$C$\underline{H_2}$O), 1.95 (s, 6H, C$\underline{H_3}$).
^{13}C-NMR (100 MHz, $CDCl_3$) δ 18.31 (C$\underline{H_3}$), 63.87 (C$\underline{H_2}$O-(C=O)), 69.12 (C$\underline{H_2}$CH$_2$O-(C=O)), 70.54 (C$\underline{H_2}$C$\underline{H_2}$O), 125.74(=C$\underline{H_2}$), 136.14(H$_3$C-C$\underline{=}$), 167.34 (C$\underline{=}$O).

5.2.3 Poly (ethylene glycol) diacrylate

The synthesis and characterization of PEG2000DA, PEG4000DA and PEG6000DA was similar to synthesis and characterization of PEG2000DMA, PEG4000DMA and PEG6000DMA. Instead of methacryloyl chloride, acryloyl chloride was used.

5.2.3.1 PEG2000DA

Poly(ethylene glycol) (M_w = 2000 g mol^{-1}) (2 g, 1 mmol, 1 eq) in CH_2Cl_2 (15 mL) with triethylamine (0.41 g, 4 mmol, 4 eq) and acryloyl chloride (0.36 g, 4 mmol, 4 eq) gave PEG2000DA (1.45 g, 0.69 mmol, 69 %) as a white waxy solid that foamed under vacuum. The NMR assignments and structure determination were made by ^{1}H-NMR (Figure 12.12) and ^{13}C-NMR (Figure 12.13).
^{1}H-NMR (400 MHz, $CDCl_3$) δ 6.16 (d, *J* = 17.3 Hz, 2H, =C$\underline{H_2}$), 6.16 (dd, *J* = 17.4, 10.4 Hz, 2H, =C$\underline{H}$), 5.84 (d, *J* = 10.4 Hz, 1H, =C$\underline{H_2}$), 4.34 – 4.30 (m, 4H, C$\underline{H_2}$O-(C=O)), 3.76 – 3.73 (m, 4H, C$\underline{H_2}$CH$_2$O-(C=O)), 3.65 (s, 103H, C$\underline{H_2}$C$\underline{H_2}$O).
^{13}C-NMR (100 MHz, $CDCl_3$) δ 63.70 (C$\underline{H_2}$O-(C=O)), 69.12 (C$\underline{H_2}$CH$_2$O-(C=O)), 70.56 (C$\underline{H_2}$C$\underline{H_2}$O), 128.28 (C$\underline{H}$),, 131.04 (=C$\underline{H_2}$), 166.17 (C$\underline{=}$O).

5.2.3.2 PEG4000DA

Poly(ethylene glycol) (M_w = 4000 g mol^{-1}) (2 g, 0.5 mmol, 1 eq) in CH_2Cl_2 (15 mL) with triethylamine (0.20 g, 2 mmol, 4 eq) and acryloyl chloride (0.18 g, 2.0 mmol, 4 eq) gave PEG4000DA (1.78 g, 0.43 mmol, 86 %) as a white waxy solid that foamed under vacuum. The NMR assignments and structure determination were made by ^{1}H-NMR (Figure 12.14) and ^{13}C-NMR (Figure 12.15).
^{1}H-NMR (400 MHz, $CDCl_3$) δ 6.43 (d, *J* = 17.3 Hz,2H, =C$\underline{H_2}$), 6.16 (dd, *J* = 17.3, 10.4 Hz, 2H, =C$\underline{H}$), 5.84 (d, *J* = 10.4 Hz, 2H, =C$\underline{H_2}$), 4.33 – 4.29 (m, 4H, C$\underline{H_2}$O-(C=O)), 3.65 (s, 462H, C$\underline{H_2}$C$\underline{H_2}$O).
^{13}C-NMR (100 MHz, $CDCl_3$) δ 63.69 (C$\underline{H_2}$O-(C=O)), 69.11 (C$\underline{H_2}$CH$_2$O-(C=O)), 70.57 (C$\underline{H_2}$C$\underline{H_2}$O), 128.29 (C$\underline{H}$),131.00 (=C$\underline{H_2}$),166.14 (C$\underline{=}$O).

5.2.3.3 PEG6000DA

Poly(ethylene glycol) (M_w = 6000 g mol^{-1}) (2 g, 0.33 mmol, 1 eq) in CH_2Cl_2 (15 mL) with triethylamine (0.14 g, 1.33 mmol, 4 eq) and acryloyl chloride (0.12 g, 1.33 mmol, 4 eq) gave PEG6000DA (1.48 g, 0.24 mmol, 73 %) as a white waxy solid that foamed under vacuum. The NMR assignments and structure determination were made by ^{1}H-NMR (Figure 12.16) and ^{13}C-NMR (Figure 12.17).

^{1}H-NMR (400 MHz, $CDCl_3$) δ 6.43 (d, *J* = 17.3 Hz, 2H, =C$\underline{H_2}$), 6.20-6.11 (m, 2H, =C$\underline{H}$), 5.84 (d, *J* = 10.4 Hz, 2H, =C$\underline{H_2}$), 4.33 – 4.30 (m, 4H, C$\underline{H_2}$O-(C=O)), 3.65 (s, 615H, C$\underline{H_2}$C$\underline{H_2}$O).

^{13}C-NMR (100 MHz, $CDCl_3$) ($CDCl_3$) δ 63.70 (C$\underline{H_2}$O-(C=O)), 69.11 (C$\underline{H_2}$CH_2O-(C=O)), 70.55 (C$\underline{H_2}$C$\underline{H_2}$O), 128.28 (C$\underline{H}$),130.06 (=C$\underline{H_2}$),166.18 (C$\underline{=}$O).

5.2.3.4 PEG1000DA

The synthesis of PEG1000DA was similar to described for PEG1000DM synthesis. The resulting crude product was purified by column chromatography using EtOAc-hexane (5:1) and then $CHCl_3$:MeOH (9:1). Compounds were visualized with phosphomolybdic acid by TLC analysis ($CHCl_3$-MeOH 9:1).

Poly (ethylene glycol) (M_w = 1000 g mol^{-1}) (2 g, 2 mmol, 1 eq) in CH_2Cl_2 (15 mL) with triethylamine (0.81 g, 8 mmol, 4 eq) and acryloyl chloride (0.73 g, 8 mmol, 4 eq) gave PEG1000DA (2.02 g, 1.82 mmol, 91 %) as a yellow waxy solid that foamed under vacuum. The NMR assignments and structure determination were made by ^{1}H-NMR (Figure 12.18), ^{13}C-NMR (Figure 12.19), DEPT (Figure 12.21) and by two dimensional NMR (COSY (Figure 12.22) and HSQC (Figure 12.20)).

^{1}H-NMR (400 MHz, $CDCl_3$) δ 6.43 (d, *J* = 17.3 Hz, 2H, =C$\underline{H_2}$), 6.16 (dd, *J* = 17.4, 10.4 Hz, 2H, =C$\underline{H}$), 5.84 (d, *J* = 10.4 Hz, 2H, =C$\underline{H_2}$), 4.34 – 4.29 (m, 4H, C$\underline{H_2}$O-(C=O)), 3.77 – 3.72 (m, 4H, C$\underline{H_2}$CH_2O-(C=O)), 3.64 (s, 86H, C$\underline{H_2}$C$\underline{H_2}$O).

^{13}C-NMR (100 MHz, $CDCl_3$) δ 63.68 (C$\underline{H_2}$O-(C=O)), 69.10 (C$\underline{H_2}$CH_2O-(C=O)), 70.55 (C$\underline{H_2}$C$\underline{H_2}$O), 128.28 (C$\underline{H}$) 130.98 (=C$\underline{H_2}$), 166.12 (C$\underline{=}$O).

5.3 MALDI-TOF MS

Due to difficult isolation of products from PEGs (starting materials) during PEGs end group modifications, quantitative functional group transformations are important. However, characterization techniques such as NMR spectroscopy have limitations in determining the efficiency of end group transformations because the signal originated from the end groups tends to be overwhelmed by the larger signal from the backbone protons (PEG protons)[129,130]. NMR spectroscopy of functionalization of PEG can be used to confirm the addition of the end groups but the low proportion of these end groups signals relative to the PEG backbone makes the completion of the reaction difficult to determine via ^{1}H-NMR integration alone. In this way,

although the NMR spectra of products show the expected peaks and the lack of additional peaks suggesting that unreacted (meth) or acryloyl chloride and trimethylamine were quantitatively removed the unreacted PEG, as well as those species with one side reacted, cannot be distinguished due to this overlapping of PEG protons[97]. Although the low molecular weight impurities might not be apparent in MALDI-TOF MS, this technique provided the necessary data for end group analysis[131].

MALDI-TOF MS can easily distinguish between macromolecules with the same repeating unit structure but different end groups providing a technique to confirm high-end group purity[129,130]. After ionization, the singly charged and structurally intact of macromolecules detected by MALDI-TOF may provide a Gaussian´s distribution of macromolecules. Thus, the mass of each macromolecule, average molecular weights (M_n and M_w) as well as polydispersities (PDI) of macromolecules, can also be determined. The macromolecules are equally spaced in a way that normally reflects the mass of repeat unit[130]. Each observed signal contains information about the end groups of that species. However, when two macromolecules vary only in the type and mass of their end group, their spectra will show two different series of m/z peaks (normally called the main and the minor series of peaks) in their MALDI-TOF mass spectra, each set of peaks separated by the mass of repeat unit[129,130]. The increase in mass measured in individual peaks of product materials compared to started material corresponds to the addition of the masses of the end groups.

The MALDI-TOF mass spectra of the starting and resulting products are shown in Figure 5.5 and in Figure 5.6, respectively. In general, end-group analysis using MALDI-TOF mass spectrometry provides after esterification two sets of peaks: the main series of peaks and a minimal minor one. This could be due to unreacted PEG are left after reaction. It is also possible that some of the molecules present in the distribution might be functionalized by a single end group rather than two. In average adjacent peaks of the same series differ in mass by 44 Da (Dalton), which corresponds to the molecular mass of the oxyethylene repeat unit.

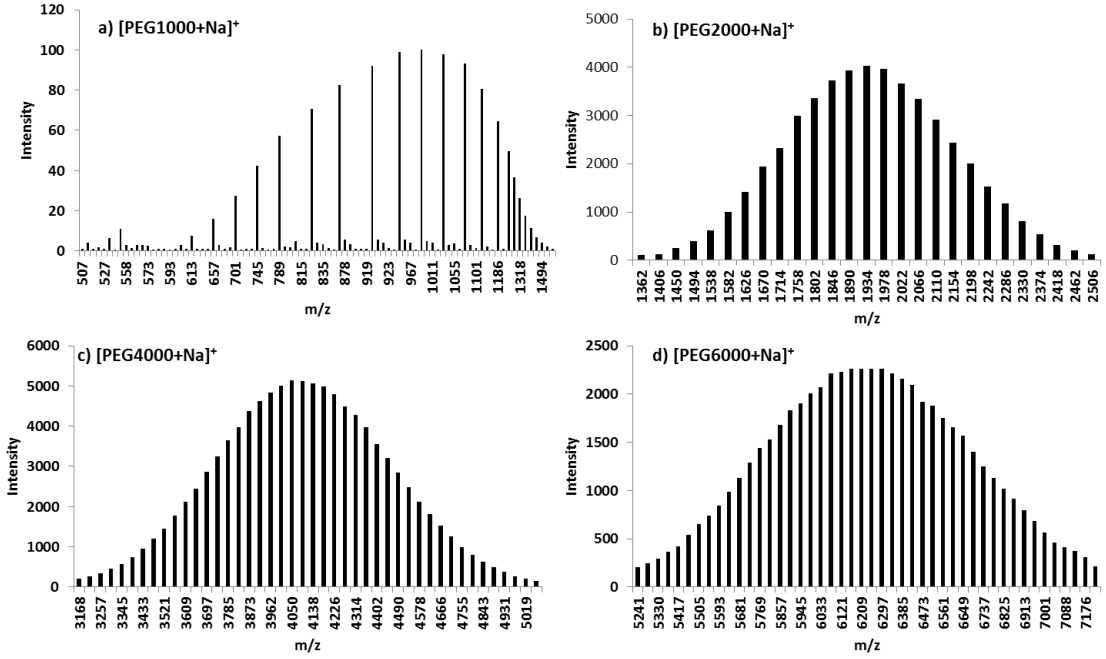

Figure 5.5 – MALDI-TOF mass spectra of $[PEG+Na]^+$: a) $[PEG1000+Na]^+$, b) $[PEG2000+Na]^+$, c) $[PEG4000+Na]^+$, d) $[PEG6000+Na]^+$.

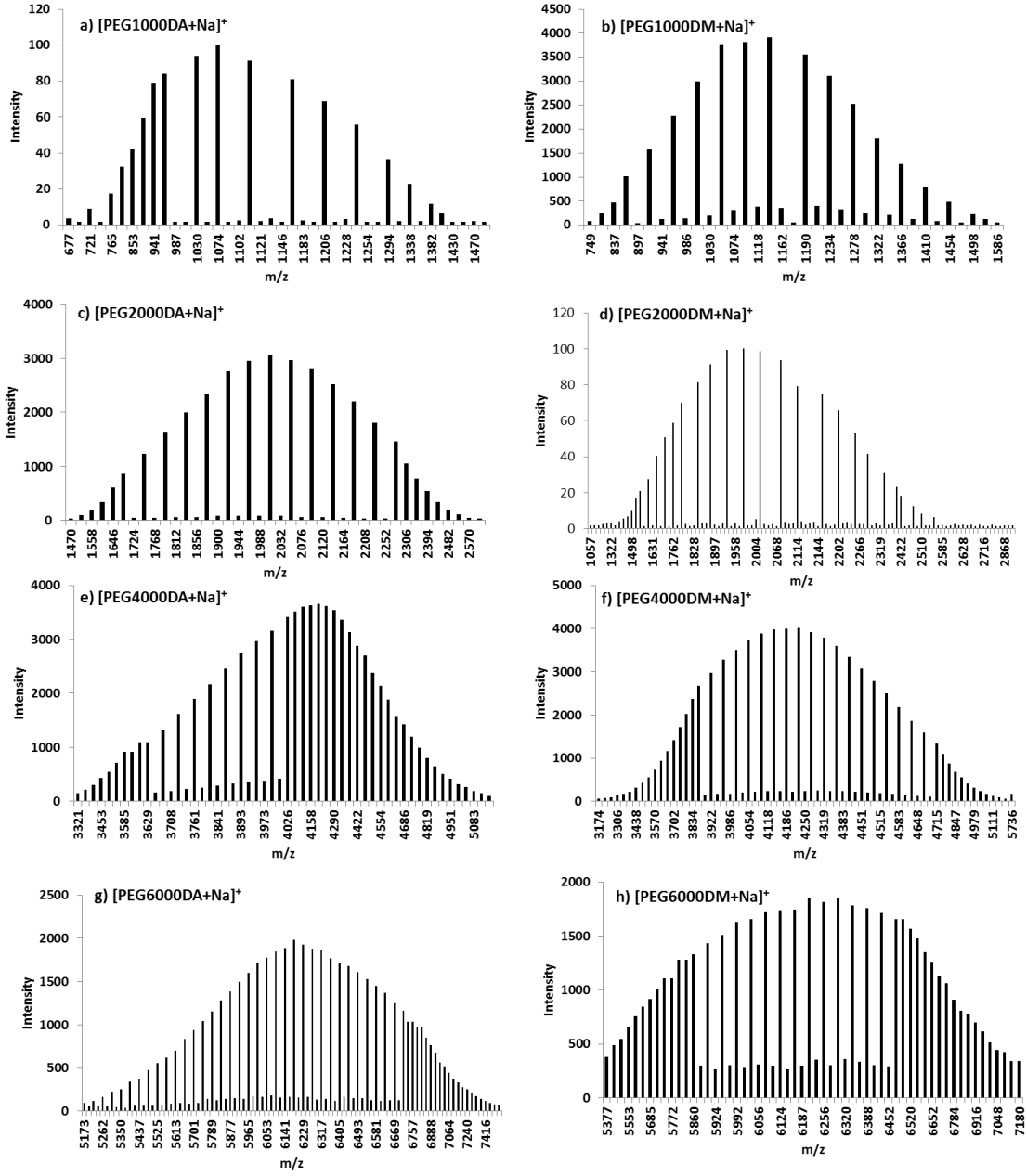

Figure 5.6 – MALDI-TOF mass spectra of [PEG di(metha)acrylate+Na]$^+$: a) [PEG1000DA+Na]$^+$, b) [PEG1000DM+Na]$^+$, c) [PEG2000DA+Na]$^+$, d) [PEG2000DM+Na]$^+$, e) [PEG4000DA+Na]$^+$, f) [PEG4000DM+Na]$^+$, g) [PEG6000DA+Na]$^+$, h) [PEG6000DM+Na]$^+$.

For the main series, the average molecular weights (M_n and M_w), polydispersities (PDI) and the number of ethylene oxide units (n) are listed in Table 5.1. The calculated molecular weights were determined from the molecular weights of the corresponding starting PEG materials. After esterification, it is expected that each individual peaks of the product exhibited a mass shift corresponding to the end groups (compared to individual peaks of starting material) in its MALDI-TOF mass spectrum.

A good correlation was observed between the average difference between the theoretical and observed values for individual peaks for PEGDMs and PEGDAs. The main series correspond

(Figure 5.6 a) ≈ 670-1500 m/z; b) ≈ 750-1600 m/z; c) ≈ 1500-2600 m/z; d) ≈ 1500-2600 m/z; e) ≈ 3300-5200 m/z; f) ≈ 3200-5200 m/z; g) ≈ 5200-7300 m/z and h) ≈ 5400-7000 m/z) to Na^+ cationized PEG di-functionalized.

Table 5.1 – The theoretical and observed molecular weights of starting material $[PEG+Na]^+$ and resulting products obtained from MALDI-TOF measurements for the main series of peaks.

[Macromolecule+Na]$^+$	M_n		M_w		PDI	
	Observed	Theoretical	Observed	Theoretical	Observed	Theoretical
[PEG1000+Na]+	1011.34	-	1044.01	-	1.03	-
[PEG1000DA +Na]+	1062.75	1062.68	1084.73	1084.67	1.02	1.02
[PEG1000DM +Na]+	1137.92	1137.74	1156.87	1156.69	1.02	1.02
[PEG2000+Na]+	1940.94	-	1963.25	-	1.01	-
[PEG2000DA +Na]+	2013.90	2013.89	2033.02	2033.02	1.01	1.01
[PEG2000DM +Na]+	1998.66	1998.81	2021.92	2022.01	1.01	1.01
[PEG4000+Na]+	4097.09	-	4127.30	-	1.01	-
[PEG4000DA +Na]+	4192.30	4192.13	4221.02	4220.87	1.01	1.01
[PEG4000DM +Na]+	4202.99	4201.59	4231.52	4228.36	1.01	1.01
[PEG6000+Na]+	6235.73	-	6264.05	-	1.01	-
[PEG6000DA +Na]+	6276.09	6277.45	6308.06	6305.82	1.01	1.01
[PEG6000DM +Na]+	6254.18	6255.21	6278.75	6279.79	1.00	1.00

The calculated mass m(n) of the most intense peak is a linear function of a number of the polymer repeat unit (n):

$$m(n) = n m_{monomer} + m_{end\ groups} + m_{cation}$$

where *n* is the number of repeats ethylene oxide units, $m_{monomer}$ is the mass of the repeat unit, m_{end} groups is the residue mass of both end groups and m_{cation} is the mass of sodium cation. The major peaks and its corresponding mass are used for calculating the number of repeat units (Table 5.1). In this way, for starting material PEG ($HO\text{-}(CH_2CH_2O)_n\text{-}H$) the theoretical peak mass should be expressed as m(n) = n44.053 + 17.007 + 1.008 + 22.990 (n x molecular weight of ethylene oxide + molecular weight of the hydroxyl terminal group + molecular weight of the hydrogen terminal group + molecular weight of the sodium cation. The di-methacrylate PEG ($(CH_3CH_2C)OCO\text{-}(CH_2CH_2O)_n\text{-}COC(CH_2CH_3)$) should be expressed as m(n) = *n*44.053 + 85.082 + 69.083 + 22.990 and finally the di-acrylate PEG ($(HCH_2C)OCO\text{-}(CH_2CH_2O)_n\text{-}COC(CH_2H)$) should be expressed as m(n) = *n* 44.026 + 71.055 + 55.066 + 22.990.

For instance, the theoretical mass value of the 22 repeat units in $[PEG1000+Na]^+$ corresponds to 22 x 44.053 + 18.015 + 22.990 = 1010.17 which is in accordance with observed mass for n = 22 of 1009.49 Da. Similarly, for PEG1000DA with the difference between the theoretical (1118.27) and observed (1117.56) mass is just 0.71 Da. Theoretical calculations and observed distributions are listed in Table 5.2. Expected masses are very close to the observed masses which indicate a minimal amount of contamination.

Table 5.2 – Calculated and experimental mass m(n) of the most intense peak in each [macromolecule+Na]$^+$ spectrum.

[Macromolecule+Na]$^+$	n	Calculated m(n)	Experimental m(n)
[PEG1000+Na]$^+$	22	1010.17	1009.49
[PEG1000DA+Na]$^+$	22	1118.27	1117.56
[PEG1000DM+Na]$^+$	21	1102.27	1101.65
[PEG2000+Na]$^+$	43	1935.28	1934.13
[PEG2000DA+Na]$^+$	41	1955.27	1954.09
[PEG2000DM+Na]$^+$	42	2027.38	2025.97
[PEG4000+Na]$^+$	91	4049.83	4049.67
[PEG4000DA+Na]$^+$	92	4201.98	4201.87
[PEG4000DM+Na]$^+$	92	4230.03	4230.51
[PEG6000+Na]$^+$	142	6296.53	6297.09
[PEG6000DA+Na]$^+$	137	6184.36	6184.65
[PEG6000DM+Na]$^+$	138	6256.47	6256.15

From a minor set of peaks of much lower intensity, Figure 5.6 c) ≈ 1700-2250 m/z; e) ≈ 3600-4000 m/z and f) ≈ 3800-4700 m/z, it is identified a residual amount of mono-functionalized PEG species (Table 5.3). However, it is possible to conclude by series peaks intensity that high reaction conversions were achieved.

Table 5.3 – The theoretical and observed molecular weights of [PEG2000A+Na]$^+$, [PEG4000A+Na]$^+$ and [PEG4000M+Na]$^+$ obtained from MALDI-TOF measurements for minor series of peaks (if only one end of PEG was functionalized).

[Macromolecule Na]$^+$	*M*n		*M*w		PDI	
	Observed	**Theoretical**	**Observed**	**Theoretical**	**Observed**	**Theoretical**
[PEG2000A+Na]$^+$	1975.06	1975.07	1985.35	1985.34	1.01	1.01
[PEG4000A+Na]$^+$	3873.62	3872.15	3876.69	3876.69	1.01	1.00
[PEG4000M+Na]$^+$	4276.44	4275.73	4287.69	4286.97	1.00	1.00

5.4 Differential scan calorimetry results and discussion

The thermal behavior of synthesized PEG-difunctionalized was investigated in the temperature range between - 80 ºC and 130 ºC with rates of 5 and 20 ºC min^{-1} in heating and cooling, details on temperatures and enthalpies are provided in Table 12.1. For thermal analysis of corresponding polymers, the thermal polymerizations were initiated inside the DSC furnace.

In PEG1000 the macromolecular chains are long and with mobility enough to form ordered arrangements and crystallize with a sharp exothermic peak characteristic of crystallization emerges followed by a broad endothermic peak corresponding to the melting of the crystalline fraction previously formed (Figure 5.7 a). In the following heating and cool runs, crystallization and melting were observed indicating a crystalline macromolecule (Figure 5.7 c, d).

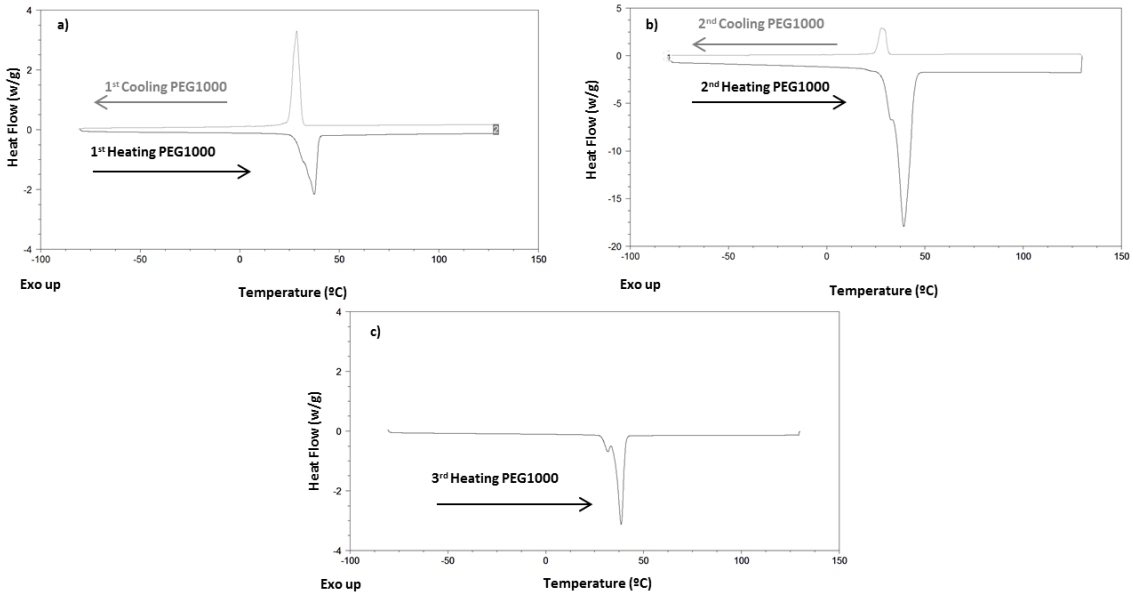

Figure 5.7 – Thermograms (heat flow vs. temperature) of PEG1000 collected at three heating and two cooling cycles at 5 ºC min^{-1}.

For PEG1000DM polymer, after melting of the oligomer (PEG 1000DM) with 1 wt.% of AIBN the temperature again increases with heating until an exothermic effect due to polymerization (Figure 5.8 a). In the following heating and cool runs, polymer glass transition temperature is observed at - 45.3 °C and no further processes were obtained indicating a fully amorphous polymer (Figure 5.8 b, c). Therefore, the presence of crosslinks in the polymer reduces the crystallinity when compared to starting PEG1000. Polymer chain sliding diffusion and disentanglement become more difficult that limited the rearrangement of chains into ordered morphology as in macromolecule PEG1000. The PEG1000DA polymer follows the same amorphous behavior as PEG1000DM polymer (Table 12.1).

In this way, the crystallization behavior of the polymer network is different from that of correspondent pre-polymers. The cross-links decrease the critical chain length and the molecular chain is no longer enough to crystallize. In addition, the crosslinks also decrease the freedom of the chains to rearrange on crystalline conformation[98,122]. In this way, the thermal behavior of PEG1000 polymer is different from that of correspondent PEG1000 oligomer.

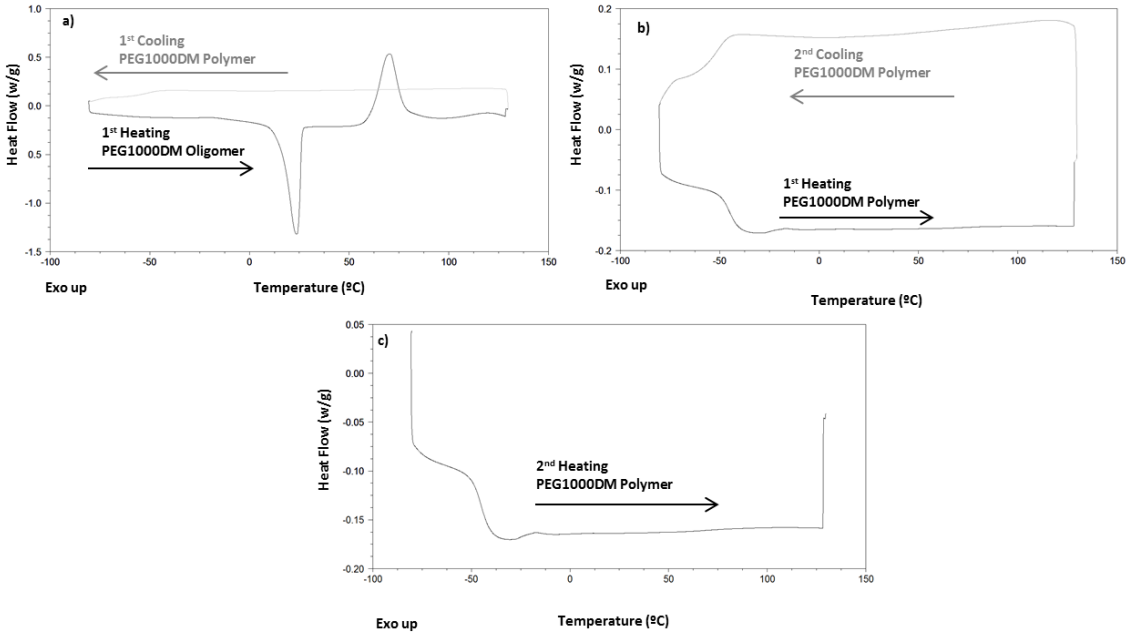

Figure 5.8 – Thermograms (heat flow vs. temperature) obtained for a mixture of PEG1000DM oligomer with 1wt.% of AIBN collected at the heating scan at 5 ºC min^{-1} and PEG1000DM polymer collected at two heating and cooling cycles at 5 ºC min^{-1}.

The thermal analysis of PEG2000DM polymer (Figure 5.9 a,b,c) shown that the sample is above of critical molecular chain length and crystal morphology result. This chain length is long enough to fold and to crystallize although the cross-linking of the polymer. For this reason, follow the same crystallization behavior of starting material PEG2000 (Figure 5.10).

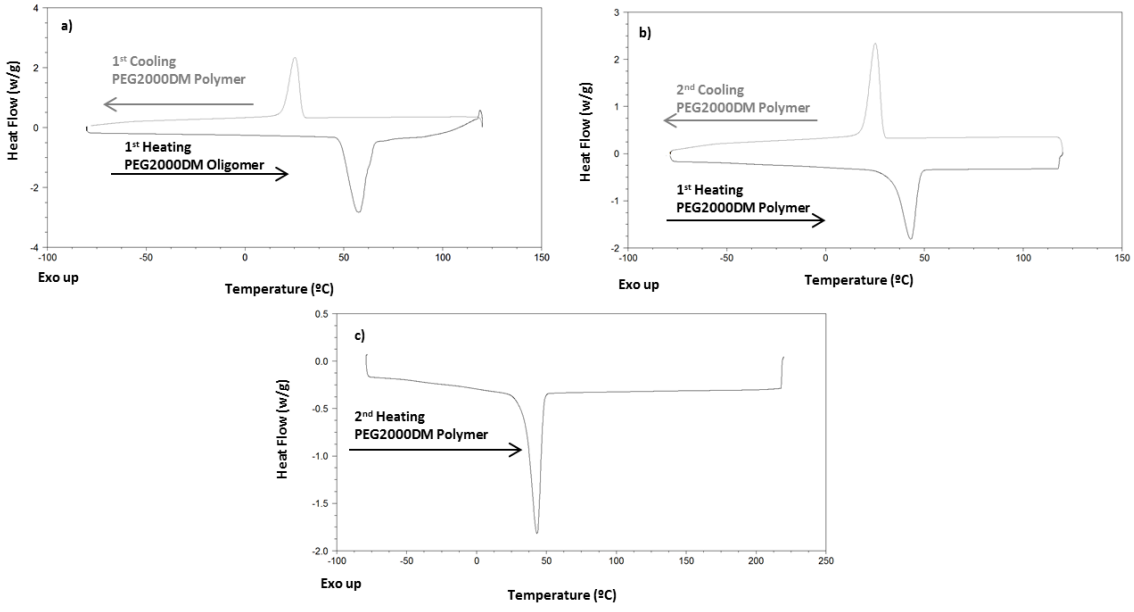

Figure 5.9 – Thermograms (heat flow vs. temperature) obtained for a mixture of PEG2000DM oligomer with 1wt.% of AIBN collected at the heating scan at 5 ºC min^{-1} and PEG2000DM polymer collected at two heating and cooling cycles at 5 ºC min^{-1}.

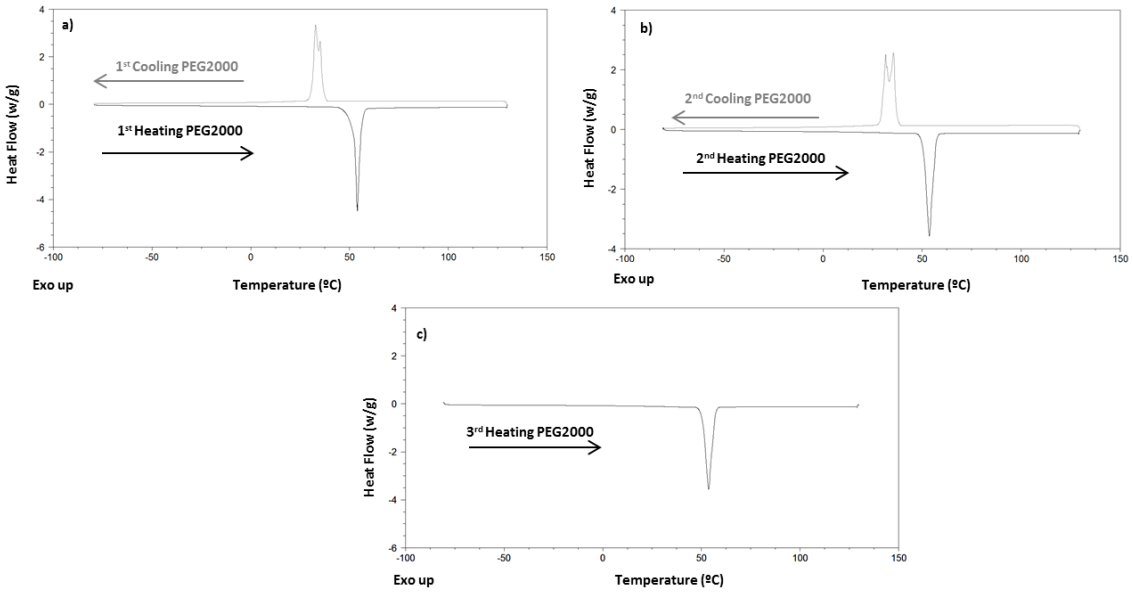

Figure 5.10 – Thermograms (heat flow vs. temperature) of PEG2000 collected at three heating and two cooling cycles at 5 ºC min^{-1}.

Although no detection of the T_g in the PEG2000 polymer (Figure 5.9) possibly it is in a semi-crystalline state with chains also in an amorphous state. The glass transition of highly crystalline macromolecules is very weak and for this reason difficult to identify. In highly crystalline macromolecules the small amorphous component is severely constrained by the crystals [31]. The cross-links in polymer reduce crystal perfectness and crystal size by the restricted of chain mobility [98,122]. This causes a decrease in the melting temperature from 54 ºC in PEG2000 (Figure 5.10) to 42 ºC in PEG2000DM polymer (Figure 5.9).

The increase of chain length could also difficult the crystallization process due to the increase of chain friction for the sliding diffusion. In this way, the freedom of the chains to rearrange themselves on crystalline morphology decreases and chain folding becomes less regular [124]. For this reason, it is expected that these samples crystallize with a larger proportion of chains in the amorphous phase[31]. Although no direct evidence of such behavior is presented in DSC thermograms collected for PEG4000 and PEG6000 and for the resulting polymers which show the same behavior of PEG2000 and the correspondent polymers (Table 12.1).

Macromolecules contain molecular chains of varying lengths possibility crystalizes in different crystal forms with more or fewer crystal arrangements and therefore molecular species can melt in different temperatures. The high molar mass component crystallizes early and the low molar mass species can crystallize in separate crystal[31,132,133]. This behavior is confirmed by the double endothermic peaks at 31.59 ºC and 38.55 ºC during the second and third heating scan that appeared in the DSC curves of the PEG1000 sample. Possible imperfect crystals melt at 37.37 ºC in a broad peak during the first heating scan (Figure 5.7 a) changing into different size distribution of crystals through the melt-crystallization, melting later in two double peaks (Figure

5.7 c). In DSC curves of PEG2000 sample (Figure 5.10 a, b) a double-crystallization peak is observed at 32.74 ºC and 35.22 ºC which also confirm the different size of crystals. However, in DSC curves of the respective polymers, the double peaks change to a single one by modifications in the polymers crystal structure. The cross-links in polymer promote a more imperfect crystal possibility with a greater dimension which shown only one simple peak.

5.5 Electro-Optical Properties

The electric field-transmittance curves as a function of PEG polymer chain length are reported in Figure 5.11 and electro-optical parameters are summarized in Table 5.4.The thermal PDLCs were prepared as described in Figure 2.10 by thermal polymerization at 70 °C, overnight.

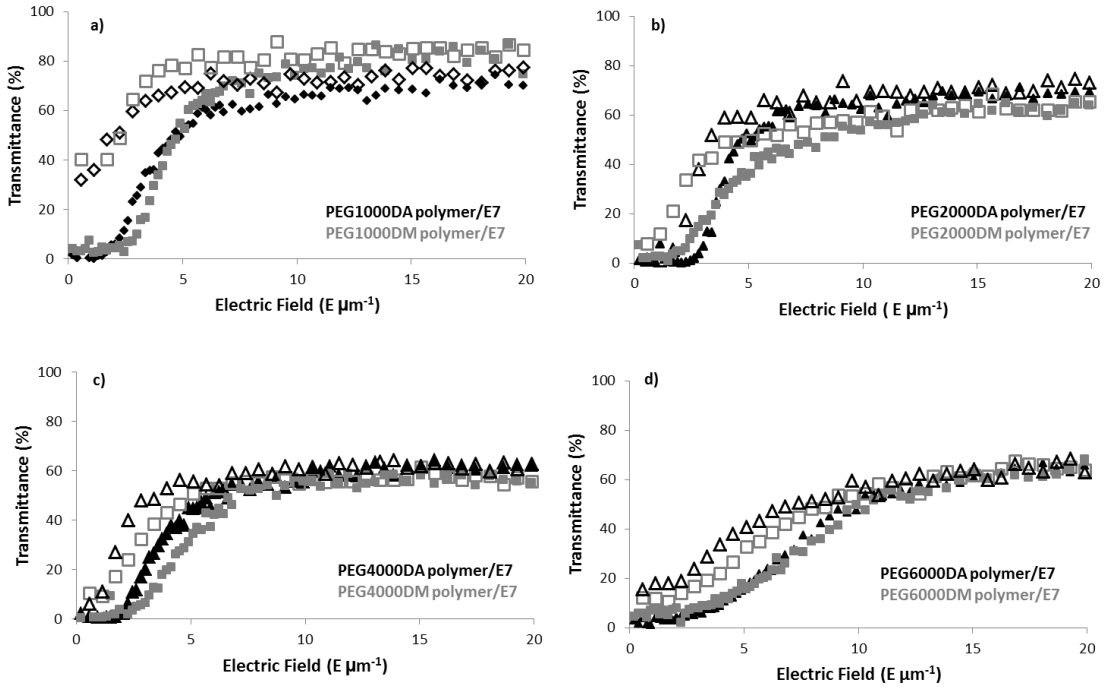

Figure 5.11 – The electro-optical response of PDLC films prepared with 30wt.% of a) PEG1000DA, PEG1000DM, b) PEG2000DA, PEG2000DM, c) PEG4000DA, PEG4000DM, d) PEG6000DA and PEG6000DM, with 1wt.% of AIBN and 70wt.% of E7, polymerized at 70 °C overnight. The transmittance was measured by applying the electrical field (filled symbols) and after removed the electric field (open symbols).

These results are intimately related to the thermal properties of the polymer matrix. It was clear that for PDLCs with amorphous flexible PEG1000 polymer chains (Figure 5.11 a) with average T_g at - 48.46 ºC (PEG1000DA polymer) and at - 45.30 ºC (PEG1000DM polymer), the transmittance at OFF state after the scan-down cycle did not return to its original scattering state and a transmittance state is displayed (in average 30 %).

Table 5.4 – Electro-optical properties of the PDLCs films prepared from 30wt.% of PEG pre-polymer with 1wt.% of AIBN and 70wt.% of E7.

PDLC Polymer	T_0 (%)	T_{OFF} (%)	T_{max} (%)	PME (%)	MSC (%)	E_{90} (V µm^{-1})
PEG1000DA	1.6	32	73	43	31	8.63
PEG1000DM	5.3	30	84	31	24	11.78
PEG2000DA	0.9	1.5	67	0.9	0.6	6.15
PEG2000DM	7.3	8.7	65	2.5	1.4	10.53
PEG4000DA	2.7	6	56	5.5	3.3	5.5
PEG4000DM	0.3	10	57	17	9.7	7.02
PEG6000DA	1.8	15.6	64	22	14	13.76
PEG6000DM	4.7	12.3	63	13	7.6	13.45

In contrast to PDLCs prepared with longer polymer chains which are arranged in crystalline structures and therefore polymers chains become rigid enough to hinder the permanent memory effect (as previously explained in chapter III). In this way, transmittance returns to a scattering state after the removal of the applied electric field. However, PDLCs with PEG6000 polymers shown an unexpected behavior with 22 % of PME for PEG6000DA PDLCs and 13 % for PEG6000DM PDLCs. The reason for this behavior could be related to the chain length too long which arrange in a more imperfect crystal by a large proportion of polymer chain in the amorphous phase (as also previously explained). This amorphous arrangement enhances the PME compared with semi-crystalline PEGs polymers but with shorter polymer chains (PEG2000 and PEG4000 polymers).

5.6 Polarized Optical Micrographs

The structure of PDLC films was characterized by POM. The images indicated that PDLC films are single layers of homogeneous structure. The effect of longer chain length in the crystalline morphology is clear by typical spherulites which grow outwards until they impinge upon neighboring spherulite[118] (Figure 5.12 j, l, n and p). For smaller polymer chain (PEG2000 polymer) crystalline shapes are smaller than in longer polymer chains leads to nonspherulitic morphology (Figure 5.12 f and h). For the smaller polymer chain (PEG1000 polymer) a typical amorphous polymer was observed where the liquid crystal is homogeneously dispersed into the polymer matrix. It is also possible to see that even for PDLC samples without PME same amount of liquid crystal molecules remain to align upon the electric field was removed (Figure 5.12 f, h, j, l). Nevertheless, this alignment is not enough to displayed higher transparency and a strong light scattering state was recovered unlike in PEG1000 polymer/E7 PDLC where a high transparency state is permanently displayed (Figure 5.11a).

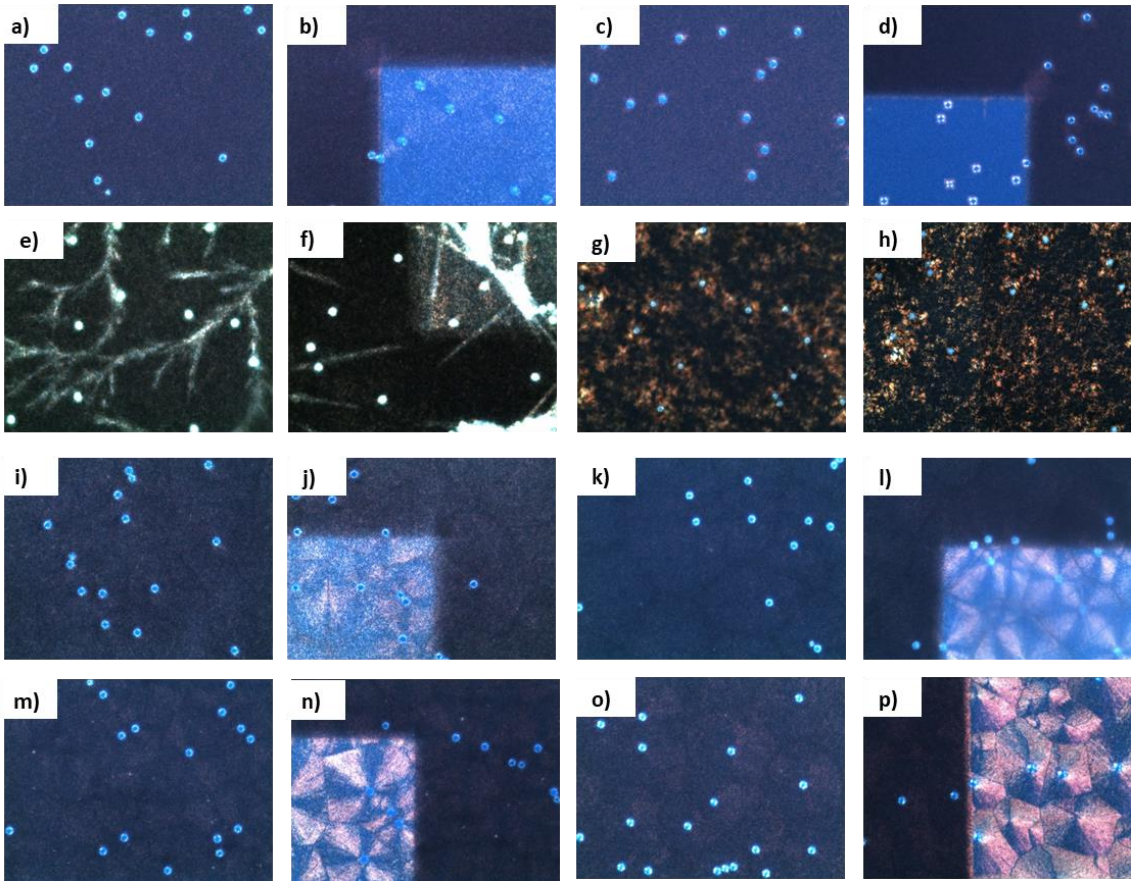

Figure 5.12 – Polarized optical micrographs observed for PDLC samples: a) initial OFF state of PEG1000DA PDLC; b) OFF state upon removal the applied electric field of PEG1000DA PDLC; c) initial OFF state of PEG1000DM PDLC; d) OFF state upon removal the applied electric field of PEG1000DM PDLC; e) initial OFF state of PEG2000DA PDLC; f) OFF state upon removal the applied electric field of PEG2000DA PDLC; g) initial OFF state of PEG2000DM PDLC; h) OFF state upon removal the applied electric field of PEG2000DM PDLC; i) initial OFF state of PEG4000DA PDLC; j) OFF state upon removal the applied electric field of PEG4000DA PDLC; k) initial OFF state of PEG4000DM PDLC; l) OFF state upon removal the applied electric field of PEG4000DM PDLC; m) initial OFF state of PEG6000DA PDLC; n) OFF state upon removal the applied electric field of PEG6000DA PDLC; o) initial OFF state of PEG6000DM PDLC; p) OFF state upon removal the applied electric field of PEG6000DM PDLC, x100 magnification.

5.7 Scanning Electron Microscopy

Figure 5.13 shows the morphology of the polymer matrix of the PEG PDLC. It is observed that morphology is affected by the degree of crystallinity of the polymer matrix. For the smallest polymer chain length (PEG 1000 polymer) and for the longest one (PEG 6000 polymer) a typical polymer ball morphology type is identified (Figure 5.13 a; b and g; h, respectively). As previously mentioned, in this morphology the polymer appears as an agglomerate of polymer beads forming an irregular network providing a high degree of interconnection between LC domains. This morphology type is in agreement with the permanent memory effect displayed by these PDLCs samples[18,134,135]. For PEG2000 polymer (Figure 5.13 c; d) and PEG4000 polymer (Figure 5.13 e; f) a ring shape was observed with an interfibrillar polymer structure possibility filled by the LC molecules.

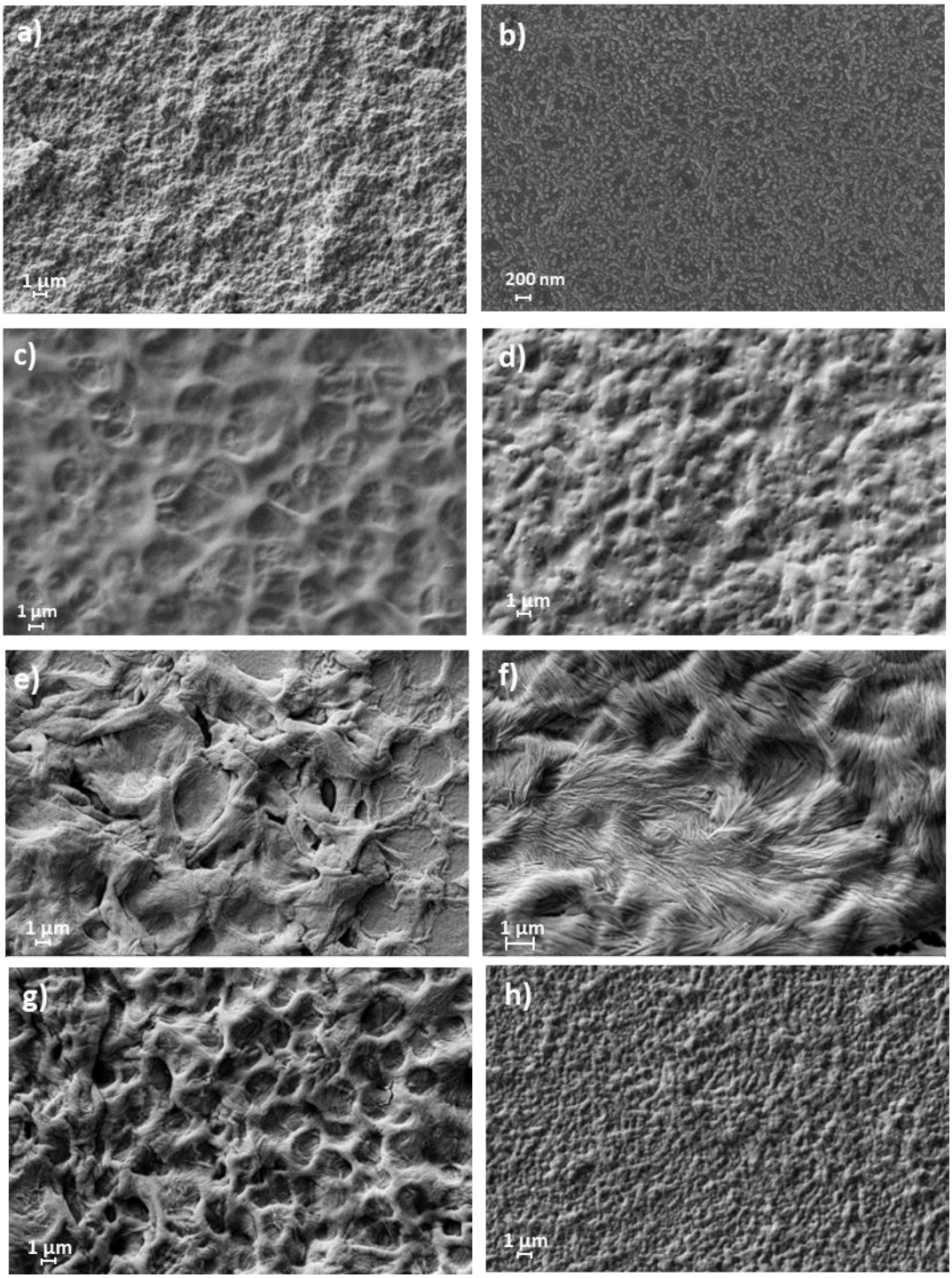

Figure 5.13 – SEM micrographs for the microstructure of the polymer matrix of PDLC films prepared with different PEG pre-polymers: a) PEG1000DA PDLC; b) PEG1000DM PDLC; c) PEG2000DA PDLC; d) PEG2000DM PDLC; e) PEG4000DA PDLC; f) PEG4000DM PDLC; g) PEG6000DA PDLC and h) PEG6000DM PDLC.

5.8 Conclusions

It was clear that the molecular weight of linear polyethylene glycol pre-polymer maintaining two functionalities affects the polymer thermal properties which in turn have direct implications in the

permanent memory effect of corresponding PDLC devices. Amorphous polymers as PEG 1000DA polymer with T_g at - 48.46 ºC and PEG 1000DM polymer with T_g at - 45.30 ºC promote permanent memory effect with 43 % and 31 %, respectively. However, for higher molecular weight polymer chains become long enough to rearrange in a semi-crystalline structure which cancels the permanent memory effect of corresponding PDLC. This correlation between permanent memory effect and amorphousness/crystallinity of polymer matrix could be related to elasticity, flexible or stiff polymer chains at the interface with LC molecules which in turn is related to anchoring energy.

In PEG1000 polymer chains are only long enough to interlink like cooked spaghetti forming amorphous regions which give to polymer enough ductility for chain segments structure can be affected by the LC alignment. Polymer chains which exist in the interface between the polymer matrix and LC domains (polymer/LC interface) may reorient by interaction with the reoriented LC molecules changing anchoring energy at polymer/LC interface. This new anchoring energy keeps the LC director aligned when the electric field is switching off giving rise to permanent memory effect. When the molecular weight increases (PEG2000 polymer and PEG4000polymer) the polymer chain length becomes long enough to semi-crystallize and polymer chain segments become stiff enough to prevent LC alignment at the polymer/LC interface. The elastic force that originates at this undistorted interface acts on LC molecules at bulk in order to restore the random LC configuration of lower energy. In this way, LC molecules return to randomly state and a higher scattering state returns.

It is possible that too longer polymer chains as PEG6000DA polymer and PEG6000DM polymer crystallize with a larger proportion of chains in the amorphous phase which enhances PME for 22 % and 13 %, respectively.

Chapter VI

6 Multi-Functional Poly(ethylene glycol)

A correlation between the polymer glass transition temperature and the degree of crosslinking of the polymer are competing effects on the appearance of the permanent memory effect. In previously studies[134,135] a stronger association between PDLCs produced from higher functional monomers and permanent memory effect was found. The increasing number of acrylate or methacrylate groups on pre-polymer enhances a cross-linking reaction. In this way, during the crosslinking reaction, bonds are formed between the macromolecules, hold them together forming enormous interconnected polymer networks[136]. The main problem found was the heavily crosslinked networks even only with partial polymerization of the systems achieve by control the polymerization time. The speed of polymer gelation is high with respect to the phase separation process. In this way, LC molecules remain trapped in a polymer matrix and are unable to respond to an applied field. In this way, although the excellent result for permanent memory effect (100 %) the use of multi-functional pre-polymers in preparation of PDLC with permanent memory effect have a second major property of high harder by unwanted high crosslink density for thermal polymerization time higher than 30 min. Which in turns result in unstable PDLCs.

In order to overcome this shortcoming of crosslinked polymer network matrix on permanent memory effect, were synthesized and characterized crosslinked pre-polymers but with arm lengthened to try significantly enhance segmental mobility decreasing the glass transition temperature and keeping the polymer structure unaffected by changes in temperature but also forming simultaneous interconnected polymer networks.

PEGs started to be commercially available only in linear chains such as diol-PEG and monomethoxy-PEG regardless of the molecular weight. In recent years, new multifunctional branched PEGs have been also commercially available. Usually, branched PEGs are a heterogeneous mixture having a distribution of arm lengths and in some cases distribution of species with different numbers of arms. The degree of branching could be not necessarily the same as the functionality because not every branched chain could carry a polymerizable group[90,91].

Flexible backbones, such as polyglycols, tend to produce softer coatings[137]. In this way, to improve segmental mobility compared to previous results[134,135], multi-armed oligomers end-functionalized were synthesized through started material of branched flexible polyols core as glycerol ethoxylate (3-armPEG) and pentaerythritol ethoxylate (4-armPEG). As in synthesis of linear di-functional PEG, the alcohol end groups of the corresponding triol and tetraol have been

functionalized by nucleophilic substitution with (meth) or acryloyl chloride, resulting in cross-linkable oligomers.

Besides the flexible branched pre-polymers to limit crosslinking to the level of crosslinking desired it is also, controlled by the time of polymerization. The crosslinking density can be extremely high with the increase of polymerization time where crosslink continues to increase as more molecules are linked together. In this way, the crosslinking reactions could be terminated prematurely achieving a desired number of crosslinks. During polymerization, the molecules start to react and crosslinks begin to form. A complete full conversion takes some time to develop, that allows controlling the desired crosslink density[136].

6.1 Synthesis and Characterization of Arm-PEG End-Functionalized

The arm-PEGs end functionalized were synthesized starting from corresponding triol and tetraol. Thus, following some literature procedures[135,138] and following the synthesis of di-functional PEG, the alcohol end groups have been functionalized by nucleophilic substitution with (meth) or acryloyl chloride, resulting in cross-linkable oligomers. Their structures were assigned on the basis of their ^{1}H-NMR, ^{13}C-NMR, DEPT, two dimensional NMR (COSY and HSQC) and MALDI-TOF mass spectrometry.

6.1.1 Tri-arm PEG with Methacrylate Ends Groups (3-armPEG TriM)

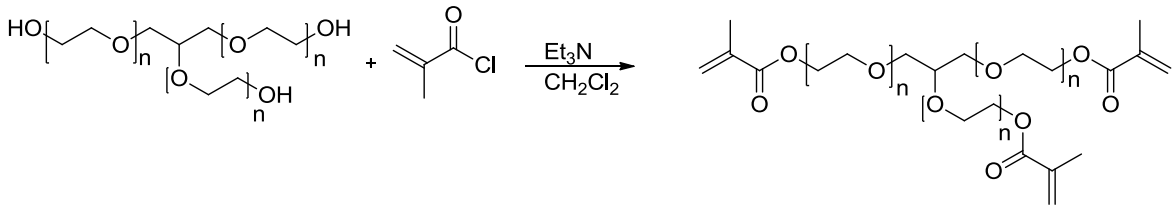

Figure 6.1 – Synthetic scheme of synthesis of Tri-armPEG with tri-methacrylate ends groups (3-armPEG TriM).

The synthetic route for tri arm-PEG with tri-methacrylate ends groups is shown in Figure 6.1. To a solution of glycerol ethoxylate (2 g, 2 mmol, 1 eq) in dry dichloromethane (CH_2Cl_2) (15 mL) was added triethylamine (Et_3N) (1.21 g, 12 mmol, 6 eq) and then cooled to 0 ºC in an ice-water bath. To this solution, methacryloyl chloride (1.25 g, 12 mmol, 6 eq) was added dropwise. After dropping, the mixture was stirred 24h at 40 ºC. The reaction mixture was washed with hydrochloric acid (HCl) 0.1M, brine and H_2O. Organic phase was dried over anhydrous sodium sulfate (Na_2SO_4) filtered and concentrated under reduced pressure. The resulting crude product was purified by column chromatography using EtOAc-hexane (5:1) and then $CHCl_3$:MeOH (9:1) as the eluents to give pure Tri-armPEG with methacrylate ends groups (2.27 g, 1.89 mmol, 94 %) as a colorless oil that foamed under vacuum. Compounds were visualized with

phosphomolybdic acid by thin layer chromatography (TLC) analysis ($CHCl_3$-MeOH 9:1). The NMR assignments and structure determination were made by ^{1}H-NMR (Figure 6.2), ^{13}C-NMR (Figure 6.4), DEPT (Figure 6.5) and by two dimensional NMR (COSY (Figure 6.6) and HSQC (Figure 6.7)).

^{1}H-NMR (400 MHz, $CDCl_3$) δ 6.13 (s, 3H, =C$\underline{H}_2$), 5.58 (s, 3H, =C$\underline{H}_2$), 4.32 – 4.27 (m, 6H, C$\underline{H}_2$O-(C=O)), 3.78 – 3.73 (m, 6H,C$\underline{H}_2$CH$_2$O-(C=O)), 3.68 – 3.53 (m, 78H, C$\underline{H}_2$C$\underline{H}_2$O,$\underline{H}$C-(C$\underline{H}_2$)$_2$), 1.95 (s, 9H, C$\underline{H}_3$).

^{13}C-NMR (100 MHz, $CDCl_3$) δ 18.18 (C$\underline{H}_3$), 63.73 (C$\underline{H}_2$O-(C=O), 68.97 (C$\underline{H}_2$CH$_2$O-(C=O)), 70.42-70.68 (C$\underline{H}_2$C$\underline{H}_2$O), 78.22 (C$\underline{H}$-CH$_2$), 125.58 (=C$\underline{H}_2$) , 136.01 (CH$_3$-C$\underline{=}$C), 167.10(C=O).

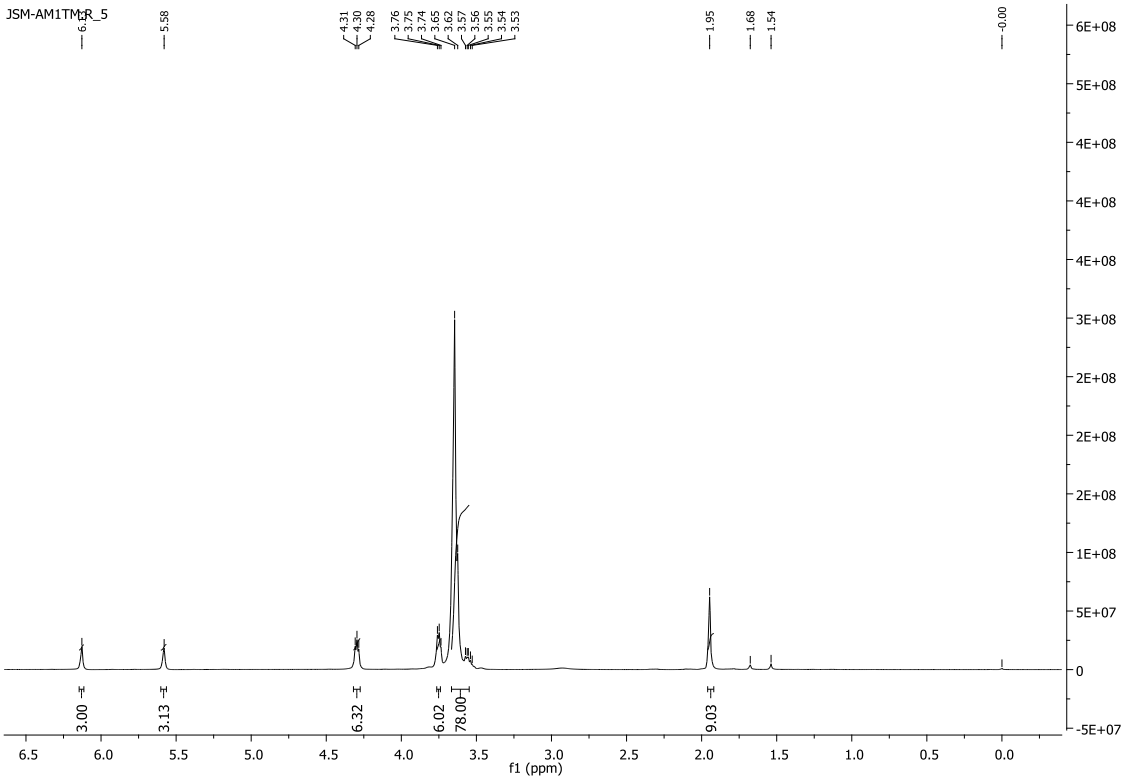

Figure 6.2 – ^{1}H-NMR spectrum of 3-armPEG TriM.

The two small singlets at 1.68 and 1.54 ppm (Figure 6.2) which by COSY spectrum (Figure 6.6) exhibits no coupling to neighboring protons are consistent with singlets at 1.72 and 1.62 ppm of methacryloyl chloride (Figure 6.3).

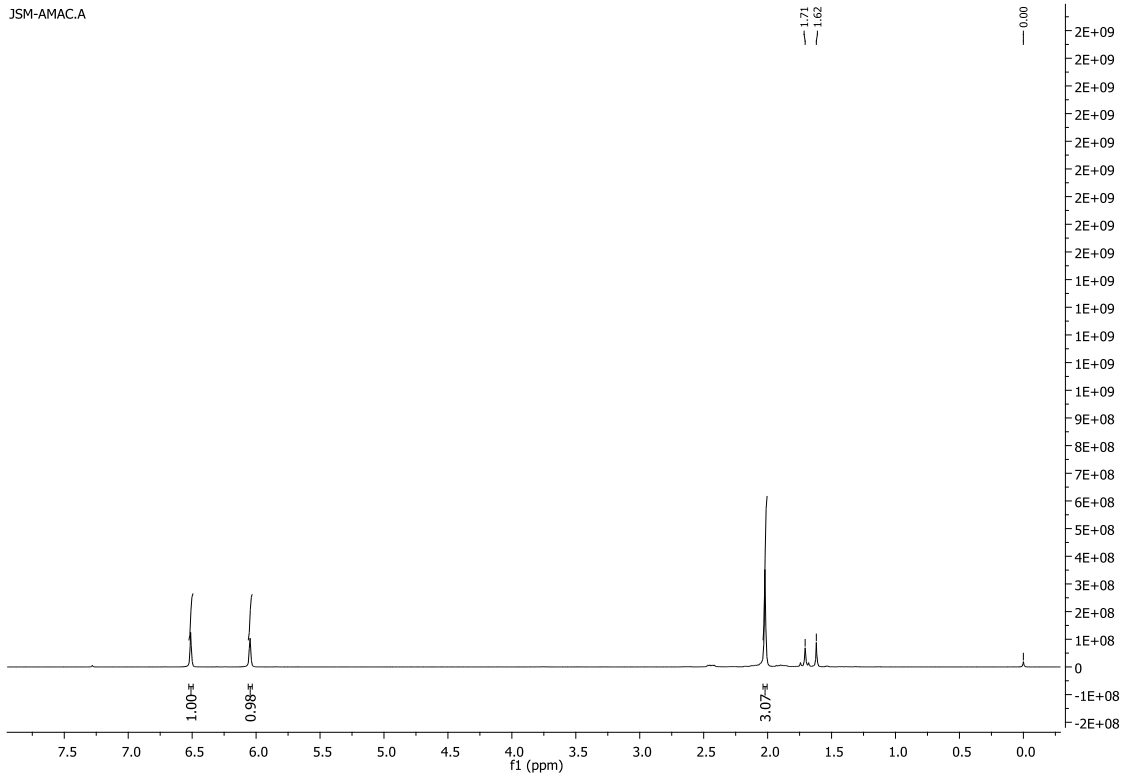

Figure 6.3 – ^{1}H-NMR spectrum of methacryloyl chloride.

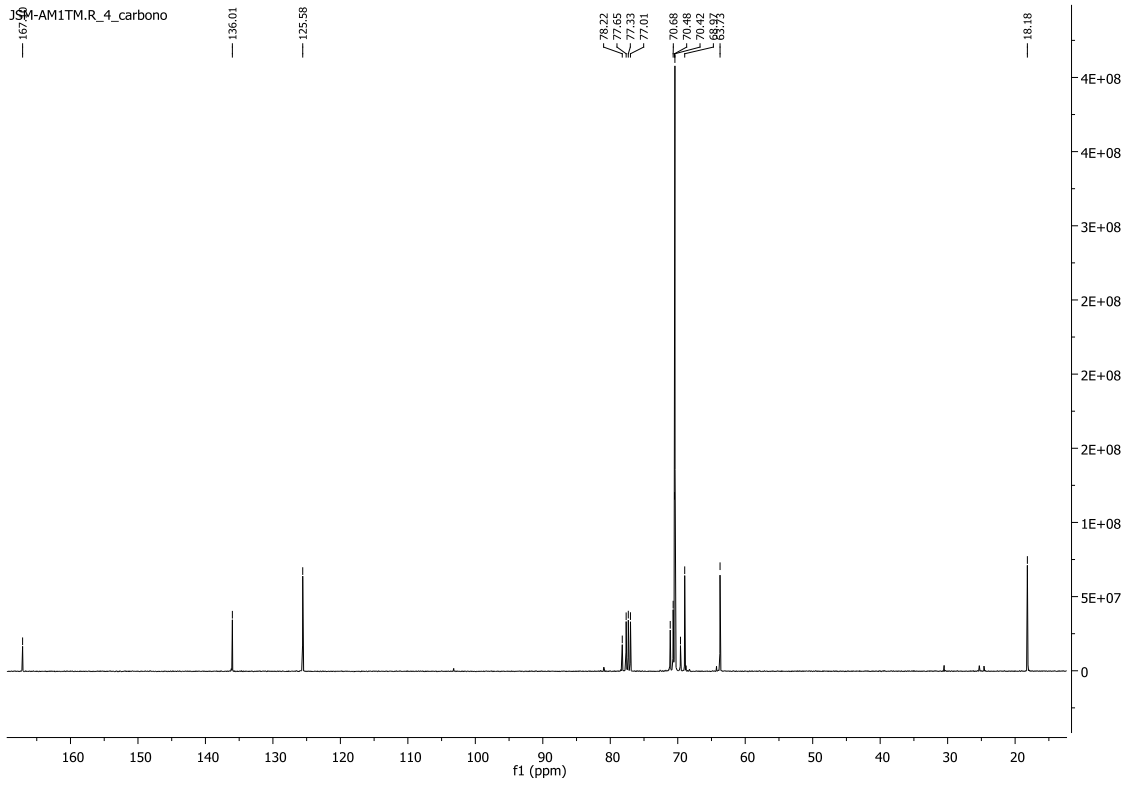

Figure 6.4 – ^{13}C NMR spectrum of 3-armPEG TriM.

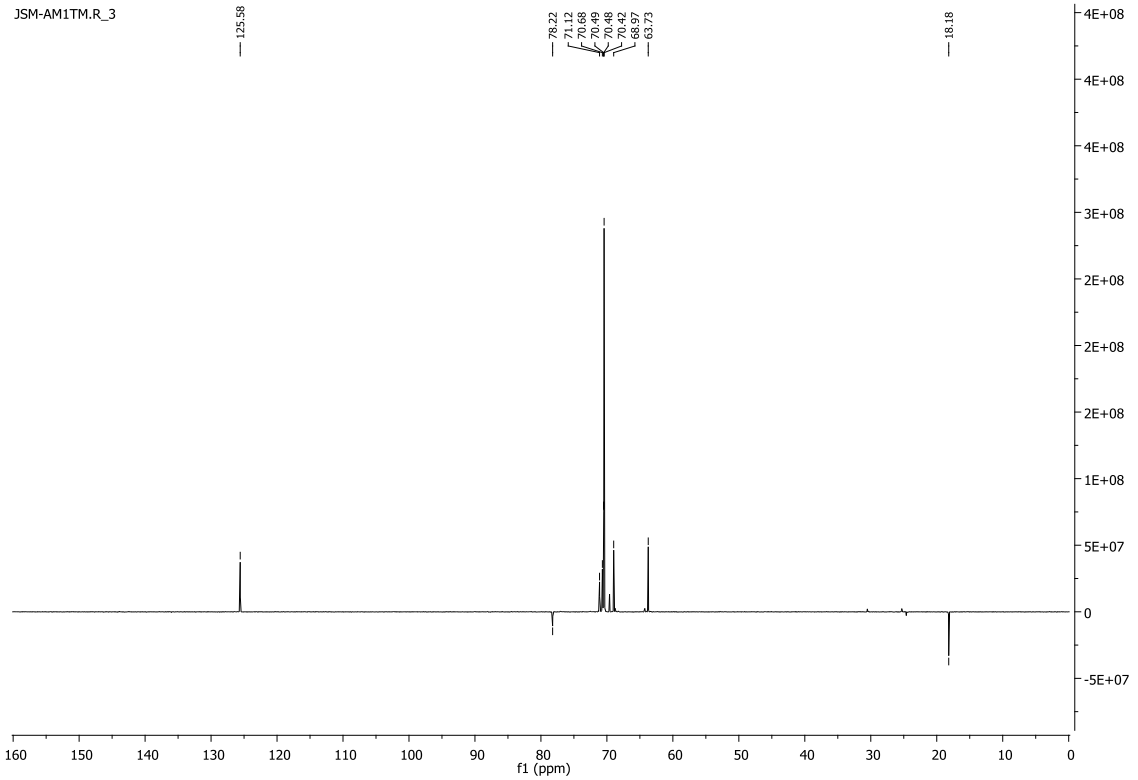

Figure 6.5 – ^{13}C DEPT spectrum of 3-armPEG TriM.

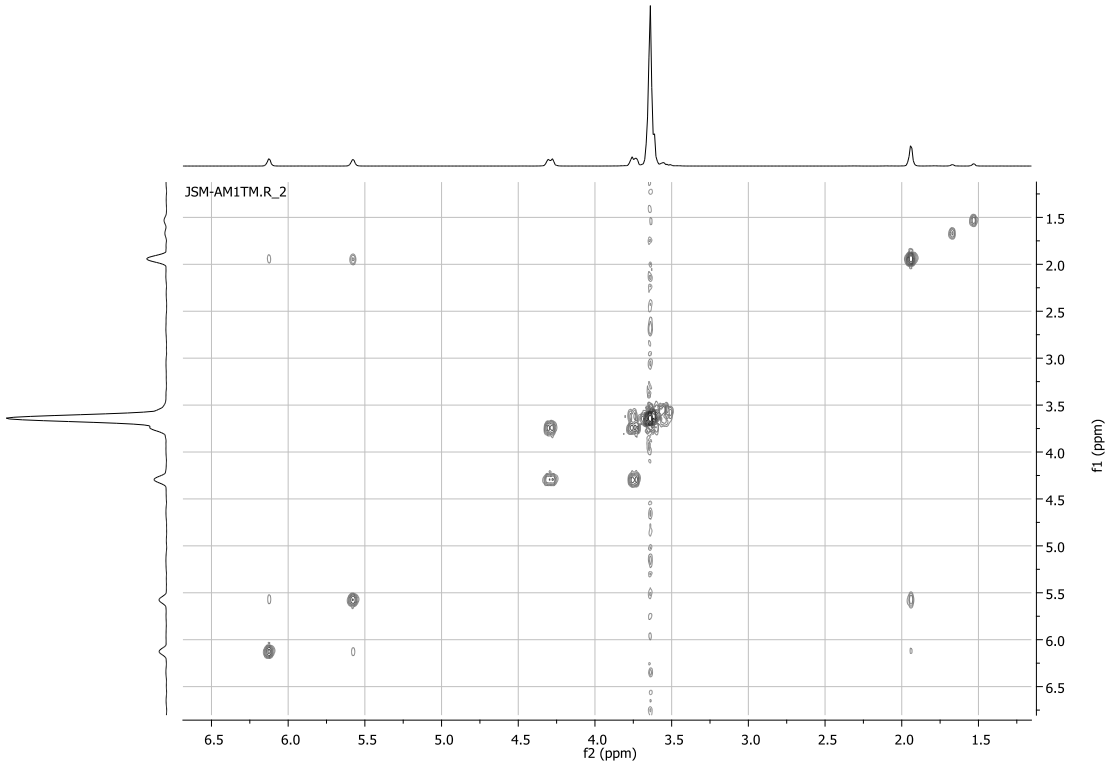

Figure 6.6 – COSY spectrum of 3-armPEG TriM.

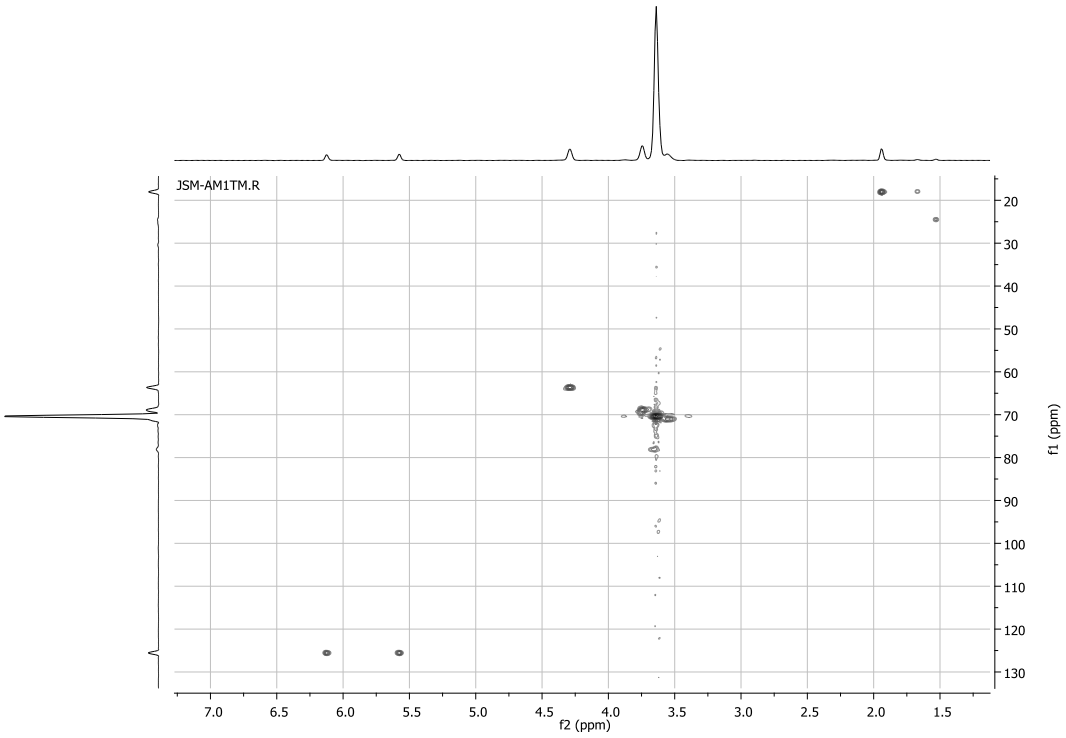

Figure 6.7 – HSQC spectrum of 3-armPEG TriM.

6.1.2 Tri-arm PEG with Acrylate Ends Groups (3-armPEG TriA)

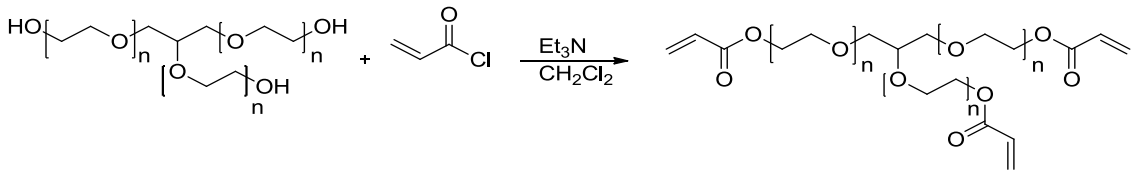

Figure 6.8– Synthetic scheme of synthesis of tri-armPEG with acrylate ends groups (3-armPEG TriA).

The synthesis (Figure 6.8) and characterization of 3-armPEG TriA was similar to synthesis and characterization of 3-armPEG TriM. Glycerol ethoxylate (2 g, 2 mmol, 1 eq) in CH_2Cl_2 (15 mL) with triethylamine (1.21 g, 12 mmol, 6 eq) and acryloyl chloride (1.09 g, 12 mmol, 6 eq) gave tri armed PEG with acrylate ends groups (2.28 g, 1.96 mmol, 98 %) as a yellow oil that foamed under vacuum. The NMR assignments and structure determination were made by ^{1}H-NMR (Figure 6.9), ^{13}C-NMR (Figure 6.10), DEPT (Figure 6.11) and by two dimensional NMR (COSY and HSQC) (Figure 6.12 and Figure 6.13).

^{1}H-NMR (400 MHz, $CDCl_3$) δ 6.43 (d, *J* = 17.3 Hz, 3H, =C$\underline{H}_2$), 6.16 (dd, *J* = 17.3, 10.4 Hz, 3H,C$\underline{H}$), 5.85 (d, *J* = 10.4 Hz, 3H, =C$\underline{H}_2$), 4.34 – 4.28 (m, 6H, C$\underline{H}_2$O-(C=O)), 3.78 – 3.73 (m, 6H, C$\underline{H}_2$CH$_2$O-(C=O)), 3.70 – 3.53 (m, 74H, C$\underline{H}_2$C$\underline{H}_2$O,$\underline{H}$C-(C$\underline{H}_2$)$_2$).

^{13}C-NMR (100 MHz, $CDCl_3$) δ 63.54 ($\underline{C}H_2O$-(C=O), 68.95 ($\underline{C}H_2CH_2O$-(C=O)), 70.42-71.10 ($\underline{C}H_2\underline{C}H_2O$), 78.21 ($\underline{C}H$-$CH_2$), 128.19 (H-$\underline{C}$=C), 130.89 (=$\underline{C}H_2$), 165.94 ($\underline{C}$=O).

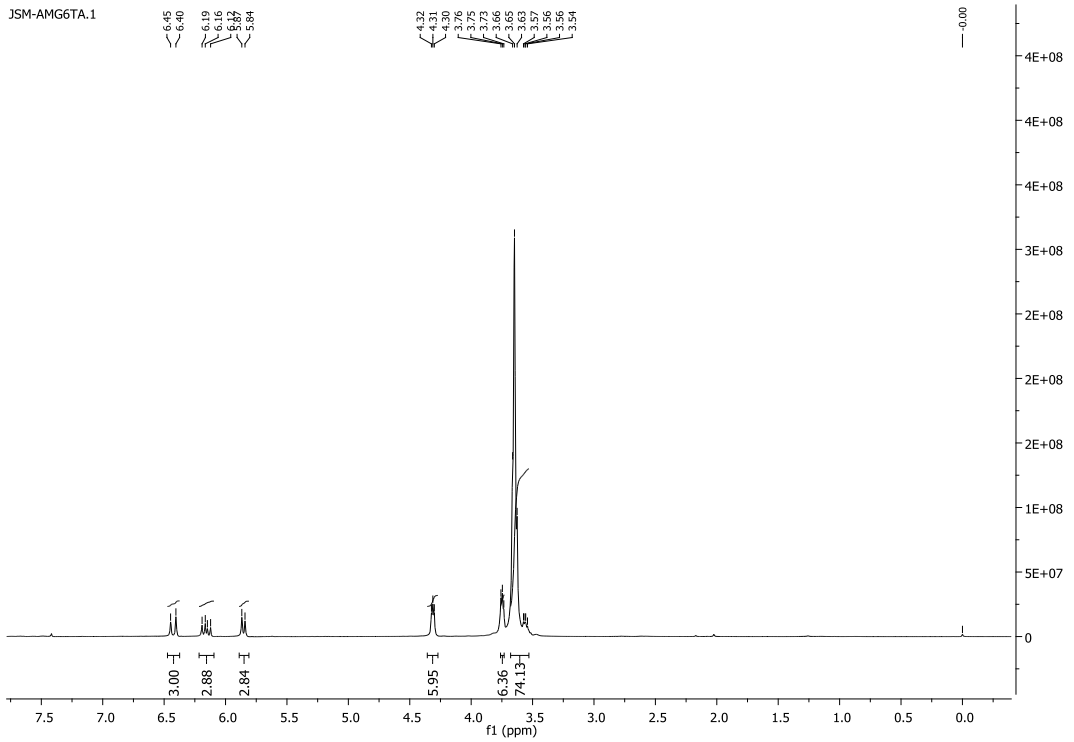

Figure 6.9 – ^{1}H-NMR spectrum of 3-armPEG TriA.

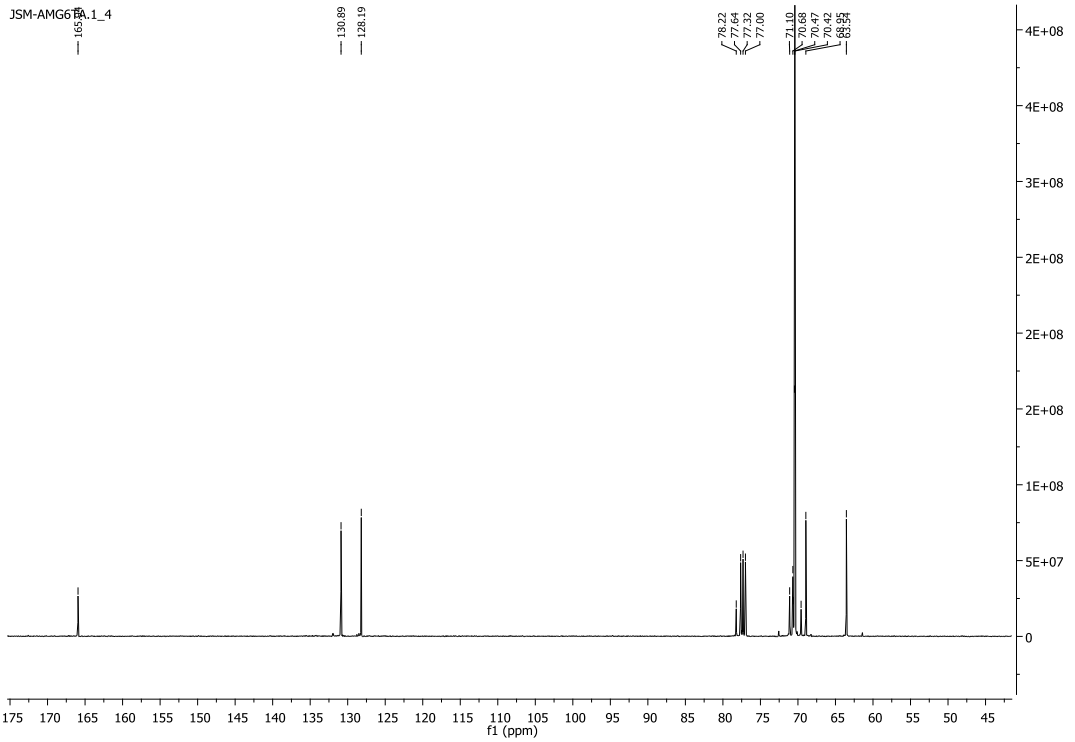

Figure 6.10 – ^{13}C NMR spectrum of 3-armPEG TriA.

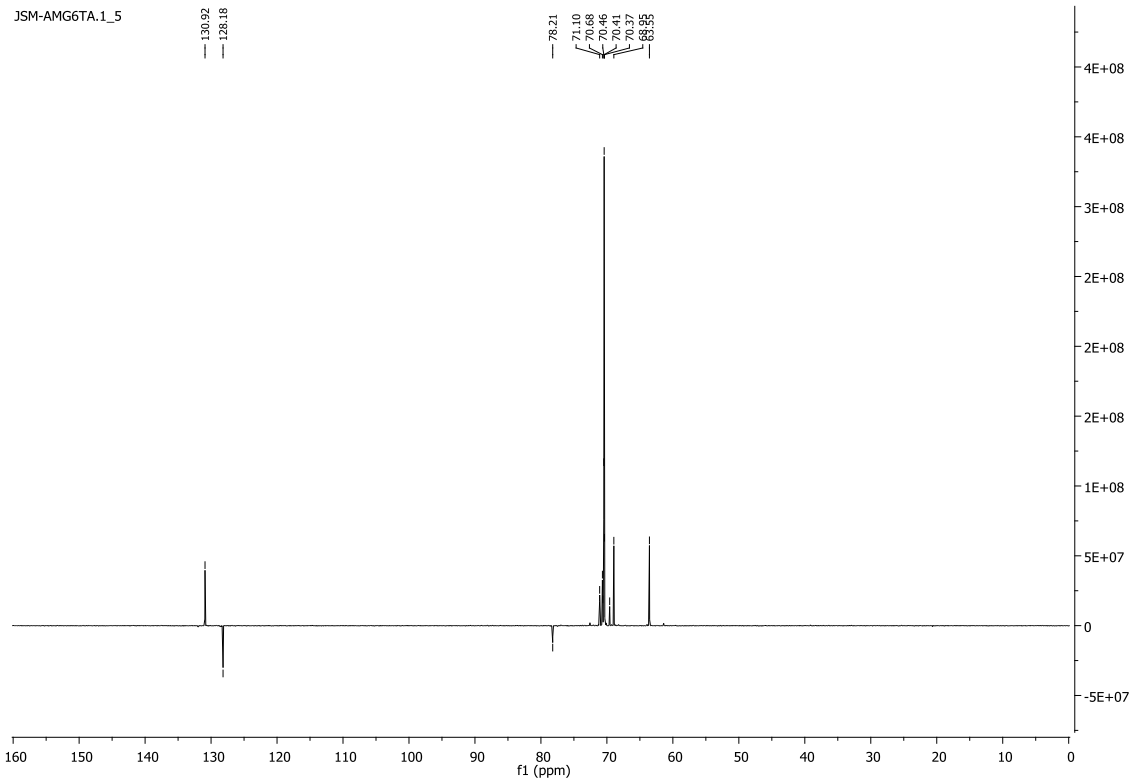

Figure 6.11 – ^{13}C DEPT spectrum of 3-armPEG TriA.

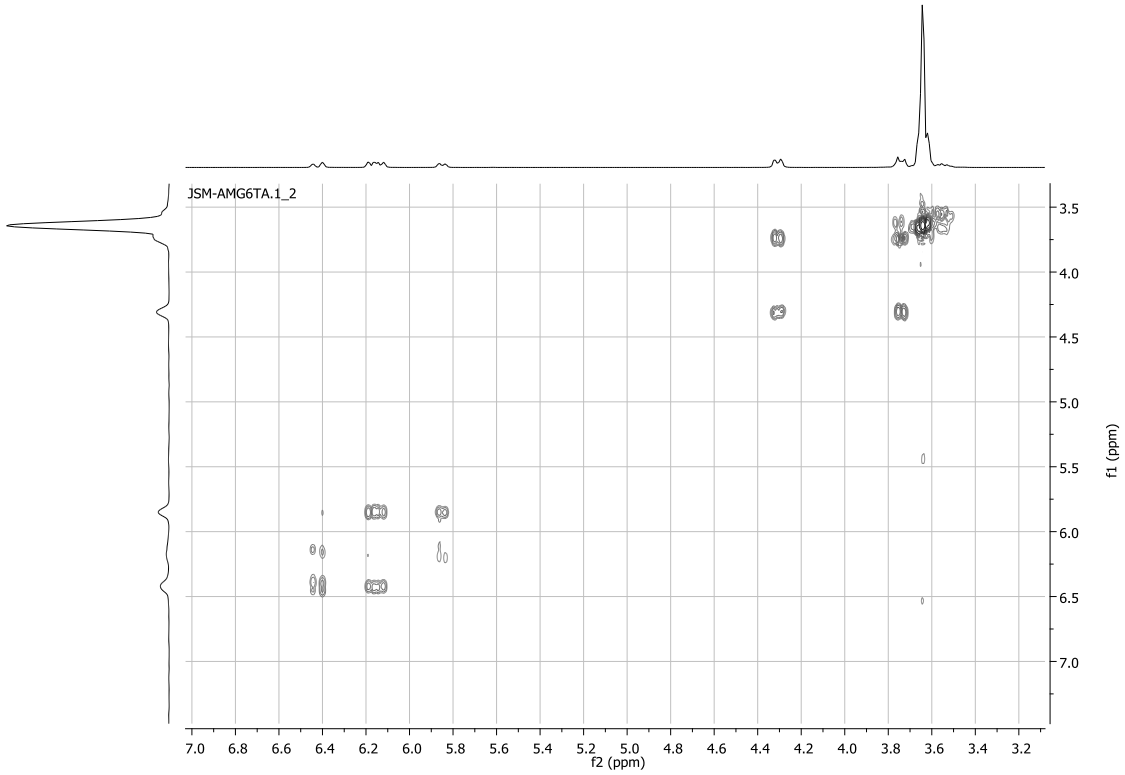

Figure 6.12 – COSY spectrum of 3-armPEG TriA.

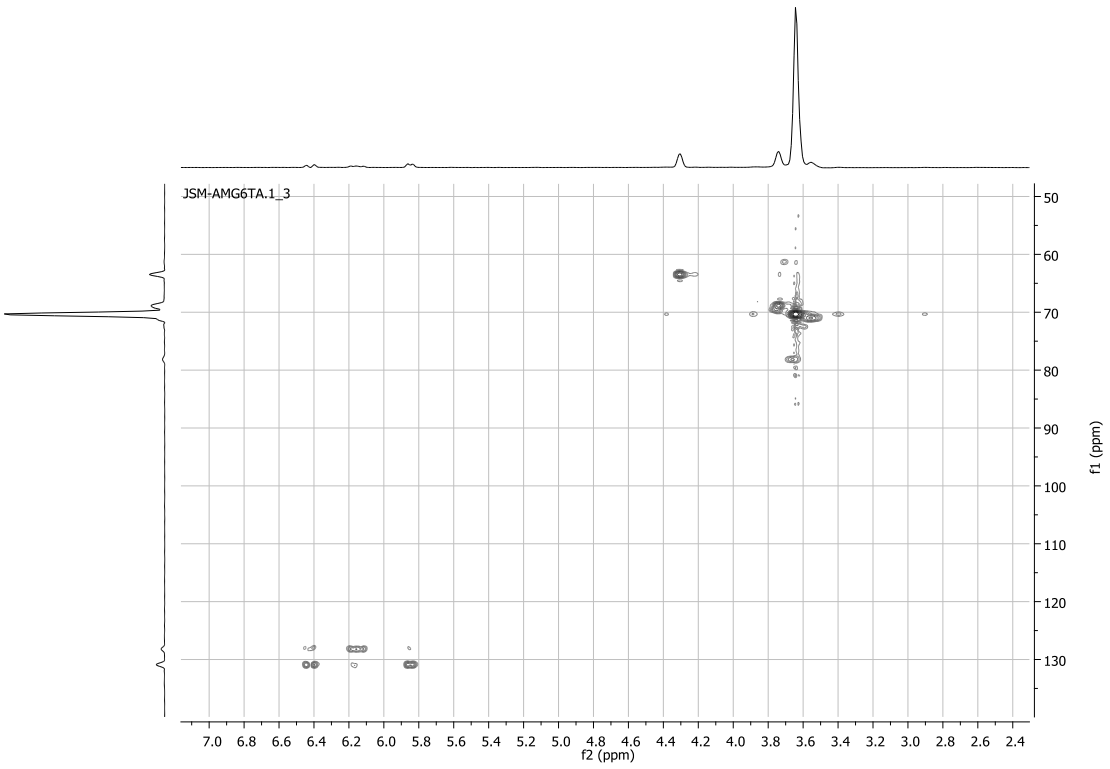

Figure 6.13 – HSQC spectrum of 3-armPEG TriA.

6.1.3 MALDI-TOF MS

The MALDI-TOF mass spectra of the $[3\text{-arm PEG+Na}]^+$ and resulting Na^+ cationized tetra-functionalized species (3-arm PEGTriM and 3-arm PEGTriA) are shown in Figure 6.14. In average adjacent peaks of the same series differ in mass by 44 Da, which corresponds to the molecular mass of the oxyethylene repeat unit. The calculated molecular weights (M_n, M_w), PDI and the number of repeat ethylene oxide units (n) were determined as described in chapter V.

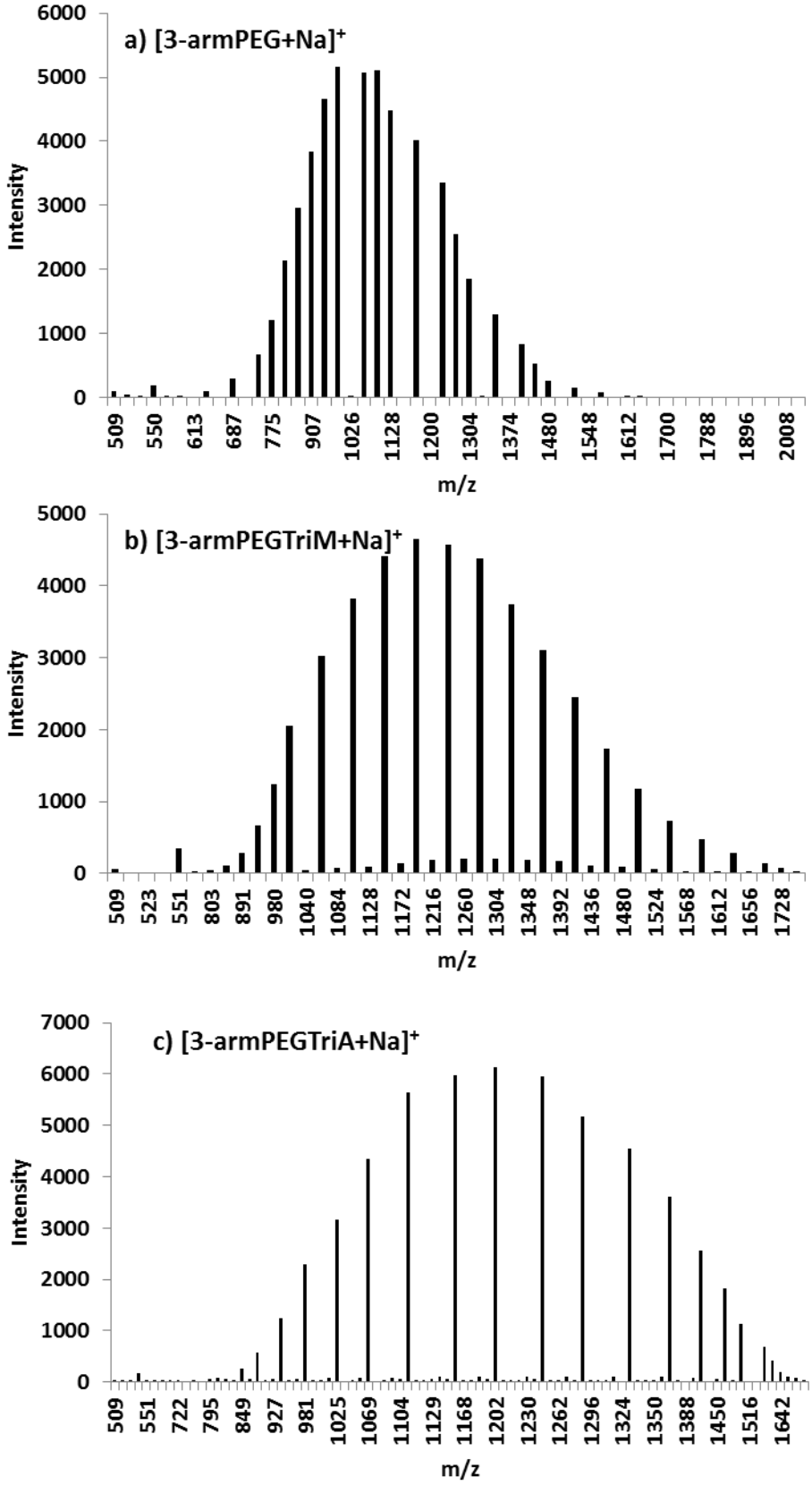

Figure 6.14 **–** MALDI-TOF mass spectra of a) [3-armPEG+Na]$^+$; b) **[**3-armPEG TriM+Na]$^+$ c) [3-armPEG TriA+Na]$^+$.

For the main series, Figure 6.14 a) ≈ 680-1700 m/z; b) ≈ 800-1800 m/z and c) ≈ 850-1800 m/z, theoretical molecular mass results are very close to the observed ones (Table 6.1) which indicate the tri-functionalization of the starting material.

Table 6.1– The theoretical and observed molecular weights of $[3\text{-armPEG+Na}]^+$ and resulting products, $[3\text{-armPEG TriM+Na}]^+$ and $[3\text{-armPEG TriA+Na}]^+$ obtained from MALDI-TOF measurements.

Macromolecule	M_n		M_w		PDI		n
	Observed	Theoretical	Observed	Theoretical	Observed	Theoretical	(total)
[3-armPEG+Na]$^+$	1063.50	-	1089.24	-	-	-	20
[3-armPEG TriM+Na]$^+$	1241.38	1242.67	1261.52	1262.37	1.02		20
[3-armPEG TriA+Na]$^+$	1218.64	1218.60	1238.44	1238.39	1.02	1.02	21

A residual amount of species of unreacted 3-armPEG was also observed in the minor series of peaks whose masses, included between ≈ 1000 m/z and 1700 m/z in $[3\text{-armPEG TriM+Na}]^+$ spectrum (Figure 6.14 b). Theoretical calculations match closely to the observed distributions in this minor series (Table 6.2). The chromatographic purification was very difficult because the variation in polarity was not enough to isolate the 3-armPEGTriM from its mixture even with repeated column chromatography. However, it is a set of peaks of much lower intensity.

Table 6.2 – The theoretical and observed molecular weights from MALDI-TOF measurements for minor series of peaks in $[3\text{-armPEG TriM+Na}]^+$ spectrum.

Macromolecule	M_n		M_w		PDI	
	Observed	Theoretical	Observed	Theoretical	Observed	Theoretical
[3-armPEG+Na]$^+$	1306.70	1306.67	1321.52	1321.49	1.01	1.01

6.1.4 Four-arm PEG with methacrylate ends Groups (4-armPEG TetraM)

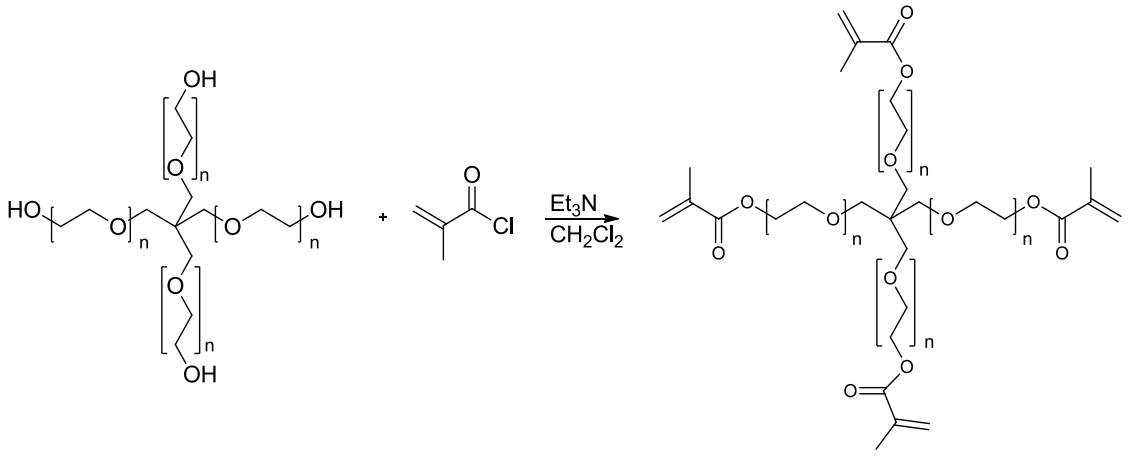

Figure 6.15 – Synthetic scheme of synthesis of four-armPEG with methacrylate ends groups (4-arm PEGTetraM).

According to the scheme shown in Figure 6.15, in a solution of pentaerythritol ethoxylate (4-arm PEG) (3 g, 3.76 mmol, 1 eq) in dry CH_2Cl_2 (15 mL) was added triethylamine (2.28 g, 22.58 mmol, 6 eq) and then was added dropwise methacryloyl chloride (2.36 g, 22.58 mmol, 6 eq) at

0 ºC. The reaction mixture was stirred for 24 h at 40 ºC. The reaction mixture was washed with HCl 0.1M, brine and H_2O. The organic phase was dried over Na_2SO_4, filtered and concentrated under reduced pressure. The resulting crude product was purified by column chromatography using EtOAc-hexane (5:1) and then $CHCl_3$:MeOH (9:1) as the eluents to give four-armed PEG with methacrylate ends groups (4-armPEG TetraM) (3.52 g, 3.29 mmol, 88 %) as a yellow oil that foamed under vacuum. Compounds were visualized with phosphomolybdic acid by TLC analysis ($CHCl_3$-MeOH 9:1). The NMR assignments and structure determination were made by ^{1}H-NMR (Figure 6.16), ^{13}C-NMR (Figure 6.17), DEPT (Figure 6.18) and by two dimensional NMR (COSY (Figure 6.19) and HSQC) (Figure 6.20)).

^{1}H-NMR (400 MHz, $CDCl_3$) δ 6.13 (s, 4H, =C$\underline{H_2}$), 5.58 (s, 4H, =C$\underline{H_2}$), 4.33 – 4.25 (m, 8H, C$\underline{H_2}$O-(C=O)), 3.78 – 3.72 (m, 8H, C$\underline{H_2}$CH_2O-(C=O)), 3.69 – 3.38 (m, 60H, C$\underline{H_2}$C$\underline{H_2}$O, C(C$\underline{H_2}$)$_4$), 1.95 (s, 12H, C$\underline{H_3}$).

^{13}C-NMR (100 MHz, $CDCl_3$) δ 18.31 (C$\underline{H_3}$), 44.71 (C(CH_2)$_4$), 63.86 (C(C$\underline{H_2}$)$_4$), 69.12-71.09 (C$\underline{H_2}$O-(C=O), C$\underline{H_2}$CH_2O-(C=O), C$\underline{H_2}$C$\underline{H_2}$O), 125.72(=C$\underline{H_2}$), 136.14 (CH_3-C=C), 167.34(C=O).

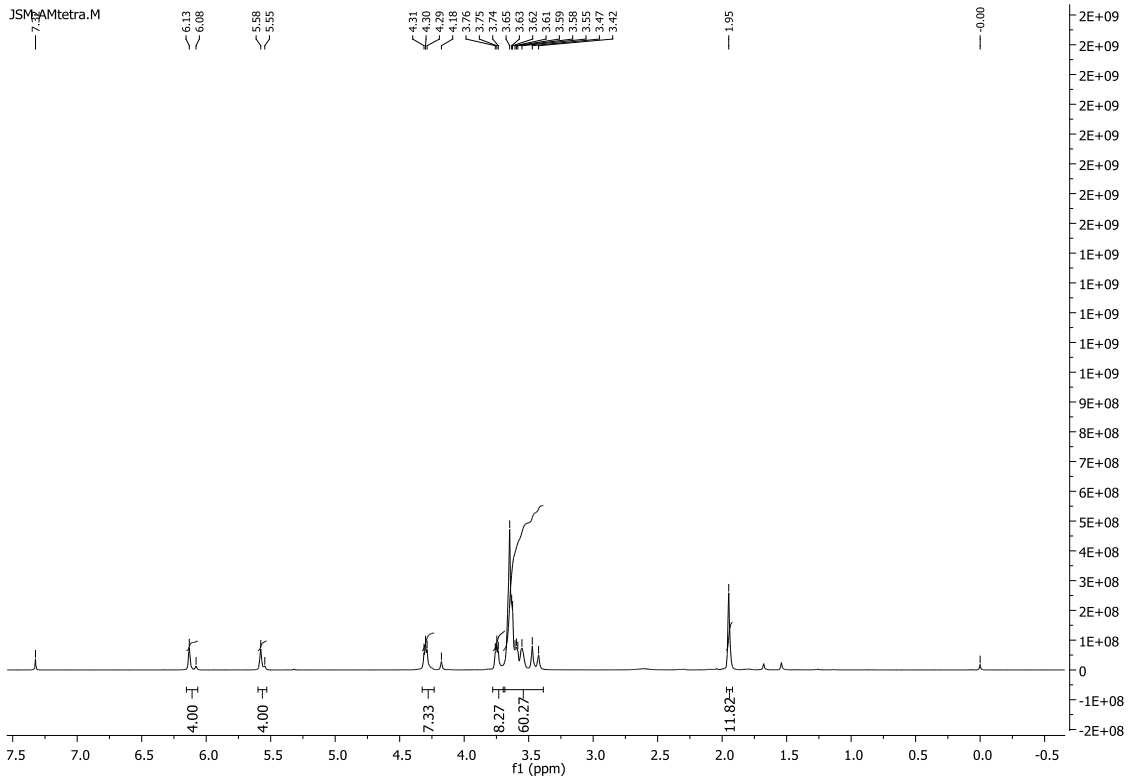

Figure 6.16 – ^{1}H-NMR spectrum of 4-arm PEGTetraM.

In the ^{1}H-NMR spectrum of 4-armPEGTetraM (Figure 6.16), methylene protons on methacrylate group resonance between 6.13 and 5.58 ppm and methylene protons immediately adjacent to the methacrylate group at 4.30 ppm. A small singlet which by COSY spectrum (Figure 6.19) exhibits no coupling to neighboring protons resonance at 4.18 ppm. This small singlet is consistent with methacrylate methylene protons but corresponds to methacrylation of the CH_2OH group directly linked to the central quaternary carbon atom (in starting material), rather

than through an ether linkage[139]. This analysis is supported by the ^{13}C NMR spectrum (Figure 6.17) where two signals, not one, at 45.5 and 44.7 ppm were observed in the range of the single quaternary carbon. In the ^{13}C DEPT spectrum (Figure 6.18) these two signals are absent, demonstrating that they are both quaternary centers. In this way, the same fraction of the mixture has 3-armPEG rather than 4-armPEG.

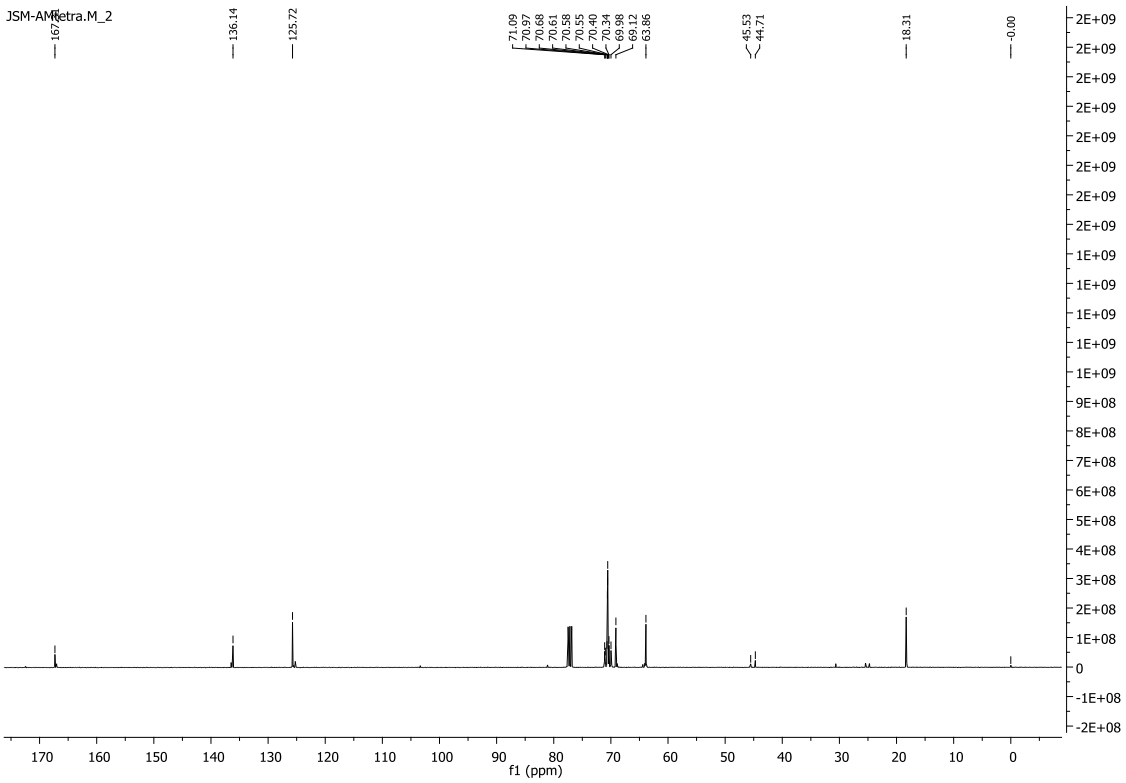

Figure 6.17 – ^{13}C NMR spectrum of 4-armPEGTetraM.

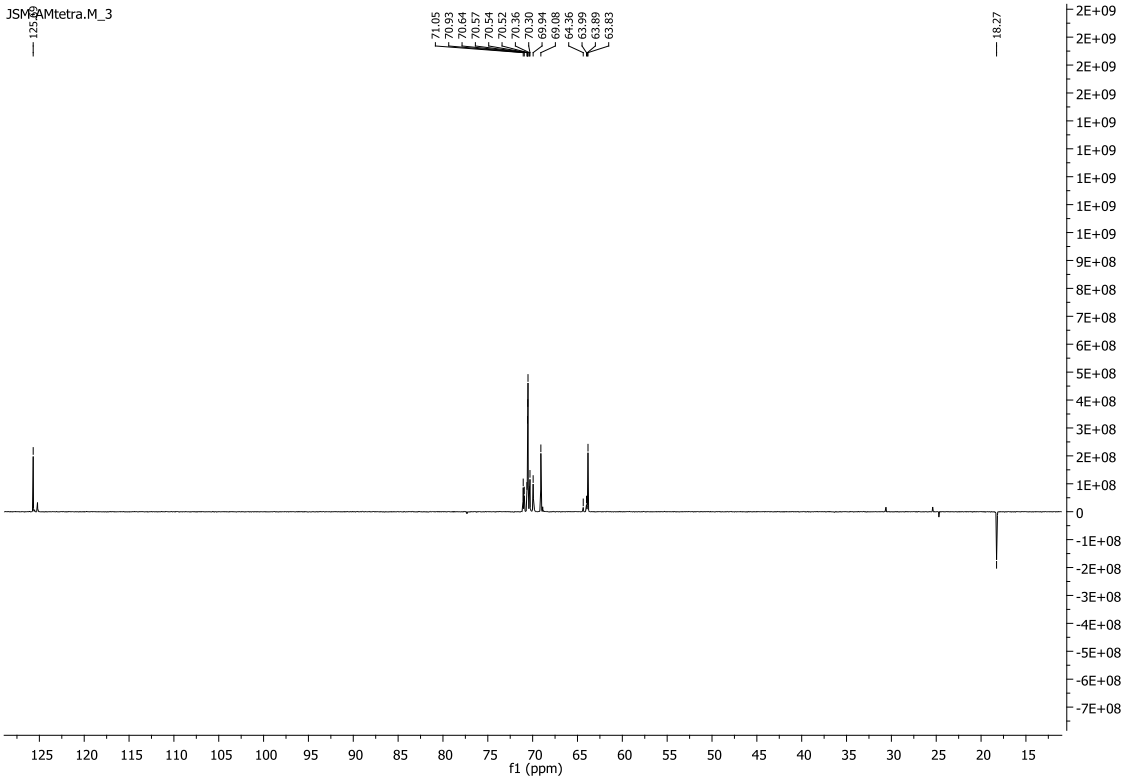

Figure 6.18 – ^{13}C DEPT spectrum of 4-armPEG TetraM.

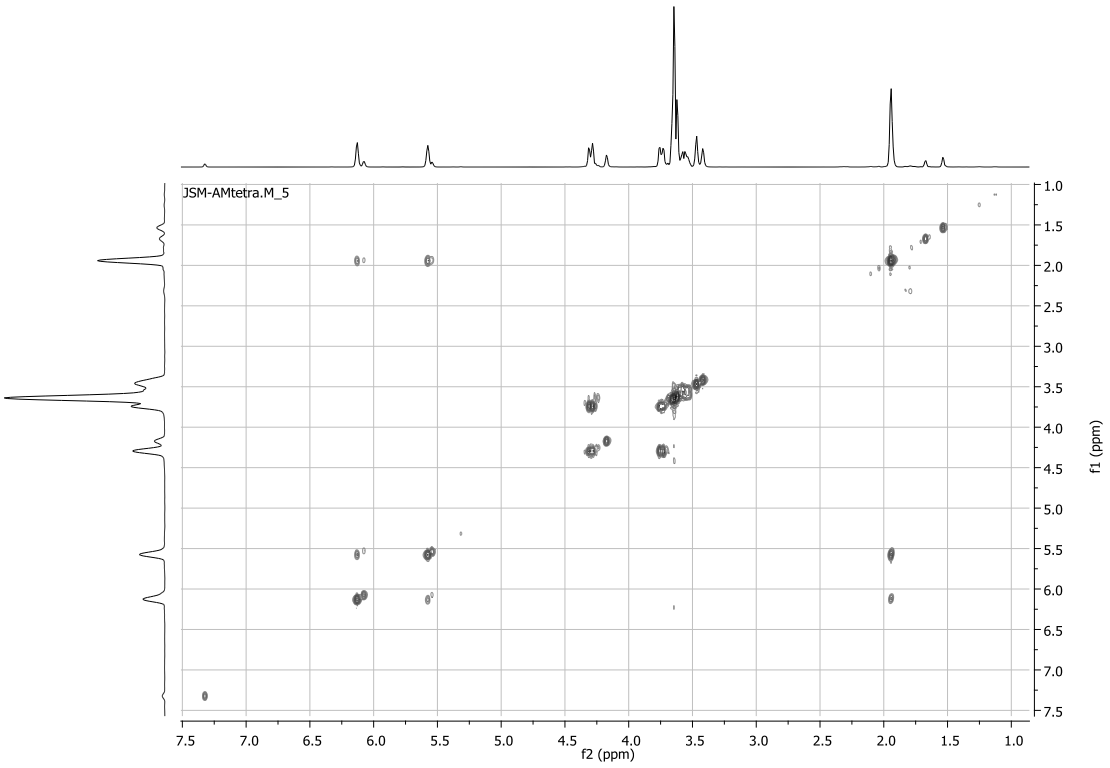

Figure 6.19 – COSY spectrum of 4-armPEG TetraM.

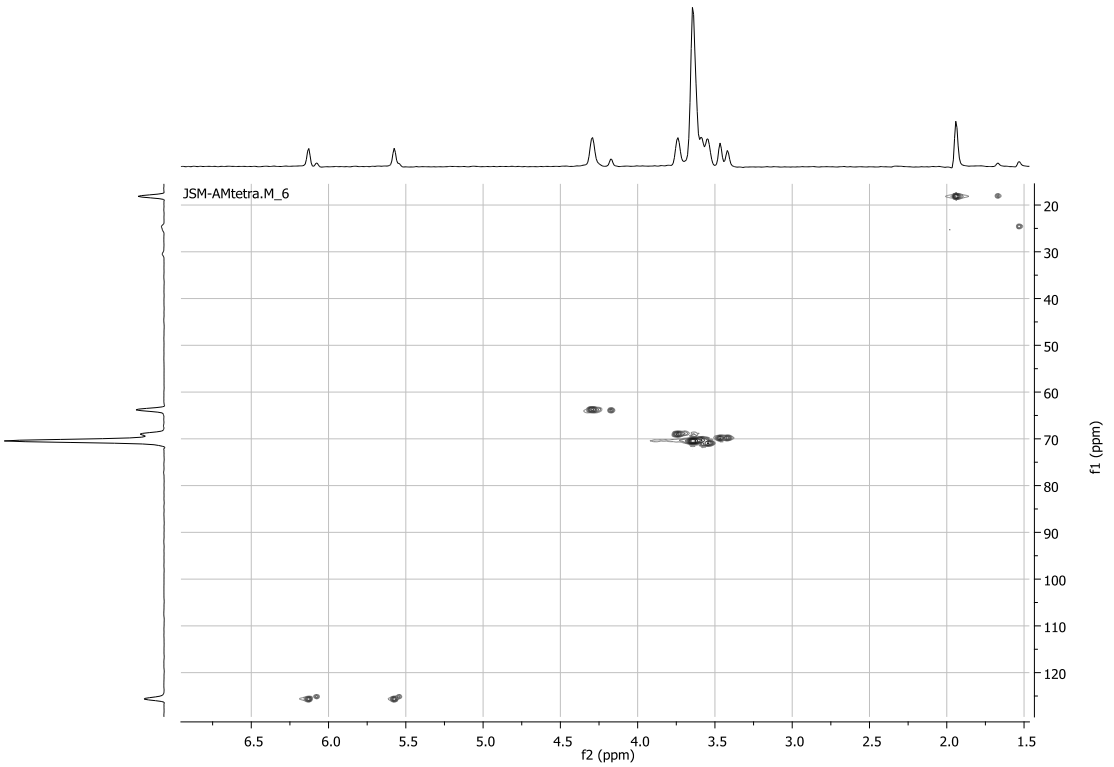

Figure 6.20 – HSQC spectrum of 4-armPEG TetraM.

6.1.5 Four-arm PEG with Acrylate ends Groups (4-armPEG TetraA)

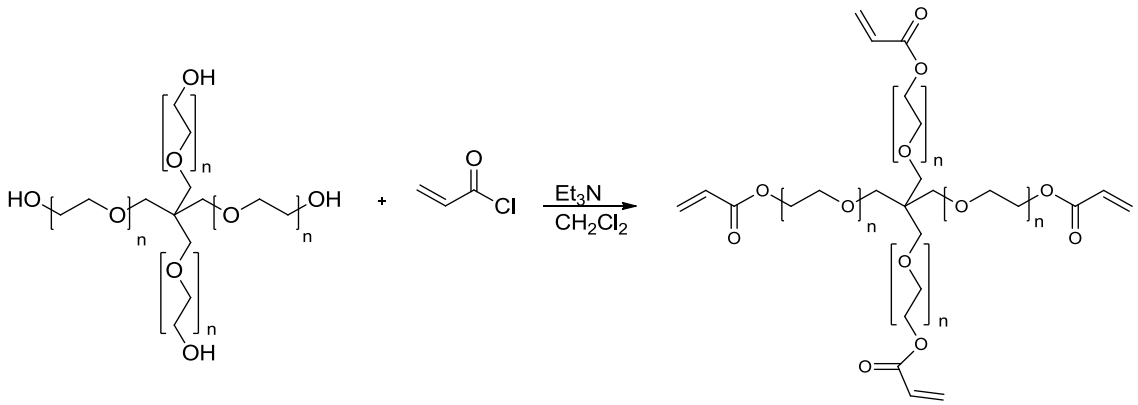

Figure 6.21– Synthetic scheme of synthesis of four-arm PEG with acrylate ends groups (4-armPEGTetraA).

In a manner similar to the preparation of four-arm oligomer with methacrylate ends groups (4-armPEG TetraM)**.** Pentaerythritol ethoxylate (4-arm PEG) (3 g, 3.76 mmol, 1 eq) in CH_2Cl_2 (15 mL) and acryloyl chloride (2.04 g, 22.59 mmol, 6 eq) gave four armed oligomers with acrylate ends groups (1.63 g, 1.60 mmol, 43 %) as a yellow oil that foamed under vacuum (Figure 6.21). The NMR assignments and structure determination were made by ^{1}H-NMR

(Figure 6.22), ^{13}C NMR (Figure 6.23), DEPT (Figure 6.24) and by two dimensional NMR (COSY (Figure 6.25) and HSQC (Figure 6.26).

^{1}H-NMR (400 MHz, $CDCl_3$) δ 6.42 (dd, *J* = 17.3, 1.2 Hz, 4H, =C$\underline{H_2}$), 6.15 (dd, *J* = 17.3, 10.4 Hz, 4H, =C$\underline{H}$), 5.85 (dd, *J* = 10.4, 1.1 Hz, 4H, =C$\underline{H_2}$), 4.33 – 4.28 (m, 8H, C$\underline{H_2}$O-(C=O)), 3.77 – 3.72 (m, 8H, C$\underline{H_2}$CH$_2$O-(C=O)), 3.68 – 3.40 (m, 60H, C$\underline{H_2}$C$\underline{H_2}$O, C-C$\underline{H_2}$)$_4$).

^{13}C-NMR (100 MHz, $CDCl_3$) δ 44.52 (C$\underline{C}$(CH$_2$)$_4$), 63.54 (C(C$\underline{H_2}$)$_4$), 68.94-77.63 ($\underline{C}$H$_2$O-(C=O), $\underline{C}$H$_2$CH$_2$O-(C=O), $\underline{C}$H$_2$C$\underline{H_2}$O), 128.20 (H-$\underline{C}$=C), 130.87 (=$\underline{C}$H$_2$), 165.91($\underline{C}$=O).

As in 4-armPEGTetraM spectrum (Figure 6.16), the additional singlet at 4.20 ppm corresponds to the possible acrylate methylene protons of the minor 3-armPEG impurity in the starting material. This is also supported by the ^{13}C NMR spectrum (Figure 6.23) where two signals, not one, at 44.52 and 45.44 ppm were observed in the range of the single quaternary carbon. This in turn is confirmed by the ^{13}C DEPT spectrum (Figure 6.24). In this way, the same fraction of the mixture has 3-arm rather than 4-arm. The penultimate methylene protons of internal ethylene glycol segment resonance at 3.74 ppm and methylene protons of internal ethylene glycol segment arms and the methylene central core protons resonance in a broad peak at 3.57 ppm.

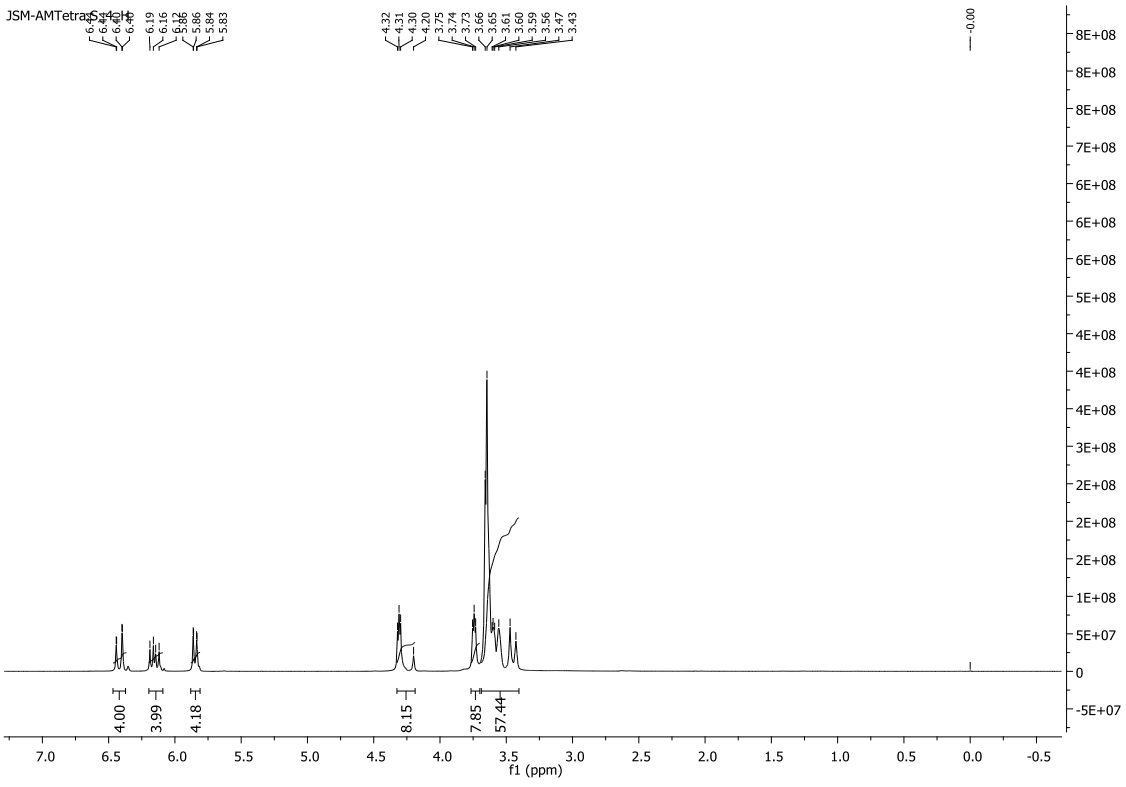

Figure 6.22 – ^{1}H-NMR spectrum of 4-armPEG TetraA.

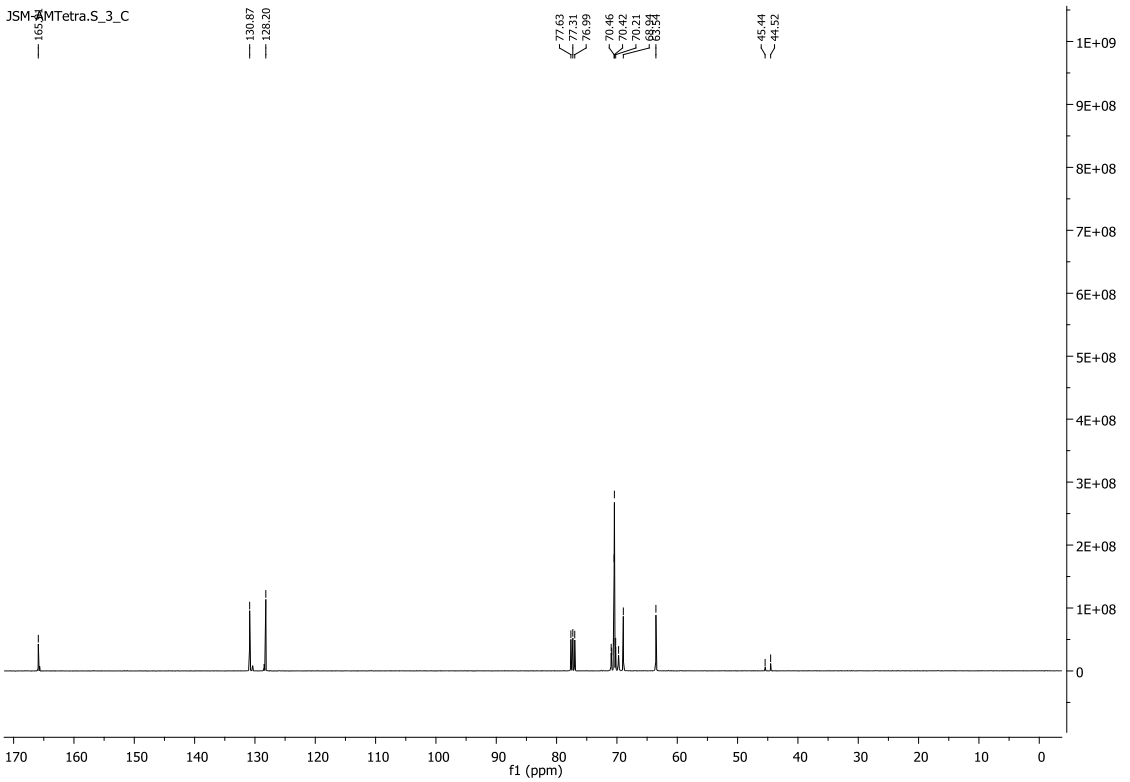

Figure 6.23 – ^{13}C NMR spectrum of 4-armPEG TetraA.

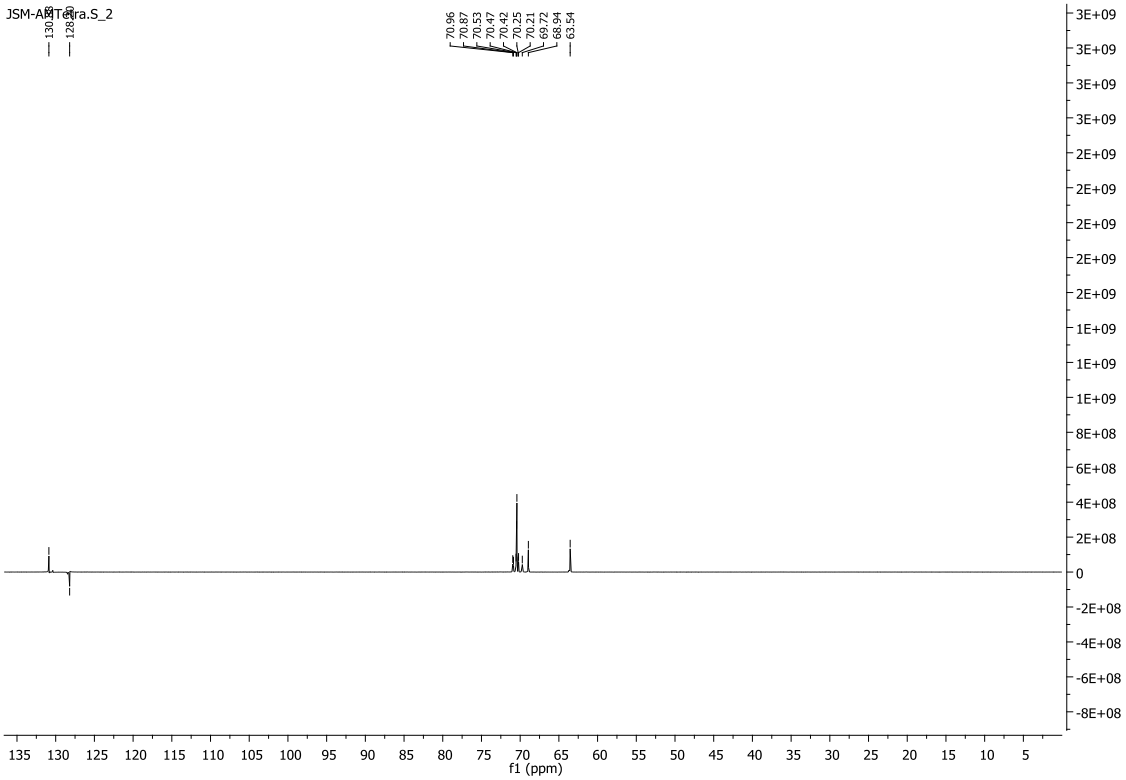

Figure 6.24 – ^{13}C DEPT spectrum of 4-armPEG TetraA.

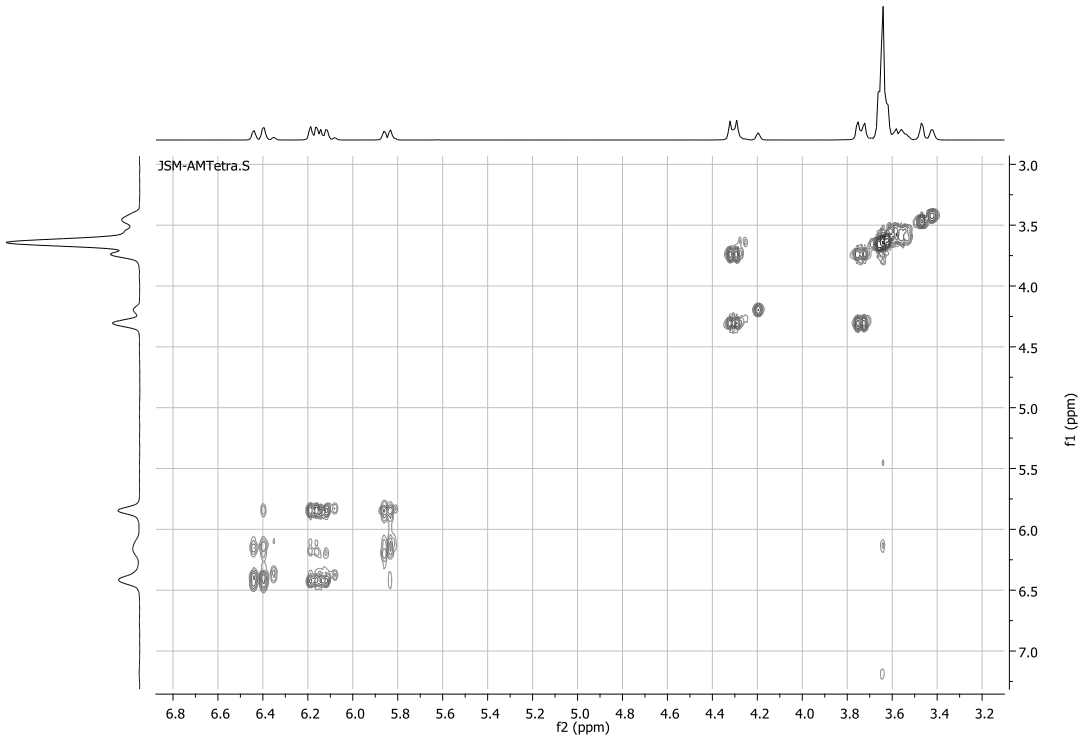

Figure 6.25 – COSY spectrum of 4-armPEGTetraA.

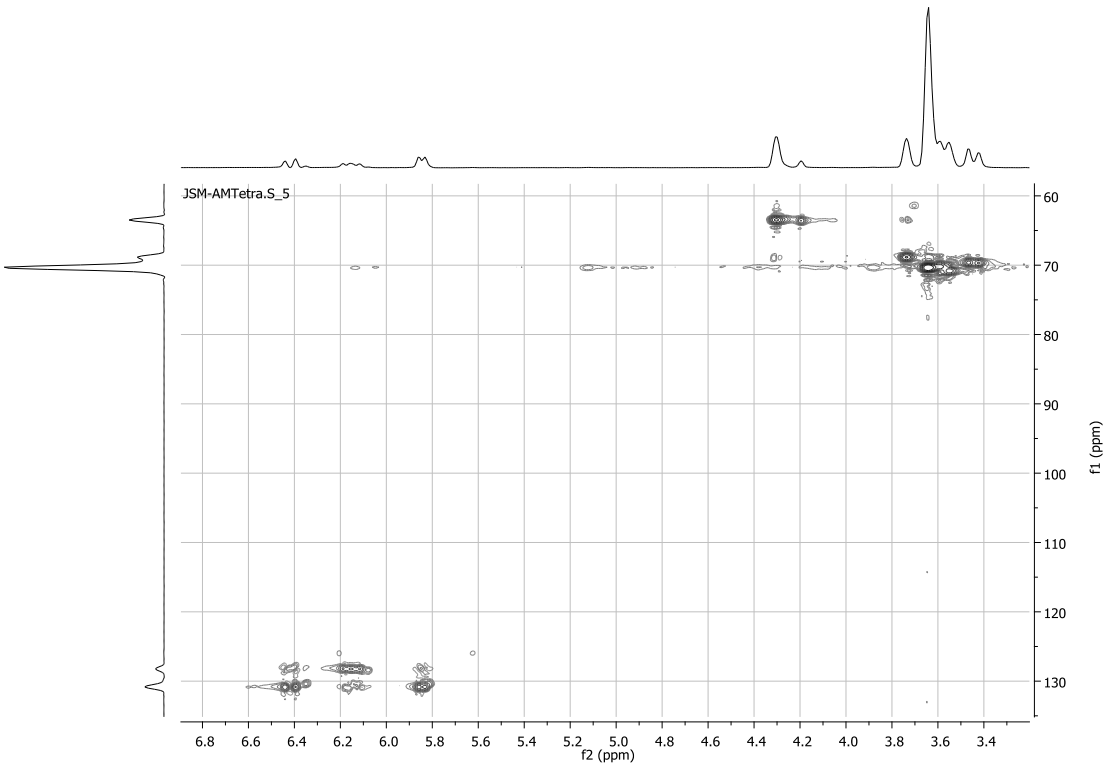

Figure 6.26 – HSQC spectrum of 4-armPEGTetraA.

6.1.6 MALDI-TOF MS

The MALDI-TOF mass spectra of the $[4\text{-armPEG+Na}]^+$ and resulting Na^+ cationized tetra-functionalized species are shown in Figure 6.27. In average adjacent peaks of the same series differ in mass by 44 Da, which corresponds to the molecular mass of the oxyethylene repeat unit. The calculated molecular weights (M_n, M_w), PDI and the number of repeat ethylene oxide units (n) are determined as described in chapter V.

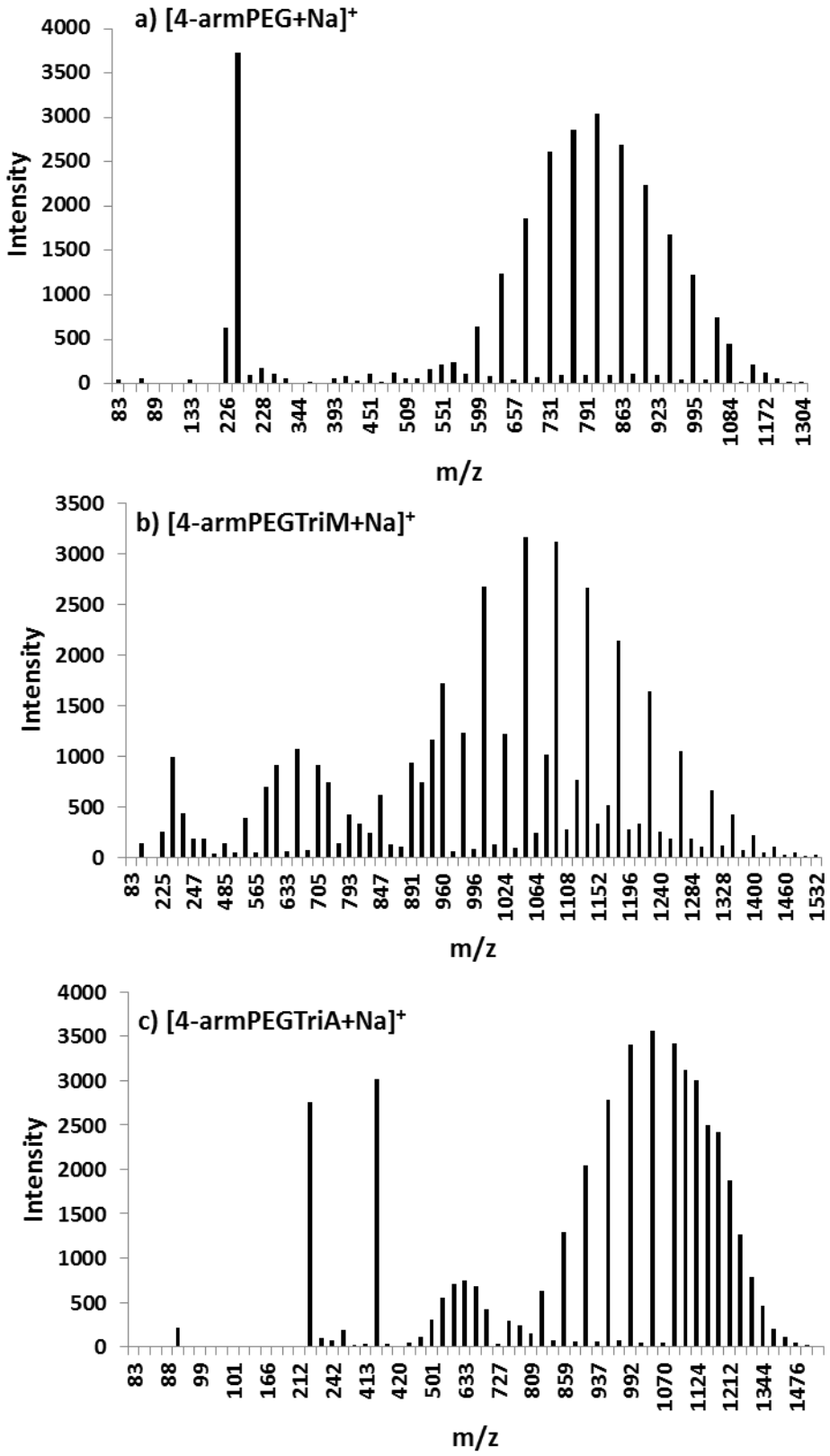

Figure 6.27– MALDI-TOF mass spectra of a) [4-armPEG+Na]$^+$; b) [4-armPEG TetraM+Na]$^+$ c) [4-armPEG TetraA+Na]$^+$.

For the main series Figure 6.27 a) ≈ 500-1300 m/z; b) ≈ 800-1550 m/z and c) ≈ 700-1600 m/z, the average molecular weights (M_n and M_w), polydispersities and the number of ethylene oxide units (n) are listed in Table 6.3. Expected masses are very close to the experimental ones and therefore the main series correspond to Na^+ cationized tetra-functionalized species.

Table 6.3 **–** The theoretical and observed molecular weights of $[4\text{-armPEG+Na}]^+$ and resulting spectra products obtained, $[4\text{-armPEG TetraM+Na}]^+$ and $[4\text{-armPEG TetraA+Na}]^+$, from MALDI-TOF measurements for the main series of peaks.

[Macromolecule +Na]$^+$	M_n		M_w		PDI		n
	Observed	Theoretical	Observed	Theoretical	Observed	Theoretical	(total)
[4-armPEG+Na]$^+$	826.32	-	846.20	-	1.02	-	15
[4-armPEG TetraM+Na]$^+$	1108.38	1108.18	1120.45	1120.25	1.01	1.01	14
[4-armPEG TetraA+Na] $^+$	1062.82	1062.47	1079.20	1078.77	1.02	1.01	15

However, an incomplete substitution of 4-armPEG was observed in the minor series peaks of $[4\text{-armPEG TetraM+Na}]^+$ spectrum (Figure 6.27b). Theoretical calculations of the peaks (whose masses, included between ≈ 700 m/z and 1300 m/z) distribution for Na^+ cationized tri-functionalized species match closely to the observed distributions, suggesting an amount of this specie (Table 6.4). An unknown minor second series of peaks whose masses are between 450 m/z and 900 m/z is also observed. As in 3-armPEG TriM purification, the purification of 4-armPEGTetraM proved to be also very difficult. The increased reaction time or temperature did not prove an alternative because it caused the formation of a polymer during reaction. However, the higher peak intensity for tetra-methacrylate PEG species could be a good indication of the higher conversion reactions.

In $[4\text{-armPEG TetraA+Na}]^+$ spectrum (Figure 6.27c) although the main series of peaks proved the presence of tetra-functionalized species, an unknown minor series of peaks between ≈ 400 and 850 m/z is also observed.

Table 6.4**–** The theoretical and observed molecular weights of tri-functionalized species cationized with Na^+obtained from MALDI-TOF measurements of minor series in $[4\text{-armPEG TetraM+Na}]^+$ spectrum (if only three ends of 4-armPEG were functionalized).

[Macromolecule +Na]$^+$	M_n		M_w		PDI	
	Observed	Theoretical	Observed	Theoretical	Observed	Theoretical
[4-armPEG TriM+Na]+	1001.19	1005.14	1014.32	1017.44	1.01	1.01

6.1.7 Differential scanning calorimetry

The thermal behavior of multi-functional PEG was investigated in the temperature range between - 80 ºC and 130 ºC with rates of 5 and 20 ºC min^{-1} in heating and cooling runs, details on temperatures and enthalpies are provided in Table 12.2. From Figure 6.28 it is observed in 3-armPEG thermogram a heat flux discontinuity at about - 55.95 ºC characteristic of the glass transition. Moreover, the detection of the previous crystallization on cooling and subsequent

melting on heating with different values of the enthalpies at 54.17 and 73.17 J g^{-1}, respectively reveals that material is in the semi-crystalline state.

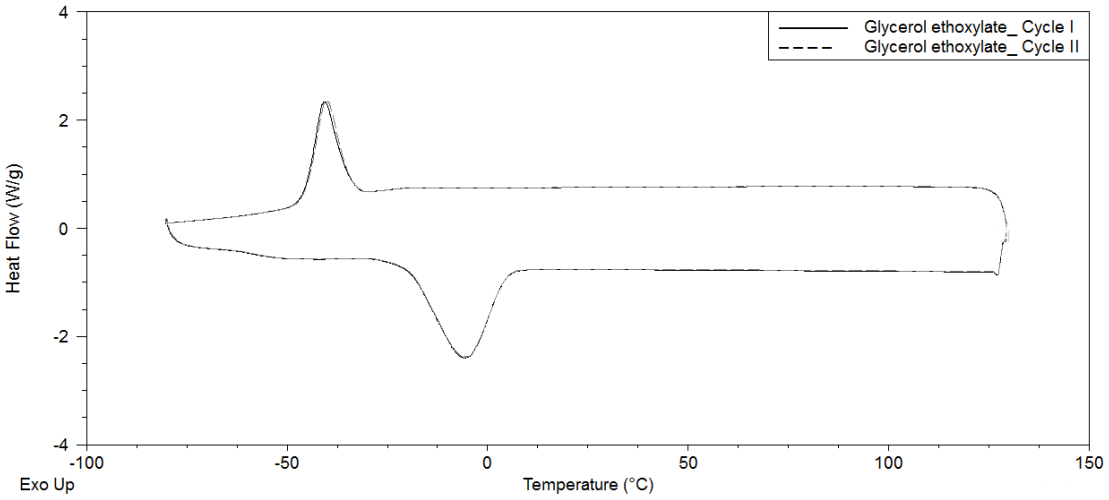

Figure 6.28 – Thermogram (heat flow vs. temperature) of 3-armPEG collected at two heating and cooling cycles at 5 ºC min^{-1}.

The end-functionalization of glycerol ethoxylate result in oligomers tri-functionalized (3-armPEG TriM and 3-armPEG TriA). For thermal analysis of corresponding polymers, the thermal polymerizations were initiated inside the DSC furnace.

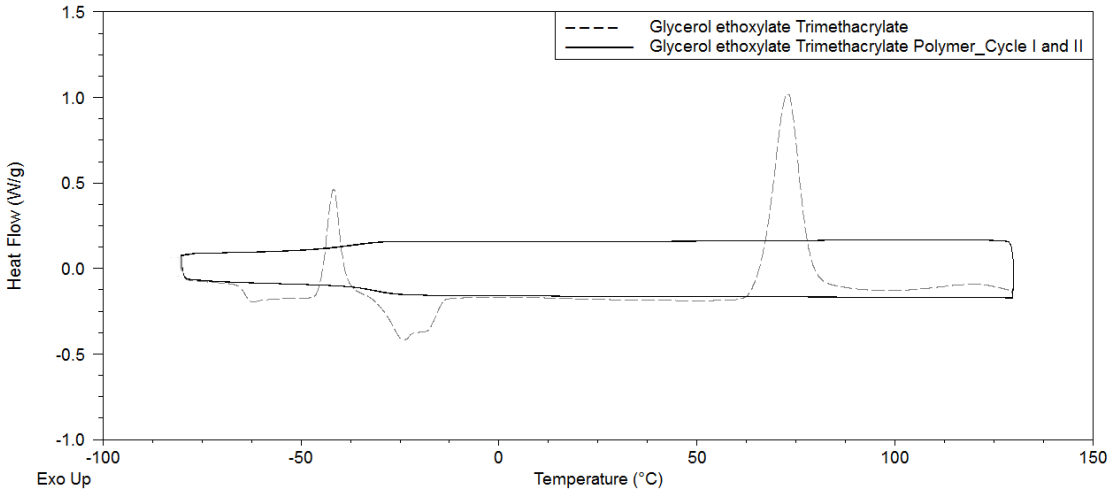

Figure 6.29 – Thermograms (heat flow vs. temperature) of 3-armPEG TriM oligomer + 1 wt.% of AIBN collected at the heating scan at 5 ºC min^{-1} (dashed lines) and for 3-armPEG TriM polymer collected at two heating and cooling cycles at 5 ºC min^{-1} (solid lines).

For 3-armPEG TriM (Figure 6.29) above the glass transition temperature at - 64.25 ºC, the oligomers chains have enough mobility to form ordered arrangements and crystallize with a sharp exothermic peak characteristic of crystallization emerges at - 41.88 ºC followed by a broad endothermic peak at - 23.84 ºC corresponding to the melting of the crystalline fraction previously formed. After melting the temperature again increases with heating until an

exothermic effect at 72.80 ºC due to the polymerization reaction. For the resulting 3-armPEG TriM polymer, in the following heating and cool runs, the glass transition temperature is observed at -31.49 ºC and - 35.97 ºC, respectively and no further processes were obtained indicating a fully amorphous polymer. DSC thermograms collected for 3-armPEG TriA and for the resulting 3-arm PEGTriA polymer showed the same behavior as shown the Figure 6.30.

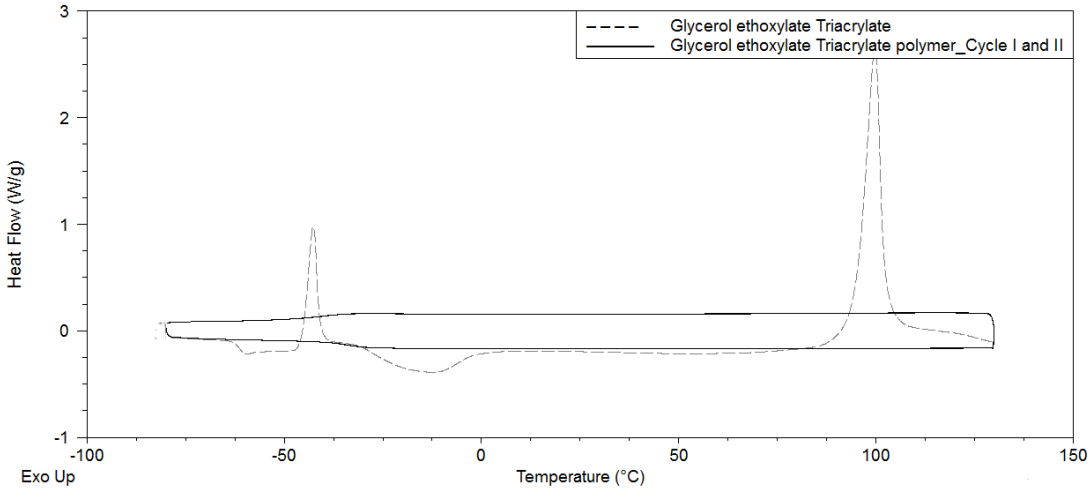

Figure 6.30 – Thermograms (heat flow vs. temperature) of 3-armPEG TriA oligomer + 1 wt.% of AIBN collected at the heating scan at 5 ºC min^{-1} (dashed lines) and for 3-armPEG TriA polymer collected at two heating and cooling cycles at 5 ºC min^{-1} (solid lines).

On closer examination, the crosslink density of the network increase the attractive forces between chains increasing the heat energy to go from a glassy to a rubbery state at about -33.73 ºC for 3-armPEG TriM polymer and - 39.91 ºC for 3-armPEG TriA polymer compared to the T_g at - 55.95 ºC (3-armPEG) and correspondent oligomers at - 64.25 ºC (3-armPEG TriM) and -62.13 ºC (3-armPEG TriA), respectively. With the cross-linking in the polymer, chain sliding diffusion and disentanglement become difficult hindering the rearrangement of chains into order morphology. The effect is that the polymer becomes fully amorphous as described above for 3-rmPEG TriM polymer (Figure 6.29) and also for 3-armPEG TriA polymer (Figure 6.30).

The cooling or heating rates affect the changes in polymer conformation. For this reason, it is also important to evaluate the influence of these rates on the thermal properties of the polymer. Polymer chains are highly entangled and sufficient time must be available for the long molecules to become ordered in the solid state. At very short times polymer chains can have not enough time for move and polymer remain in a glassy state, preventing the development of significant crystallinity. At intermediate times polymer chains can start to move between uncoil and recoil in a stable rubbery state. At long times the chains can move past each other and polymer behaves as a viscous liquid or partially crystallizes[118]. The influence of rate velocities on the thermal properties of 3-armPEG TriA polymer was also evaluated carrying out cooling/heating cycles with rates at 20ºC min^{-1} (Figure 6.31). It was observed that in this study

the glass transition temperature not depend on the rate velocities confirming a fully amorphous polymer.

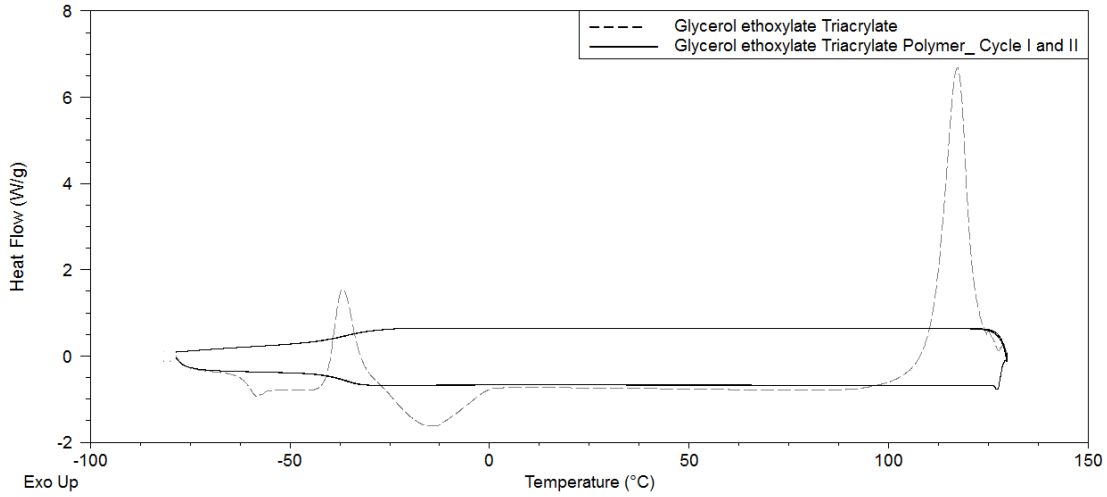

Figure 6.31 – Thermograms (heat flow vs. temperature) of 3-armPEG TriA oligomer + 1 wt.% of AIBN collected at the heating scan at 20 ºC min^{-1} (dashed lines) and for 3-arm PEG TriA polymer collected at two heating and cooling cycles at 20 ºC min^{-1} (solid lines).

The decrease of the linear polymeric arm's length (from n ≈ 20 to n ≈ 15) decreases chain flexibility and the increase of linear arms (from 3 to 4) compared to 3-armPEG make it difficult for 4-armPEG also pack in a regular array as 3-armPEG (Figure 6.28) decreasing the degree of crystallinity. The smaller and more branched chains lead to the formation of amorphous materials where no melting peaks were observed as a result of the lack of crystallinity. The glass transition region at - 62.81 ºC occurs in all heating scans evidencing a fully amorphous 4-armPEG (Figure 6.32).

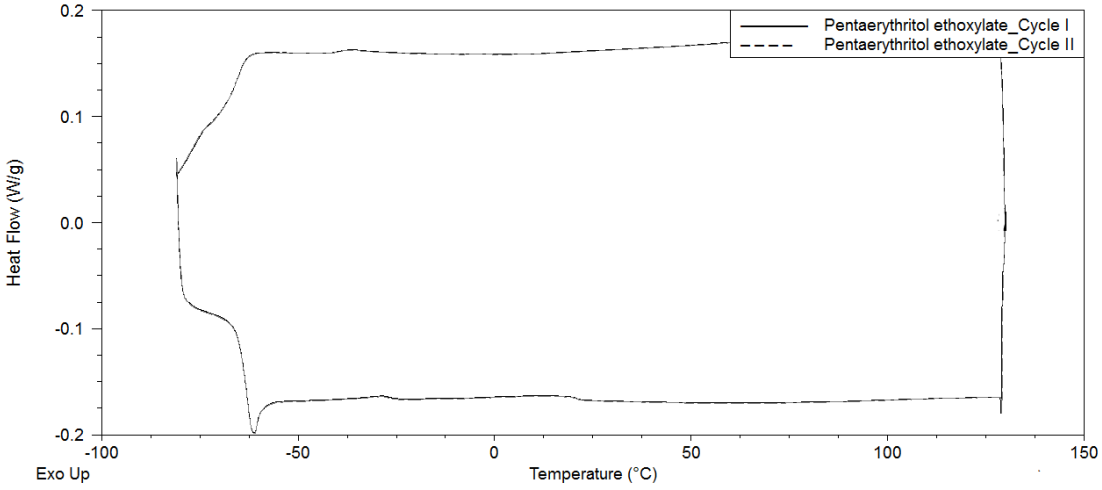

Figure 6.32 – Thermograms (heat flow vs. temperature) of 4-armPEG collected at two heating and cooling cycles at 5 ºC min^{-1}.

The end-functionalization of 4-armPEG result in oligomers tetra-functionalized (4-armPEG TretraM and 4-armPEG TretraA) for preparation of crosslinked polymers (4-armPEG TretraM polymer and 4-armPEG TretraA polymer). The crosslinked polymerizations were also monitored by DSC and initiated inside the furnace.

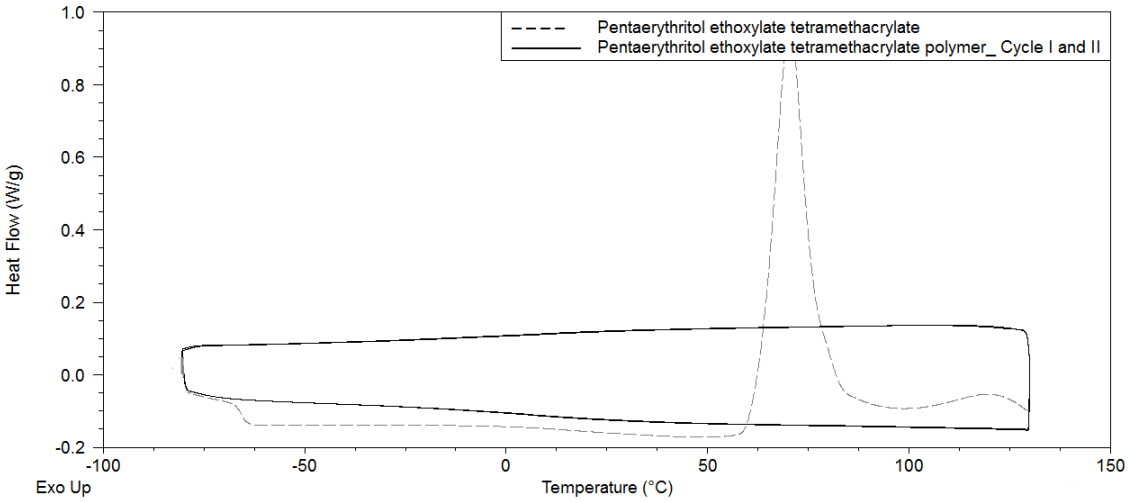

Figure 6.33 – Thermograms (heat flow vs. temperature) of 4-armPEG TetraM + 1 wt.% of AIBN collected at the heating scan at 5 ºC min^{-1} (dashed lines) and for 4-armPEG TetraM polymer (solid lines) collected at two heating and cooling cycles at 5ºC min^{-1}.

Initially for 4-armPEG TetraM, even above of glass transition temperature at - 65.80 ºC, the macromolecule chains cannot melt resulting in an amorphous material that polymerized with a sharp exothermic peak at 70.40 ºC. For the result 4-armPEG TetraM polymer, in the following heating and cool runs, a flat and diffuse transition region is observed with nonexistent of melting point indicating also a fully amorphous polymer (Figure 6.33). DSC thermograms collected for 4-armPEG TetraA (Figure 6.34) with a T_g at - 64.36 ºC and for the result crosslinked polymer (4-armPEG TetraA polymer) showed similar behavior as that report above.

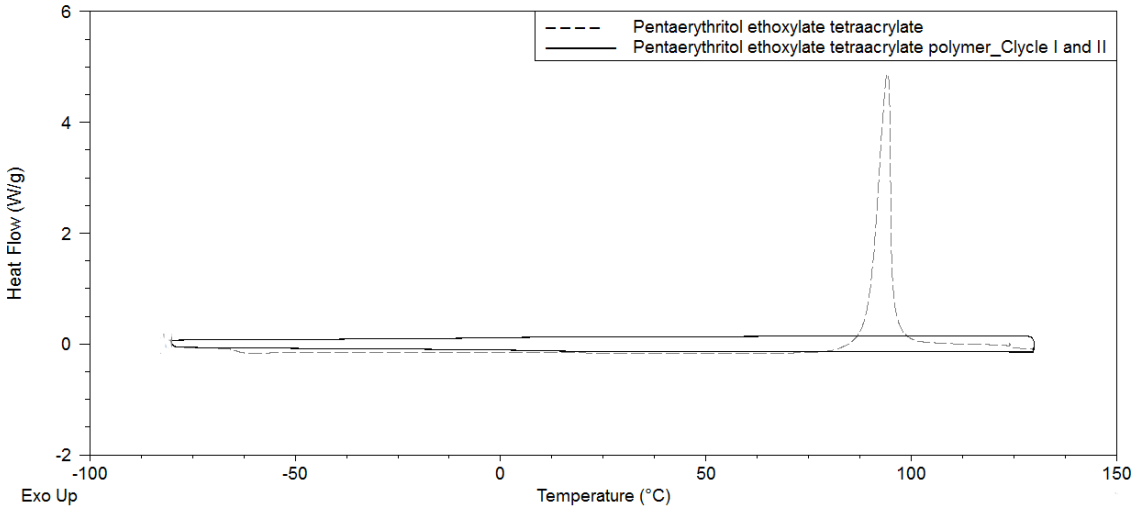

Figure 6.34 – Thermograms (heat flow vs. temperature) of 4-armPEGTetraA oligomer + 1 wt.% of AIBN collected at the heating scan at 5 ºC min^{-1} (dashed lines) and for 4-armPEGTetraA polymer collected at two heating and cooling cycles at 5 ºC min^{-1} (solid lines).

The highly densely crosslinked polymer results from tetra functionalized oligomers make glass transition become too flat and diffuse in DSC thermograms. On this way, the DSC is not sensitive enough to detect the T_g of this highly crosslinked polymer network due to the small heat capacity values between glassy and rubbery regions[103]. In this way, although it is not possible to detect the T_g value, the DSC confirms the high densely crosslinked.

6.1.8 Electro-Optical Properties

The electro-optical response curves shown in Figure 6.35 are presented in terms of the light transmittance in percentage versus electric field. The PDLCs were prepared as described in Figure 2.10 by thermal polymerization at 70 °C.

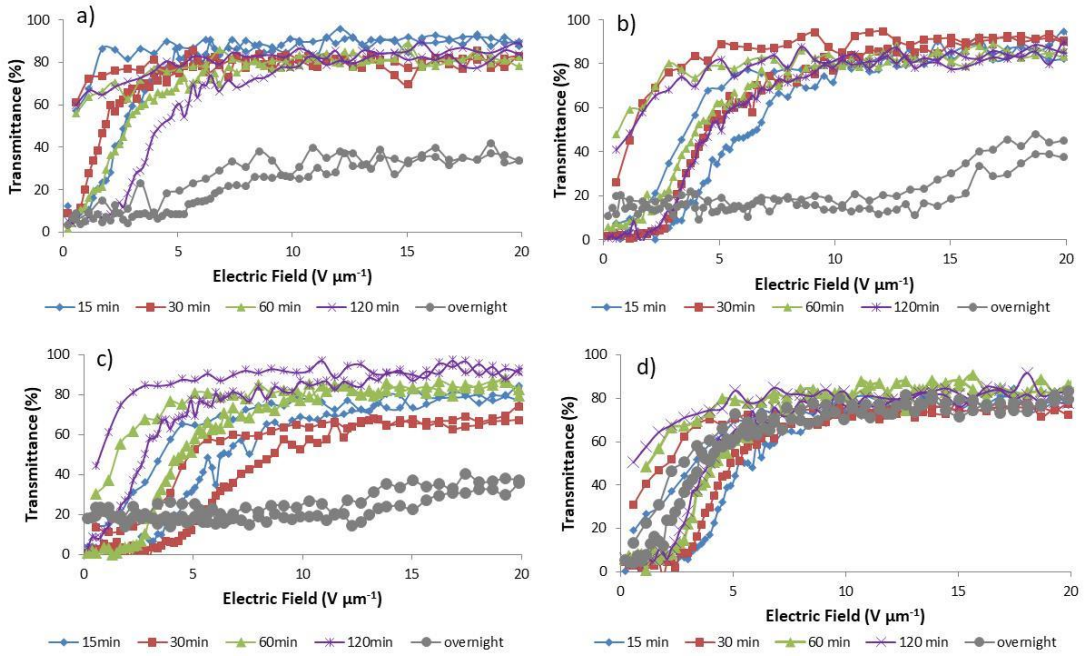

Figure 6.35 – Dependence of the polymerization time on the transmittance versus applied electric field of a) 4-armPEG TetraM(1 wt.% of AIBN)+E7 in a weight ratio of 30/70 (wt.%); b) 4-armPEG TetraA(1 wt.% of AIBN)+E7 in a weight ratio of 30/70 (wt.%); c) 3-armPEG TriA(1 wt.% of AIBN)+E7 in a weight ratio of 30/70 (wt.%) and d) 3-armPEG TriM (1 wt.% of AIBN)+E7 in a weight ratio of 30/70 (wt.%).

It could be found that electro-optical curves of the PDLCs prepared with four-arm PEG with methacrylate (4-armPEG TetraM) and acrylate (4-armPEG TetraA) ends groups as precursor of polymer matrix, polymerized by different times (15, 30, 60, 120 min and all night) exhibit different response as shown in (Figure 6.35 a) and (Figure 6.35 b), respectively. The samples polymerized by lower times of 15 min exhibited poorer electro-optical response because the phase-separation process is not completed, compared with that of the samples prepared by longer polymerization time. With this low polymerization time, the polymer cannot form enough stable matrix to incorporate the LC domains.

When polymerization time is increased to 60 min leads to a sufficient denser network, improving the phase separation process for a better electro-optical response with approximately 70 % of PME for 4-armPEG TetraM PDLCs (Figure 6.35 a) and 57 % for 4-armPEG TetraA PDLCs (Figure 6.35 b) PDLCs. Although the crosslink density rises when increasing the functionality of the pre-polymer, the relative conversion (ratio between the number of polymerized double bonds and the total number of double bonds) simultaneously could diminish because double bonds are highly entangled to react decreasing polymer segments mobility[140]. The remaining polymerizable double bonds can cause undesirable polymer degradation which in turn affected the electro-optical properties. In this way, in order to check the PDLC thermal stability, the polymerization continues for another 60 min. The electro-optical curves obtained for 60 and 120 min of polymerization are close to each other which indicate temperature stability and durability of PDLCs.

In this way, the effect is a polymer matrix more thermal stabilized compared with that of the corresponding polymer without flexible chains [134,135]. This follows from the fact that for this last oligomers type the stages of polymerization are readily achieving an undesirable higher crosslinked for more than 30-40 min of thermal polymerization. For longer polymerization times, the LC diffusion and coalescence cannot follow the polymer matrix gelation point. However, PDLC films prepare with crosslinked oligomers with linear longer polymeric arms (4-arm PEG TetraM and 4-armPEGTetraA) exhibits more electro-optical stabilized properties even with thermal polymerization between 60 and 120 min with no significant impact in PME. Nevertheless, longer polymerization time during overnight lead to a polymer crosslinking so higher that LC could remain trapped in the polymer matrix canceling the PME.

In all the experiments, the electro-optical response of PDLC samples prepared with tri-arm PEG with methacrylate ends groups (3-armPEG TriM; Figure 6.35 d) and tri-arm PEG with acrylate ends groups (3-armPEG TriA; Figure 6.35 c) as the precursor of polymeric matrix follow the same behavior of electro-optical response shown in four-arm oligomer PDLCs. The best PME for these tri-functionalized PDLCs was 60 % for 3-armPEGTriM PDLCs and 47 % for 3-armPEGTriA PDLCs both with 120 min of polymerization time.

The comparison of the electro-optical response of acrylate and methacrylate systems indicates that the methacrylate systems substantially improve PME of corresponding PDLC films. The chemical environment of radically curable double bonds influences their reactivity. As previously mentioned, the acrylate functional pre-polymer is more reactive than their methacrylate functional analogs. In this way, for the same polymerization time, the acrylates systems enhance more the densification of polymer network diminishing the LC-rich domains which in turn affect the PME.

6.1.9 Co-Polymerization

The desired crosslink density could be also achieved by co-polymerization between multi-functional and mono-functional pre-polymers. The mono-functional pre-polymer leads to an increase of polymer flexibility but not ensure a stable polymer network to support the LC domains[141]. On the other hand, as seen, multi-functional pre-polymers lead to heavily crosslinked polymer networks trapping liquid crystal. In this way, the effect of pre-polymer mixtures of crosslinked and uncrosslinked pre-polymers in PME was also studied.

The co-polymerization mixtures were prepared through mixtures of the mono-functional pre-polymer, poly(propylene glycol)methacrylate (PPGM) or poly(propylene glycol)acrylate (PPGA) with synthesized multi-functional (meth) acrylate PEGs in the weight ratios shown in Table 6.5.

Table 6.5 – Composition of samples for PDLCs films preparation by co-polymerization.

System	30 wt.% (multi-functional:mono-functional)	E7 (wt. %)
1	25 wt.%4-armPEGTetraM:75 wt.% PPGM	70
2	50 wt.%4-armPEGTetraM:50 wt.% PPGM	70
3	75 wt.%4-armPEGTetraM:25 wt.% PPGM	70
4	25 wt.%4-armPEGTetraA:75 wt.% PPGA	70
5	50 wt.%4-armPEGTetraA:50 wt.% PPGA	70
6	75 wt.%4-armPEGTetraA:25 wt.% PPGA	70
7	25 wt.%3-armPEGTriA:75 wt.% PPGA	70
8	50 wt.% 3-armPEG TriA:50 wt.% PPGA	70
9	75 wt.% 3-armPEG TriA: 25 wt.% PPGA	70
10	25 wt.% 3-armPEG TriM: 5 wt.% PPGM	70
11	50 wt.% 3-armPEG TriM:50 wt.% PPGM	70
12	75 wt.% 3-armPEG TriM:25 wt.% PPGM	70

The electro-optical properties of PDLCs prepared with multi-functional and mono-functional pre-polymers at a variety of compositions (Table 6.5) and polymerization times (30, 60 and 120 min) is illustrated from Figure 12.23 to Figure 12.26 and summarized in Table 6.6.

Table 6.6 – Electro-optical properties of PDLCs prepared by co-polymerization.

System	Polymerization Time (min)	T_0(%)	T_{OFF}(%)	T_{max}(%)	PME(%)	MSC(%)	E_{90} (V µm^{-1})
1	30	7.0	50.0	65	74	43	3.1
	60	2.3	45.0	65	68	43	2.1
	120	7.4	48.0	80	56	41	4.5
2	30	2.0	64.0	75	83	62	3.2
	60	10.o	65.0	80	79	55	3.0
	120	14.9	38.7	80	37	24	5.5
3	30	0.0	29.0	80	36	29	4.1
	60	0.0	48.0	80	60	48	4.7
	120	2.8	13.4	70	16	11	9.8
4	30	5.9	63.0	75	83	57	2.0
	60	1.7	60.0	75	80	58	1.5
	120	9.6	51.7	75	65	42	2.8
5	30	7.0	77.0	80	96	70	5.5
	60	14.0	57.0	70	77	43	4.3
	120	8.2	13.3	55	11	5	5.8
6	30	0.8	4.7	65	6	4	5.8
	60	0.9	27.0	80	33	26	9.1
	120	2.5	3.6	80	1	1	5.6
7	30	5.1	57.0	85	65	52	2.6
	60	12.1	68.0	85	77	56	4.2
	120	0.3	14.7	85	17	15	4.4
8	30	66.7	80.0	80	100	13	5.7
	60	11.0	74.0	74	100	63	3.2
	120	12.0	60.0	72	80	48	2.9
9	30	4.5	70.0	85	81	66	3.4
	60	2.2	70.0	85	82	68	4.6
	120	4.7	6.2	85	2	2	1.9
10	30	2.3	63.0	80	78	63	2.8
	60	2.9	52.0	80	64	50	4.0
	120	17.1	45.5	80	45	28	2.8
11	30	0.0	47.0	80	59	47	6.3
	60	11.0	60.0	75	77	49	5.6
	120	1.7	37.8	75	50	37	5.7
12	30	0.3	36.0	80	45	36	6.9
	60	0.2	61.0	85	72	60	6.5
	120	3.6	30.4	80	35	27	6.7

In general, the best percentages of PME are achieved by the weight ratio of 50 % of mono-functional and 50 % of multi-functional pre-polymer with 60 min of polymerization time (Table 6.6). This weight ratio provides an adequate degree of crosslinking in the polymer matrix to incorporate the liquid crystal.

The 30 min time also seems not to be enough time for phase separation between the polymer matrix and the liquid crystal to allow an optimized PME. With 60 min of polymerization time, it is possible that multi-functional pre-polymers reacts more than mono-functional ones resulting in a fraction of unreacted monomer retained in the polymer matrix as plasticizers. This affects the interactions between polymer chains by spacing out the chains giving sufficient free volume for polymer chains mobility [134,135]. The unreacted monomer could also form a layer between polymer and LC domains during phase separation decreasing anchoring energy [18].

With 120 min of polymerization time, the unreacted monomer concentrations decrease which lead to more heavily crosslinked networks. Therefore, LC molecules swell the polymer matrix

becoming strongly anchored to the surface of the polymer weakening the PME. This represents a disadvantage to the thermal stability of the PDLC by limiting the applicability of them.

For instance, although the noticeable response for PDLCs prepared with system 8 (Table 6.6) where the 100 % of the PME remains unaffected between 30 and 60 min of polymerization time this percentage starts decreasing for polymerization time longer than 120 min.

In a previous discussion published for polymer matrix morphology with this type of co-polymerization with structurally similar monomer without spacer length showed that regardless of weight ratios used in co-polymerization and the polymerization time the polymer matrix morphology is a polymer ball morphology type[134,135]. Such results could be extending in this present co-polymerization.

6.2 Synthesis and Characterization of 3-armPEG-PPG with Highly Length Chains

6.2.1 Synthesis and Characterization of 3-armPEG-PPG with Methacrylate Ends Groups

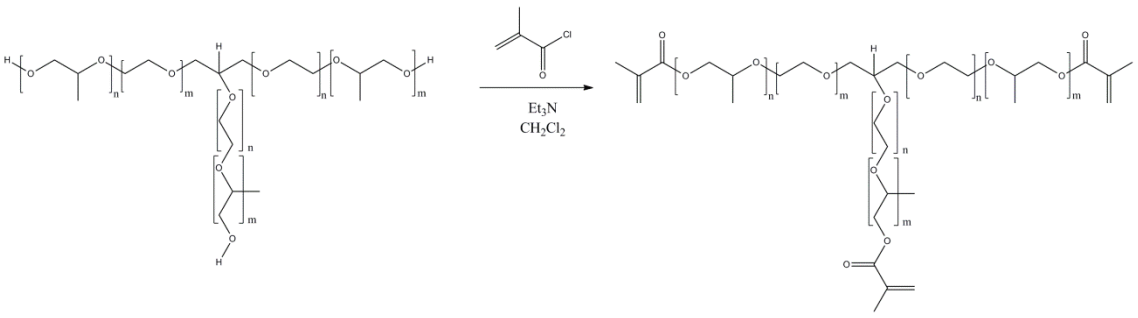

Figure 6.36 – Synthetic scheme of synthesis of Tri-armPEG-PPG with methacrylate ends groups (3-armPEG-PPG TriM).

According to the general method above described (Figure 6.36), to a solution of glycerol ethoxylate-co-propoxylate triol (3-armPEG-PPG) (M_w ≈ 2600 g mol^{-1}) (2 g, 0.77 mmol, 1 eq) in dry CH_2Cl_2 (15 mL) was added triethylamine (0.47 g, 4.62 mmol, 6 eq) and then cooled to 0 ºC in an ice-water bath. To this solution, methacryloyl chloride (0.48 g, 4.62 mmol, 6 eq) was added dropwise and the solution was stirred at 40 ºC for 24 h. The reaction mixture was washed with HCl 0.1 M, brine and H_2O. In the end, the organic extract phase was dried with anhydrous Na_2SO_4, filtered and concentrated in vacuum. The resulting crude product was purified by column chromatography using ($CHCl_3$-MeOH 9:1) as eluent. Compounds were visualized with phosphomolybdic acid by TLC analysis. White oil (0.73 g, 0.26 mmol, 34 %) was obtained as a product. The NMR assignments and structure determination were made by ^{1}H-NMR (Figure

6.37), ^{13}C-NMR (Figure 6.38), DEPT (Figure 6.39) and by two dimensional NMR (COSY (Figure 6.40) and HSQC (Figure 6.41)).

^{1}H-NMR (400 MHz, $CDCl_3$) δ 6.09 (s, 3H, =C$\underline{H}_2$), 5.56 (s, 3H, =C$\underline{H}_2$), 3.77 – 3.38 (m, 275H, C$\underline{H}_2$C$\underline{H}_2$O, CH(C$\underline{H}_2$)$_2$), 1.94 (s, 9H, C$\underline{H}_3$C=CH$_2$), 1.15 (d, *J* = 5.9 Hz, 79H, CH$_2$CHC$\underline{H}_3$).

^{13}C-NMR (100 MHz, $CDCl_3$) δ 17.24 (C$\underline{H}_3$C=CH$_2$), 18.34 (CH$_2$CH$\underline{C}$H$_3$), 68.51 (CH(C$\underline{H}_2$)$_2$), 70.57-70.98 (C$\underline{H}_2$C$\underline{H}_2$O), 75.00 (CH$_2$C$\underline{H}$CH$_3$), 75.18 (C$\underline{H}_2$CHCH$_3$),125.33 (=C$\underline{H}_2$), 136.68 (CH$_3$-C=C), 166.8(C=O).

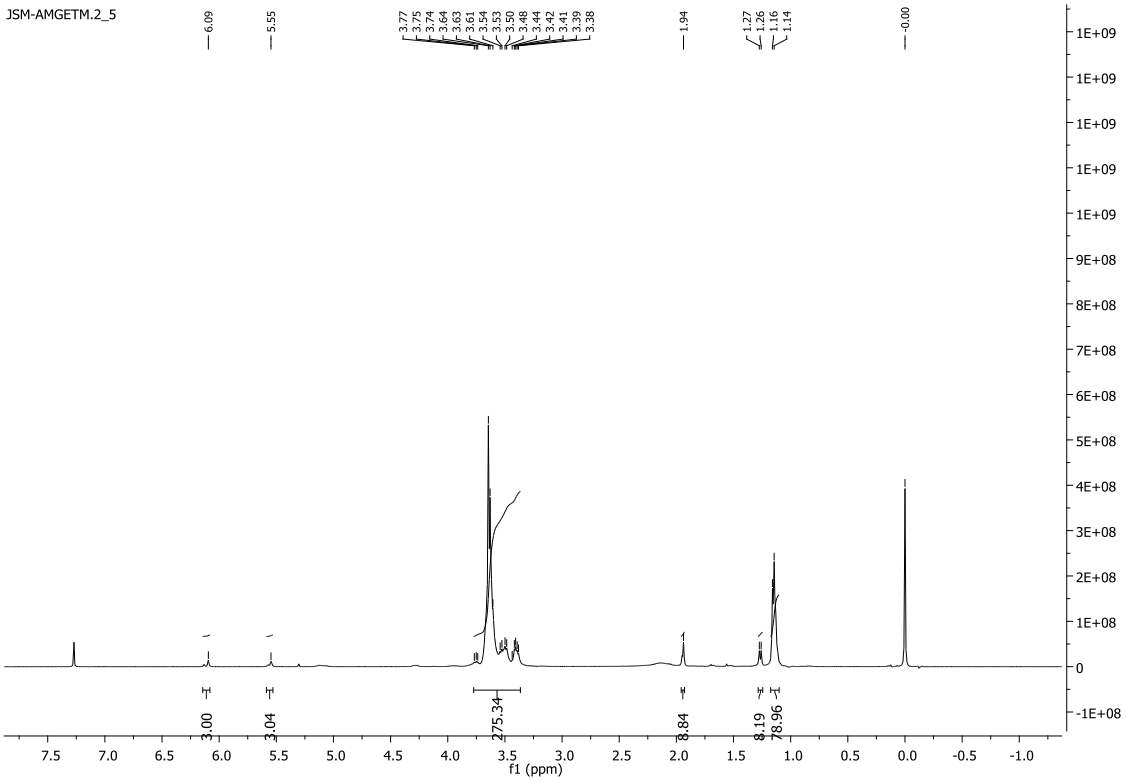

Figure 6.37 – ^{1}H-NMR spectrum of 3-armPEG-PPG TriM.

The small duplet at 1.27 ppm (Figure 6.37) is also consistent with the methyl of propylene unit. It is possible that a fraction of propylene glycol units had been directly methacrylate. This is support by the ^{13}C-NMR spectrum (Figure 6.38) where three signals, not two, at 17.2, 17.4 and 18.3 ppm were observed in the range of the methyl carbon.

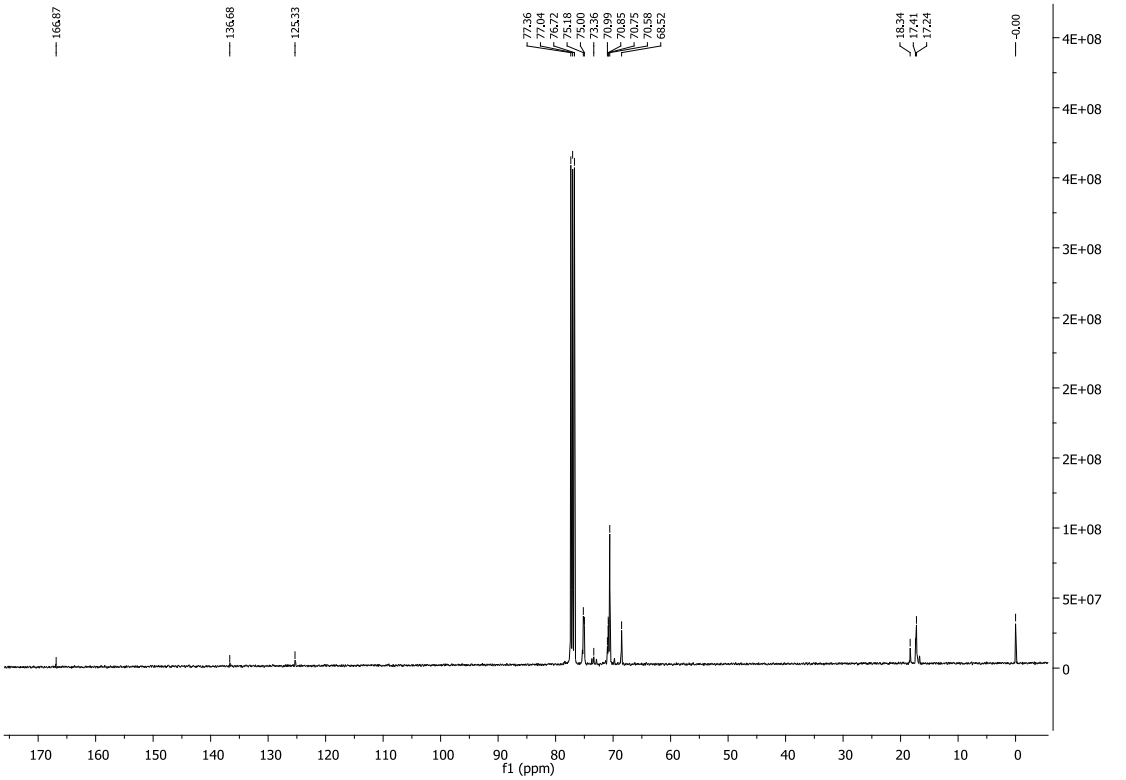

Figure 6.38 – ^{13}C-NMR spectrum of 3-armPEG-PPG TriM.

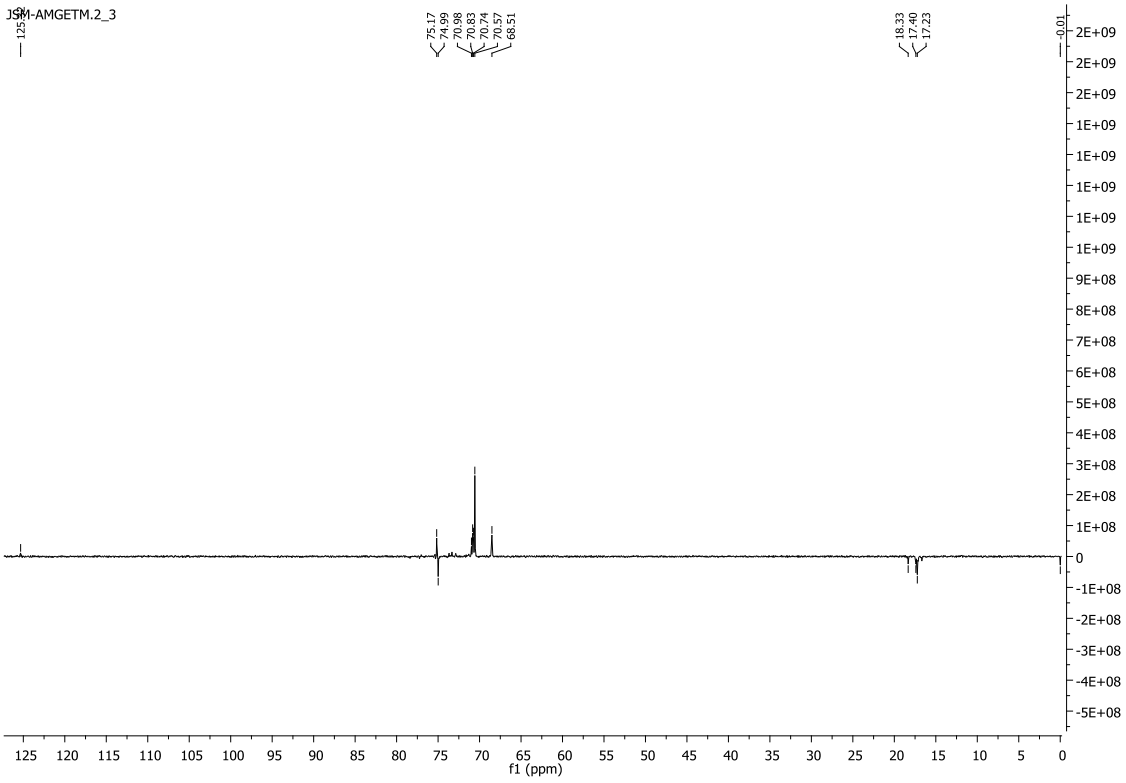

Figure 6.39 – ^{13}C DEPT spectrum of 3-armPEG-PPG TriM.

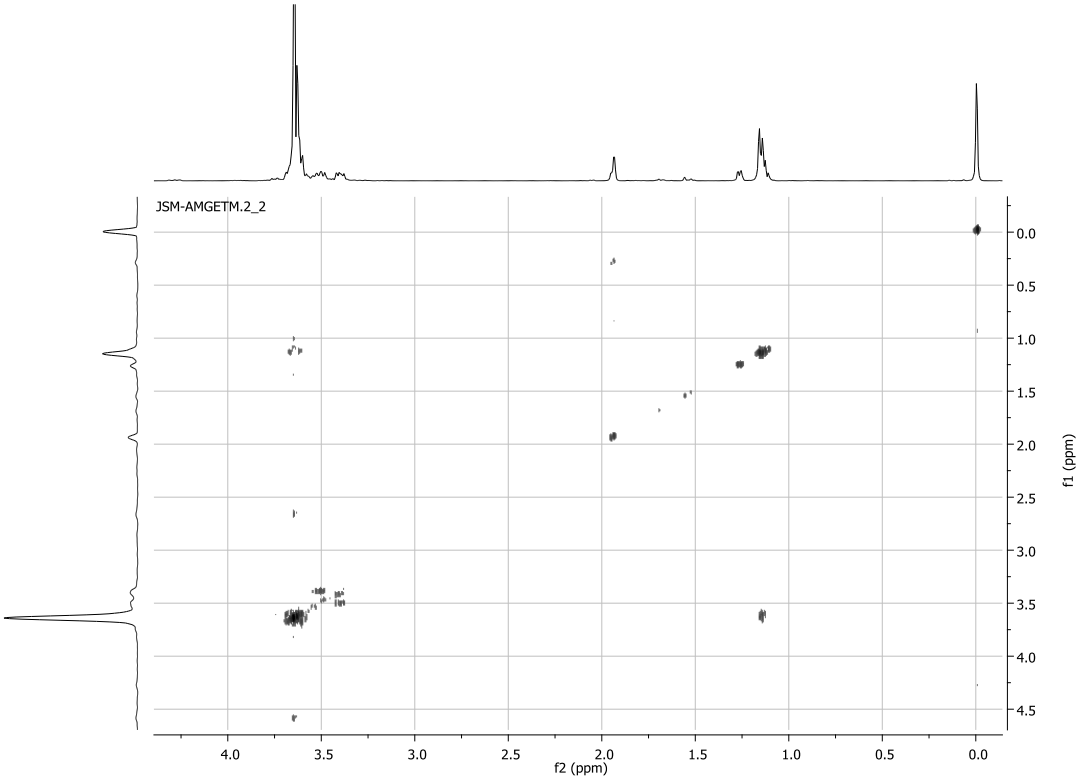

Figure 6.40 – COSY spectrum of 3-armPEG-PPG TriM.

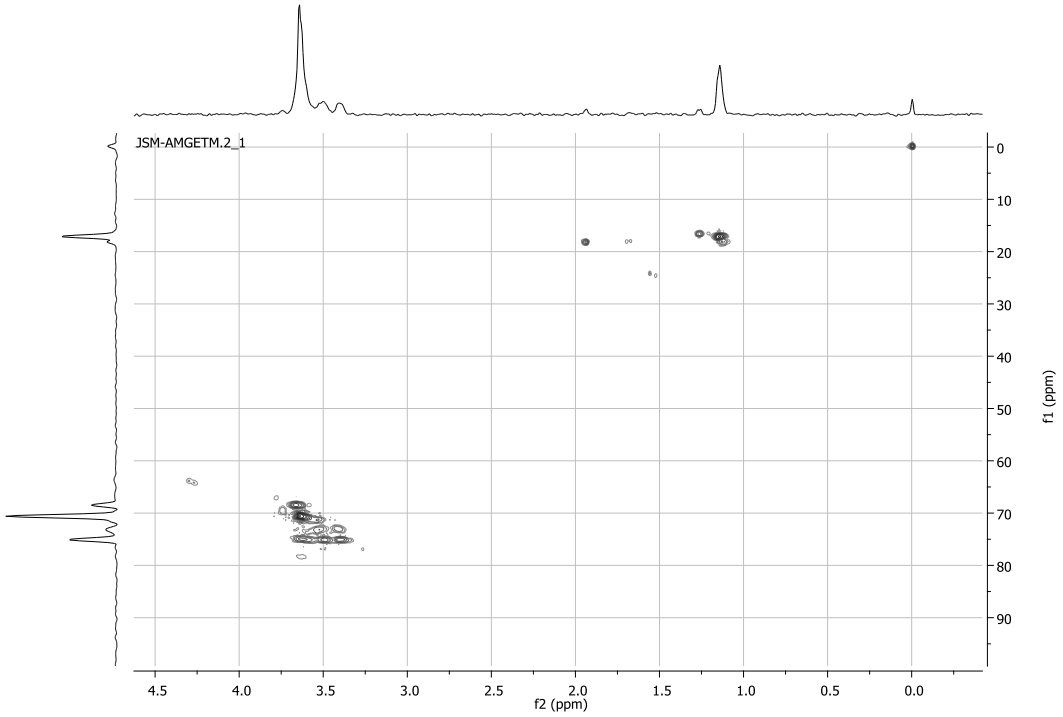

Figure 6.41 – HSQC spectrum of 3-armPEG-PPG TriM.

6.2.2 Synthesis and characterization of 3-armPEG-PPG with acrylate ends groups

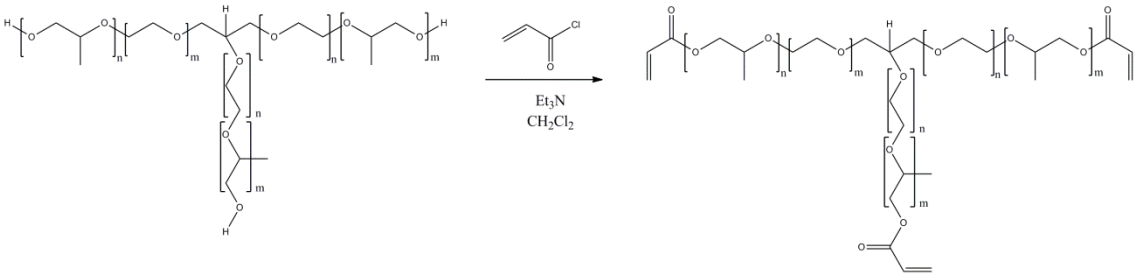

Figure 6.42 – Synthetic scheme of synthesis of Tri-armPEG-PPG with acrylate ends groups (3-arm PEG-PPG TriA).

The synthesis (Figure 6.42) and characterization of 3-armPEG-PPG TriA was similar to synthesis and characterization of 3-armPEG-PPG TriM. Glycerol ethoxylate-co-propoxylate triol (3-armPEG-PPG) (2 g, 0.77 mmol, 1 eq) in CH_2Cl_2 (15 mL) with triethylamine (0.47 g, 4.62 mmol, 6 eq) and acryloyl chloride (0.42 g, 4.62 mmol, 6 eq) gave 3-armPEG-PPG TriA (0.97 g, 0.35 mmol, 45 %) as a yellow oil that foamed under vacuum. The NMR assignments and structure determination were made by ^{1}H-NMR (Figure 6.43), ^{13}C-NMR (Figure 6.44), DEPT (Figure 6.45) and by two dimensional NMR (COSY (Figure 6.46) and HSQC (Figure 6.47)).

^{1}H-NMR (400 MHz, $CDCl_3$) δ 6.40 (d, *J* = 17.3 Hz, 3H, =C$\underline{H}_2$), 6.12 (dd, *J* = 17.3, 10.4 Hz, 3H, =C$\underline{H}$), 5.81 (d, *J* = 10.3 Hz, 3H, =C$\underline{H}_2$), 3.78 – 3.36 (m, 279H, C$\underline{H}_2$C$\underline{H}_2$O, CH(C$\underline{H}_2$)$_2$), 1.15 (d, *J* = 5.9 Hz, 76H, $CH_2CHC\underline{H}_3$).

^{13}C-NMR (100 MHz, $CDCl_3$) δ 17.31 ($CH_2CH\underline{C}H_3$), 68.60 (CH($\underline{C}H_2$)$_2$) 70.52-70.93 ($\underline{C}H_2\underline{C}H_2O$), 75.08 ($CH_2\underline{C}HCH_3$), 75.25 ($\underline{C}H_2CHCH_3$),128.88 (H$\underline{C}$=C), 130.57 (=$\underline{C}H_2$), 165.81($\underline{C}$=O).

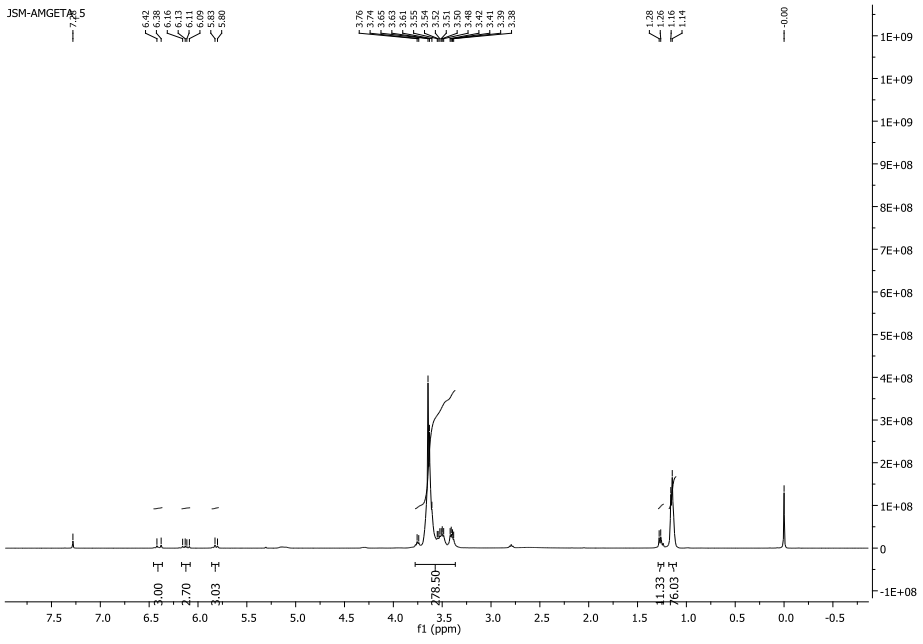

Figure 6.43 – ^{1}H-NMR spectrum of 3-armPEG-PPG TriA.

The small duplet at 1.27 (Figure 6.43) is also consistent with the methyl of propylene unit but corresponds to the direct acrylation of propylene glycol units. This is support by the ^{13}C NMR spectrum (Figure 6.44) where two signals, not one, at 16.61 and 17.31 ppm were observed in the range of the methyl carbon. Two signals at carbonyl region were also observed at 165.8 and 169.9 ppm. In this way, it is possible the presence of a heterogeneous mixture having a distribution of species.

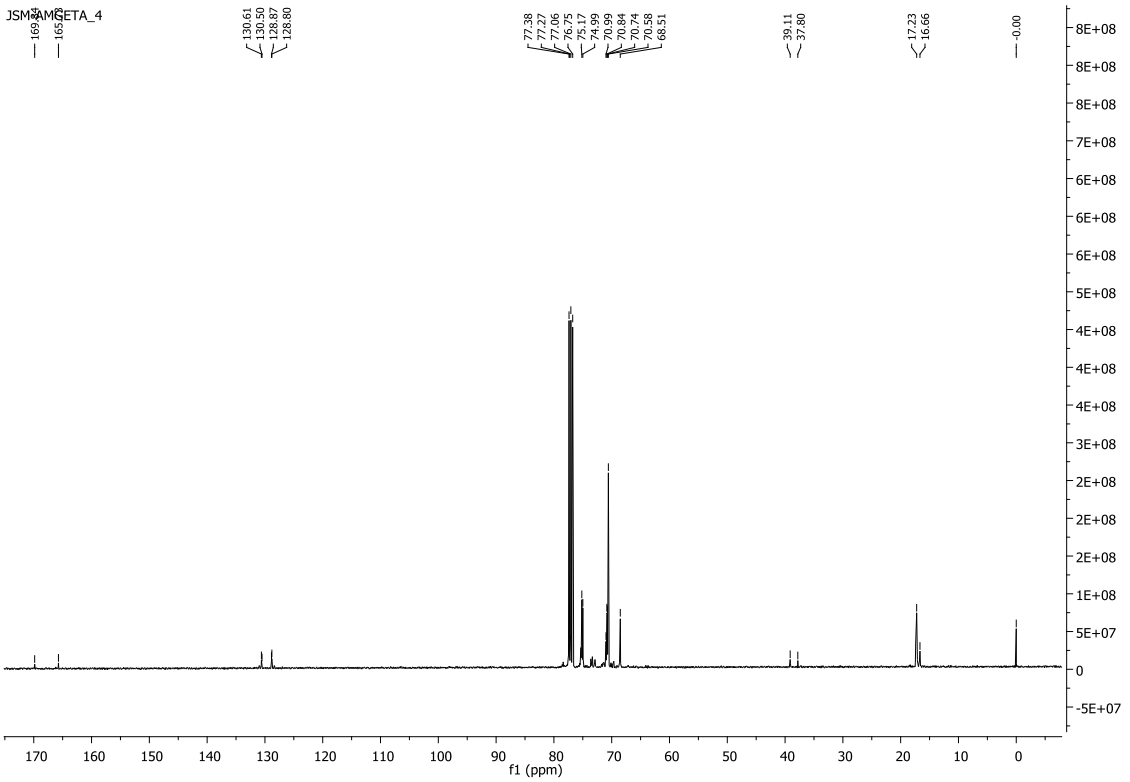

Figure 6.44 – ^{13}C-NMR spectrum of 3-armPEG-PPG TriA.

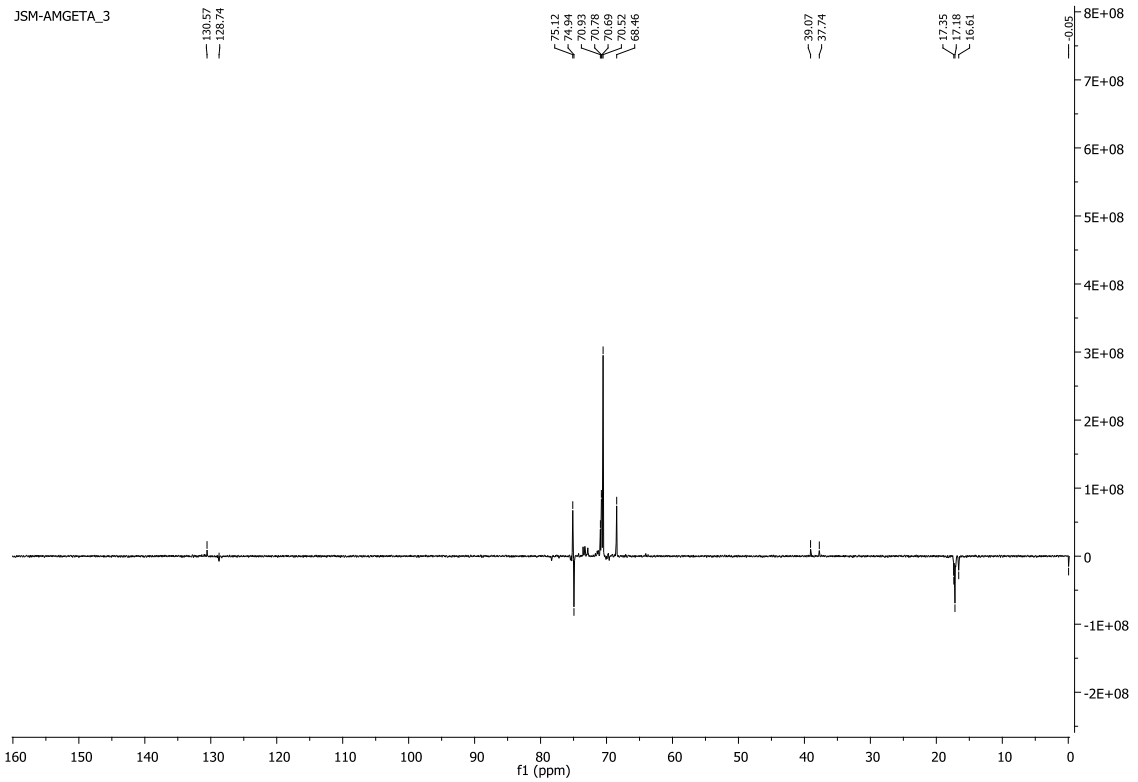

Figure 6.45 – ^{13}C DEPT spectrum of 3-armPEG-PPG TriA.

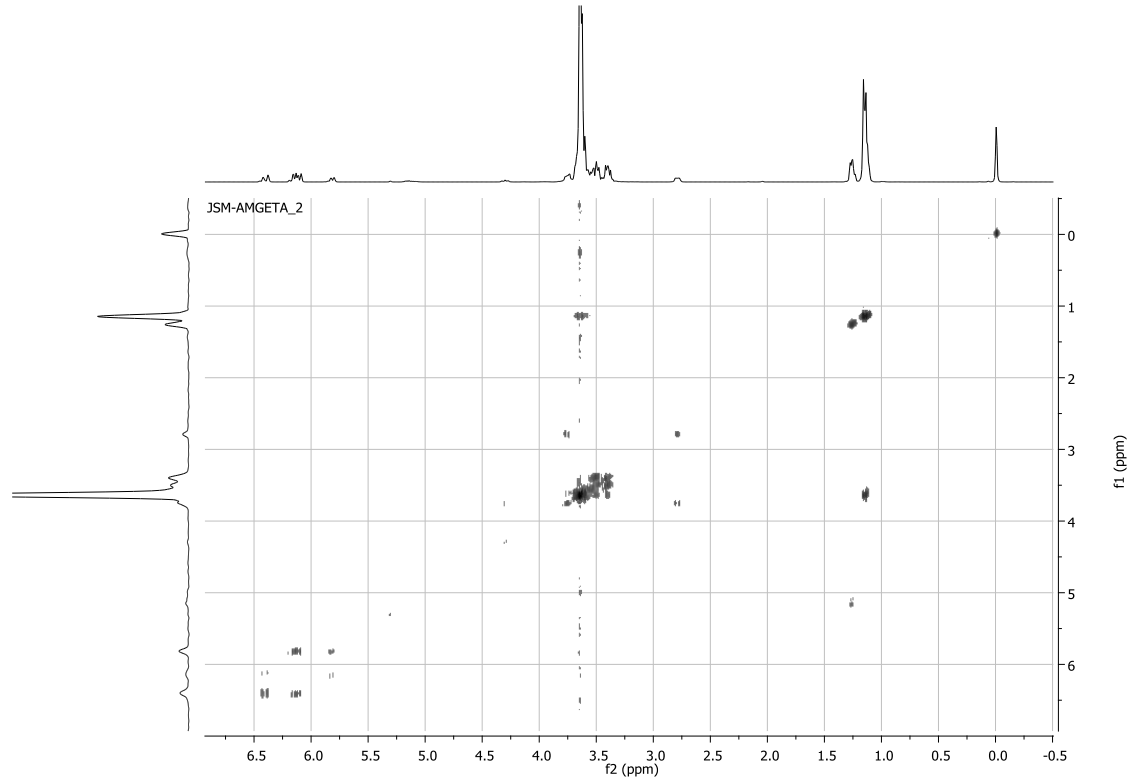

Figure 6.46 – COSY spectrum of 3-armPEG-PPG TriA.

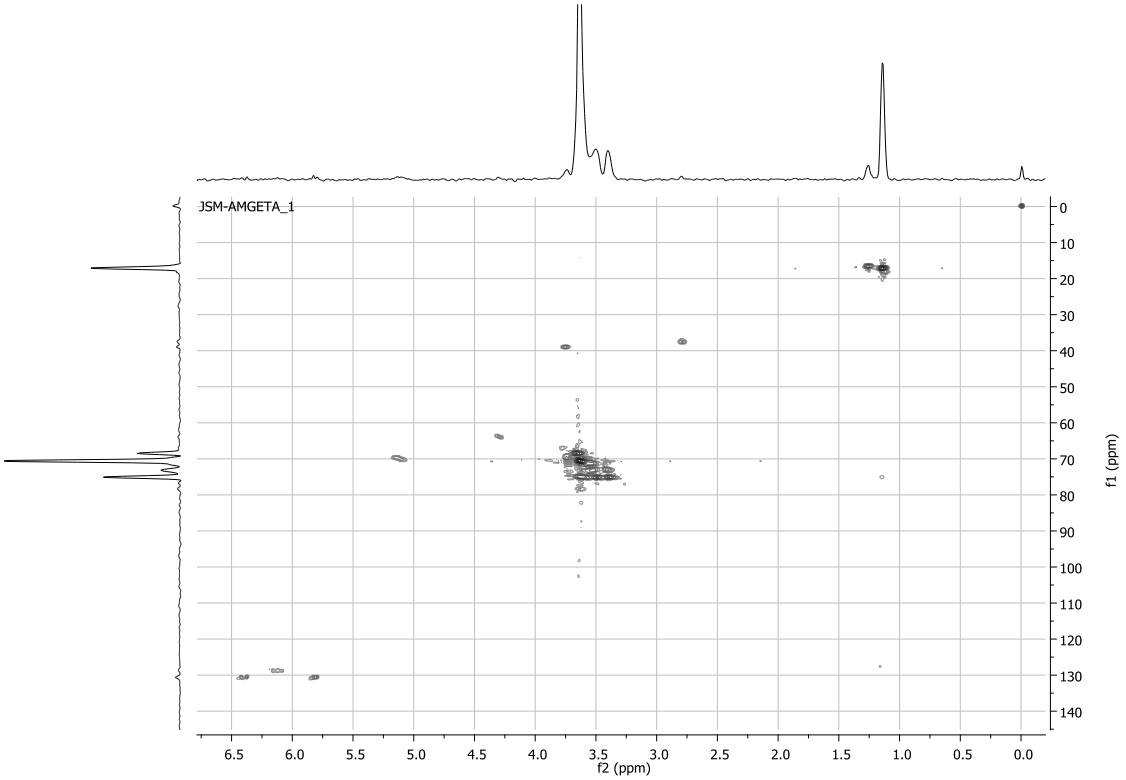

Figure 6.47 – HSQC spectrum of 3-armPEG-PPG TriA.

6.2.3 MALDI-TOF MS

The MALDI-TOF mass spectra of the [3-armPEG-PPG +Na]$^+$ and for resulting tri-functionalized products cationized with Na^+ are shown in Figure 6.48. The obtained results for average of molecular mass (both M_n and M_w) and PDI are reported in Table 6.7.

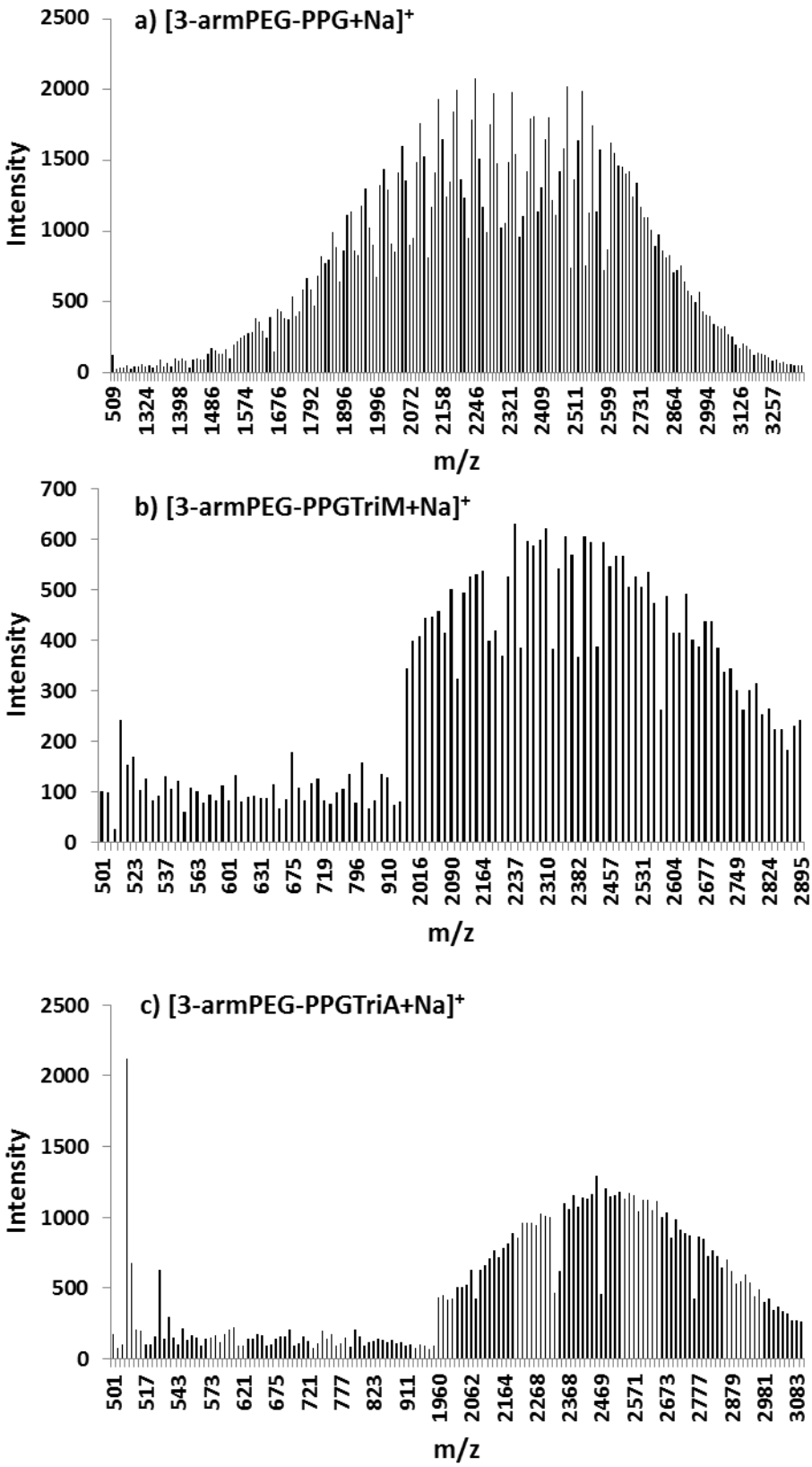

Figure 6.48 – MALDI-TOF mass spectra of a) [3-armPEG-PPG+Na]$^+$; b) [3-armPEG-PPG TriM+Na]$^+$ c) [3-armPEG-PPG TriA+Na]$^+$.

A good correlation was observed between the theoretical and experimental values of M_n, M_w and PDI for a series of peaks (m/z range of ≈ 2000 to ≈ 3000) in $[3\text{-armPEG-PPG TriA+Na}]^+$ spectrum (Table 6.7) . In this way, the series of peaks correspond to Na^+ cationized 3-armPEG-PPG TriA species (Figure 6.48 c). However, an incomplete substitution of 3-armPEG-PPG was observed in the series peak (m/z range of ≈ 2000 to ≈ 3000) of $[3\text{-armPEG-PPG TriM+Na}]^+$ spectrum (Figure 6.48 b)**.** Theoretical calculations of this peaks distribution for Na^+ cationized di-functionalized species match closely to the observed distributions (Table 6.7), suggesting that only di-methacrylate functionalized species result. However, for simplicity, the sample keeps the name as 3-armPEG-PPG TriM.

Table 6.7 – The theoretical and observed molecular weights of $[3\text{-armPEG-PPG+Na}]^+$ and resulting spectra products obtained, $[3\text{-armPEG-PPG DiM+Na}]^+$ and $[3\text{-armPPG-PEG TriA+Na}]^+$, from MALDI-TOF measurements.

[Macromolecule+Na]$^+$	**M_n**		**M_w**		**PDI**	
	Observed	**Theoretical**	**Observed**	**Theoretical**	**Observed**	**Theoretical**
[3-armPEG-PPG+Na]$^+$	2310.5	-	2368.9	1.02	1.03	-
[3-armPEG-PPGDiM+Na]$^+$	2405.28	2404.88	2429.61	2429.23	1.01	1.01
[3-armPEG-PPGTriA+Na]$^+$	2501.24	2499.07	2532.45	2530.64	1.01	1.01

6.2.4 Electro-Optical, Morphological and DSC properties

The PDLCs were prepared by 3-armPEG-PPG tri-functionalized with 1 wt. % of AIBN and E7 in a weight ratio of 30/70 (wt. %) and thermally polymerized at 70 ºC, overnight. However, the light scattering intensity in OFF state became too small. In order to increase the light scattering in OFF state, it was also prepared PDLCs with weight ratios of 40/60 (wt. %). However, the low light scattering remains that enable the electro-optical response of these PDLCs. A polarized optical microscopic observation of PDLC films reveals heterogeneous dispersion between liquid crystal and polymer, as shown in Figure 6.49 and Figure 6.50.

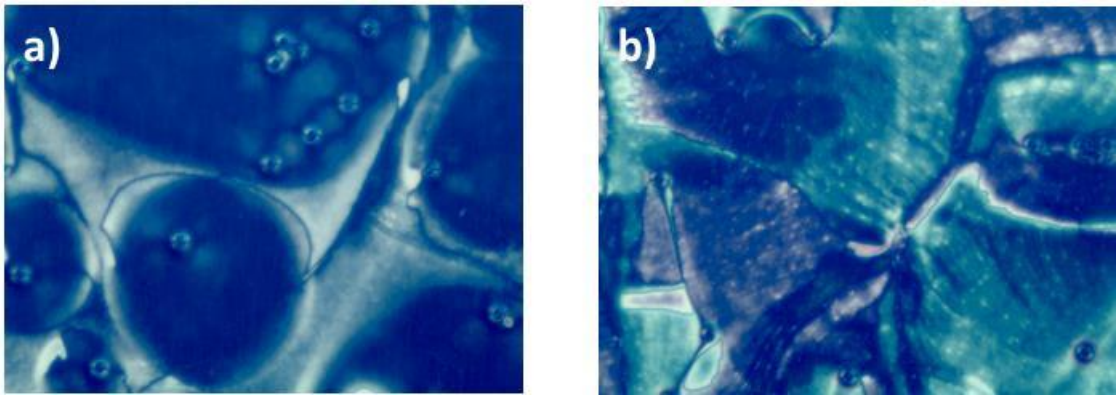

Figure 6.49 – Crossed Polarized optical micrographs observed for PDLC samples prepared with 3-armPEG-PPG TriM with 1wt.% of AIBN and E7 with weight ratios of a) 30/70 (wt.%) and b) 40/60 (wt.%), x100 magnification.

This inhomogeneous morphology promotes the poor light scattering which enabled the electro-optical response of these PDLCs. This could be to the polymer matrix which cannot support LC domains.

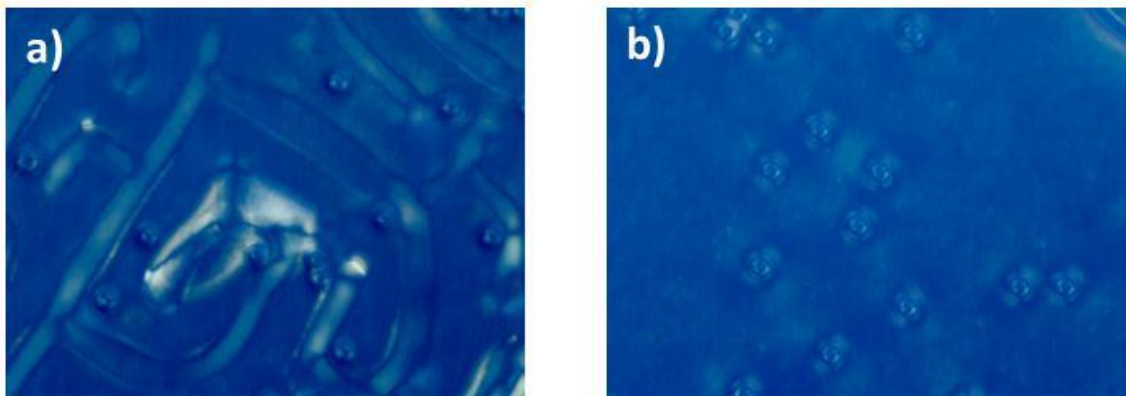

Figure 6.50 – Crossed Polarized optical micrographs observed for PDLC samples prepared with 3-arm PEG-PPGTriA with 1wt.% of AIBN and E7 with weight ratios of a) 30/70 (wt.%) and b) 40/60 (wt.%), x100 magnification.

The thermal behavior was investigated in the temperature range between - 80 ºC and 130 ºC with rates of 5 ºC min^{-1} in heating and cooling runs. From Figure 6.51 it is evident that for 3-armPEG-PPG the heat flux presents a discontinuity characteristic of the glass transition at -68 ºC. The absence of other transition confirmed the full amorphous compound.

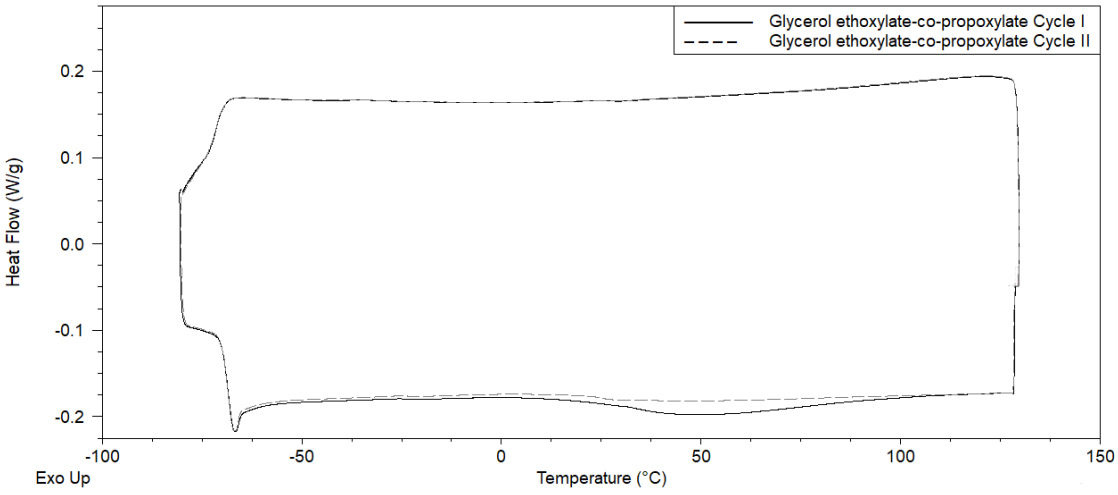

Figure 6.51 – Thermogram (heat flow vs. temperature) of 3-armPEG-PPG collected at two heating and cooling cycles at 5 ºC min^{-1}.

The end functionalization of glycerol ethoxylate-co-propoxylate triol results in oligomers tri-functionalized (3-armPEG-PPG TriM and 3-armPEG-PPG TriA). For the thermal analysis of correspondent polymers, the thermal polymerizations were initiated inside the DSC furnace.

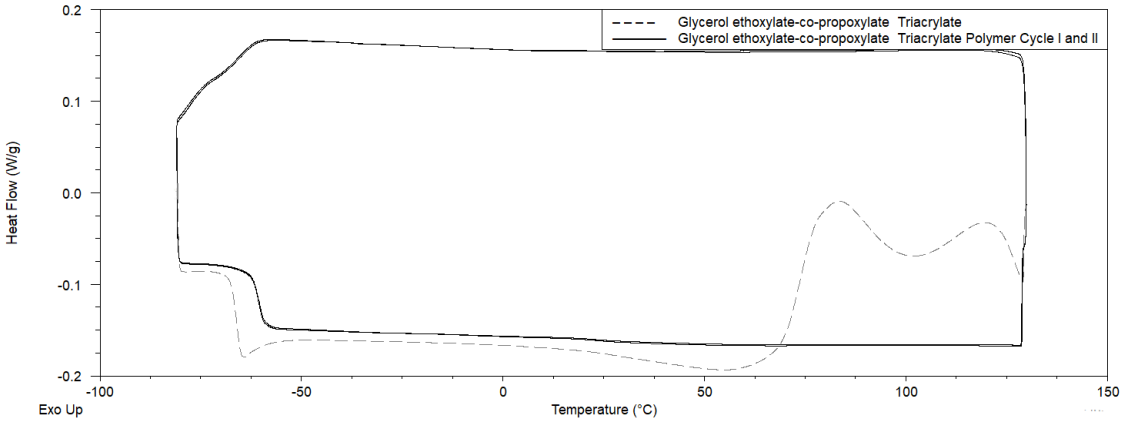

Figure 6.52 – Thermograms (heat flow vs. temperature) of 3-armPEG-PPG TriA + 1wt.% of AIBN collected at the heating scan at 5 ºC min^{-1} (dashed lines) and for 3-armPEG-PPG TriA polymer (solid lines) collected at two heating and cooling cycles at 5 ºC min^{-1}.

For 3-armPEG-PPG TriA (Figure 6.52) above the glass transition temperature at - 64.25 ºC, only exothermic effect at 72.80 ºC due to polymerization reaction occurs. The lack of addition transition represents a fully amorphous material, in contrast, to also tri-arm pre-polymer (3-armPEG TriA) but only with oxyethylene repeat units (Figure 6.30). It is possible that the methyl group in propoxylate units enable the arrangement of chains in an ordered arrangement.

For the resulting polymer, in the following heating and cool runs, the glass transition temperature is observed at - 60.68 ºC and - 60.54 ºC, respectively and no further processes were observed indicating a fully amorphous 3-armPEG TriA polymer (Figure 6.52). The propoxylate units lower the glass transition temperature from about - 39.91 ºC for 3-armPEG TriA polymer to about - 60 ºC for 3-armPEG-PPG TriA polymer. DSC thermograms collected for 3-armPEG-PPG TriM and for the result 3-armPEG-PPG TriM polymer show the same behavior as is shown in Figure 6.53.

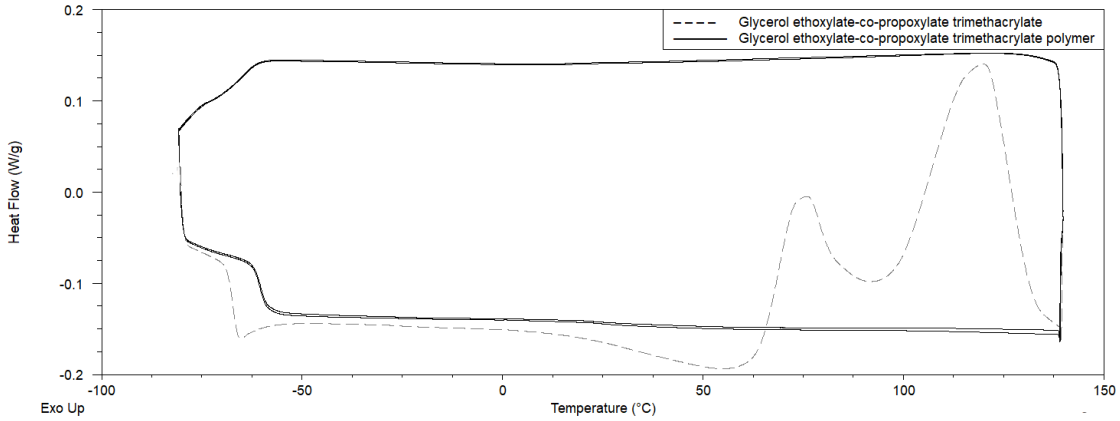

Figure 6.53 – Thermograms (heat flow vs. temperature) of 3-armPEG-PPG TriM + 1wt.% of AIBN collected at the heating scan at 5 ºC min^{-1} (dashed lines) and for 3-armPEG-PPG TriM polymer (solid lines) collected at two heating and cooling cycles at 5 ºC min^{-1}.

6.2.5 Nematic to Isotropic Transitions

The PDLC samples were heated at a rate of 1 ºC min^{-1} from 25 ºC to 70 ºC and observed by POM. The nematic to isotropic transitions were taken at the temperature where the sample became optically clear under crossed polarizers. The same heating was repeated two times for each sample. The liquid crystal phase transition temperature from nematic to isotropic determined by POM are reported in Table 6.8.

Table 6.8 – Nematic to isotropic transition temperatures determine by POM under crossed polarized during heating at the rate of 1 ºC min^{-1} from 25 to 70 ºC for 3-armPPG-PEG TriA polymer/E7 and 3-armPPG-PEG TriM polymer/E7 PDLCs.

PDLC sample	T_{NI}(ºC)
3-armPEG-PPG TriA polymer /E7 (30/70 wt.%) PDLCs	54.8
3-armPEG-PPG TriM polymer /E7 (40/60 wt.%) PDLCs	51.5
3-armPEG-PPG TriA polymer /E7 (30/70 wt. %) PDLCs	56.0
3-armPEG-PPG TriM polymer /E7 (40/60 wt. %) PDLCs	54.6

The T_{NI} obtained in 3-armPPG-PEG PDLCs (Table 6.8) is lower than in pure LC E7 (58 ºC) and also lower than in other PDLCs films studies (Table 3.2). In this way, the heterogeneity in PDLC films lower the order parameter of LC molecules which in turn makes more easily LC molecules reach a T_{NI} by thermal motions of LC molecules.

6.3 Conclusions

Multi-arm meth(acrylate) functionalized oligomers were synthesized using single step esterification with (meth) and acryloyl chloride and corresponding triol and tetraols as starting materials. As no pure mono-disperse multi-arm starting materials are commercially available the polydispersity of products difficult the chromatographic purification even with extensive purification. Although the difficult of purification of desired species, higher degrees of conversion were achieved. The MALDI-TOF mass spectrometric results were further supported by the NMR spectra.

The control of polymerization time is of enormous importance in achieving the level of desired crosslinking. The crosslink density increases continuously as polymerization time increases, more polymer chains are linked together growing molecular weight reaching maximum double bond conversion. Clearly, the lowest polymerization time of 15 and 30 min is insufficient to form stable PDLCs. When polymerization time is approximately between 60 and 120 min, PDLCs cell exhibits much better properties than for lower polymerization times. However, increasing polymerization time during the night leads to a decreased in phase separation with liquid crystal molecules trapped in the polymer matrix.

Mono-functional oligomers form a linear polymer chain while multi-functional one forms a crosslinked polymer network when polymerized. It is also possible to reduce the extent of crosslinking by a combination of these two oligomers types. It was clearly shown that with the desired ratio between multi-functional and mono-functional oligomers and polymerization time the permanent memory effect percentage increased until 100 % but the increase of polymerization time decreased this effect.

Although, the crosslinked PEG with linear longer arms significantly enhancement thermal stability, keeping the permanent memory effect unaffected in the time range from 60 to 120 min of thermal polymer curing at 70 ºC, the main problem remains with further polymerization. With multi-functional PEG a substantial number of unreacted functional groups remain after complete gelation. In this way, the development of a highly cross-linked network does not necessarily mean that the polymerization has completely ceased. Which represent a problem by the deterioration of the PDLCs.

The 3-armPPG-PEG polymers cannot support the LC domains increasing the heterogeneity of PDLC film which enable electro-optical properties of the PDLC films. These requirements eliminate these polymer types to be used in PDLCs films.

Chapter VII

7 Effect of Surface Alignment Layers on Permanent Memory Effect

As previously mentioned, in chapter I it is necessary to promote the director orientation to induce the anisotropy for an efficient response of liquid crystal molecules. This can be achieved by liquid crystal in contact with a substrate that induces a preferential alignment, where the director alignment is extended to the bulk. Usually, these alignment configurations include a homeotropic (LC director perpendicular to the substrate) and homogeneous (LC director parallel to the substrate) alignment[1,2,12]**.** The type of response with the applied voltage depends on the dielectric anisotropy of the liquid crystal. For a positive dielectric anisotropy, the electric field applied will reorient the nematic n-director parallel with the electric field. In this way, the liquid crystal molecules should be sandwiched between two parallel conductive glass plates with surface treated in order to obtain a homogeneous alignment[2,12]. In this configuration, when the electrical field is applied perpendicular to the LC director, the electric dipoles along to the long axis add together to give an electric polarization along the electrical field (positive charge moving in the direction of the electrical field and negative charge moving in the opposite direction) and perpendicular to the director. This separated charge exerts a torque that rotates the n-director parallel to the applied electrical field. However, the decrease in the amount of orientational order decreases the electric polarization induced by the applied electrical field. In other words, decrease of LC molecules with their long axis in a perpendicular orientation to the applied electric field and in this way able of being polarized. Therefore, the electric polarization creates by the applied field is not enough for LC molecules to align in the electric field direction[2]**.**

In this way, the type of orientations of liquid crystal molecules in pure LC devices induce by alignment surface methods is determinant for an efficient response to externally applied electric fields. Assuming that LC directors are held fixed in one direction the average dipole moment per molecule is in the same direction for each molecule. The applied electrical field causes a slight charge creating weak dipole moments but these dipole moments add together causing a large polarization. The larger the polarization more easily LC will align with the applied electric field.

In an ITO surface, the van der Waals interaction between ITO surface and LC molecules are more effective than between LC molecular interactions and a random LC alignment at the surface is produced, affecting the LC orientation in the bulk [142]. Thus, when a perpendicular electric field is applied to the surface of this system, this electric field is not very effective to orient the LC molecules ($\Delta\varepsilon>0$) due to the decrease of orientational order and the LC orientation remains mostly unchanged because anchoring ability remains dominant.

In a homogeneous alignment, the LC directors are parallel to the bounding surfaces of the cell, propagating the LC orientation to the bulk by molecular interactions. When LC molecules are in

contact with this surface LC molecules align parallel to the rubber polymer adopting a homogenous alignment[1]. The surface energy is minimized and the van der Waals interactions between LC molecules and substrate are sufficiently decreased[142].

As also previously mentioned, during electric field application there will be a competition between cell surface anchoring ability for LC and electrical force which would dictate how the LC director has to be oriented in the substrate surface. The LC director orientation is determined by a balance between the elastic, electrical and the interfacial contributions to the free energy of the nematic. The application of an electric field in a dielectrically positive liquid crystal makes mostly LC molecules rotate out-of-plane parallel with the applied field. Conversely, in a homeotropic alignment of a dielectrically negative nematic liquid crystal cell mostly LC molecules rotate out-of-plane perpendicular with the applied field.

When the electric field is removed, it is the orientation of the LC at boundaries that dictates the preferential LC director orientation in order to restore the configuration of lower elastic energy. However, in a memory system, the application of a sufficiently strong electric field oriented the LC molecules in a bulk but also changes the orientation of LC at boundaries to the surface cell to a closed orientation of the LC in a bulk and sufficiently different that in it was before application of the electric field[105]. This new preferred anchoring orientation will exert influence on the free molecules trying to keep the LC director align even when the electric field is removed.

In a liquid crystal cell with LC molecules with positive dielectric anisotropy but without alignment layer at boundaries of the substrate (only ITO coated substrate) even when the voltage is greater than the threshold voltage the n-director at boundaries has a fixed orientation and LC molecules cannot tilt. In this way, the elastic ability that originates at the unchanged LC molecules orientation at the substrate of ITO coated glass will restore the random LC configuration when the electric field is removed.

The effect of alignment layers on the properties of PDLC although has been reported[18,143–145] as expected no significant effect has been found in PDLC performance. However, all PDLCs discussed have no permanent memory effect. In this chapter, PDLC cells configurations were studied to report the effect of the alignment layer on the permanent memory effect.

In this way, six types of PDLC cells were constructed by allowing the unidirectional rubbing direction of polyimide (ITO coated glass substrate that was covered with rubber polyimide alignment layer (Figure 2.11)) on upper glass substrate, to be perpendicular, parallel and anti-parallel to that at the lower glass substrate with a cell gap of 23 μm by mylar spacers. The cells were denoted by Perpendicular-PDLC, Parallel-PDLC and anti-parallel-PDLC, respectively. It is also assembled a cell with random planar alignment by non-rubbed ITO coated glasses and the cell gap was also ensured to be 23 μm by mylar spacers. This cell was denoted as ITO-PDLC. It

was also prepared cells with homeotropic alignment by orientation layers with lecithin (lecithin-PDLC). Finally, it was also compared to a homogeneous alignment in anti-parallel configurations of unidirectional rubbed polyimide orienting substrates in commercial LC cell with 20 μm (Figure 2.12).

The effect of alignment layers surface on the alignment of liquid crystal molecules (E7) was confirmed by observations of the conoscopic images formed in a monochromatic beam converging in the glass cell filled with liquid crystal. When the n-director of E7 molecules is parallel to the light´s path, form a maltese cross in the center, as shown in Figure 7.1 a). This confirms that in a liquid crystal cell with a homeotropic alignment of n-director, the optic axis is oriented normal to the substrate surface. In the cell with homogeneous boundary conditions produced by rubbed polyimide, the E7 n-directors adopt a parallel orientation to the substrate surface, as shown in Figure 7.1 b).

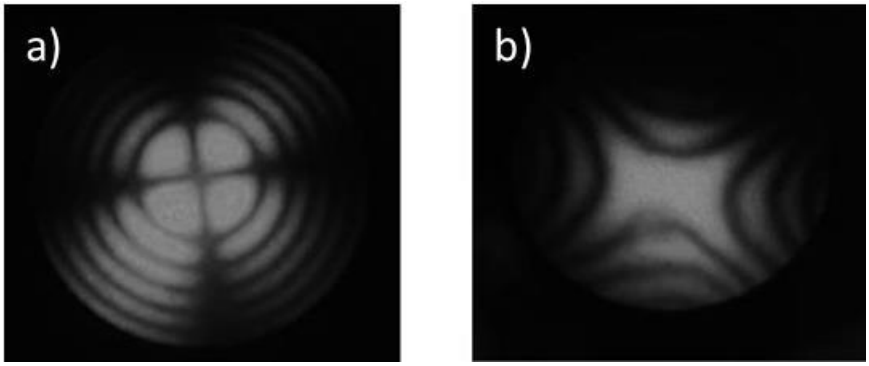

Figure 7.1 – Conoscopic images of a) homeotropic aligned of E7 and b) homogeneous alignment of E7.

The electro-optical properties of PDLCs films were compared and it was found that the presence of an alignment layer greatly affected the permanent memory effect (Figure 7.2).

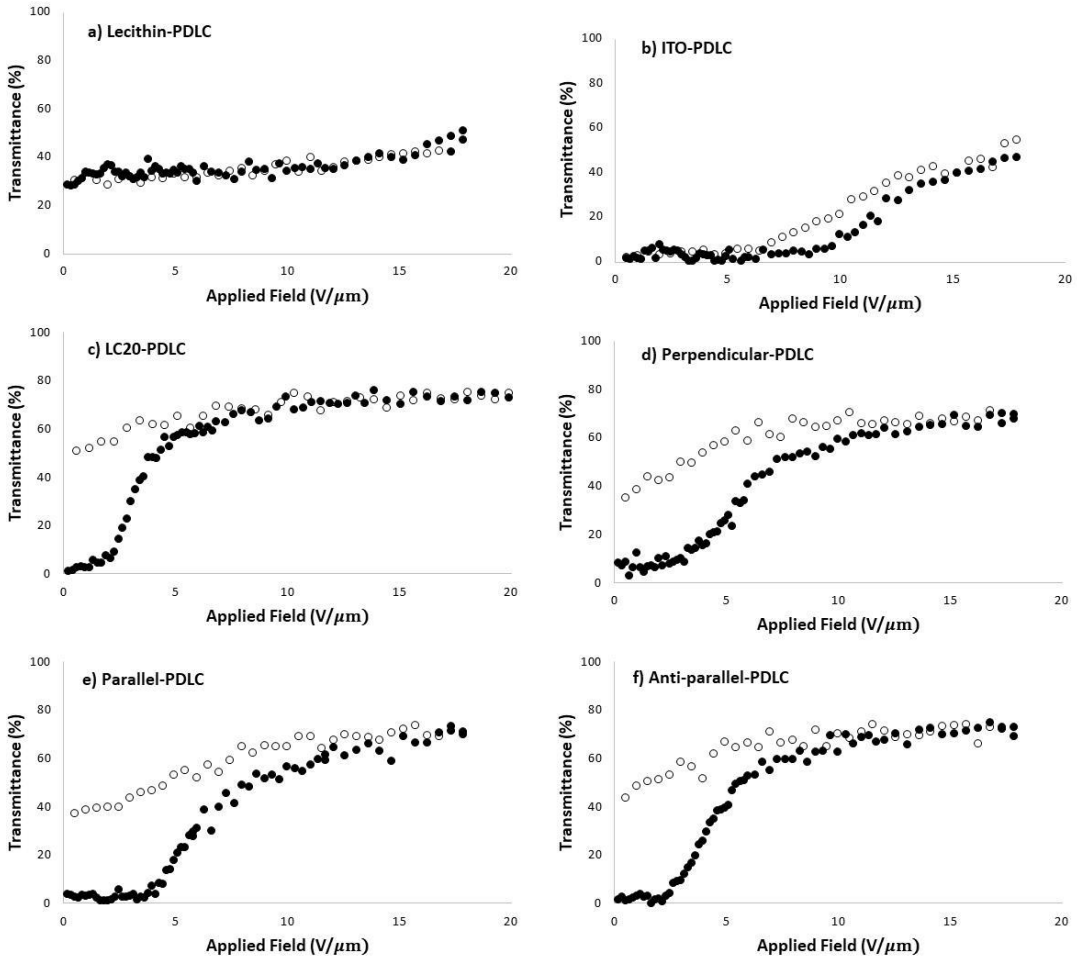

Figure 7.2 – The effect of the alignment layer on electro-optical (transmittance-electrical field) properties of PDLCs prepared by PEGDM875 (1 wt.% of AIBN)+E7 in a weight ratio of 30/70 (wt.%) and polymerized at 70 ºC, overnight: a) lecithin-PDLC cell cell (23 μm thick); b) ITO-PDLC cell (23 μm thick); c) commercial LC20-PDLC cell (20 μm thick); d) perpendicular-PDLC (23 μm thick); e) Parallel-PDLC (23 μm thick) and f)anti-parallel-PDLC (23 μm thick).

In this way, it is possible to hypothesize some explications, based on the above results, for the increase of PME with the presence of surface alignment layers.

The mixture of PEGDM875 and LC E7 is an isotropic liquid containing manly mesogenic molecules that start being order in contact with the substrate. During polymerization/phase separation the LC domains are dispersed into the polymer matrix and also anchored to the boundaries of the cell following the anchoring orientation of substrates[144]. In another case the anchoring ability of boundaries substrate for LC propagate same distance into the LC/polymer composite and a possible thin layer of free LC (without polymer matrix) lies between the LC/polymer matrix and alignment layer [18]. In a PDLC cell without alignment layer (ITO coated glass substrate) the nematic director is random planar alignment in contact to the substrate and in a presence of an alignment layer LC molecular orientation follow the alignment layer: along the polyimide rubbing direction by a homogeneous alignment or in a homeotropic orientation induce by the lecithin alignment layer.

The PDLCs studies are characterized by a polymer ball morphology in which an interconnected liquid crystal channel as continuity of the LC domains exist in an agglomerate of polymer beads. This morphology type, favorable a propagating of anchoring orientation of the alignment layer from boundaries to the bulk of the PDLC (high degree of interconnection between LC domains). A possible self-alignment of LC-pre-polymer chain on the surfaces of substrates is proposed in Figure 7.3.

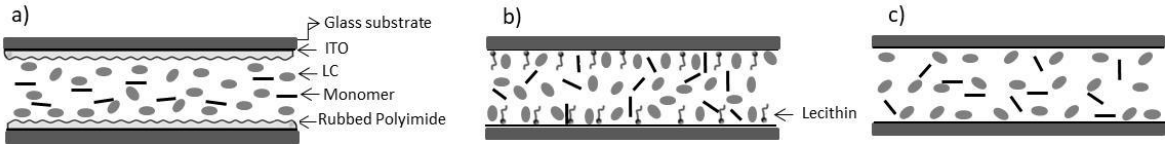

Figure 7.3 – Schematics of the arrangement of the pre-polymer and liquid crystal in a) homogeneous alignment-PDLC cell; b) homeotropic alignment-PDLC and c) random planar alignment- PDLC cell[145,146].

Under an electrical field, the LC domains director aligned parallel to the electrical field and incident light passes through the PDLC without scattering by matching the ordinary refractive index of the LC to the refractive index of the polymer matrix and PDLC becomes transparent. When the electric field is removed a higher transparent state is displayed by PDLC-homogeneous (Figure 7.2 c);d);e) and f) unlike for ITO-PDLC cell configuration where scattering sate return (Figure 7.2 b).

Using a homeotropic anchoring result in high transparency in the initial OFF state (30 %). The LC molecules are preferably oriented perpendicularly to the cell surface. For this reason, even at electric-field off light goes through the PDLC without scattering by matching the ordinary refractive index of the LC to the refractive index of the polymer matrix (Figure 7.2 a).

The main difference between the preparations of these PDLCs is the alignment layer of boundaries of the glass cell. In this way, the permanent memory effect on the PDLC-homogeneous cell configuration could be promoted by the LC director orientation on the alignment surface layer also be disturbed by the electrical field applied. When electrical field return at zero, the LC director at these surfaces exert influence on the LC molecules at PDLC film bulk (LC molecules are in a continuous phase dispersed in the polymer matrix) and LC molecules remain in a stable align state although different from the initial one.

In an ITO-PDLC cell, the random planar LC molecules orientation on the ITO layer remains unchanged or only partially disturbed when the electrical field is applied. When the electrical field is removed the LC orientation impose by applied electrical field is lost because LC molecules in PDLC films return to a minimum energy state by elastic reorientation ability imposed by random LC alignment of ITO substrates. Therefore, a scattering state is observed once again (Figure 7.2 b).

Chapter VIII

8 Manufacturing Passive PDLC Film Matrixes: Digital Memory PDLCs Devices based on Electrical Writing Digital Information

Optical storage information in LC composites has been described [52–55,147] and the applications of these properties in developing a novel digital memory devices based on write-read-erase cycles can be envisaged by the permanent memory effect of PDLCs development in this work. The electro-optical characterization of a test PDLC cell with PME is depicted in Figure 3.2 d). The 70 % of permanent memory effect, the thermal stability and the reproducibility even after multiple repetitions of the heating and electric field cycle application make this PDLC film promising for recording, storing and erasing digital information.

For optical storage information in PDLCs by electrically writes, optically read and thermally erased a multiplexing drive pixel array is needed where optical elements (pixels) are formed by PDLC units with PME. The PDLC units are individually controllable and can be transparent or opaque whether or not an electric field is applied to define the ON and OFF state, respectively. The principle of digital memory devices based on write-read-erase cycles can be described by a robust representation of a PDLCs pixels array in a passive matrix shown in Figure 8.1. The conducting rows and columns end are the contact areas and the rectangular pixels (PDLC units) can be electrically addressed from those contact areas. In this way, information can be electrically written by electric field individually applied to different PDLC units that turn these pixels to the transparent state and if no electric field is applied to a given pixel it remains in the opaque state. The transparent state is preserved after the field is removed, due to the permanent memory effect. As previously mentioned, the storage information given by transparent or opaque pixels can be optically read and thermally erase (until to the T_{NI} of LC). Later, information can be electrically written again.

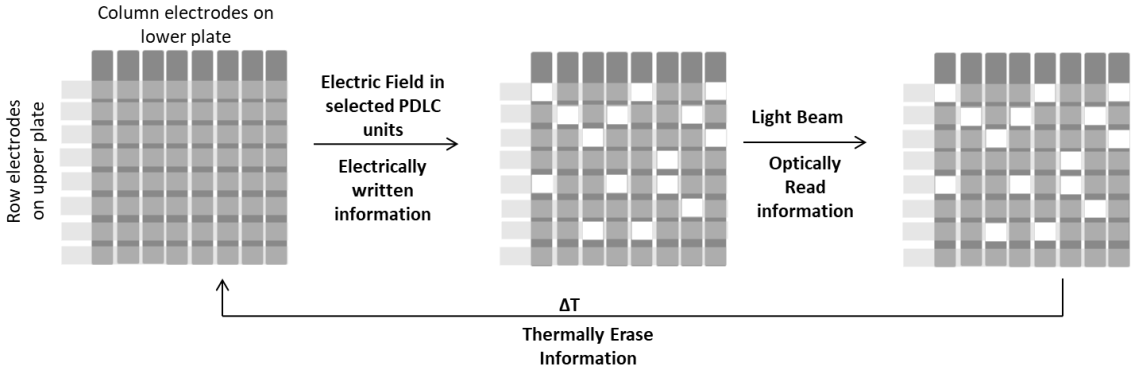

Figure 8.1 – Top view of a schematic representation of the working principle of optical storage materials in an 8 x 8 passive matrix using PDLC with permanent memory effect units (rows of electrodes on one piece of glass and columns of electrodes on the opposing piece of glass).

8.1 Pattern Fabrication on ITO Covered with an Alignment Layer

The PDLCs with permanent memory effect developed in this work constitute the starting point of new investigations with a view to use these PDLCs as material for optical storage. For this, a passive PDLC matrix display with a pixel number of 8x8 and a pixel size of 1x1 mm^2 was manufactured. In the whole fabrication process, the formation of the patterned ITO substrate is a crucial process starts with a photolithography technique.

The photolithography process starts with spin coating the ITO coated (16x16 mm) glass substrate (20x25x1.1) that was covered with rubbing polyimide alignment layer, with a photoresist. The positive photoresist used is known as AZ-1518 and is composed by photoactive species denominated diazonaphthoquinone (DNQ) (Figure 8.2)[148].

Once the substrate has been coated with this photoresist, the substrate is then soft baked at 110 ºC during 4 min in order to remove the solvents and improve the adhesion. Subsequently, the developed photomask is aligned by contact to the substrate and for this reason, only some individual areas of the photoresist are selectively exposed to the UV light for several seconds. The photoresist areas that were exposed to UV light changes chemically. The nitrogen molecule in the photoactive compound is liberated of the aromatic ring turning the unoccupied orbital highly reagent. In this way, one of the carbon atoms moves outside of the ring and the oxygen atom is then covalently bonded to it (Wolff rearrangement). In the presence of water a final rearrangement occurs in which a double bond of the external carbon is changed by a single bond with an OH group, giving a final carboxylic acid product (Figure 8.2) more soluble in a developing solution (NaOH solution) than started material (photoresist)[148].

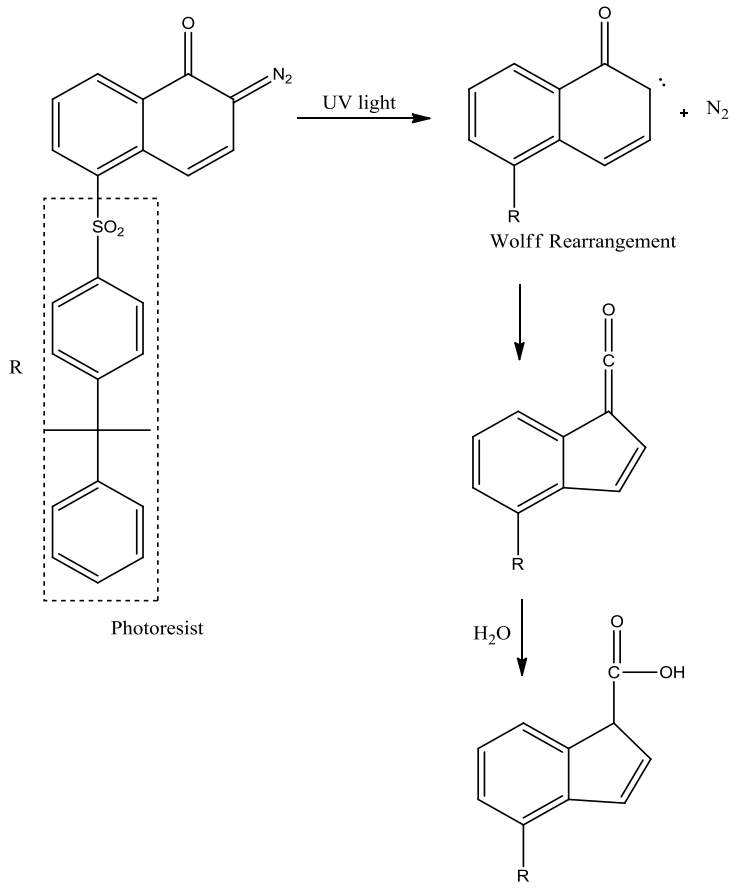

Figure 8.2 – Photodisintegration of the photoactive compound and subsequent reactions[1].

After development, the masked photoresist serves as a masking area for individual areas of polyimide exposed could be etching using oxygen and fluorine gas mixture (O_2-SF_6 plasma)[149,150].

Next, the expose indium tin oxide areas were chemical etching by an aqua regia solution of HCl:HNO_3. For this, substrates were immersed vertically in the etching solution for 1 minute, without stirring.

The etching rate increases with temperature and in this way, the etching process was performed at 40 ºC. The photoresist was then stripped with acetone. The line-shaped ITO electrodes with a width of 1 mm and a spacing of 1 mm could be observed clearly in the substrate (Figure 8.3).

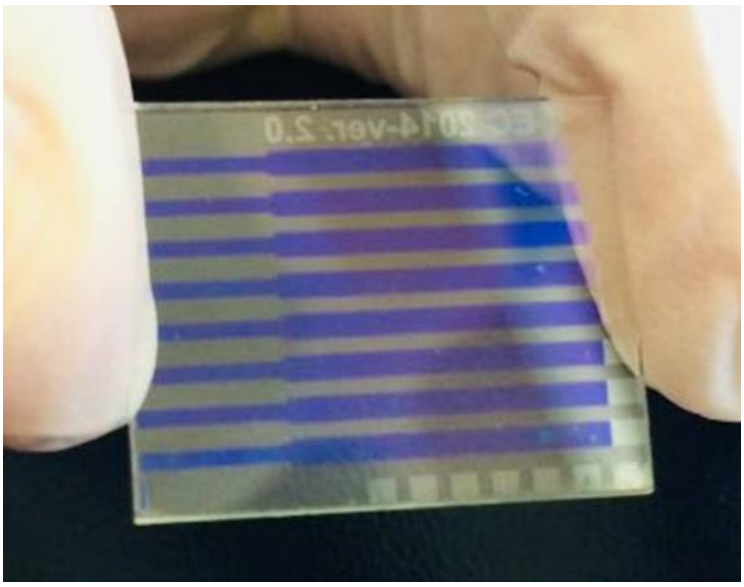

Figure 8.3 – Image of line-shaped ITO electrodes coated on the glass substrate.

Following the generation of the photomask, the lithography process can be schematic proceed as shown in Figure 8.4.

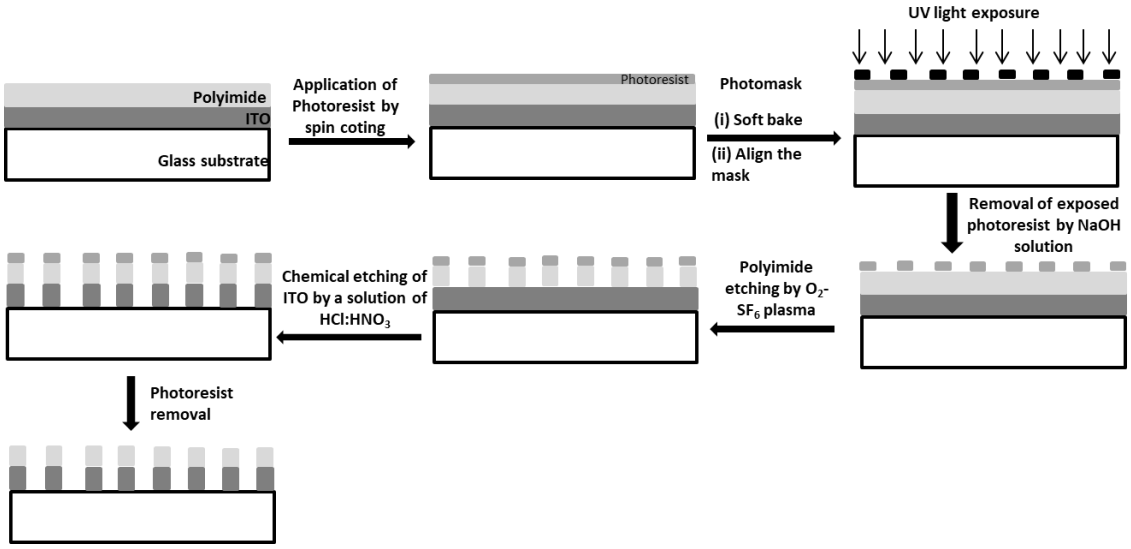

Figure 8.4 – Schematic illustration of photolithography process for making line-shaped ITO electrodes covered with polyimide.

8.1.1 Line-shaped ITO Electrodes Covered with Polyimide Thickness Measurement

A mechanical profilometer (Ambios XP-Plus 200 Stylus) was used to estimate the film thickness of each eight line-shaped ITO covered with polyimide previously development in the

photolithography process, as illustrated by Figure 8.5 a). In average each line has a thickness of 160nm. The line thickness profile exemplification is shown in Figure 8.5 b).

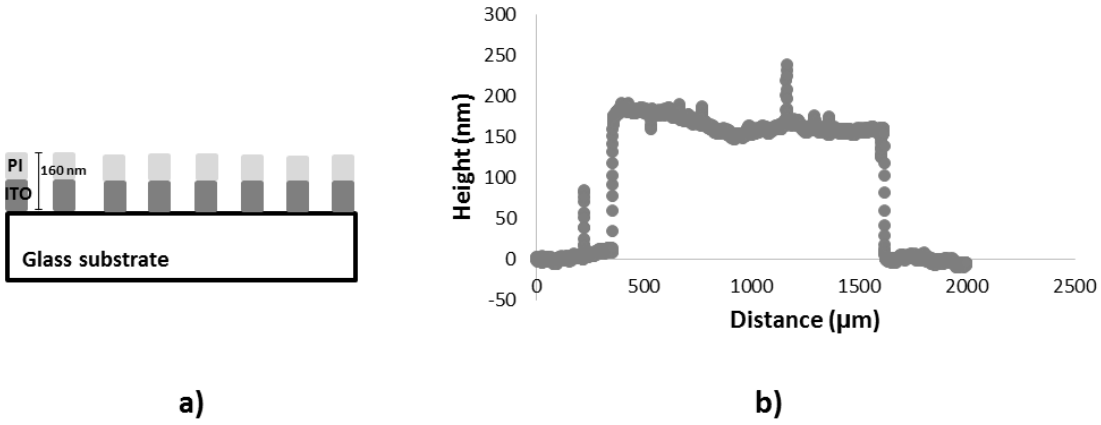

Figure 8.5 – Schematic illustration of the line thickness measure (a) and line thickness profile (b).

8.2 PDLC Passive Matrix Assembly Device

To prove the principle of passive matrix addressing, passive matrixes were constructed by two glass substrates sandwiched the PDLC mixture, where the top and bottom electrodes are patterned ITO covered with polyimide previously developed in rows and columns, respectively (or vice versa). The row electrodes and the column electrodes are perpendicular to each other and the rows and column intersect is a display element referred to as a pixel. The thickness of the cell was controlled by mylar spacers (thickness, 23 µm), placed along the perimeter of the substrates plates and sealed with epoxy resin. The cell cavity was filled with the PDLC mixture (PEGDM875 (1 wt.% of AIBN) and E7 in a weight ratio of 30:70 (wt.%) by capillary action. Finally, this sample is cured at 70 ºC, overnight. Each pixel is a PDLC unit sandwiched in the area of intersection of rows address lines and column address lines. The main specifications of this passive matrix PDLC device are summarized in Table 8.1.

Table 8.1– Specifications of passive matrix PDLC device.

Substrate type	**Patterned ITO covered with polyimide coated glass**
Glass type	soda lime
Substrate size (mm^2)	25x25
Active area (mm^2)	21x20
Number of pixels	8x8
Pixel size (mm^2)	1x1
Gap between pixels (mm)	0.023

8.3 PDLC Passive Matrix Device Operation

The macroscopic effect of electrically written information in a passive PDLC matrix device was direct observation, as shown in Figure 8.6. The applied AC with 75.3 V_{RMS} results in a desired selected pixel that switches to the transparent state and the unselected pixels remain in a scattering state. However, for applied AC higher than 254.2 V_{RMS} an undesirable complete row and column of pixels addressed was observed (Figure 8.6 c)).

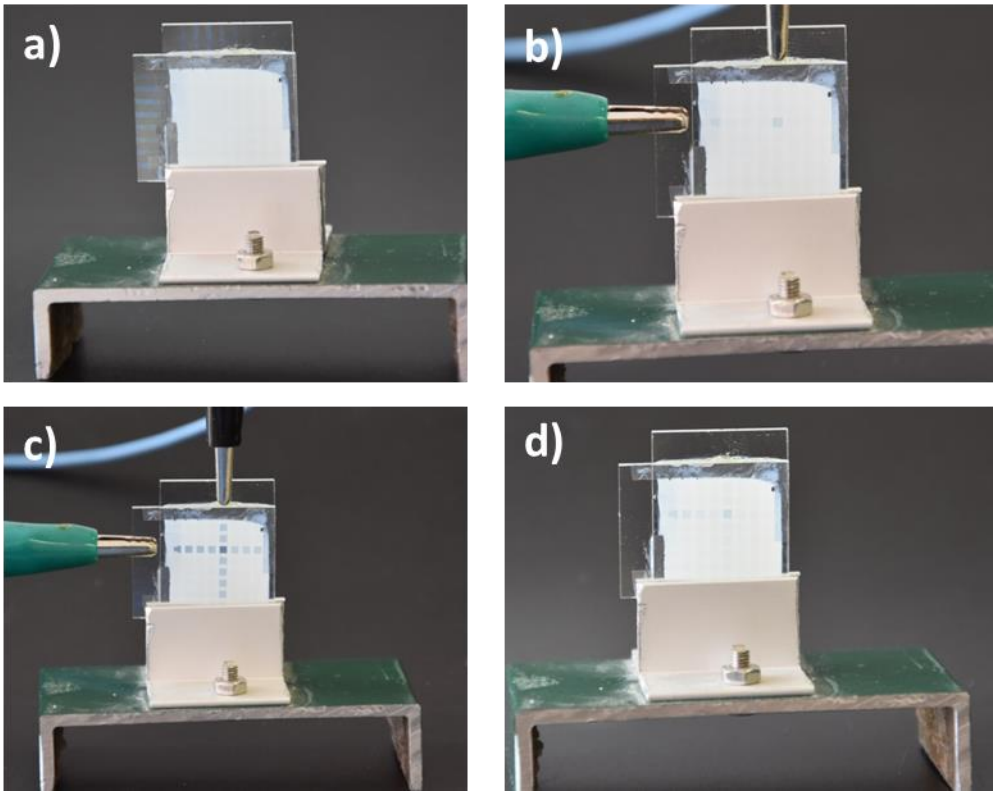

Figure 8.6 – Photographs of direct observation of the macroscopic performance of PDLC display example in an 8x8 passive matrix: Electrically written at 1 KHz with an applied voltage of a) 0 V_{RMS}, b) 75.3 V_{RMS}, c) 254.4 V_{RMS} and d) after the applied voltage is switched off.

After the above pixel selected, optical information was also written in another pixel as shown in Figure 8.7.

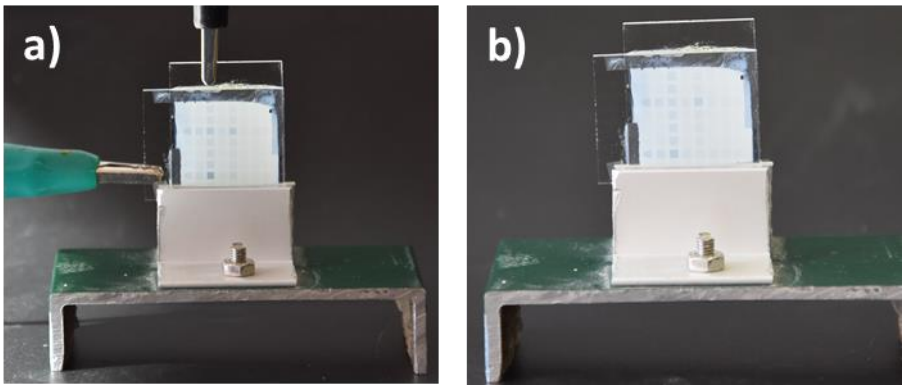

Figure 8.7 – Photographs of direct observation of the macroscopic performance of PDLC display example in an 8x8 passive matrix, demonstrating the electrically written information effect at 1 KHz with an applied voltage of a) 126.2 V_{RMS} and in b) after the applied voltage is switched off.

A new working device of passive matrix addressing PDLC display with PME of 8x8 pixels was presented. It is clear that this result can represent an important starting point for potential applications in terms of the optical storage devices. However, to accurately describe the optical storage information in passive PDLC matrix devices further experimental and theoretical studies are needed.

Chapter IX

9 Erase Stored Information and Rewrite it again

The transparent state displayed by a PDLC device due to permanent memory effect can be converted into a scattering state by heating up to T_{NI} of the liquid crystal and cooling it down later on, or by changing the bulk alignment with an external electrical field[18].

In a PDLC film with thermotropic nematic liquid crystal, heat causes an increase in the thermal motion of the LC molecules. The kinetic energy of LC molecules becomes too large to preserve the memorized aligned state of the molecular orientation retained by the electric field previously applied (permanent memory effect). When the PDLC film is heated up to the isotropic phase, the molecular align orientation of LC molecules is disturbed by the heat application, resulting in a random disordered isotropic phase. As the material cools down from the isotropic phase to the nematic phase, liquid crystal molecules in each domain adopt a different orientation by polymer surface anchoring. Liquid crystal molecules align themselves in a different arrangement from domain to domain which left scattering sites for incident light[6,18,151].

Heat transfer to PDLC film may take place by conduction or radiation [152]. From these two modes of heat transfer to achieve T_{NI} of a PDLC, radiation heat transfer may be more infeasible due to setup constraints. This thermal radiation needs a mechanism for propagation of electromagnetic radiation while heat transfer by conduction is made by direct contact between materials. For this reason, heat transfer from ITO conductive layers to PDLC film by conduction is more practical and effective than by radiation taking advantage of direct contact between ITO layers and PDLC film.

Thermal energy may be conducted in conductive solids by lattice vibration and transport by free electrons. In electrical conductors, free electrons move about in the lattice structure of the material[152]. One way to convert this electrical energy into a heat flux on the material surface is by Joule heating effect. In this way, when a potential difference is applied across the ends of a conductor such as ITO, the free electrons are accelerated. The collisions between electrons and atoms transfer energy to atoms which manifest itself as heat[153]. This heat energy can be transfer by conduction to PDLC film.

ITO is an electrical conductor by Ohm´s law:

$$I = \frac{V}{R}$$

where R is the resistance of the conductor in units of ohms, V is the voltage measured across the conductor in units of volts and I is the electrical current intensity applied through the conductor in units of the ampere.

The energy released when current flows through the ITO layer is denoted by *P* in watts. It is assumed that all the power is dissipated through heat[154] and can be calculated by the following equation:

$$P = VI$$

That means:

$$P = I^2R$$

An electrical DC voltage by independent electrodes used to apply an AC electrical field to the PDLC layer is coupled to one ITO layer to transfer heat to PDLC film by the Joule heating effect. The power supply, *EX4210R* from *TTi* provides an output voltage from 0 to 42 V at 0 to 10 A.

The current provided by the power source flows through the conductive ITO layer encountering resistance (100 ohms/square) and some electrical energy is transformed into thermal energy. This thermal energy is transferred to the PDLC film by conduction. As previously mentioned, by Ohm equation the larger the current intensity, the greater the energy loss by the Joule heating effect. If the amount of current intensity is large enough, it could reach the T_{NI} of PDLC film. Which totally erases the written information.

To evaluate the effect of thermal erase optical information by Joule heating, the PDLC transmittance has used to determine the period of time and electrical current intensity needed to reach the transparent state (isotropic state) and the period of time to reach the scattering state (nematic state) by cooling it down, as shown in Figure 9.1.

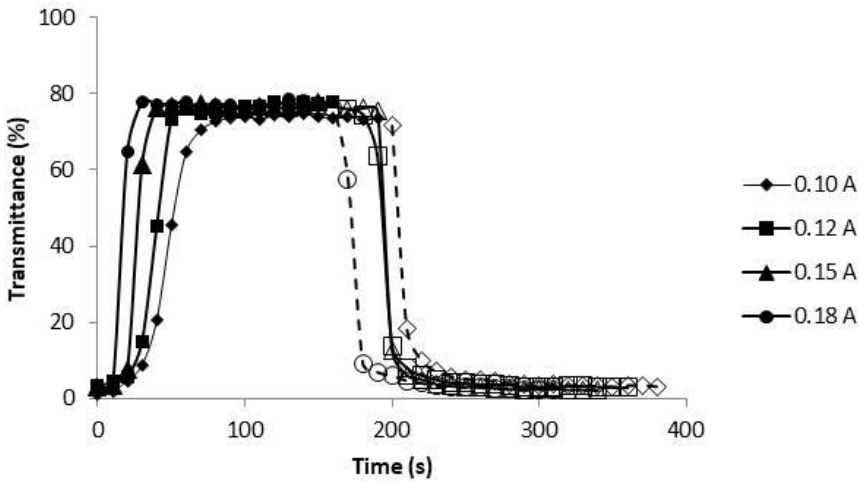

Figure 9.1 – PDLC transmittance variation in time depending on turn-on time by Joule heating effect with electrical current intensity at 0.10 A; 0.12 A; 0.15 A and 0.18 A and turn-off time after Joule heating effect during cooling for each electrical current intensity applied. Solid lines denote to the application of the Joule heating effect and dotted lines denote to the cooling period of time. The PDLC sample was prepared by commercial *Instec* LC cell (20 μm of thickness) filled with PEGDM875 (1 wt. % of AIBN) + E7 in a ratio of 30/70 (wt.%) mixture thermally polymerized at 70 ºC, overnight.

As expected, the higher the electric current intensity, the quicker the higher transmittance is reached (Figure 9.1). That means, as electrical current intensity increases more quickly the PDLC film temperature overcomes the phase transition temperature to the isotropic state. The time needed for the PDLC reach the highest transmittance decreases as the electrical current intensity increases from 70 s for 0.10 A to 30 s for 0.18 A. Electrical current intensity lower than 0.10 A is insufficient to produce enough thermal energy to erase the PME.

When the electrical current applied was switched off and the PDLC cools down, LC turns to the nematic phase and transmittance decreases again to initial values due to random LC orientation. The time at which the PDLC becomes totally opaque by cooling after the electrical current is turned off slightly increases as electrical current increase. From 80 s for 0.10 A to 110 s for 0.18 A. Mostly because higher PDLC temperatures are reached by applying higher currents.

In this way, the Joule heating effect and cooling treatment could be used to erase the permanent memory effect. In order to use this effect to erasing the written information (PME), the transmittance of a PDLC sample with PME was monitored as the electrical current intensity was applied and removed (Figure 9.2). To test the reproducibility of this process, after the erase of the permanent memory effect, 120 V_{RMS} AC were applied to the PDLC sample to rewrite again information.

The process of writing information, heating to the isotropic phase, cooling to the nematic phase (writing information and erase it) was repeated for three times (Figure 9.2). For 0.15 A as working electrical current intensity chosen, it is necessary near 30 s of Joule heating effect to

disturbed LC orientation by reaching the isotropic state and more than 65 s to restore the scattering state after removal Joule heating by reaching the nematic phase. In a total of 95 s for complete erasing of the permanent memory effect by heating and cooling treatment.

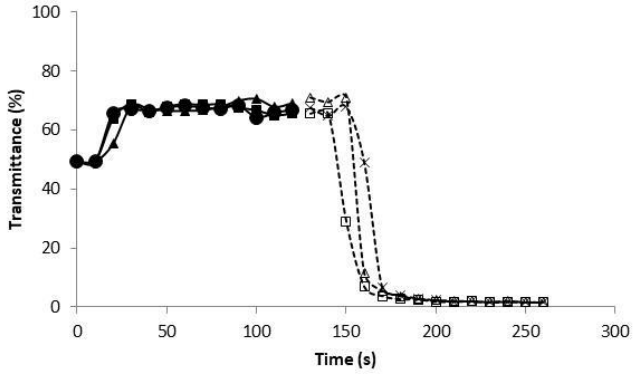

Figure 9.2 – Three repetition of PDLC transmittance variation in time depending on the Joule heating effect with electrical current intensity at 0.15 A and turn-off time after Joule heating by cooling treatment. Solid lines denote to the application of the Joule heating effect and dotted lines denote the cooling period of time. The PDLC sample was prepared in commercial *Instec* LC cell (20 μm of thickness) filled with PEGDM875 (1 wt. % AIBN) +E7 in a ratio of 30/70 (wt. %) mixture thermally polymerized at 70 ºC, overnight.

Chapter X

10 Final Conclusions

A series of di-, tri- and tetra meth(acrylate) pre-polymers were synthesized using a single step of esterification with (meth) and acryloyl chloride and correspond alcohols as starting materials. Combined analyses of ^{1}H-NMR, ^{13}C-NMR and two-dimensional NMR (COSY and HSQC), as well as MALDI-TOF mass spectroscopy, was used to confirm the structure and purity of the products.

In this work, it has been shown that PDLCs can not only be operated in their conventional mode as light shutters scattering in the OFF state and transparent in the ON state but also in an operational way where even after the applied electric field has been switched OFF, a highly transparent state is preserved. This electro-optical characteristic called permanent memory effect (PME) depends on appropriate conditions.

This work provided an intimate relationship between thermal properties of the polymer matrix, polymer morphology type, free radical polymerization conditions and surface alignment layer type coated on glass substrates cell in the development of the PDLCs with permanent memory effect property. The T_g of the polymer matrix determines the degree of interaction between the polymer matrix and LC molecules. Polymer matrix with T_g low than room temperature decreases the interaction with LC molecules which enhance the stability of LC in keeping align when the electrical field is removed. The type of polymerization used for preparation PDLCs determines the polymer matrix morphology type which in term influence the PME. The thermal polymerization, with temperature and polymerization time optimized, produces polymer ball morphology where LC molecules are in a continuous LC phase which stabilizes the keeping of LC alignment even when the electrical field was removed. The LC alignment layers in PDLCs cell determine the energy of adhesion between LC molecules and alignment layers. The PDLC cells with a homogeneous alignment layer type give rise to PME unlike the homeotropic or even without any alignment layer. In this way, in this work, the main requirements for achieving a stable permanent memory effect (70 %) are a di-functional pre-polymer (PEGDM875), with a T_g of the polymer matrix (- 35.51 ºC) lower than room temperature and a PDLCs cell with a homogeneous alignment layer.

In nematic LC systems, the duration of the retention of a switching state is usually not significant enough for the application. However, based on these improvements results for permanent memory effect a simple proof-of-principle prototype to be used in the digital process of recording information in opaque and transparent states was successfully tested. The erase of the stored information by heat with the Joule effect makes the experimental setup developed simpler.

Chapter XI

11 Bibliography

(1) Yang, D.-K.; Wu, S.-T. *Fundamentals of Liquid Crystal Devices*; Lowe, Anthony, C., Sage, I., Eds.; John Wiley & Sons, Inc., 2015.

(2) *Handbook of Visual Display Technology*; Chen, J., Cranton, W., Fihn, M., Eds.; Springer-Verlag, 2012.

(3) Pieranski, P. *Nematic and Cholesteric Liquid Crystals*; Gray, G. W., Goodby, J. W., Fukuda, A., Eds.; Taylor & Francis, 2005.

(4) Rizvi, T. Z. *J. Mol. Liq.* **2003**, *1*, 43–53.

(5) Chen, Robert, H. *Liquid Crystal Displays:Fundamental Physics and Technology*; Anthony, C. L., Ed.; Wiley, 2011.

(6) *Introduction to Liquid Crystals*; Priestley, E. B., Wojtowicz, Peter, J., Sheng, P., Eds.; RCA laboratories, 1974.

(7) Collings, P. J.; Michael, H. *Introduction to Liquid Crystals: Chemistry and Physics*; Gray, G. W., Goodby, J. W., Fukuda, A., Eds.; Taylor & Francis, 2009.

(8) Meier, G.; Sackmann, E.; Grabmaier, J. G. *Applications of Liquid Crystals*; Springer Verlag, 1975.

(9) Pochi, Y.; Claire, G. *Optics of Liquid Crystal Display*; Boreman, G. D., Ed.; John Wiley & Sons, Ltd, 2010.

(10) Zakerhamidi, M. S.; Ara, M. H. M.; Maleki, a. *J. Mol. Liq.* **2013**, *181*, 77–81.

(11) Barbero, G.; Evangelista, L. R. *Adsorption Phenomena and Anchoring Energy in Nematic Liquid Crystals*; Taylor & Francis, 2006.

(12) Takatoh, K.; Hasegawa, M.; Koden, N.; Itoh, N.; Hasegawa, R.; Sakamoto, M. *Alignment Technologies and Applications of Liquid Crystal Devices*; Gray, G.W., Goodby, J.W., Fukuda, A., Ed.; Taylor & Francis, 2005.

(13) *Optical Applications of Liquid Crystals*; Vicari, L., Ed.; Institute of Physics Publishing, 2003.

(14) Brás, A. R. E.; Henriques, S.; Casimiro, T.; Aguiar-ricardo, A.; Sotomayor, J.; Caldeira, J.; Santos, C.; Dionísio, M. *Liq. Cryst.* **2007**, *34*, 591–597.

(15) Pauluth, D.; Tarumi, K. *J. Mater. Chem.* **2004**, *14*, 1219–1227.

(16) Pasechnik, S. V; Chigrinov, V. C.; Shmeliova, D. V. *Liquid Crystal: Viscous and Elastic Properties*; Wiley-VCH, 2009.

(17) Mucha, M. *Prog. Polym. Sci.* **2003**, *28*, 837–873.

(18) Drzaic, P. S. *Liquid Crystal Dispersions*; Ong, H. L., Ed.; World Scientific Publishing, 1995.

(19) Bulgakova, S. A.; Mashin, A. I.; Kazantseva, I. A.; Kashtanov, D. E.; Jones, M. M.; Tsepkov, G. S.; Korobkov, A. V.; Nezhdanov, A. V. *Russ. J. Appl. Chem.* **2008**, *81*, 1446–1451.

(20) He, J.; Yan, B.; Yu, B.; Wang, S.; Zeng, Y.; Wang, Y. *Eur. Polym. J.* **2007**, *43*, 2745–2749.

(21) Li, W.; Cao, H.; Kashima, M.; Liu, F.; Cheng, Z.; Yang, Z.; Zhu, S.; Yang, H. *J. Polym. Sci. Part B Polym. Phys.* **2008**, *46*, 2090–2099.

(22) Amundson, K.; Blaaderen, A. van; Wiltzius, P. *Am. Phys. Soc.* **1997**, *55*, 1646–1654.

(23) Du, X.; Yan, B.; Wang, Y. *J. Polym. Sci. Part B Polym. Phys.* **2010**, *48*, 729–732.

(24) Ahmad, F.; Jamil, M.; Jeon, Y. J.; Woo, L. J.; Jung, J. E.; Jang, J. E.; Lee, G. H.; Park, J. *J. Appl. Polym. Sci.* **2011**, *121*, 1424–1430.

(25) He, J.; Yan, B.; Wang, X.; Yu, B.; Wang, Y. *Eur. Polym. J.* **2007**, *43*, 4037–4042.

(26) Han, J. *J. Korean Phys. Soc.* **2006**, *49*, 1482–1487.

(27) Bower, D. I. *An Introduction to Polymer Physics*; Cambridge University Press: Cambridge, 2002.

(28) Ravve, A. *Principles of Polymer Chemistry*; Springer, 2012.

(29) Mandelkern, L. *An Introduction to Macromolecules*; Springer-Verlag: k, 1972.

(30) Raju, G. G. *Dielectrics in Electric Fields*; Marcel Dekker, Inc., 2003.

(31) Gedde, Ulf, W. *Polymer Physics*; Springer-Science+Business Media, B.V., 2001.

(32) Moad, G.; Solomon, D. H. *The Chemistry of Radical Polymerization*; Elsevier, 2006.

(33) Scharf, T. *Polarized Light in Liquid Crystals and Polymers*; John Wiley & Sons, Inc., 2007.

(34) Nomura, H.; Suzuki, S.; Atarashi, Y. *Jpn. J. Appl. Phys.* **1990**, *3*, 522–528.

(35) Vaz, N. A.; Montgomery, G. P. *J. Appl. Phys.* **1987**, *62*, 3161–3172.

(36) Jain, S. C.; Rout, D. K. *J. Appl. Phys.* **1991**, *70*, 6988–6992.

(37) Roussel, F.; Buisine, J.-M.; Maschke, U.; Coqueret, X. *Liq. Cryst.* **2010**, *24*, 555–561.

(38) Deshmukh, R. R.; Malik, M. K. *J. Appl. Polym. Sci.* **2008**, *109*, 627–637.

(39) Maschke, U.; Coqueret, X.; Benmouna, M. *Macromol. Rapid Commun.* **2002**, *23*, 159–170.

(40) Han, J. *J. Korean Phys. Soc.* **2003**, *43*, 45–50.

(41) Jeong, E. H.; Sun, K. R.; Kang, M. C.; Jeong, H. M.; Kim, B. K. *Express Polym. Lett.* **2010**, *4*, 39–46.

(42) Rumiko, Y.; Susumu, S. *Jpn. J. Appl. Phys.* **1991**, *30*, L616–L618.

(43) Fuh, Andy, Y.-G.; Ko, T. C.; Li, Mo, H. *Jpn. J. Appl. Phys.* **1992**, *31*, 3366–3369.

(44) Mouquinho, A. I.; Petrova, K.; Barros, M. T.; Sotomayor, J. *New Polymers Networks for PDLC Films Application*; Souza Gomes, A., Ed.; InTech, 2012.

(45) Yamaguchi, R.; Sato, S. *Liq. Cryst.* **1993**, *14*, 929–935.

(46) Buscaglia, M.; Bellini, T.; Chiccoli, C.; Mantegazza, F.; Pasini, P.; Rotunno, M.; Zannoni, C. *Am. Phys. Soc.* **2006**, *74*, 011706(1)-011706(8).

(47) Yamaguchi, R.; Sato, S. *Jpn. J. Appl. Phys.* **1992**, *31*, L254–L256.

(48) Jákli, A. *Mol. Cryst. Liq. Cryst.* **1994**, *251*, 289–301.

(49) Brás, A. R. E.; García, O.; Viciosa, M. T.; Martins, S.; Sastre, R.; Dias, C. J.; Figueirinhas, J. L.; Dionísio, M. *Liq. Cryst.* **2008**, *35*, 429–441.

(50) *Technological Applications of Dispersions (Surfactant Science)*; McKay, R. B., Ed.; Marcel Dekker, Inc.: New York, 1994.

(51) Ivashchenko, A. V. *Dichroic Dyes for Liquid Crystal Displays*; CRC Press, 1994.

(52) Lucchetti, L.; Bella, S. Di; Simoni, F. *Liq. Cryst.* **2002**, *29*, 515–519.

(53) Torgova, S.; Dorozhkina, G.; Novoseletskii, N.; Umanskii, B. *Mol. Cryst. Liq. Cryst.* **2004**, *412*, 513–517.

(54) Simoni, F.; Bella, S. D. I.; Lucchetti, L.; Cipparrone, G.; Mazzulla, A. *Mat.Res.Soc.Symp.Proc.* **1999**, *559*, 65–74.

(55) Cipparrone, G.; Mazzulla, A.; Nicoletta, F. P.; Lucchetti, L.; Simoni, F. *Mol. Cryst. Liq. Cryst.* **1998**, *320*, 249–263.

(56) Khrushudov, A. *The Essential Guide to Computer Data Storage: From Floppy to DVD*; Prentice Hall, 2001.

(57) Ivanković, A.; Dronjić, A.; Bevanda, A. M.; Talić, S. *Int. J. Sustain. Green Energy* **2017**, *6*, 39–48.

(58) Welton, T. *Proc.R.Soc.A* **2015**, *471*, 0502.

(59) Shameli, K.; Ahmad, M. Bin; Jazayeri, S. D.; Sedaghat, S.; Shabanzadeh, P.; Jahangirian, H.; Mahdavi, M.; Abdollahi, Y. *Int. J. Mol. Sci.* **2012**, *13*, 6639–6650.

(60) Zhong, X.; Dou, G.; Wang, D. *Molecules* **2013**, *18*, 13139–13147.

(61) Tiwari, A. R.; Bhanage, B. M. *Green Chem.* **2016**, *18*, 144–149.

(62) Chen, J.; Spear, S. K.; Huddleston, J. G.; Rogers, R. D. *Green Chem.* **2005**, *7*, 64–82.

(63) Anastas, P.; Eghbali, N. *Chem.Soc.Rev.* **2010**, *39*, 301–312.

(64) Murphy, D. B. *Fundamentals of Light Microscopy and Electronic Imaging*; Wiley-Liss, 2001.

(65) Parry-Hill, M.; Sutter, R. T.; Davidson, M. W. Microscopy: The Source for Microscopy Education.

(66) Mescher, A. L. *Junqueira's Basic Histology:Text & Atlas*; McGraw-Hill Education, 2013.

(67) Reimer, L. *Scanning Electron Microscopy: Physics of Image Formation and Microanalysis*; Spring, 1998.

(68) Carter, S. A.; LeGrange, J. D.; White, W.; Boo, J.; Wiltzius, P. *J. Appl. Phys.* **1997**, *81*, 5992–5999.

(69) Ohta, S.; Inasawa, S.; Yamaguchi, Y. *J. Polym. Sci. Part B Polym. Phys.* **2012**, *50*, 863–869.

(70) *Handbook of Thermal Analysis and Calorimetry:Principles and Practice*; Brown, M. E., Ed.; Elsevier, 1998.

(71) *Principles of Thermal Analysis and Calorimetry*; Haines, P. J., Ed.; The Royal Society of Chemistry, 2002.

(72) Park, J.; Lakes, R. S. *Biomaterials: An Introduction*; Springer, 2007.

(73) Holding, S. R.; Meehan, E. *Molecular Weight Characterization of Synthetic Polymers*; Rapra Technology, 1995.

(74) Gross, J. H. *Mass Spectrometry*; Springer, 2011; Vol. 40.

(75) Watson, J. T.; Sparkman, O. D. *Introduction to Mass Spectrometry: Instrumentation, Applications, and Stategies for Data Interpretation*, 4th ed.; John Wiley & Sons, Ltd, 2007.

(76) Bedjaoui, L.; Gogibus, N.; Ewen, B.; Pakula, T.; Coqueret, X.; Benmouna, M.; Maschke, U. *Polymer (Guildf).* **2004**, *45*, 6555–6560.

(77) Kuriyama, T. O. and A. *Polym. Bull.* **1984**, *142*, 135–142.

(78) Ward, J. .; Shahar, a; Peppas, N. . *Polymer (Guildf).* **2002**, *43*, 1745–1752.

(79) Kannurpatti, A. R.; Anderson, K. J.; Anseth, J. A. Y. W.; Bowman, C. N. *J. Polym. Sci. Part B Polym. Phys.* **1997**, *35*, 2297–2307.

(80) Qiu, J.; Charleux, B.; Matyjaszewski, K. *Prog. Polym. Sci.* **2001**, *26*, 2083–2134.

(81) Instec. Instec Focus On Excellence: Liquid Crystal Products www.instec.com.

(82) *Nonlinear Dynamics : Materials , Theory and Experiments*; Tlidi, M., Clerc, Marcel, G., Eds.; Springer, 2016.

(83) Brás, A.; Henriques, S.; Casimiro, T.; Aguiar Ricardo, A.; Sotomayor, J.; Caldeira, J.; Santos, C.; Dionísio, M. *Electron. Cryst. Commun.* **2005**, 1–9.

(84) Zhang, F. Z.; Xinxian, M.; Wang, H.; Ye, F. *Appl. Phys. A Mater. Sci. Process.* **2018**, *124*, 1–6.

(85) Mori, S.; Barth, H. G. *Size Exclusion Chromatography*; Springer, 1999.

(86) Crich, D.; Brebion, F.; Suk, D.-H. *Radicals in Synthesis I:Methods and Mechanisms*; Gansauer, A., Ed.; Springer, 2006; Vol. 263.

(87) Takacs, E.; Wojnarovits, L. *Radiat.Phys.Chem* **1995**, *46*, 1007–1010.

(88) Jansen, Johan, F. G. A.; Dias, Aylvin, A.; Dorschu, M.; Coussens, B. *Macromolecules* **2003**, *36*, 3861–3873.

(89) Ottani, S.; Vitalini, D.; Comelli, F.; Castellari, C. *J. Chem. Eng. Data* **2002**, *47*, 1197–1204.

(90) Zacchigna, M.; Cateni, F.; Drioli, S.; Bonora, G. M. *Polymers (Basel).* **2011**, *3*, 1076–1090.

(91) *Poly(Ethylene Glycol):Chemistry and Biological Applications*; Harris, J. M., Zalipsky, S., Eds.; American Chemical Society, 1997.

(92) Nuttelman, C. R.; Tripodi, M. C.; Anseth, K. S. *J. Biomed. Mater. Res. A* **2004**, *68*, 773–782.

(93) Lin-Gibson, S.; Bencherif, S.; Antonucci, J. M.; Jones, R. L.; Horkay, F. *Macromol. Symp.* **2005**, *227*, 243–254.

(94) Imani, M.; Sharifi, S.; Mirzadeh, H.; Ziaee, F. *Iran. Polym. J.* **2007**, *16*, 13–20.

(95) Priola, A.; Gozzelino, G.; Ferrero, F.; Malucelli, G. *Polymer (Guildf).* **1993**, *34*, 3653–3657.

(96) Li, H.; Fu, Y.; Niu, R.; Zhou, Z.; Nie, J.; Yang, D. *J. Appl. Polym. Sci.* **2013**, *127*, 1737–1743.

(97) Lin-Gibson, S.; Bencherif, S.; Cooper, J. a; Wetzel, S. J.; Antonucci, J. M.; Vogel, B. M.; Horkay, F.; Washburn, N. R. *Biomacromolecules* **2004**, *5*, 1280–1287.

(98) Qiao, C.; Jiang, S.; Dong, D.; Ji, X.; An, L.; Jiang, B. *Macromol. Rapid Commun.* **2004**, *25*, 659–663.

(99) Bryant, S. J.; Chowdhury, T. T.; Lee, D. A.; Bader, D. L.; Anseth, K. S. *Ann. Biomed. Eng.* **2004**, *32*, 407–417.

(100) *Comprehensive Analytical Chemistry Molecular Characterization and Analysis of Polymers*; Chalmers, J. M., Meier, Robert, J., Eds.; Elsevier, 2008.

(101) Han, J.-W. *J. Korean Soc.* **2002**, *40*, 849–855.

(102) Bouriche, A.; Alachaher, L. B.; Maschke, U. *Liq. Cryst.* **2018**, *45*, 656–665.

(103) Anseth, K. S.; Bowman, C. N.; Peppas, N. A. *Polym. Bull.* **1993**, *31*, 229–233.

(104) Oh, B.; Jung, W. Il; Kim, D.; Rhee, H. W. *Bull. Korean Chem. Soc.* **2002**, *23*, 683–687.

(105) Loiko, V. A.; Zyryanov, V. Y.; Konkolovich, A. V.; Miskevich, A. A. *Opt. Spectrosc.* **2016**, *120*, 143–152.

(106) Shao, L.; Zhang, Y.; Liu, C.; Li, J.; Qin, A.; Wang, Y. *Liq. Cryst.* **2012**, *39*, 1458–1464.

(107) Koenig, J. L.; Wang, S.; West, J. L. *Appl. Spectrosc.* **1993**, *47*, 942–951.

(108) Mirau, P. A.; Srinivasarao, M. *Soc. Appl. Spectrosc.* **1997**, *51*, 1639–1643.

(109) Ahn, W.; KiRyong, H. *Korea Polym. J.* **1999**, *7*, 130–135.

(110) Serbutoviez, C.; Kloosterboer, J. G.; Boots, H. M. J.; Touwslager, F. J. *Macromolecules* **1996**, *29*, 7690–7698.

(111) Li, W.; Cao, Y.; Cao, H.; Kashima, M.; Kong, L.; Yang, H. *J. Polym. Sci. Part B Polym. Phys.* **2008**, *46*, 1369–1375.

(112) Shao, L.; Li, J.; Zhang, Y.; Gong, S.; Wang, Y. *Liq. Cryst.* **2017**, *41*, 652–661.

(113) Yang, K.; Kim, K. P.; Kim, D. H.; Choi, B. D. *Mol. Cryst. Liq. Cryst.* **2009**, *498*, 83–88.

(114) Osipov, M. . *Liquid Crystalline and Mesomorphic Polymers*; Shibaev, V. P., Lam, L., Eds.; Springer-Verlag, 1994.

(115) Araki, T.; Buscaglia, M.; Bellini, T.; Tanaka, H. *Nat. Mater.* **2011**, *10*, 303–309.

(116) Thakur, V.; Kessler R., M. *Liquid Crystalline Polymers*; Springer Cham Heidelberg, 2015.

(117) Strobl, G. *The Physics of Polymers*; Springer, 2007.

(118) Ward, I. M.; Sweeney, J. *An Introduction to the Mechanical Properties of Solid Polymers*; John Wiley & Sons, Ltd., 2004.

(119) Pielichowski, K.; Flejtuch, K. *Polym. Adv. Technol.* **2002**, *13*, 690–696.

(120) Godovsky, Y. K.; Slonimsky, G. L.; Garbar, N. M. *J. Poymer Sci. C* **1972**, *21*, 1–21.

(121) Gao, W.; Bai, Y.; Chen, E.; Zhou, Q. *Chinese J. Polym. Sci.* **2005**, *23*, 275–285.

(122) Nishi, M.; Hikosaka, M.; Ghosh, S. K.; Toda, A.; Yamada, K. *Polym. J.* **1999**, *31*, 749–758.

(123) Muthukumar, M. *Nucleation In Polymer Crystallization*; John Wiley & Sons, Inc., 2004; Vol. 128.

(124) Bower, D. I. *An Introduction to Polymer Physics*; Cambridge University Press, 2002.

(125) Li, Y.; Ma, Q.; Huang, C.; Liu, G. *Mater. Sci.* **2013**, *19*.

(126) Cheng, S. Z. D. *Phase Transitions In Polymers*; Elsevier, 2008.

(127) Clayden, J.; Greeves, N.; Warren, S. *Organic Chemistry*; Oxford University Press Inc., 2012.

(128) Salaklang, J.; Maes, V.; Conradi, M.; Dams, R.; Junkers, T. *React. Chem. Eng.* **2018**, *3*, 41–47.

(129) Zhang, B.; Zhang, H.; Myers, B. K.; Elupula, R.; Jayawickramarajah, J.; Grayson, S. M. *Anal. Chim. Acta* **2014**, *816*, 28–40.

(130) Yu, D.; Vladimirov, N.; Fréchet, J. M. J. *Macromolecules* **1999**, *32*, 5186–5192.

(131) Casey, B. K.; Lapucha, J. E.; Grayson, S. M.; Myers, B. K.; Lapucha, J. E.; Grayson, S. M. *Brazilian J. Pharm. Sci.* **2012**, *49*, 45–55.

(132) Ginos, J. M.; Arias, M. J.; Rabasco, A. M.; Novák, C. *J. Therm. Anal.* **1996**, *46*, 291–304.

(133) Craig, D. Q. M.; Newton, J. M. *Int. J. Pharm.* **1991**, 33–41.

(134) Santos, R.; Silva, M. C.; Mouquinho, A.; Sotomayor, J. *Mol. Cryst. Liq. Cryst.* **2015**, *611*, 123–131.

(135) Mouquinho, A.; Luís, N.; Sotomayor, J. *J. Appl. Polym. Sci.* **2016**, *133*, 1–7.

(136) Strong, B. A. *Fundamentals of Composites Manufacturing: Materials, Methods and Applications*; Society of Manufacturing Engineers, 2008.

(137) *Radiation Curing: Science and Technology*; Pappas, P. S., Ed.; Spring Science + Business Media, LLC: New Jersey, 1992.

(138) Figuly, G. D.; Richardson, L. B. *Method For Embolization Using Liquid Embolic Materials*; United States patent 2009/0054535, 2009.

(139) Yau, H. C.; Bayazit, M. K.; Gaffney, P. R. J.; Livingston, A. G.; Steinke, J. H. G.; Shaffer, M. S. P.

Polym. Chem. **2015**, *6*, 1056–1065.

(140) Glockner, P.; Jung, T.; Struck, S.; Studer, K. *Radiation Curing: Coating and Printing Inks*; Vincentz Network, 2008.

(141) Mouquinho, A.; Saavedra, M.; Maiau, A.; Petrova, K.; Barros, M. T.; Figueirinhas, J. L.; Sotomayor, J. *Mol. Cryst. Liq. Cryst.* **2011**, *542*, 132/[654]-140/[662].

(142) Lee, W. K.; Hwang, S. J.; Cho, M. J.; Park, H. G.; Han, J. W.; Song, S.; Jang, J. H.; Seo, D. S. *Nanoscale* **2013**, *5*, 193–199.

(143) No, Y.; Jeon, C. *Mol. Cryst. Liq. Cryst.* **2009**, *513*, 98–105.

(144) Marinov, Y. G.; Hadjichristov, G. B.; Petrov, A. G.; Marino, S.; Versace, C.; Scaramuzza, N. *J. Appl. Phys.* **2013**, *113*, 064301-1/064301-10.

(145) Rajaram, C. V; Hudson, S. D. *Am. Chem. Soc.* **1995**, *7*, 2300–2308.

(146) Parshin, A. M.; Zyryanov, V. Y.; Shabanov, V. F. *Sci. Rep.* **2017**, *7*, 1–8.

(147) Kato, K.; Tanaka, K.; Tsuru, S.; Sakai, S. *Jpn. J. Appl. Phys.* **1994**, *33*, 2635–2640.

(148) Mendes, L. A. V; Pinho, R. R.; Ácila, L. F.; Lima, C. R. A.; Rocco, M. L. M. *Polym. Degrad. Stab.* **2007**, *92*, 933–938.

(149) Turban, G.; Rapeaux, M. *J.Electrochem.Soc.Solid-state Sci. Technol.* **1983**, *120*, 2231–2236.

(150) Koretsky, M. D.; Reimer, J. A. *Am. Inst. Phys.* **1992**, *72*, 5081–5088.

(151) Toshiaki, N.; Masuda, S.; Sato, S. *Jpn. J. Appl. Phys.* **1991**, *30*, 3450–3455.

(152) Holman, J. P. *Heat Transfer*; Holman, J., Lioyd, J., Eds.; McGraw-Hill, 2010.

(153) Brindley, K. *Electronics Engineer ' s Pocket Book Newnes*; Newnes-Butterworth-Hein, 1993.

(154) Ageorges, C.; Ye, L. *Fusion Bonding of Polymer Composites: From Basic Mechanisms to Process Optimisation- (Engineering Materials and Processes)*; Derby, B., Ed.; Springer-Verlag, 2002.

12 Appendix

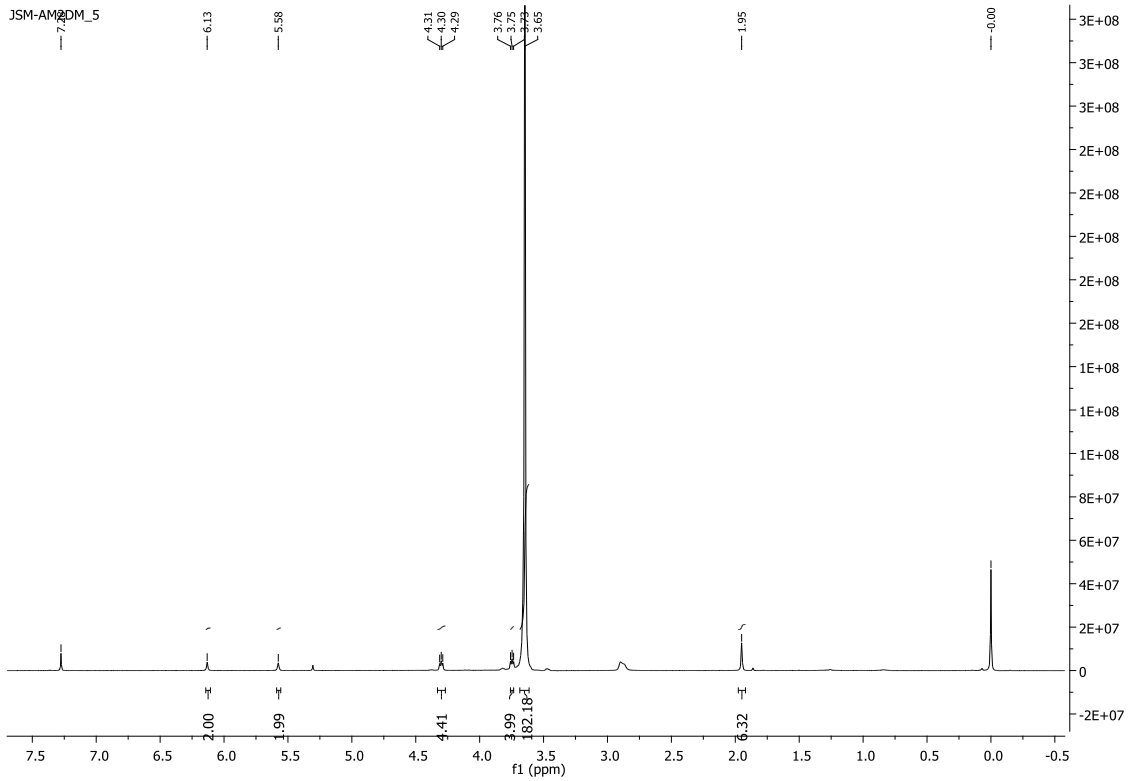

Figure 12.1 – ^{1}H-NMR spectrum of PEG2000DM.

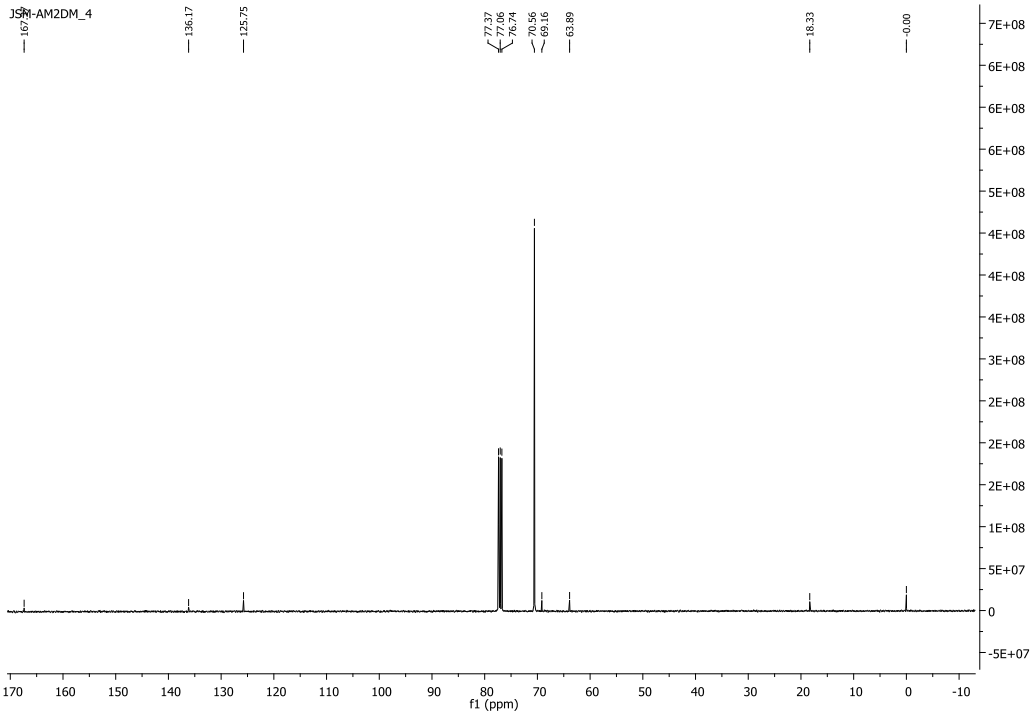

Figure 12.2 – ^{13}C-NMR spectrum of PEG2000DM.

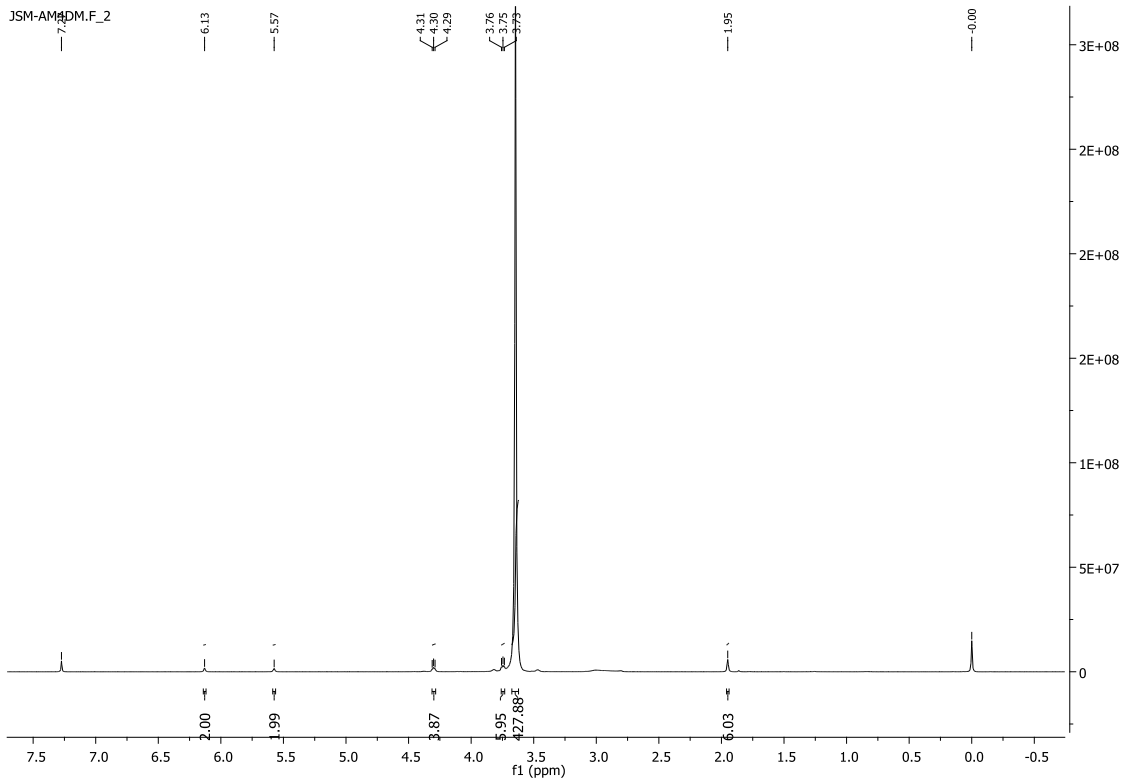

Figure 12.3 – ^{1}H-NMR spectrum of PEG4000DM.

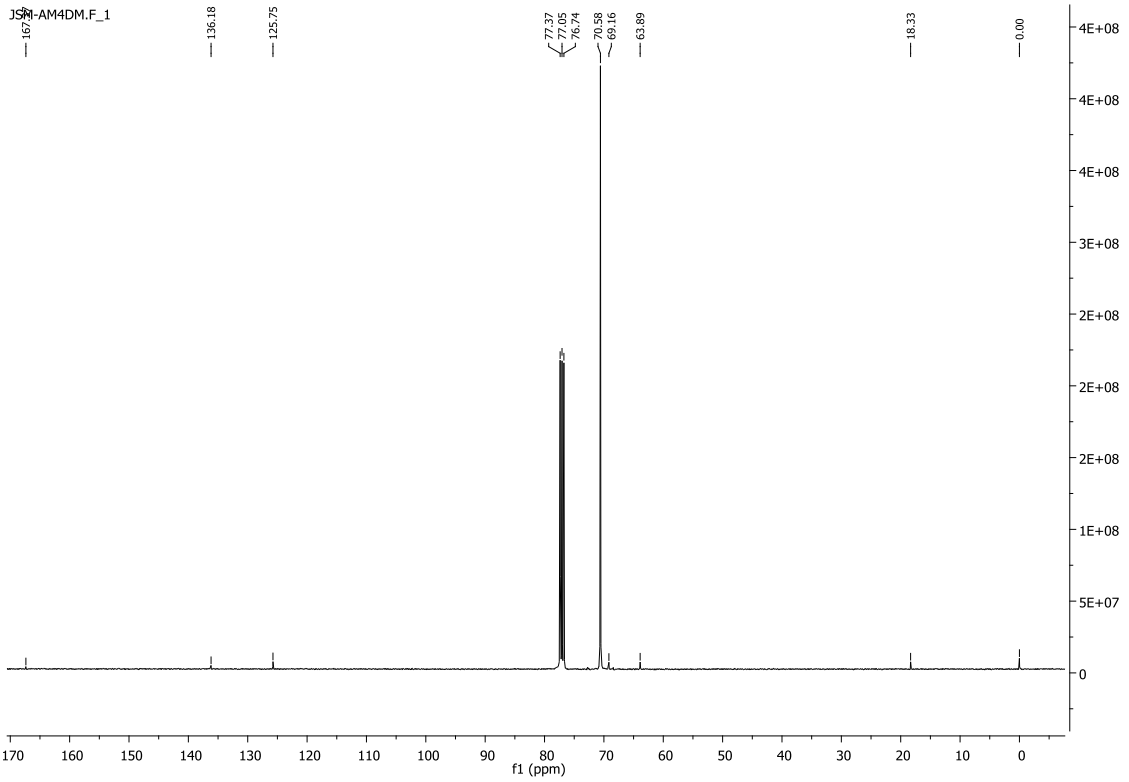

Figure 12.4 – ^{13}C-NMR spectrum of PEG4000DM.

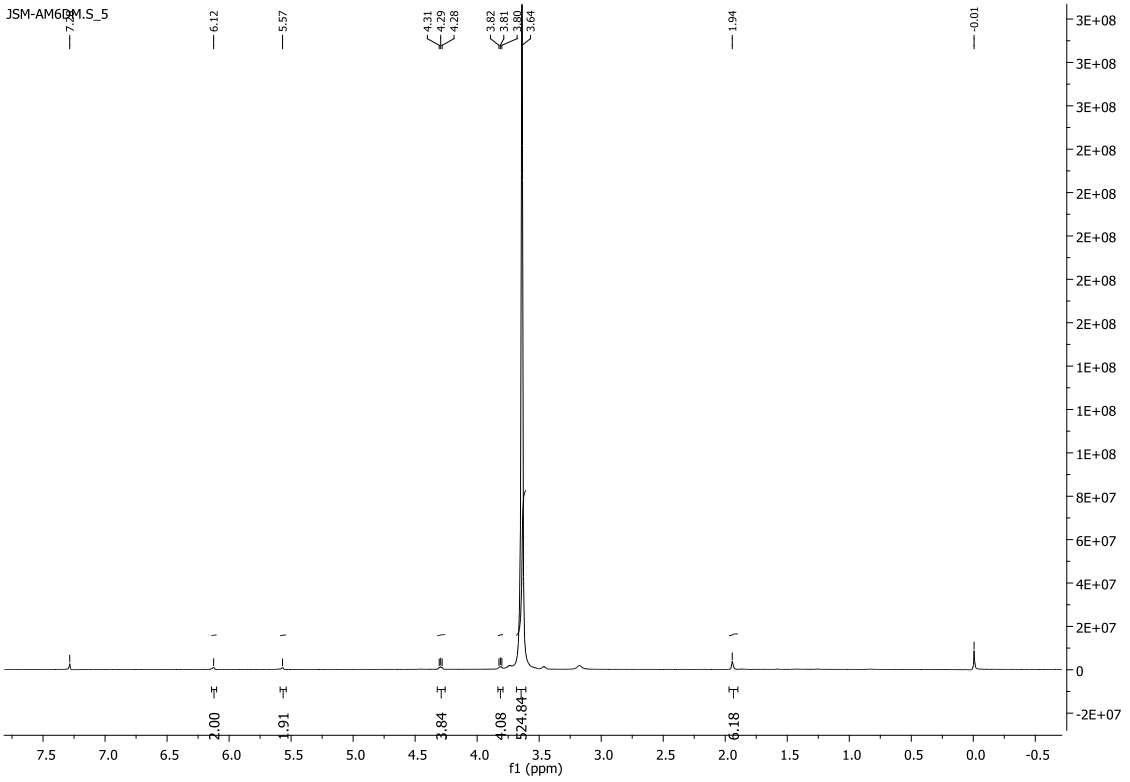

Figure 12.5 – ^{1}H-NMR spectrum of PEG6000DM.

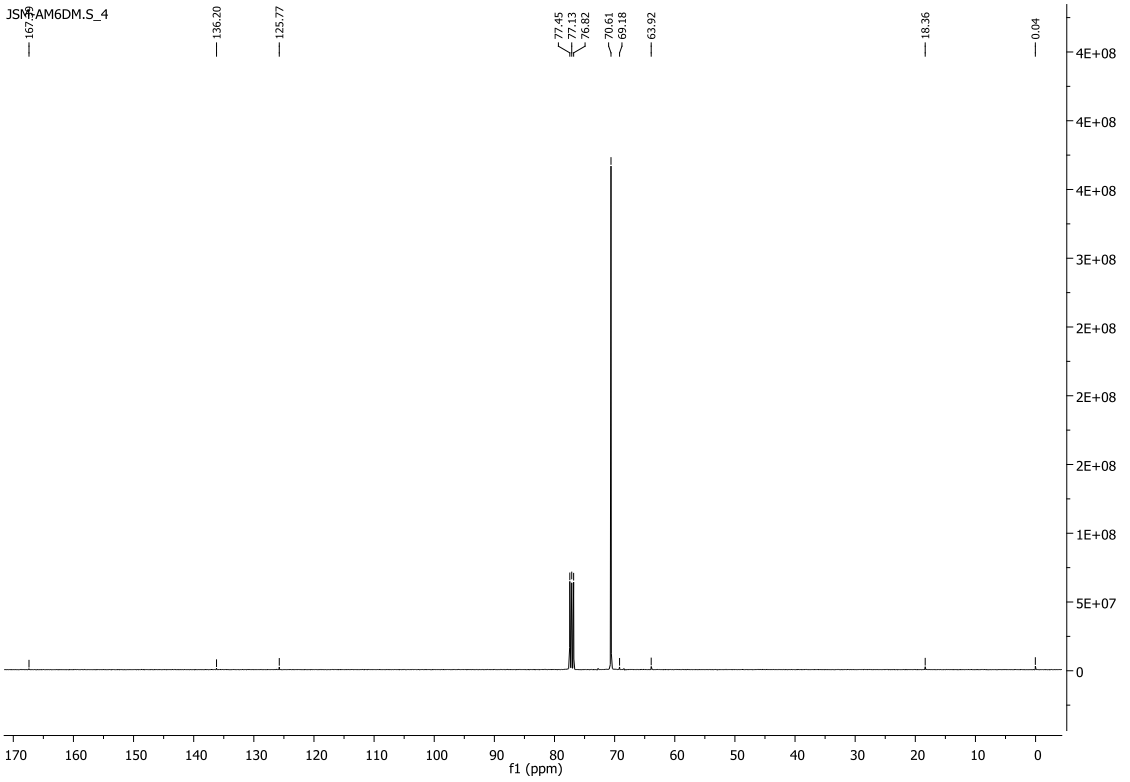

Figure 12.6 – ^{13}C-NMR spectrum ofPEG6000DM.

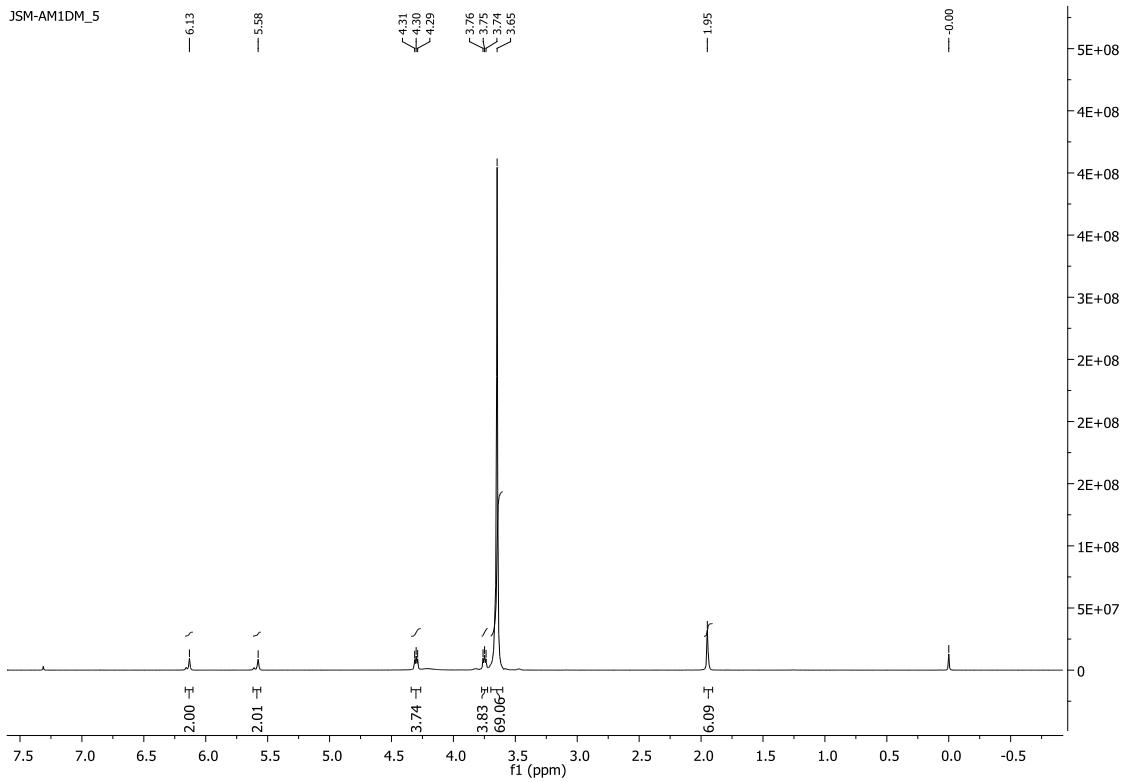

Figure 12.7 – ^{1}H-NMR spectrum of PEG1000DM.

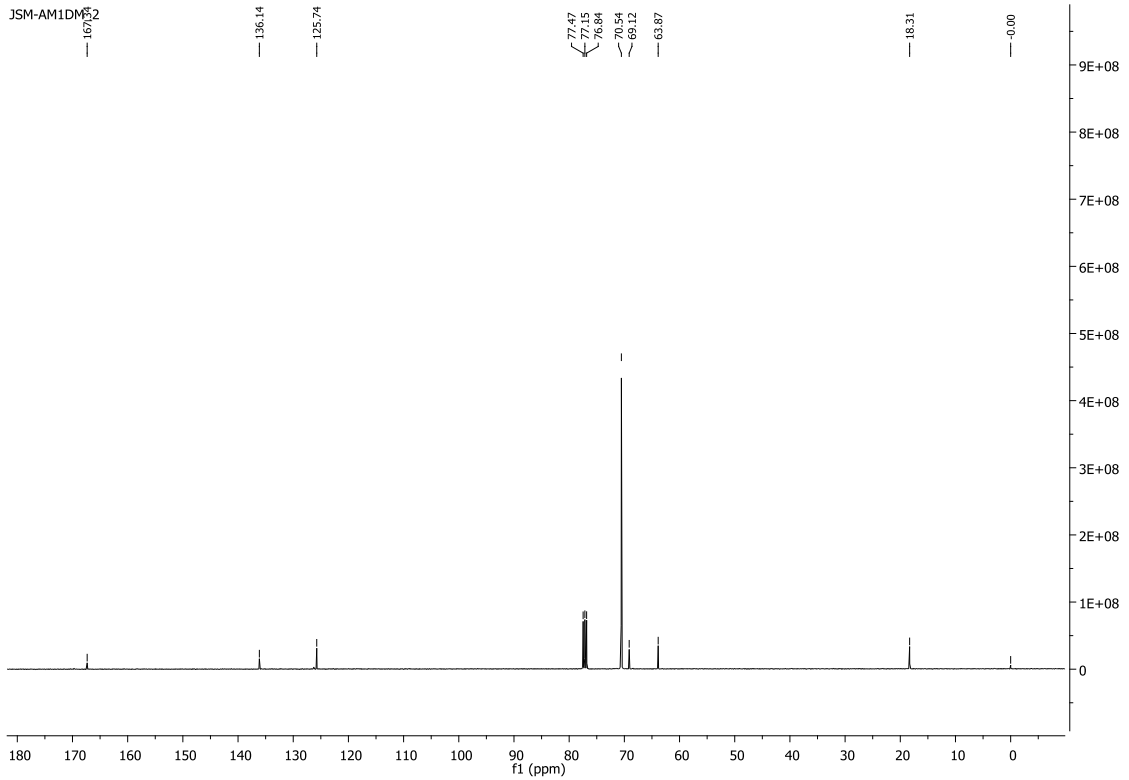

Figure 12.8 – ^{13}C-NMR spectrum of PEG1000DM.

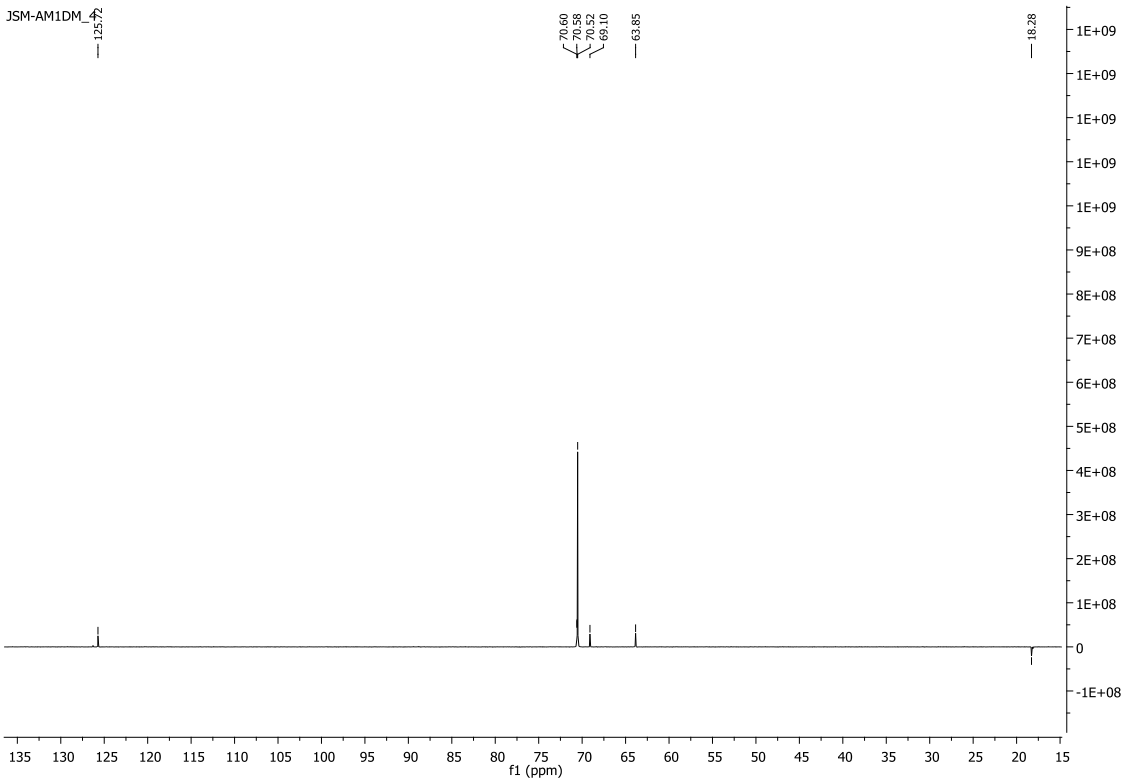

Figure 12.9 – ^{13}C DEPT spectrum of PEG1000DM.

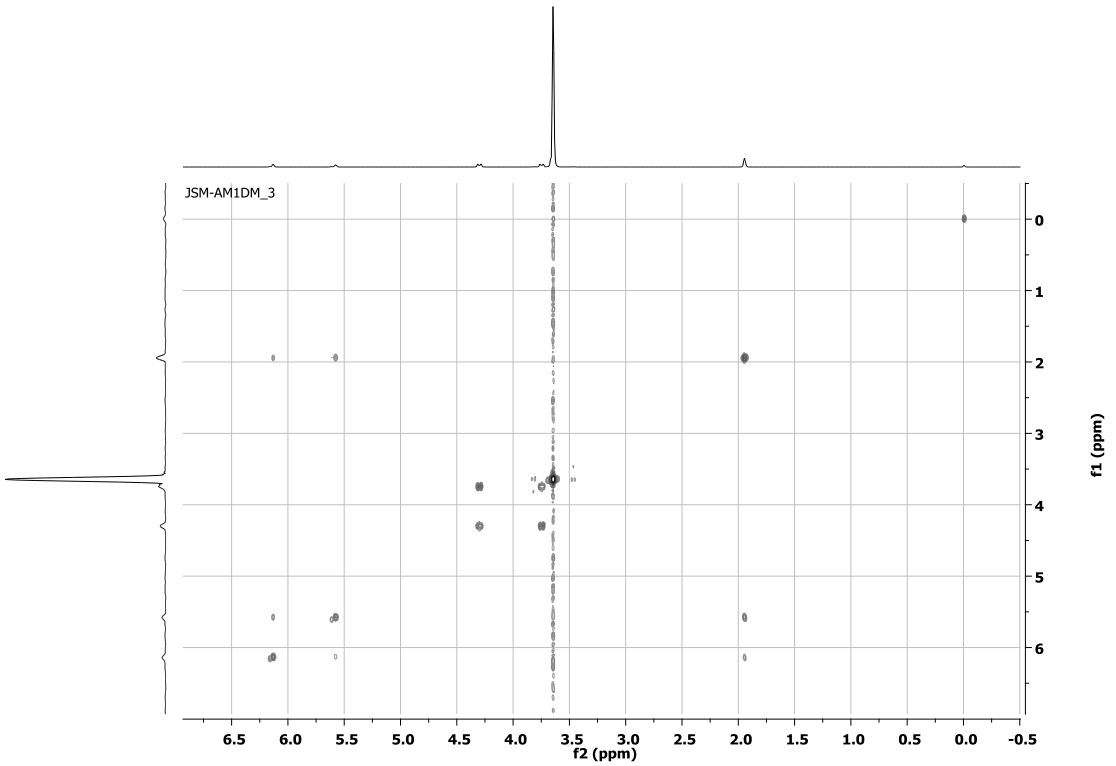

Figure 12.10 – COSY spectrum of PEG1000DM.

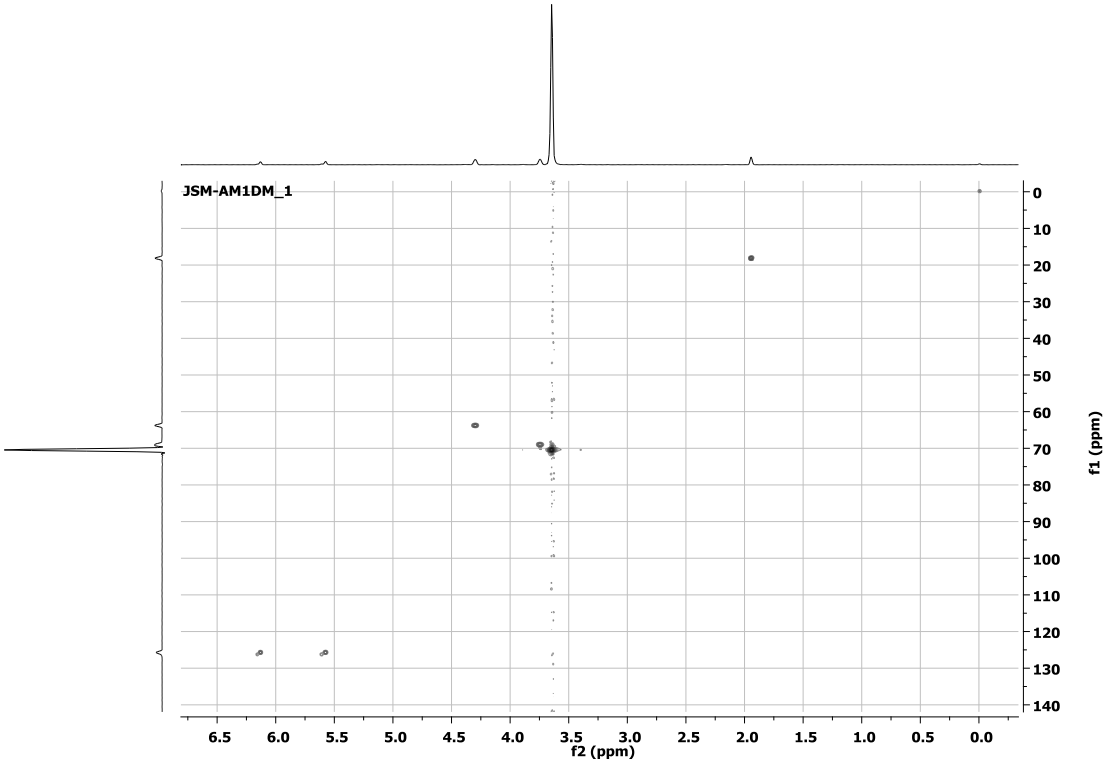

Figure 12.11 – HSQC spectrum of PEG1000DM.

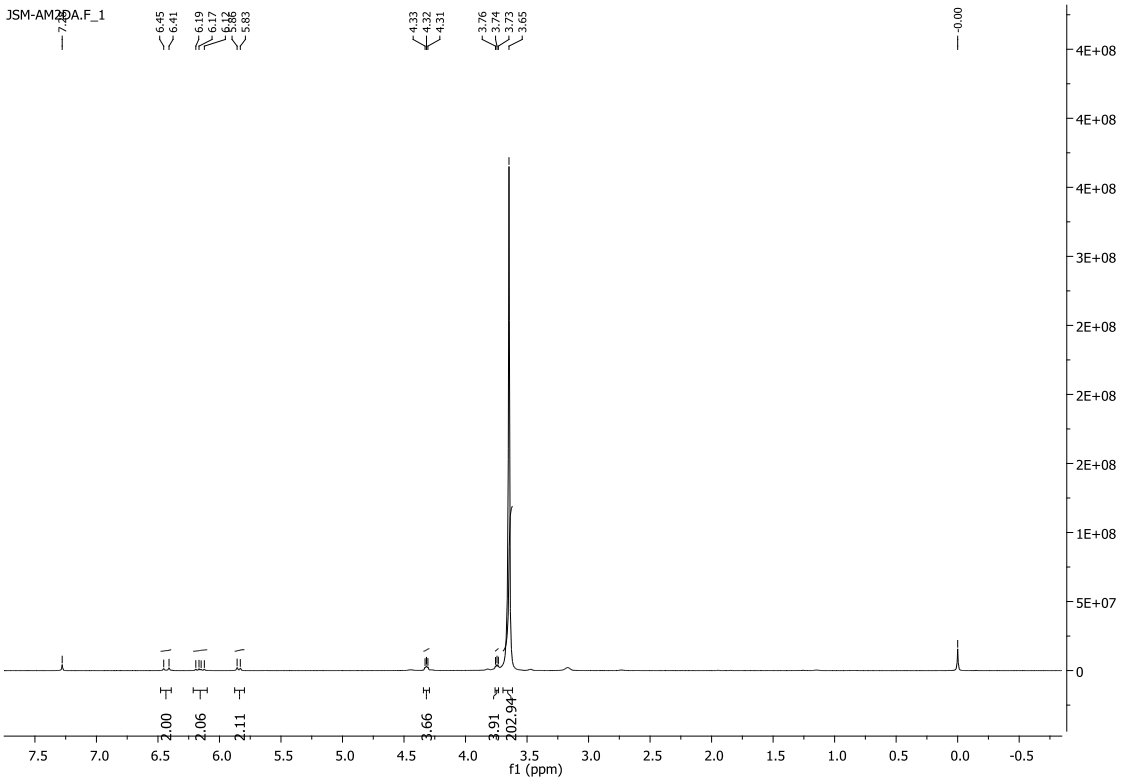

Figure 12.12 – ^{1}H-NMR spectrum of PEG2000DA.

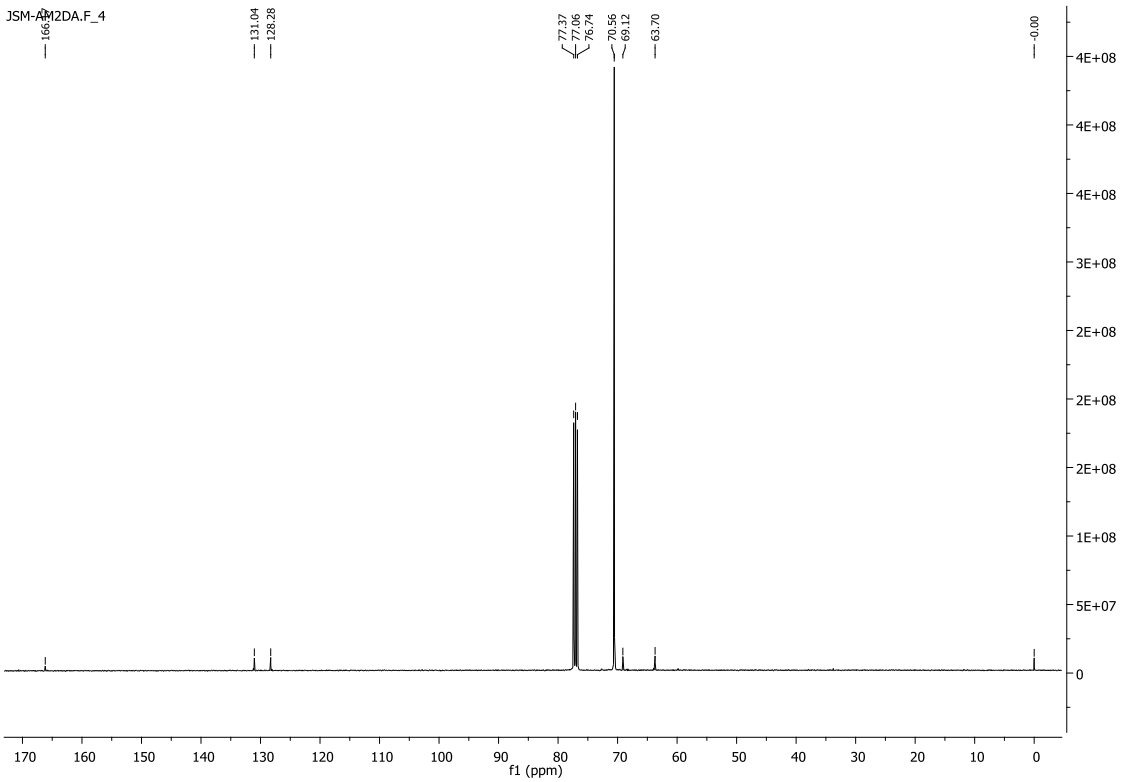

Figure 12.13 – ^{13}C-NMR spectrum of PEG2000DA.

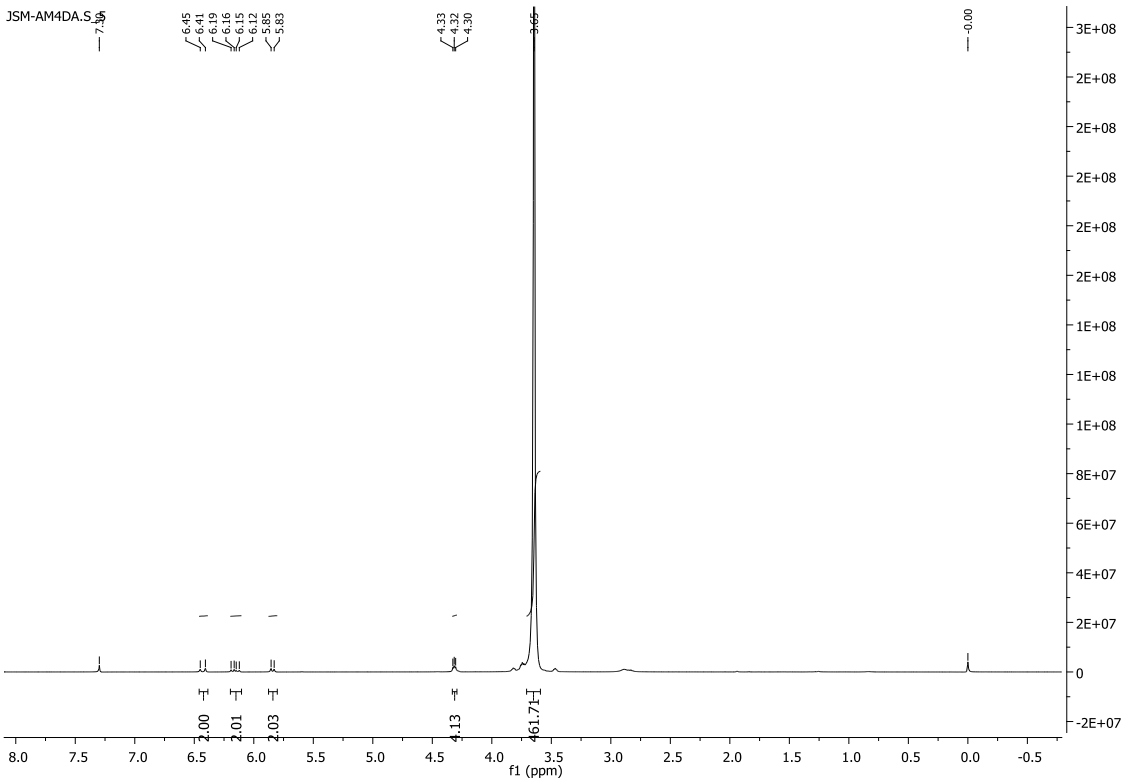

Figure 12.14 – ^{1}H-NMR spectrum of PEG4000DA.

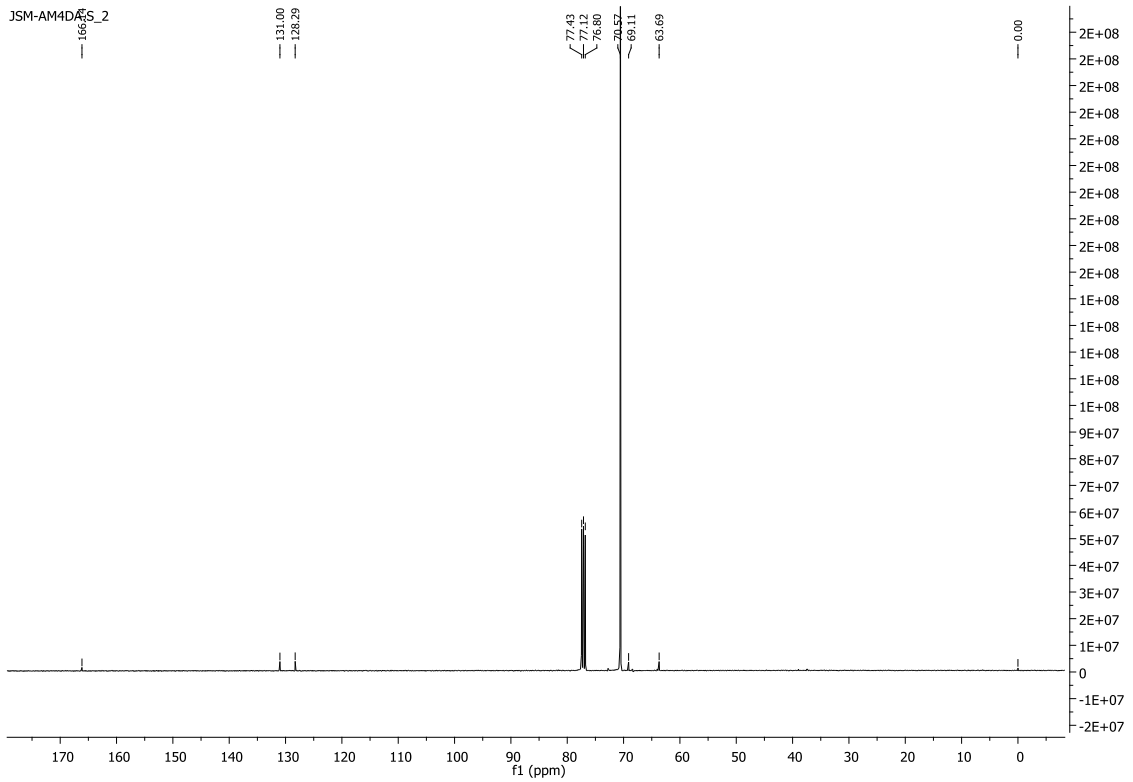

Figure 12.15 – ^{13}C-NMR spectrum of PEG4000DA.

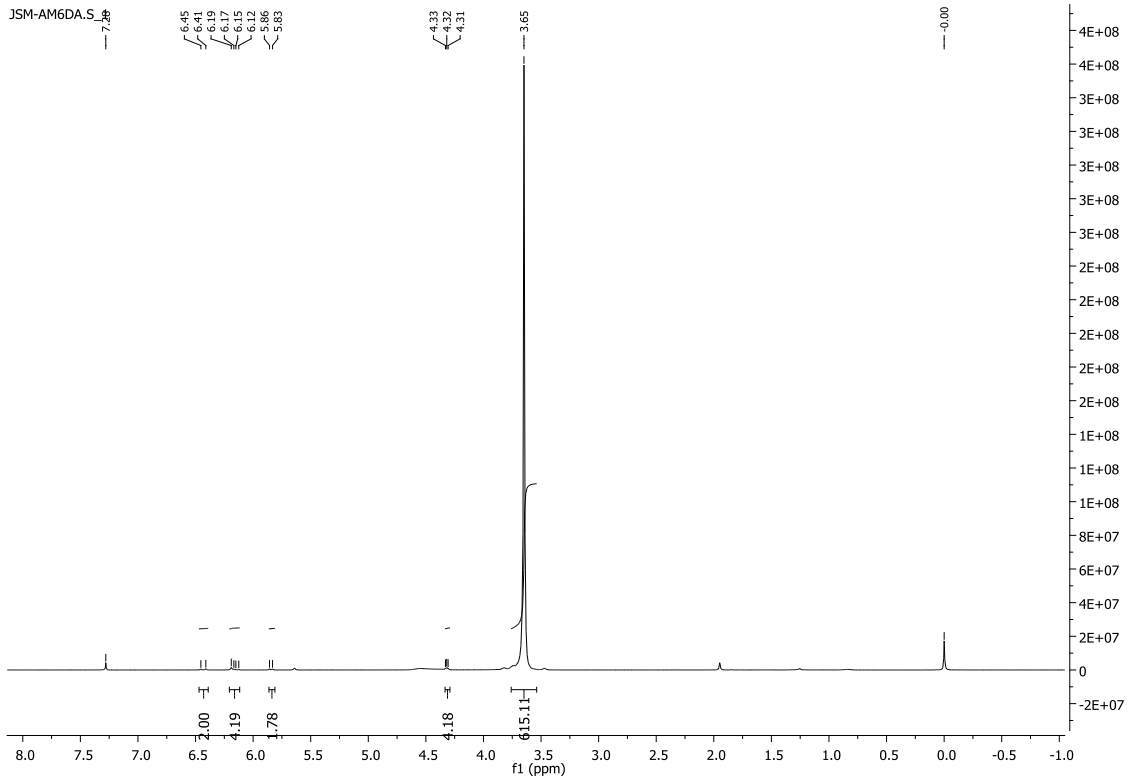

Figure 12.16 – ^{1}H-NMR spectrum of PEG6000DA.

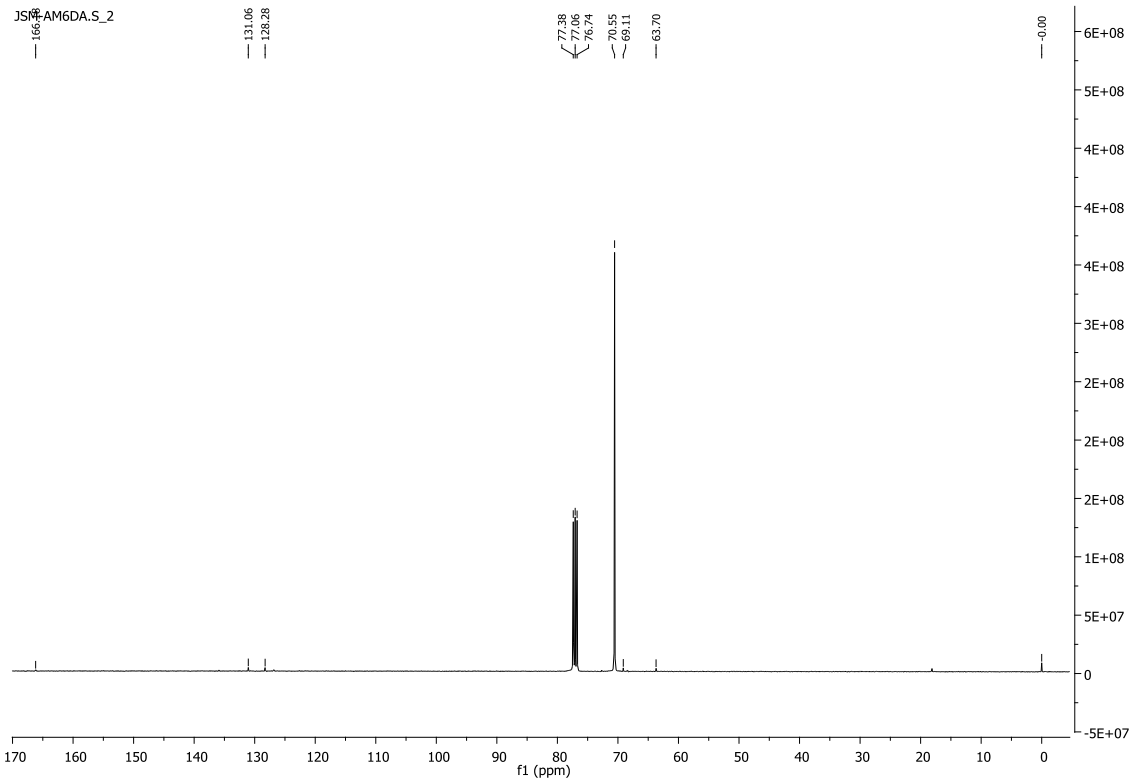

Figure 12.17 – ^{13}C-NMR spectrum of PEG6000DA.

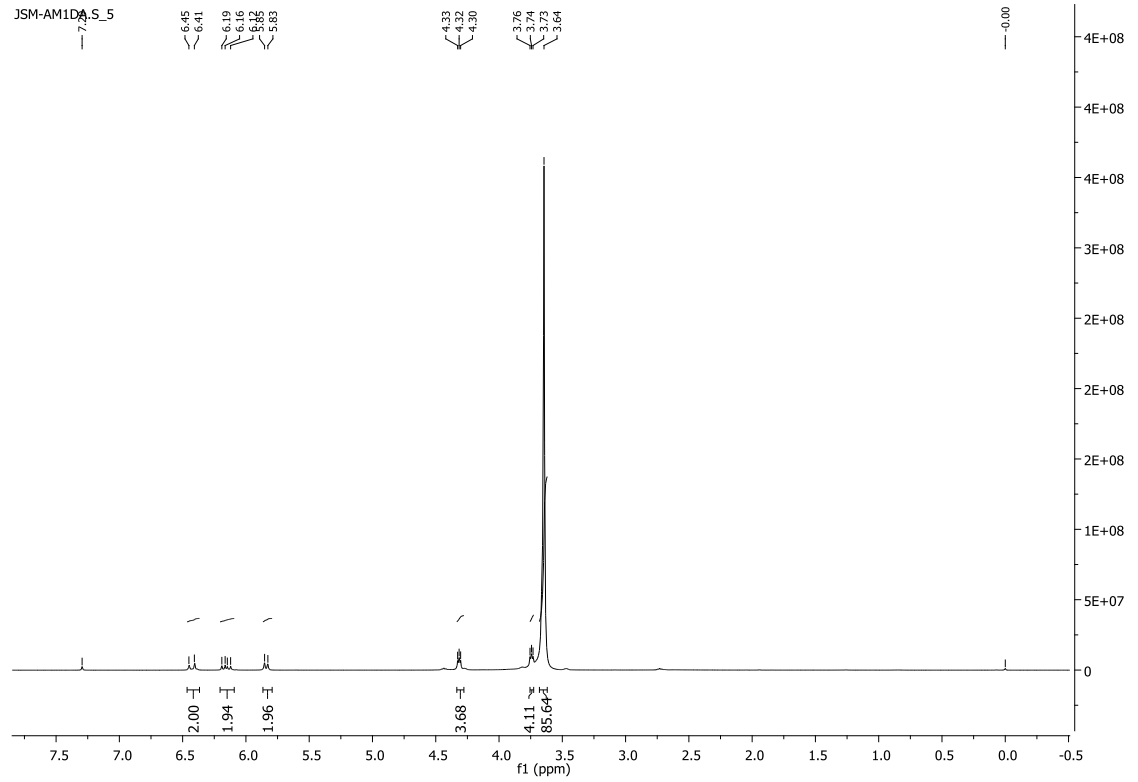

Figure 12.18 – ^{1}H-NMR spectrum of PEG1000DA.

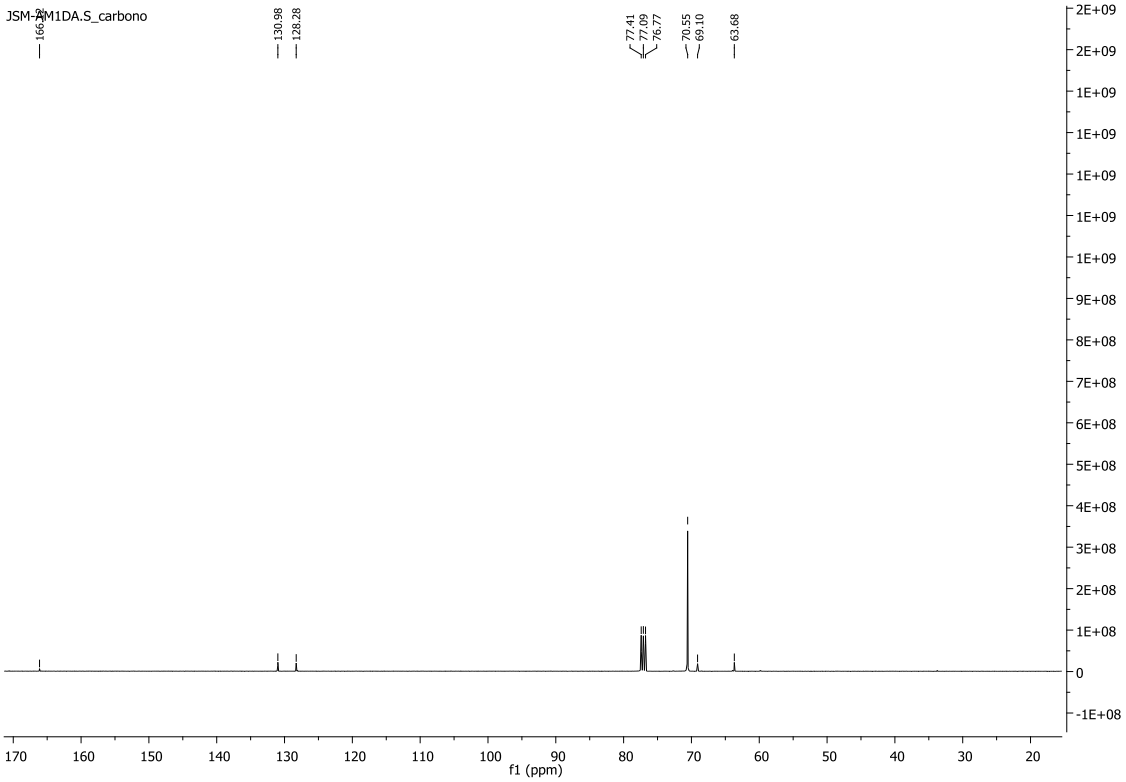

Figure 12.19 – ^{13}C-NMR spectrum of PEG1000DA.

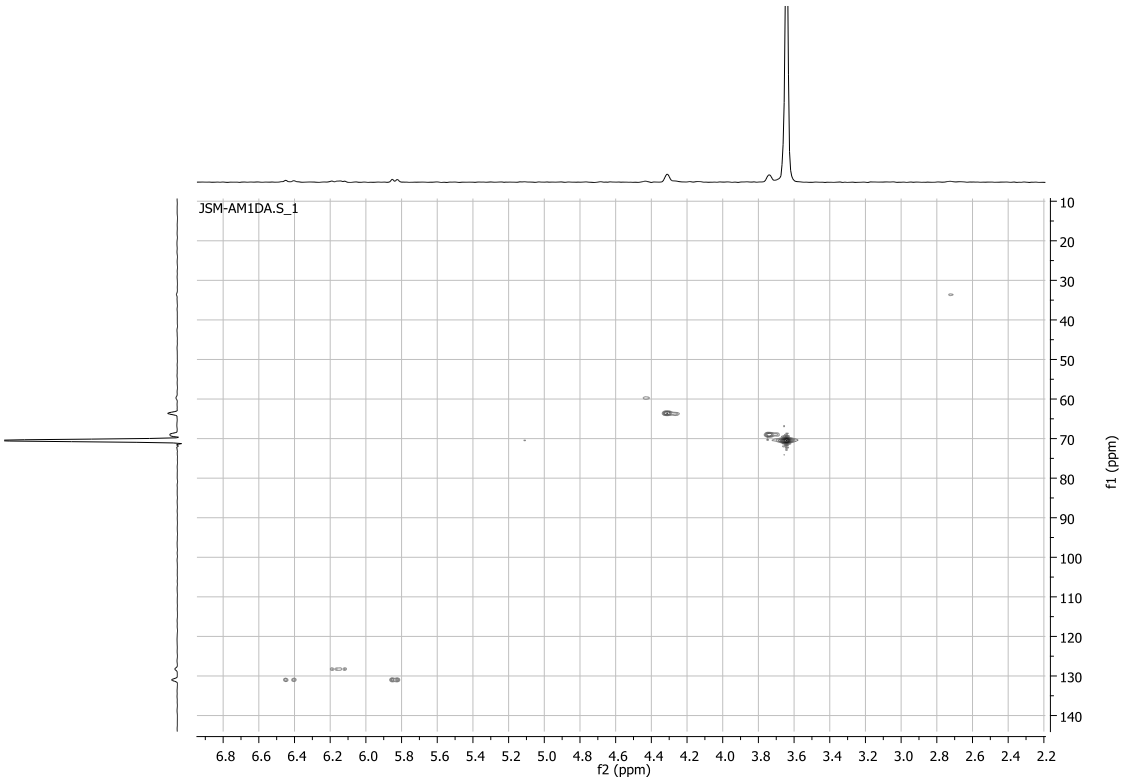

Figure 12.20 – HSQC spectrum of PEG1000DA.

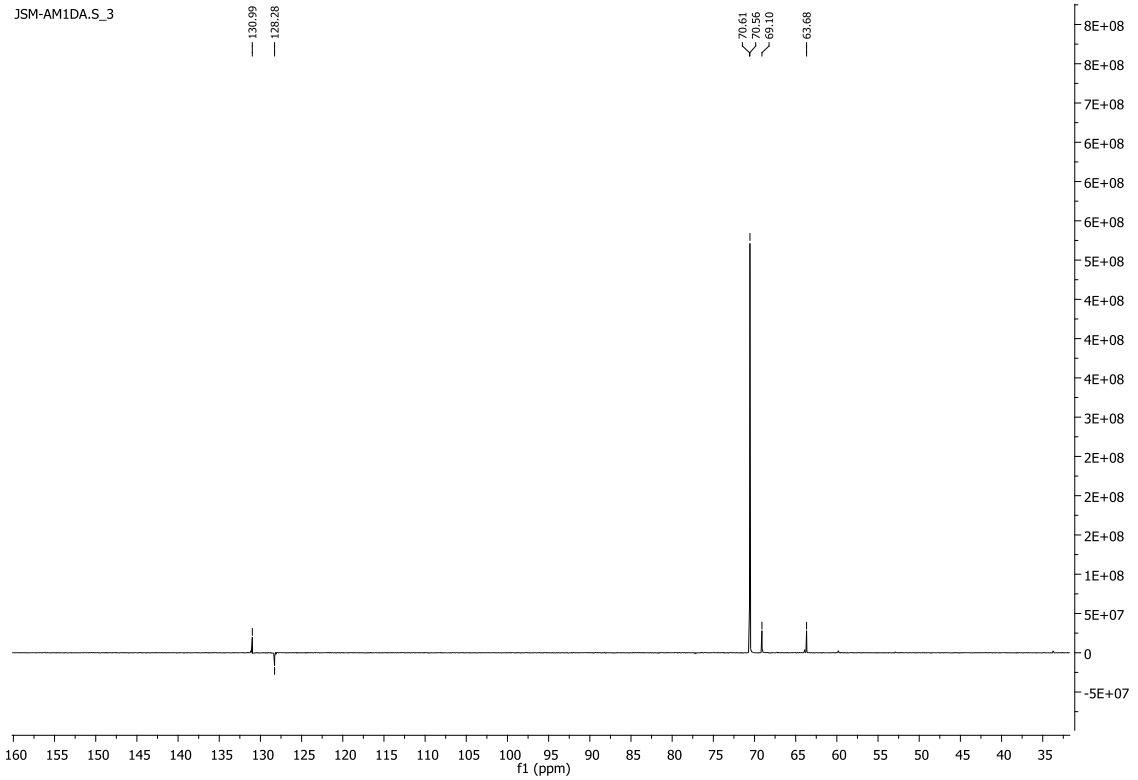

Figure 12.21 – ^{13}C DEPT NMR spectrum of PEG1000DA.

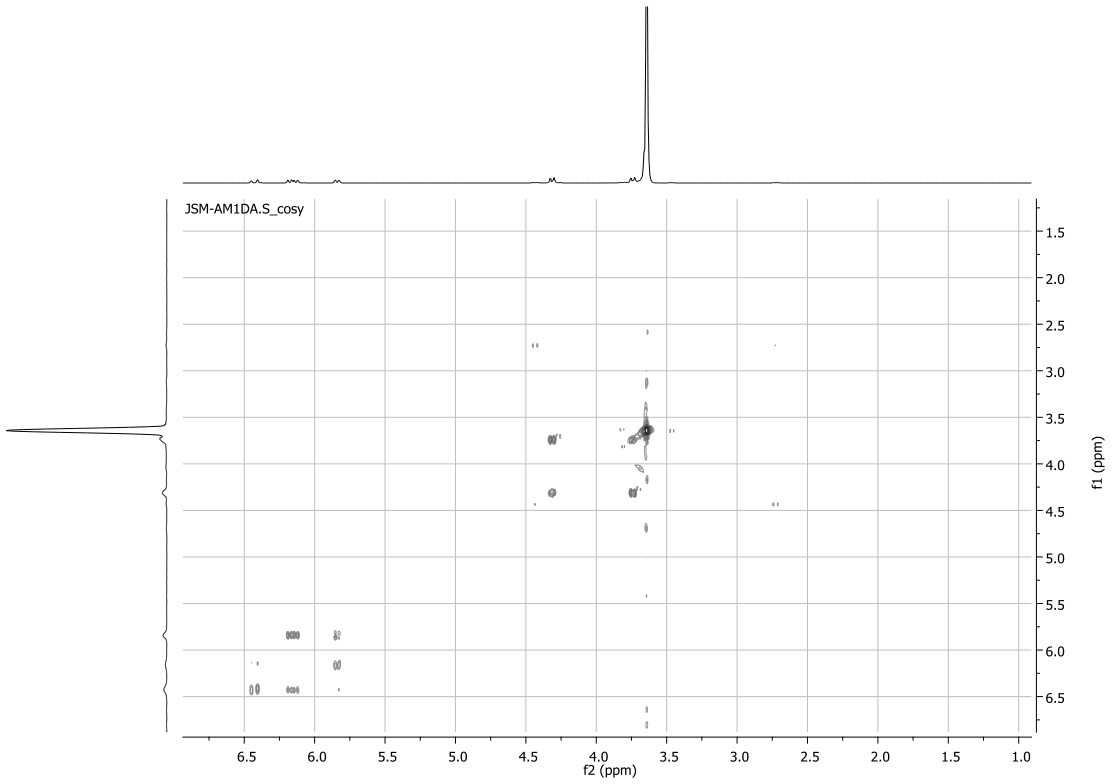

Figure 12.22 – COSY spectrum of PEG1000DA.

Table 12.1 – Thermal properties of PEG macromolecules obtained by DSC during two cooling/heating cycles. T_g: glass transition temperature; Tm: melting temperature; Tc: crystallization temperature, ΔHm and ΔHc: melting and crystallization enthalpies, respectively.

		Cooling Scan			Heating Scan		
Sample		**glass transition**	**melt-crystallization**		**glass transition**	**melting**	
	scan	**T_g /°C**	**Tc/°C**	**ΔHcr/J g-1**	**T_g / °C**	**Tm/°C**	**ΔHm/J g^{-1}**
PEG1000	**I**	-	28.61	152.8		**37.37**	**153.8**
	II	-	27.73	154.6		**31.59/38.55**	**160.5**
	III					**38.50**	**161.3**
PEG1000DA oligomer	**I**	-	-	-		**36.66**	**127.1**
PEG1000DA Polymer	**I**	-50.68	-	-	**-48.41**	-	-
	II	-51.56	-	-	**-48.50**	-	-
PEG1000DM oligomer	**I**	-	-	-	-	**23.52**	**101.8**
PEG1000DM Polymer	**I**	-51.00	-	-	**-45.71**	-	-
	II	-51.09	-	-	**-44.89**	-	-
PEG2000	**I**	-	32.79	163.5	-	**53.96**	**174.8**
	II	-	35.52	163.8	-	**53.67**	**166.6**
	III	-	-	-	-	**53.65**	**166.6**
PEG2000DA oligomer	**I**	-	-	-	-	**52.25**	**141.8**
PEG2000DA Polymer	**I**	-	24.65	70.24	-	**41.64**	**69.28**
	II		24.88	75.05	-	**42.25**	**70.52**
PEG2000DM oligomer	**I**	-	-	-	-	**55.38**	**140.9**
PEG2000DM Polymer	**I**	-	24.65	70.24		**41.64**	**69.28**
	II	-	24.88	75.05		**42.25**	**70.52**
PEG4000	**I**	-	41.58	180.8		**62.27**	**199.4**
	II	-	41.95	181.5		**61.36**	**186.0**
	III	-	-	-		**61.36**	**186.7**
PEG4000DA oligomer	**I**	-	-	-	-	**57.91**	**176.2**
PEG4000DA Polymer	**I**	-	24.92	72.32	-	**41.43**	**72.05**
	II	-	25.24	73.21	-	**41.59**	**73.69**
PEG4000DM oligomer	**I**	-	-	-	-	**50.36**	**134.8**
PEG4000DM Polymer	**I**	-	16.78	55.61	-	**35.42**	**52.93**
	II	-	18.56	58.85	-	**35.42**	**52.93**
PEG6000	**I**	-	38.90	164.4	-	**62.91**	**171.5**
	II	-	38.46	163.2	-	**62.80**	**168.85**
	III	-	-	-	-	**62.87**	**167.9**
PEG6000DA oligomer	**I**	-	-	-	-	**59.01**	**76.31**
PEG6000DA Polymer	**I**	-	31.06	74.87	-	**42.63**	**76.31**
	II	-	31.53	76.67	-	**42.97**	**77.14**
PEG6000DM oligomer	**I**	-	-	-	-	**54.88**	**149.5**
PEG6000DM Polymer	**I**	-	38.81	80.14	-	**48.34**	**77.85**
	II		34.83	86.52	-	**49.14**	**77.79**

Table 12.2 – Thermal properties of multi-functional PEG obtained by DSC during two cooling/heating cycles. Tg: glass transition temperature; Tm: melting temperature; Tc: crystallization temperature; TCC: cold-crystallization temperature; ΔHm and ΔHc: melting and crystallization enthalpies, respectively.

			Cooling Scan			Heating Scan				
			glass transition	melt-crystallization		glass transition	cold-crystallization		melting	
Sample	Rate °C min^{-1}	Cycle	Tg / °C	Tc/°C	ΔHcr/ J g-1	Tg / °C	Tcc/°C	ΔHcr/ J g^{-1}	Tm/°C	ΔHm/ J g^{-1}
3-arm PEG	5	I	-	-40.83	53.44	-55.93	-	-	-6.36	71.45
	5	II	-	-40.25	54.90	-55.98	-	-	-6.22	74.90
3-arm PEG TriM	5	I	x	x	x	-64.25	-41.88	28.00	-23.84	31.78
	5	II	x	x	x	x	x	x	x	x
3-arm PEG TriM polymer	5	I	-36.40	-	-	-31.47	-	-	-	-
	5	II	-35.53	-	-	-31.52	-	-	-	-
3-arm PEG TriA	5	I	x	x	x	-61.13	-42.64	37.46	-13.91	49.33
	5	II	x	x	x	x	x	x	x	x
3-arm PEG TriA polymer	5	I	-39.94	-	-	-35.21	-	-	-	-
	5	II	-39.88	-	-	-34.67	-	-	-	-
3-arm PEG TriA	20	I	x	x	x	-59.72	-36.80	37.89	-15.02	39.08
	20	II	x	x	x	x	x	x	x	x
3-arm PEG TriA polymer	20	I	-36.13	-	-	-37.16	-	-	-	-
	20	II	-35.94	-	-	-35.50	-	-	-	-
4-arm PEG	5	I	-65.78			-62.85				
	5	II	-65.79			-62.77				
4-arm PEG TetraA	5	I	x	x	x	-64.36	-	-	-	-
	5	II								
4-arm PEG TetraA polymer	5	I	Flat and diffuse heat flux jump							
	5	II	Flat and diffuse heat flux jump							
4-arm PEG TetraM	5	I	x	x	x	-65.80	-	-	-	-
	5	II	x	x	x	x	x	x	x	x
4-arm PEG TetraM polymer	5	I	Flat and diffuse heat flux jump							
		II	Flat and diffuse heat flux jump							

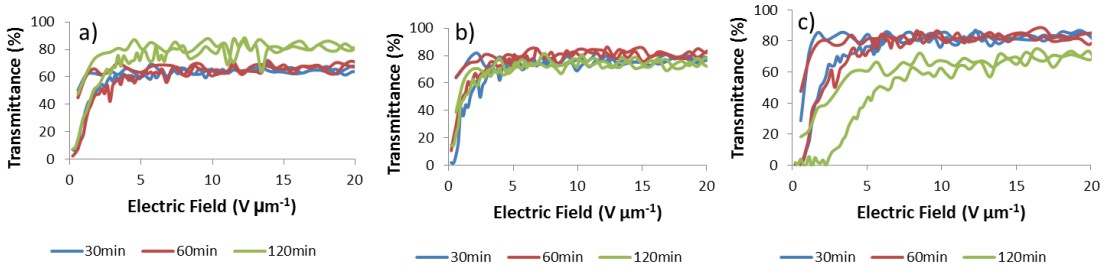

Figure 12.23 – Dependence of the polymerization time on the transmittance versus applied electric field of a) ((25 wt.% 4-armPEGTetraM, 75 wt.% PPGM)(1 wt.% AIBN))+E7 in a ratio of 30/70 (wt.%); b) ((50 wt.% 4-armPEG TetraM, 50 wt.% PPGM)(1 wt.% AIBN))+E7 in a ratio of 30/70 (wt.%); c) ((75 wt.% 4-armPEG TetraM, 25 wt.% PPGM)(1 wt.% AIBN))+E7 in a ratio of 30/70 (wt.%).

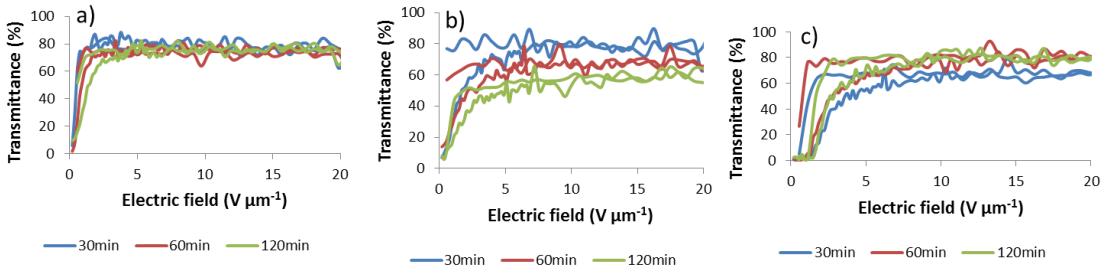

Figure 12.24 – Dependence of the polymerization time on the transmittance versus applied electric field of a) ((25 wt.-% 4-armPEG TetraA, 75 wt.-% PPGM)(1 wt.% AIBN))+E7 in a ratio of 30/70 (wt.%); b) ((50 wt.% 4-armPEG TetraA, 50 wt.% PPGM)(1 wt.% AIBN))+E7 in a ratio of 30/70 (wt.%) and c) ((75 wt.% 4-armPEG TetraA, 25 wt.% PPGM)(1 wt.% AIBN))+E7 in a ratio of 30/70 (wt.%).

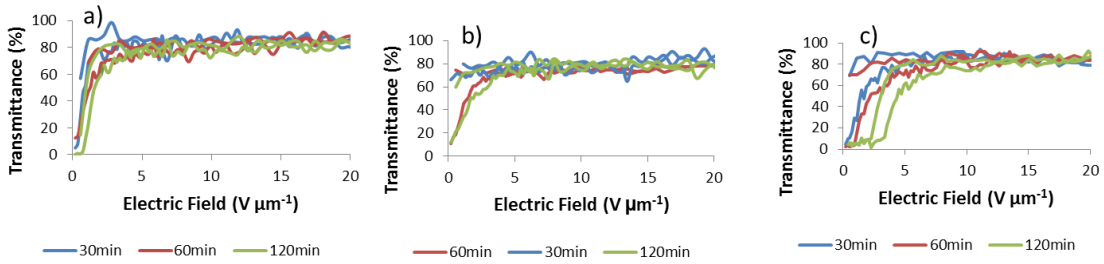

Figure 12.25 – Dependence of the polymerization time on the transmittance versus applied electric field of a) ((25 wt.-%3-armPEGTriA, 75 wt.% PPGM)(1 wt.% AIBN))+E7 in a ratio of 30/70 (wt.%);b) ((50 wt.% 3-arm PEG TriA, 50 wt.% PPGM)(1 wt.% AIBN))+E7 in a ratio of 30/70 (wt.%) and c) ((75 wt.% 3-armPEG TriA, 25 wt.% PPGM)(1 wt.% AIBN))+E7 in a ratio of 30/70 (wt.%).

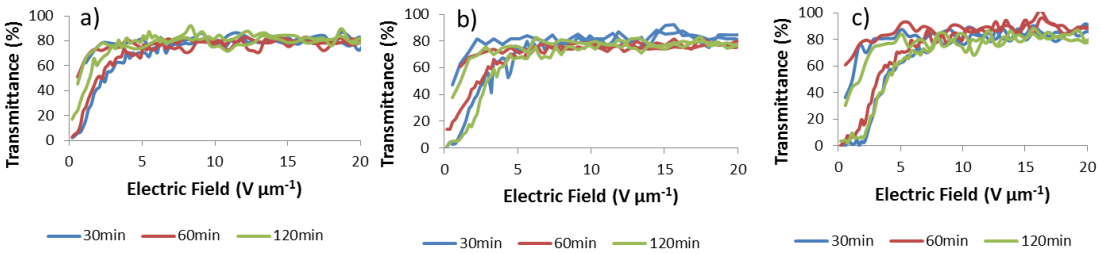

Figure 12.26 – Dependence of the polymerization time on the transmittance versus applied electric field of a) ((25 wt.% 3-armPEG TriM, 75 wt.% PPGM)(1wt.% AIBN))+E7 in a ratio of 30/70 (wt.%);b) ((50 wt.% 3-arm PEG TriM, 50 wt.% PPGM)(1 wt.% AIBN))+E7 in a ratio of 30/70 (wt.%) and c) ((75 wt.% 3-arm PEG TriM, 25 wt.% PPGM)(1 wt.% AIBN))+E7 in a ratio of 30/70 (wt.%).